POST-DEPOSITIONAL ALTERATION OF THE VENTERSDORP CONTACT REEF AT VAAL REEFS No.10 SHAFT, KLERKSDORP GOLDFIELD

Volker Heinrich Gartz

March 1996

A thesis submitted in fulfilment for the degree of Master of Science at the Department of Geological Sciences, University of Cape Town.

POST-DEPOSITIONAL ALTERATION OF THE VENTERSDORP CONTACT REEF AT VAAL REEFS No.10 SHAFT, KLERKSDORP GOLDFIELD

Volker Heinrich Gartz

March 1996

A thesis submitted in fulfilment for the degree of Master of Science at the Department of Geological Sciences, University of Cape Town.

In memory of Aidan Coulthard.

CONTENTS

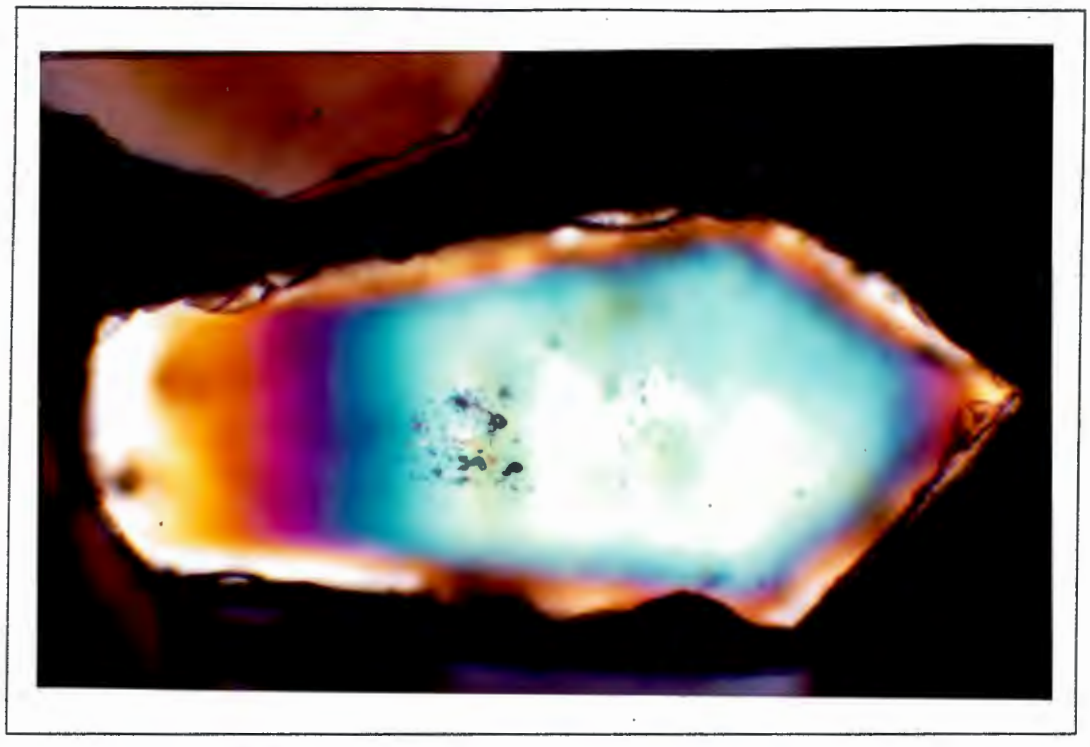

Cover Plate: Euhedral quartz crystal from the auriferous quartz vein, containing fluid inclusions and solid calcite inclusions in the centre (top). The complex growth zonations in this quartz crystal only become visible through cathodoluminescence imaging (bottom) and suggest a complex growth history of this vein quartz. (sample VHG163(A), XPL (top) and CL (bottom), length of quartz crystal = 0.65 mm).

LIST OF FIGURES

Fig.6.6: Composition-volume diagrams comparing (a) white phenocryst sample VHG069 to dark phenocryst sample VHG081, and (b) sample VHG081 to contact zone sample VHG084.

Fig.6.7: Variation of CIA in footwall quartzites with increasing proximity to the VCR.

Fig.6.8: Bulk rock alteration trends in (a) footwall quartzites and (b) hangingwall metabasalts as indicated on A'KF and ACF diagrams, respectively.

Fig.6.9: Primitive mantle-normalised REE abundances in four hangingwall metabasalt samples (samples VHG084(A), VHG084, VHG081 and VHG069) and in two footwall quartzite samples (VHG096 and VHG101).

Fig.7.1.1: Plot of the sum of non-interlayer cations vs total Al content illustrating chlorite end-member compositions (after Robinson *et al.*, 1993). Enlarged portion shows the chlorite compositions of different rock types (excluding the VCR).

Fig.7.1.2: Plot of Al/(Al+Fe+Mg) vs X_{Fe} ratios of chlorites from different rock types. For symbols see Fig.7.1.1.

Fig.7.1.3: Plot of calculated temperature of chlorite formation (after Zang and Fyfe, 1995) vs chlorite content X_{Chl} (after Robinson *et al.*, 1993). The presence of an apparently lower-temperature chlorite population is interpreted as incomplete equilibration of chlorite with the fluid. For symbols see Fig.7.1.1.

Fig.7.1.4: Histogram of X_{Fe} of chlorite analyses from three different chloritised footwall quartzite samples, showing the range in X_{Fe} within and between samples.

Fig.7.1.5: Plot of calculated temperature of chlorite formation (after Zang and Fyfe, 1995) and Al^{IV} content vs X_{Fe} of two, petrographically distinct, chlorite populations in bedding-parallel quartz vein sample VHG169.

Fig.7.1.6: Plot of the sum of non-interlayer cations vs total Al content for selected VCR chlorites.

Fig.7.1.7: Plot of Al/(Al+Fe+Mg) vs X_{Fe} of selected VCR chlorites. For symbols see Fig.7.1.6.

Fig.7.1.8: Plot of calculated temperature of chlorite formation (after Zang and Fyfe, 1995) vs chlorite content X_{Chl} (after Robinson *et al.*, 1993). For symbols see Fig.7.1.6.

Fig.7.1.9: Plot of Al^{IV} vs X_{Fe} content of VCR and footwall quartzite chlorites (of presumably the same generation) in sample VHG074, showing a positive correlation between Al^{IV} and Fe/Mg contents.

Fig.7.1.10: Plot of Al^{IV} vs X_{Fe} illustrating the wide range in Al^{IV} and/or X_{Fe} present in chlorites in four VCR samples.

Fig.7.1.11: Plot of Al^{IV} vs X_{Fe} of chlorite analyses from 4 samples of Fe-metasomatised VCR shown in Plate 7.1.1. Note the small compositional range in the Fe-rich chlorites

compared to the larger range of the more magnesian VCR type II chlorites.

Fig.7.2.1: Ternary $CaCO_3$-$FeCO_3$-$MnCO_3$ compositional plot of calcite from different rock types.

Fig.7.2.2: Ternary $CaCO_3$-$FeCO_3$-$MnCO_3$ compositional plot of carbonates from three Fe-metasomatised VCR samples.

Fig.7.2.3: Compositional core-rim zonation of four siderite grains.

Fig.7.3.1: Histogram of weight per cent composition of (a) Au, (b) Ag and (c) Hg of 349 individual gold particles from the VCR (this study) and the average of gold particles from 94 Vaal Reef samples (after Reid *et al.*, 1988) from the Klerksdorp goldfield.

Fig.7.3.2: Histogram comparison of gold fineness from the VCR No.10 Shaft (this study) and VCR from other localities in the Klerksdorp goldfield (after Utter, 1979).

Fig.7.3.3: Plot of Au vs Ag contents (wt%) illustrating the inhomogeneous composition of two gold particles from the auriferous quartz vein (sample VHG163(B)) (analytical totals normalised to 100 wt%).

Fig.7.3.4: Plot of Ag vs Hg contents (wt%) of gold particles in samples (a) VHG062, (b) VHG164, (c) VHG074 and (d) VHG093(B).

Fig.7.3.5: Plot of Ag vs Hg contents (wt%) of all quartz-, chlorite-, and pyrite-associated gold particles in the VCR samples.

Fig.7.3.6: Plot of Ag vs Hg contents (wt%) of gold particles from samples VHG163(B) and VHG163(C) from the auriferous quartz vein.

Fig.8.1: Fluid inclusion types and inclusion morphology.

Fig.8.2: Histogram of T_h and salinity of (a) VCR quartzite, (b) bedding-parallel (Par QV) and (c) bedding-perpendicular (Perp QV) quartz vein hosted aqueous fluid inclusions.

Fig.8.3: Histograms of T_h and salinity of primary type II and type III fluid inclusions from an Fe-metasomatised, siderite-rich VCR quartzite (sample VHG158(B)).

Fig.8.4: Histograms of T_h and salinity of primary and secondary type II and type III fluid inclusions from the auriferous quartz vein (sample VHG163(A)). Although the salinities of all the fluid inclusions are similar, two groups of fluid inclusions with distinctly different T_h are present in the central and marginal zones.

Fig.8.5: Examples of salinity (wt% $NaCl_{eq}$) vs T_h plots for secondary type II and type III fluid inclusions from (a) a bedding-perpendicular quartz vein, (b) the Nooitgedacht Fault zone quartz vein and (c)-(d) VCR quartzite. Open symbols: individual fluid inclusions; Filled symbols: mean of 3 or more fluid inclusions from a microfracture.

Fig.8.6: Histograms of T_h and salinity of secondary fluid inclusions from a bedding-parallel quartz vein (sample VHG087). Two distinct groups of fluid inclusions are present in this sample. For legend see Fig.8.3.

Fig.8.7: Histograms of T_h and salinity of secondary fluid inclusions from a bedding-parallel quartz/calcite vein (sample VHG137). For legend see Fig.8.3.

Fig.9.1: Typical quartz CL spectra of (a) detrital quartz (spectrum S1 from VCR sample VHG063(A) and spectra S2/S3 from sample VHG158(B)), (b) authigenic/metamorphic quartz (spectra S1/S2 from footwall quartzite sample VHG173(B), spectrum S3 from quartz adjacent to the gold particle shown in Plate 9.7 (sample VHG063(A)) and (c) hydrothermal quartz (spectra S1/S2 from zoned euhedral quartz crystal from quartz vein (sample VHG181); spectra S3 and S4 are from a quartz/calcite vein at the VCR-footwall contact (sample VHG172) and the auriferous quartz vein (sample VHG163(A), respectively).

Fig.9.2: Quartz CL spectra, the areas of acquisition are shown in Plate 9.6. Note the asymmetry of the orange peak in some of the spectra. S1/S2: detrital quartz; S3: fractured detrital grain with authigenic/metamorphic signature; S4: authigenic/metamorphic quartz rim; S5: hydrothermal quartz from a quartz vein in the same sample.

Fig.9.3: Quartz CL spectra from gold- and chlorite-bearing quartz grains from VCR sample VHG063(A). Spectrum S1 was acquired 30 μm away from the pseudohexagonal chlorite flake in the detrital quartz grain on the right hand side, spectrum S4 is from the authigenic/metamorphic quartz rim surrounding the pseudohexagonal chlorite flake (see CL image of Plate 9.7). Spectrum S2 come from immediately adjacent to the gold particle in the left hand quartz grain and spectrum S3 was acquired 30 μm away from that gold particle.

Fig.9.4: Quartz CL spectra from footwall quartzite sample VHG173(B) (areas of spectra acquisition are shown in Plate 9.8). S1: detrital quartz grain; S2/S3/S4: authigenic/ metamorphic quartz surrounding the detrital quartz grain and enclosing galena and chlorite.

Fig.9.5: Hydrothermal quartz CL spectra from the euhedral quartz crystal (sample VHG163(A)) shown in Plate 9.9. S1/S2: core zone containing minute calcite and fluid inclusions; S3: intermediate dark grey/black CL zone; S4: dissolution zone towards the margin of the quartz crystal.

Fig.9.6: Effects of instrument set-up/operating conditions on CL spectra. (a) Shows the effect of changing the scan area, (b) the effect of increasing scan time and probe current and (c) the acquisition of spectra after rescanning an area after 155 seconds (S1 an S2) and another area after 130 seconds (S3 and S4).

Fig.10.1: Calculated temperature of chlorite formation (after Zang and Fyfe, 1995) vs X_{Fe} of regionally metamorphosed hangingwall metabasalt samples VHG126 and VHG183.

Fig.10.2: F(M)ASH system for the footwall quartzites is defined by the phases quartz (Qtz), pyrophyllite (Prl) and chloritoid (Cld) (H_2O in excess).

Fig.10.3: P-T diagram (after Frimmel, 1994) showing several metamorphic reactions in the FASH system. Solid lines represent stable mineral reactions involving the phases quartz (qtz), kaolinite (kln), pyrophyllite (prl), chlorite (chl), chloritoid (cld) and kyanite (ky) (H_2O in excess). Dashed line represents mineral reaction in the absence of quartz. Shaded area outlines the approximate P-T conditions of regional metamorphism as interpreted for the VCR in the study area.

Fig.10.4: Calculated temperature of chlorite formation (after Zang and Fyfe, 1995) vs X_{Fe} of chlorites.

Fig.10.5: Isochores calculated for primary fluid inclusions (sample VHG158(B) and VHG163(A)) and secondary fluid inclusions along microfractures in hydrothermal vein quartz (sample VHG087), using the equation of state of Brown and Lamb (1989).

Fig.11.1: Sulphur vs oxygen fugacity diagram showing the stability fields for pyrite (Py), pyrrhotite (Po), magnetite (Mag), haematite (Hem), rutile (Ru) and ilmenite (Ilm) at $T = 300^0C$, $P = 2$ kbar. Differently hatched areas indicate the possible ranges in fugacities which may have existed around the VCR, the metabasalts (HW) and in quartz veins (QV). Phase boundaries were calculated using the GEO-CALC program of Brown *et al.* (1989).

Fig.12.1: Gold solubility of $Au(HS)_2^-$ and $AuCl_2^-$ complexes as a function of $f(O_2)$ and $f(S_2)$ in a solution at $T = 350^0C$, $pH = 6$, salinity = 6 wt% NaCl and 320 ppm S (after (Romberger, 1991). Also shown are the stability fields of pyrite (Py), pyrrhotite (Po), magnetite (Mag) and haematite (Hem).

Fig.12.2: Diagram illustrating the time required to homogenise a gold particle with respect to Ag at different temperatures, assuming an initial variation of 10 wt% Ag. Diffusion coefficients are from Askill (1989).

LIST OF TABLES

LIST OF PLATES

Plate 9.2: Subangular, fractured detrital quartz grains showing varying degrees of CL intensity. Note dark grey authigenic/metamorphic quartz cement and fracture-filling quartz. Pyrite and chlorite are black. (sample VHG136, CL, length of photo = 3.4 mm, area of Plate 9.1 is outlined).

Plate 9.3: Detrital quartz grains surrounded by dark grey authigenic/metamorphic quartz over-growth rims. Note embayed grain margins (arrows) of detrital quartz grains. (sample VHG093(A), CL, length of photo = 1.3 mm).

Plate 9.4: Hydrothermal auriferous quartz vein showing euhedral quartz crystals (on right handside), fine grained anhedral quartz (towards left hand side) and a large anhedral hydrothermal quartz grain (purple) on the extreme left hand side. (sampleVHG163(A), XPL, length of photo = 2.3 mm).

Plate 9.5: Approximately the same field of view as in Plate 9.4. The zonation of the euhedral quartz crystals is clearly visible under CL, as is the fine grained quartz towards the left hand side. (sample VHG163(A), CL, length of photo = 3 mm).

Plate 9.6: Areas of spectra acquisition S1-S4 shown in Fig.9.2. Spectra S1 and S2 are from two adjacent detrital quartz grains. Spectrum S3 comes from a brecciated and re-cemented dark grey detrital quartz grain with an authigenic/metamorphic signature. Spectrum S4 is from the dark grey authigenic/metamorphic quartz overgrowth rim separating the two detrital quartz grains. Note the lighter grey rectangular boxes (radiation damaged areas) caused by electron bombardment during acquisition of CL spectra. (sample VHG093(A), CL, length of photo = 0.4 mm).

Plate 9.7: Comparison of backscatter electron image (left) and CL image (right) of VCR sample VHG063(A). Two very brightly reflectant grains in the backscatter image are gold grains, one of them is attached to type III chlorite (in the left hand quartz grain) and the other one adjacent to chlorite/pyrite (medium grey grain along top edge of backscatter image). A pseudohexagonal chlorite flake is p resent in the right hand quartz grain. (sample VHG063(A), backscatter and CL image, length of each photo = 0.3 mm).

Plate 9.8: Detrital quartz grain from footwall quartzite (showing very bright CL intensity) surrounded by authigenic/metamorphic quartz with very low (dark grey) CL intensity. Galena (Gn) and chlorite (black) are closely associated with the latter. Areas of spectra acquisition S1-S4 (shown in Fig.9.4) are as indicated. (sample VHG173(B), CL, length of photo = 0.8 mm).

Plate 9.9: CL image of a euhedral quartz crystal from the auriferous quartz vein, showing complex growth zonation. The jagged nature of the outer zone indicates a quartz dissolution and subsequent precipitation event. Areas of acquisition of spectra S1-S4 (shown in Fig.9.5) are as indicated. (sample VHG163(A), CL, length of photo = 0.3 mm).

ABSTRACT

The Ventersdorp Contact Reef (VCR) is an auriferous conglomerate which unconformably overlies the rocks of the Witwatersrand Supergroup. It acted as a palaeo-aquifer and is capped by relatively impermeable metabasalts of the Ventersdorp Supergroup.

Three post-depositional alteration events, which form an alteration halo in the footwall and hangingwall rocks around the VCR, can be recognised. The first of these alteration events is attributed to regional metamorphism and is identified by the formation of pyrophyllite in the footwall quartzites and a lower greenschist facies mineral assemblage in the hangingwall metabasalts. The second and third alteration events are interpreted as metasomatic fluid infiltration events which were focused along the VCR horizon. The second alteration event involved K^+ metasomatism which affected the footwall and hangingwall rocks up to a distance of several metres away from the VCR. The third alteration event, during which the muscovite was partially replaced, was associated with the formation of chlorite in and immediately around the VCR. Chlorite thermometry suggests a temperature of 307 ± 14^0C for this event.

The close mineralogical association of gold with chlorite, secondary pyrite and secondary quartz in the VCR is interpreted to indicate that gold remobilisation was associated with the chlorite-forming alteration event. The inhomogeneity found in gold particles within a hydrothermal quartz vein indicates a sharp drop in temperature after gold precipitation, suggesting a very short period of hydrothermal fluid infiltration. The chlorite metasomatism and gold mobilisation post-date the formation of pseudotachylite and can be explained by the Vredefort event at c. 2024 Ma.

ACKNOWLEDGEMENTS

I would like to thank the Vaal Reefs Exploration and Mining Company Limited for permission to conduct this study at Vaal Reefs No.10 Shaft, and for being allowed to collect underground sample material. I thank my collegues on the mine for their assistance, be it for moral support or keeping an eye open for interesting samples. The expertise of Lydia Loubser, who very professionally draughted several of the figures in this text, is acknowledged. Much appreciation goes to Dave Wilson for preparing the thin and polished sections at the Department of Geological Sciences (UCT), and to Dick Rickard for guidance on the electron microprobe at the department. Special thanks go to Dane Gerneke and the rest of the team at the Electron Microscope Unit at UCT for their tremendous help, not only technically but also logistically for providing the photographs of the CL images. For the production of the colour photographs I would like to thank Nick Fox at the Gold and Mineral Exploration Services branch of the Anglo American Corporation.

Finally, I would like to thank two people in particular, without whose help this study would not have been possible. To my supervisor Hartwig Frimmel, not only for his financial support but in particular also for his patience, guidance and immensely helpful discussions. To my wife Colleen, for her patience and support during the three year's of part-time studying.

ABBREVIATIONS

$a(H_2O)$	activity of water
$a(Ca^{2+})$	Ca^{2+} activity in fluid
$a(K^+)$	K^+ activity in fluid
Al^{IV}	tetrahedral Al
bd	below detection
CIA	chemical index of alteration
CL	cathodoluminescence
CLI	cathodoluminescence imaging
EMP	electron microprobe
$f(O_2)$	oxygen fugacity
$f(S_2)$	sulphur fugacity
F_v	volume factor
i/l	interlayer cations
LLD	lower limit of detection
LOI	loss on ignition
L/V	liquid/vapour ratio
$NaCl_{eq}$	wt % $NaCl_{equivalent}$
nd	not determined
non i/l	non-interlayer cations
PPL	plane polarised light
ppm	parts per million
REE	rare earth element
RL	reflected light
SEM	scanning electron microscope
T_e	first melting (eutectic) temperature
T_h	temperature of homogenisation
T_m	temperature of final melting
VCR	Ventersdorp Contact Reef
wt %	weight per cent
X_{Chl}	chlorite content
X_{Fe}	Fe/(Fe+Mg) (in wt %)
XPL	cross-polarised light
XRD	X-ray diffraction
XRF	X-ray fluorescence

1. Introduction

Gold in the Witwatersrand Basin typically occurs in quartz pebble conglomerate horizons which define erosional unconformities. These conglomerate horizons, which can vary in thickness from <10 cm to several metres, are separated from each other by up to several hundreds of metres of quartzites. Within these conglomerates, gold is often closely associated with carbonaceous matter (in form of nodules and seams) and with heavy minerals such as pyrite, chromite, altered titanomagnetite grains and uraninite along foresets.

The controversy of the origin of the gold in the Witwatersrand conglomerates is almost as old as the discovery of the gold in the Witwatersrand Basin itself. Two opposing theories explaining the origin of the gold are an epigenetic/hydrothermal theory (e.g. Graton, 1930; Davidson, 1955; Phillips, 1988) and a metamorphosed placer theory (e.g. Mellor, 1916; Reimer and Mossman, 1990(b); Robb and Meyer, 1990; Frimmel *et al.*, 1993). The former model proposes that all the gold was introduced by hydrothermal fluids. In contrast, the latter theory envisages the local remobilisation of originally detrital gold particles through post-depositional alteration processes.

Recent work by Minter *et al.* (1993) involving an SEM study of the morphology of gold particles has provided strong evidence in support of the metamorphosed placer theory. Attempts have also been made to explain the presence of rounded pyrite grains in the conglomerates through a large-scale sulphidisation process (e.g. Myers *et al.*, 1993). Evidence in favour of a detrital origin of some of the rounded pyrite grains (as has previously been suggested by Hallbauer, 1986; MacLean and Fleet, 1989), however, comes from the wide range in sulphur isotope ratios which have been identified within and between morphologically different pyrite grains (e.g. Eldridge *et al.*, 1993; Armstrong *et al.*, 1995).

The Ventersdorp Contact Reef (VCR) forms the upper-most auriferous conglomerate horizon which is currently being mined for gold. It is unique in the sense that it is overlain by c. 2800 m of metabasalt (in the Klerksdorp goldfield) (Antrobus *et al.*, 1986; Bowen *et al.*, 1986) and it has, in recent years, become one of the most important ore bodies in the Witwatersrand Basin. It can

be expected that the capping of the VCR by relatively impermeable basalts would have made the VCR a favourable horizon along which post-depositional fluids could have been channelled. This implies that the VCR was probably characterised by fairly high fluid:rock ratios, which would have been particularly favourable for gold mobilisation.

Vaal Reefs No.10 Shaft is currently the only shaft belonging to the Vaal Reefs Exploration and Mining Company Ltd where the VCR is being mined as the major ore body. The Vaal Reefs No.10 Shaft lease area is located c. 5 km west of Orkney and c. 180 km south-west of Johannesburg along the western margin of the Klerksdorp goldfield (Fig.1.1) in the North West Province.

Numerous studies dealing with sedimentological, mineralogical and geochemical aspects of the VCR in the Carletonville goldfield have been conducted (e.g. Krapez, 1985; Stefan and Martin, 1993; Germs and Schweitzer, 1994; Hall, 1994; Henckel and Schweitzer, 1994; Henning *et al.*, 1994; Reddy and Germs, 1994; Schweitzer *et al.*, 1994; Zhao *et al.*, 1994) but very little research has been done on the VCR in the Klerksdorp goldfield.

An MSc dissertation by Thomas (1977) concentrated on the sedimentology of the VCR at Vaal Reefs No.6 & 7 Shafts (several kilometres to the north-east of No.10 Shaft). More recently, a pseudotachylite fault rock study (yielding an age of 2006 ± 17 Ma for the pseudotachylite formation event) was carried out by Trieloff *et al.* (1994) at Vaal Reefs No.10 Shaft. In addition, an investigation of the composition of fluid inclusions and the conditions of gold mobilisation in the VCR at Vaal Reefs No.10 Shaft was done by Boer *et al.* (1995). Apart from this research, the present study is the first detailed investigation dealing with the post-depositional alteration events that have affected the VCR at Vaal Reefs No.10 Shaft.

The age of 2714 ± 8 Ma for the Ventersdorp Supergroup lavas (Armstrong *et al.*, 1991) is also the minimum age of the VCR. This, together with the age of 2006 ± 17 Ma for the pseudotachylite formation suggests that a period of at least 700 Ma was available for post-depositional alteration of the VCR. It therefore becomes important to distinguish between the different post-depositional alteration effects such as contact metamorphism, regional metamorphism and metasomatic alteration processes.

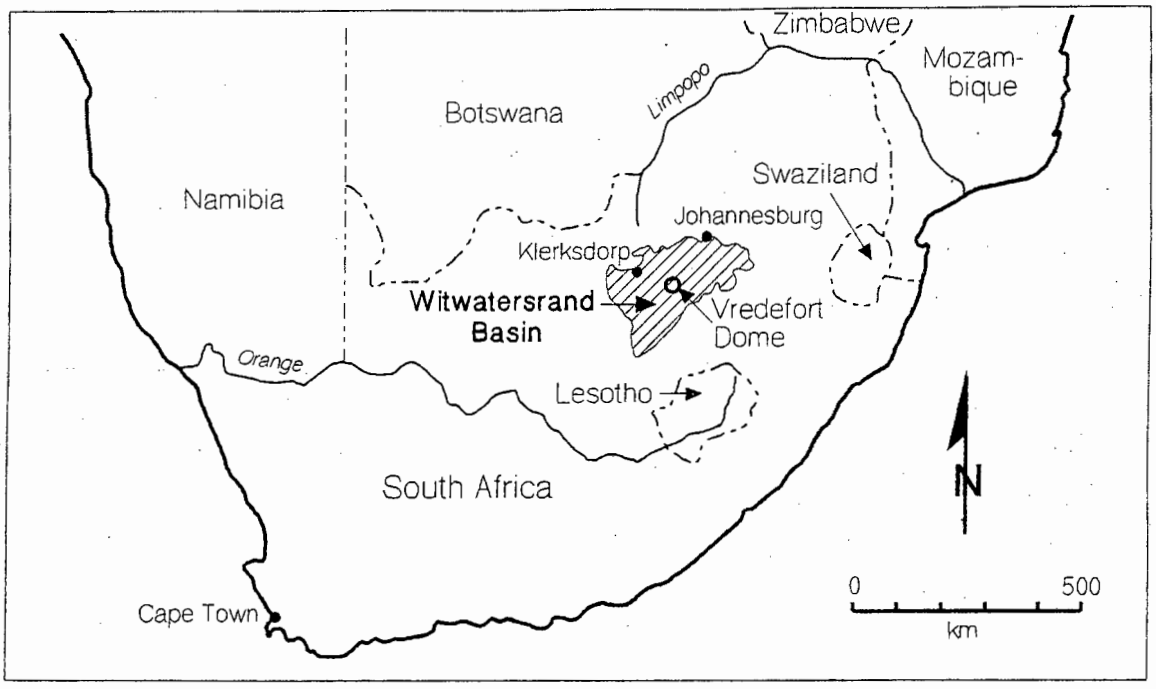

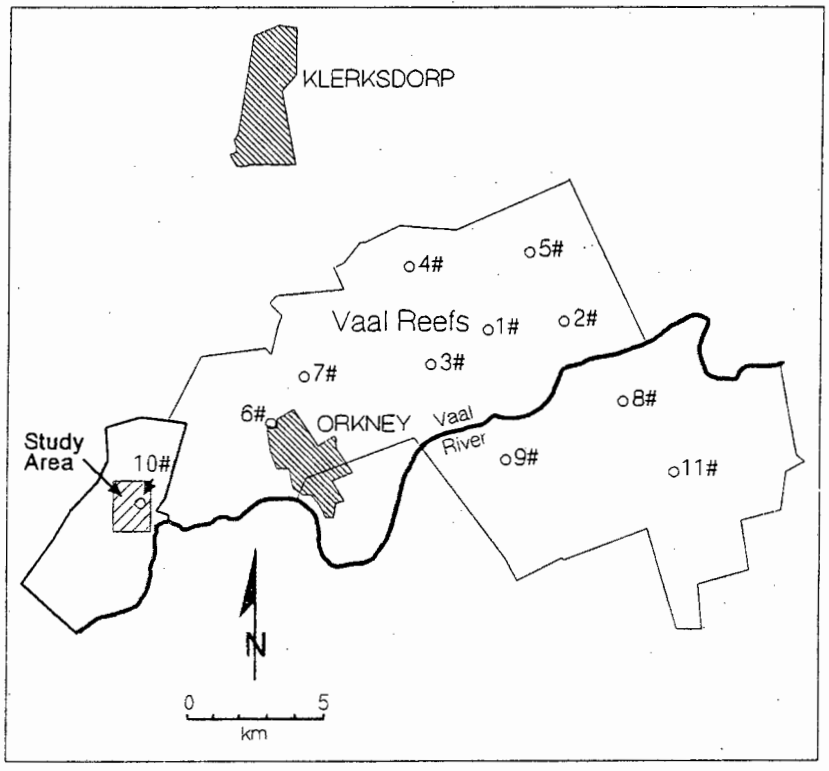

Fig.1.1: Locality plan of the Witwatersrand Basin in South Africa (top) and the locality of the Vaal Reefs No.10 Shaft study area (bottom).

Chlorite and sericitic muscovite in the VCR in the Carletonville goldfield have been interpreted as products of metasomatic alteration (Henckel and Schweitzer 1994; Zhao *et al.*, 1994). Although some effects of post-depositional alteration were visible around the VCR at Vaal Reefs No.10 Shaft (e.g. discolouration of footwall quartzites and hangingwall metabasalts, quartz veining, massive secondary pyrite crystallisation), the relative timing and extent of these metamorphic/metasomatic alteration events has remained unknown. One of the aims of this study therefore was firstly, to distinguish between different post-depositional alteration events and secondly, to document the effects of these events on the VCR and the surrounding rocks in the study area.

For this purpose, bulk rock geochemical analyses and modelling were important in determining what compositional changes occurred in the footwall and hangingwall rocks with increasing proximity to the VCR and to what extent an exchange of components between the rock and the fluid(s) had taken place. The secondary fluid inclusions in quartz veins and in the VCR quartzite fraction were examined to aid in the identification and characterisation of different fluids. In addition, cathodoluminescence imaging (CLI) was used to identify textures which might provide information on the extent of secondary quartz formation and to identify fluctuations in quartz solubility. Mineral analyses of gold particles in the VCR was done to determine the extent of gold homogenisation. Furthermore, the compositions of different textural types of chlorites in the VCR and surrounding rocks were analysed to establish at what scale compositional variations existed.

2. Regional Geology

The conglomerates of the Witwatersrand Basin are unique in the world because of their age and the quantity of gold which is found in them. The dimensions of the basin are c. 300 km x 150 km, with the long axis of the basin striking approximately north-east/south-west (Fig.2.1). Five major goldfields lie around the western, northern and north-eastern margins of the Witwatersrand Basin.

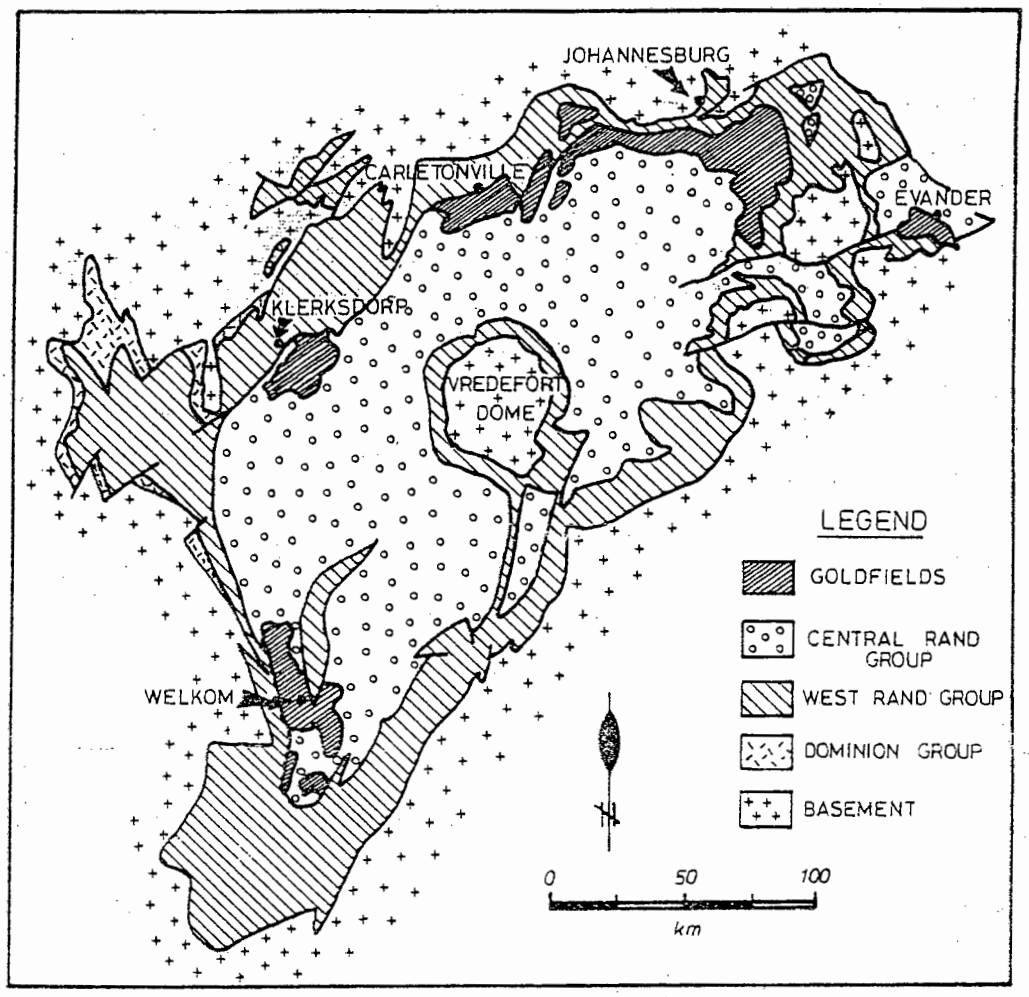

Fig.2.1: Subsurface distribution of the Witwatersrand Supergroup rocks and the location of the five major goldfields around the margin of the Witwatersrand Basin.

The subsurface distribution of the rocks belonging to the Witwatersrand Supergroup are shown in Fig.2.1. The Witwatersrand Supergroup has been subdivided into three groups, namely the Dominion Group, the West Rand Group and the Central Rand Group (Fig.2.2). The predominantly sedimentary rocks of the Witwatersrand Basin were deposited on Archaean granitic basement rocks in the Kaapvaal Craton. Volcanic rocks from the Dominion group have been dated at 3074 ± 6 Ma (Armstrong *et al.*, 1991), whereas mafic and felsic volcanic rocks of the Ventersdorp Supergroup (which overlie the Witwatersrand Supergroup rocks) have been dated at 2714 ± 8 and 2709 ± 4 Ma, respectively (Armstrong *et al.*, 1991). A period of c. 350 Ma was therefore available for the deposition of the Witwatersrand Supergroup, which attains a maximum thickness of c. 10 km (Tankard *et al.*, 1982).

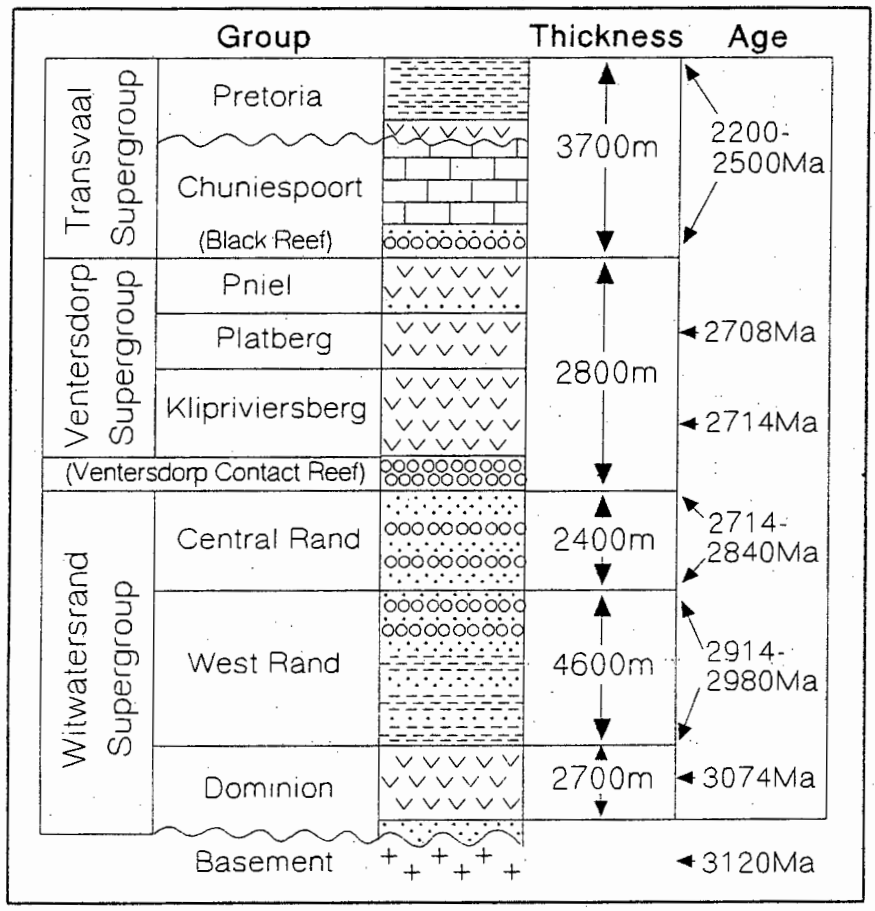

Fig.2.2: Generalised stratigraphic column of the Witwatersrand, Ventersdorp and Transvaal Supergroups from the Klerksdorp goldfield.

The base of the Dominion Group is defined by quartzites and conglomerates which rest unconformably on the basement granites. The bulk of the Dominion Group, however, consists of predominantly basic to intermediate lavas. A maximum thickness of 2700 m for this group has been reported from the Klerksdorp goldfield (Tankard *et al.*, 1982).

The rocks of the West Rand Group attain a maximum thickness of c. 7500 m to the north-west of Krugersdorp, but in the Klerksdorp goldfield they average 4600 m (Tankard *et al.*, 1982). They consist of argillaceous quartzites and magnetic shales in approximately equal proportions and minor (250 m thick) lavas. The presence of magnetic shales and banded iron formations and the absence of any sedimentary structures indicates that deposition of these sediments probably occurred in a distal shelf marine environment during periods of transgression (Tankard *et al.*, 1982). Eight such transgressive events are recorded in the Klerksdorp area (Tankard *et al.*, 1982). The auriferous conglomerate horizons are found in a predominantly quartzite sequence in the Government and Jeppestown Subgroups.

By far the most important gold-bearing conglomerates, however, occur in the Central Rand Group. This group attains a thickness of c. 2400 m in the Klerksdorp goldfield and a maximum thickness of c. 2900 m near Vredefort (Tankard *et al.*, 1982). The rocks consist predominantly of quartzites and lesser amounts of fine grained argillites (shales). Intercalated with the quartzites and the argillites are conglomerate horizons which host a significant portion (c. 40 %) of the world's gold.

These conglomerate horizons (also called "reefs") can be described as quartz ± chert, small pebble to large cobble conglomerates which vary in thickness from <10 cm to several metres. Volumetrically the conglomerates amount to only a small fraction (<1 %) of the total volume of rocks in the Witwatersrand Basin. The conglomerates are interpreted to be products of degradation in a braided fan/delta system (Tankard *et al.*, 1982). All the conglomerates define erosional unconformities and although the typical angle of unconformity is hardly noticeable and is usually $<4^0$ (Tankard *et al.*, 1982), unconformity angles of nearly 90^0 have been reported (Myers *et al.*, 1992) along the upturned and thrusted margins of the basin.

The unconformable relationship of the VCR with the underlying footwall rocks and the contemporaneous extrusion of lavas during VCR sedimentation (leading to so-called "inter-reef lavas", Hall, 1993) has resulted in the VCR being grouped separately into the Venterspost Conglomerate Formation (SACS, 1980). The age of 2714 ± 8 Ma which was obtained for the overlying mafic Klipriviersberg lavas (Armstrong *et al.*, 1991) is, by implication, also the age when sedimentation of the VCR was terminated.

Evidence from the Carletonville goldfield indicates that basalt extrusion was diachronous and commenced in the north (Linton *et al.*, 1994), resulting in the formation of "inter-reef lavas". The rocks of the Ventersdorp Supergroup fill an elliptical basin of similar extent as the rocks of the Witwatersrand Supergroup, the former being subdivided into the Klipriviersberg Group, the Platberg Group and the Pniel Group (Fig.2.2). In is estimated that these predominantly volcanic continental flood basalts covered an area >300000 km^2 (Pretorius, 1976). In the Klerksdorp region the maximum thickness attained by rocks of the Ventersdorp Supergroup was c. 2800 m (Antrobus *et al.*, 1986; Bowen *et al.*, 1986).

A coastal-marine depositional environment has been interpreted for the rocks of the Witwatersrand Basin (e.g. Eriksson *et al.*, 1981), based on the interbedded nature of the quartzites, argillites, magnetic shales (in the West Rand Group) and the presence of conglomerates along erosional surfaces. The cyclic nature of the Witwatersrand Supergroup sediments and the overall coarsening-upwards nature suggests that changes in relative sea level led to a series of regressive and transgressive events. Deposition of conglomerates in a fluvio-marine setting is interpreted to have occurred during regression events.

The structural setting at the time of deposition of the Dominion Group was probably in a failed rift basin in an extensional regime (Burke *et al.*, 1986). An age of 3100 - 3010 Ma has been suggested for this event (Robb *et al.*, 1990). The accumulation of West Rand Group sediments only began c. 100 Ma after the eruption of the Dominion lavas. Deposition of the sediments probably occurred in a foreland basin (Robb *et al.*, 1990). Initiation of the foreland basin compressive tectonics has tentatively been related to the convergence of the Zimbabwe and

Kaapvaal Cratons (e.g. McCarthy, 1994).

The sediments of the Central Rand Group were deposited in a continually shrinking basin under an increasingly compressive tectonic regime, resulting in southerly verging thrusts (Winter, 1995). The rate of sedimentation and the interaction between marine and fluvial depositional systems within the Witwatersrand Basin is interpreted to have been strongly influenced by 19 fault-bounded basement blocks (Fig.2.3) (Stanistreet and McCarthy, 1991; Myers *et al.*, 1992). These fault-bounded blocks are also thought to have exerted an important control on the preservation potential of the conglomerate horizons (McCarthy, 1994). In the Klerksdorp goldfield, disconformities and unconformities were produced when the continued tectonic movement resulted in the uplift of the beds to the north-west (Antrobus *et al.*, 1986).

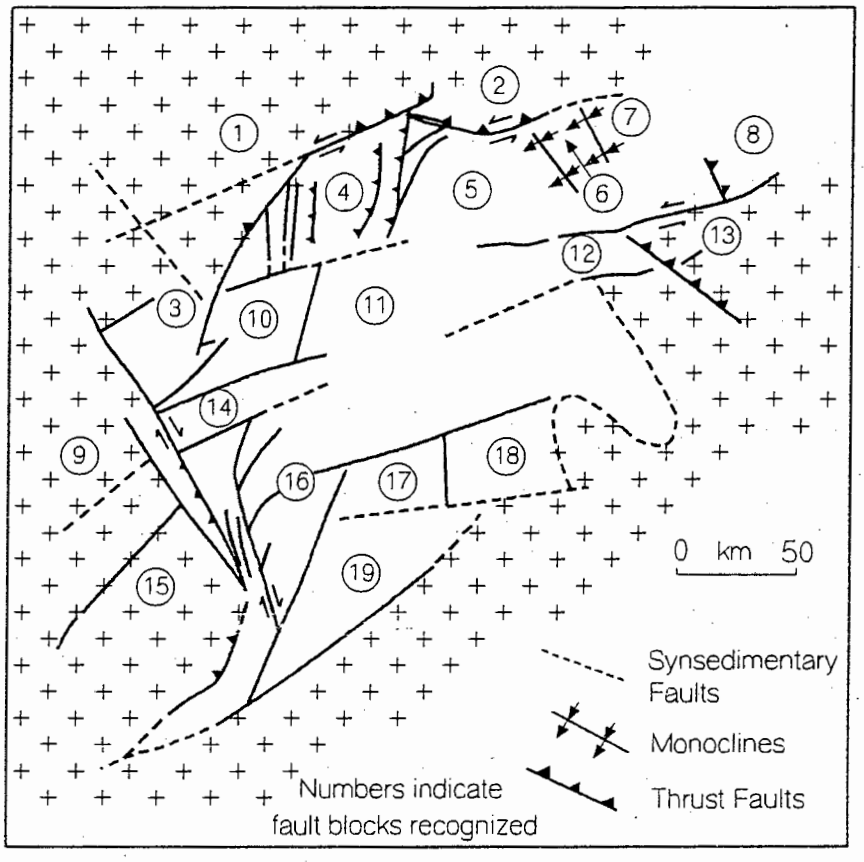

Fig.2.3: Structural map of the Witwatersrand Basin showing the major syn-sedimentary fault and deformation zones which define the margins of basement blocks. Major blocks are numbered (after Myers *et al.*, 1992).

The deposition of Witwatersrand Supergroup sediments was finally terminated by crustal extension and the extrusion of Klipriviersberg lavas. The development of normal faults during this extensional phase occurred during Ventersdorp times and resulted in the preservation of Platberg Group sediments in several fault-bounded graben blocks. Folding, tilting and faulting of Transvaal age have also been identified in the Klerksdorp goldfield (Antrobus *et al.*, 1986), some of the faults being reactivated older bedding-plane faults.

The metamorphic mineral assemblage in the metabasaltic rocks of the Witwatersrand Basin indicate lower greenschist facies. In the quartzites, however, a metamorphic mineral assemblage consisting of quartz, pyrophyllite, muscovite, chlorite and chloritoid has been used to infer regional peak P-T conditions of 2 - 3 kbar and 350 ± 50^{0}C (Phillips, 1987; Wallmach and Meyer, 1990) or 300 - 350^{0}C (Frimmel, 1994).

Kaolinite, which has been identified in the rocks of the West Rand and Central Rand Groups (Schreyer and Bisschoff, 1982; Phillips and Law, 1994) is considered either to be a product of the breakdown of feldspars or a late-stage retrograde alteration product. Up to 30 % feldspars have been recorded in some quartzites of the West Rand Group (Fuller, 1958), but the Central Rand Group rocks are characteristically devoid of feldspars.

The widespread occurrence of pyrophyllite in particular has been interpreted to indicate regional temperatures >290^{0}C (Phillips, 1987; Frimmel, 1994). Although pyrophyllite is generally regarded as a hydrothermal alteration mineral indicative of advanced argillic alteration (e.g. Guilbert and Park, 1986), it is now also widely recognised as a regional metamorphic mineral (Frey, 1987). The maximum regional metamorphic temperature which was attained is constrained by the breakdown of pyrophyllite to form kyanite+quartz. Kyanite has only been identified together with pyrophyllite locally in shear zones and quartz veins in the Central Rand Group (Schreyer and Bisschoff, 1982), suggesting that the local pressures and temperatures attained were above 2.5 kbar and 380^{0}C, respectively. The possible interpretation of sericite aggregates in the Black Reef (McCarthy *et al.*, 1986) as pseudomorphs after chiastolite (Frimmel, 1994) would indicate a maximum pressure of 2.5 - 3.5 kbar for the Witwatersrand Supergroup.

A similar peak metamorphic mineral assemblage has been observed in the rocks of the West Rand and the Central Rand Groups. This may, however, be an artifact of sampling because the West Rand Group is accessible for sampling only near the basin margin where it was, in places, never overlain by the Central Rand Group. The peak metamorphic mineral assemblage indicates an anomalously high geothermal gradient of 35 - 40^{0}C/km, in contrast to a geothermal gradient of 15 - 20^{0}C/km for stable cratonic areas. This suggests that a thermal event of basin-wide extent occurred at some stage during the post-depositional history of the Witwatersrand Basin.

Higher-grade metamorphic mineral assemblages (consisting of garnet, cordierite, staurolite and/or sillimanite) are found only locally in vicinity to intrusions such as those around the Vredefort Dome (Bisschoff, 1982). Although most researchers attribute these amphibolite facies minerals to thermal metamorphism, others (e.g. Gibson and Stevens, 1995) suggest that they reflect the association between regional metamorphism and the Bushveld/Vredefort events.

Numerous studies which deal with the composition of pre- and post-depositional fluid inclusions for which evidence exists in the quartzites, quartz veins and amygdales of the rocks of the Witwatersrand Basin have been done (e.g. Shepherd, 1977; Hallbauer and Kable, 1982; Frimmel *et al.*, 1993; Boer *et al.*, 1995; Drennan *et al.*, 1995). Two main groups of fluid inclusions have been identified in pre- and post-depositional fluid inclusions, namely low to moderately saline (generally <20 wt% $NaCl_{equivalent}$) aqueous inclusions and CO_2-rich inclusions (Table 2.1).

Table 2.1: Fluid Inclusion Compositions from Witwatersrand Quartz as Determined by Other Authors

Author	Robertson (1985)	Frimmel et al. (1993)		Boer et al. (1995)	Klemd et al. (1994)
Locality	'C' Reef - Evander & Klerksdorp	Basal Reef Welkom		VCR (No.10#) Klerksdorp	Granitoids around Wits Basin
Quartz investigated	Quartz veins	Authigen. quartz	Detrital quartz	Detrital quartz & quartz veins	Quartz veins
Low-salinity type					
Th	155±30	137±5	160 - 190	115 - 190	130±10
Salinity	6 - 18	0 - 4	<5	<9	0 - 9
Cation Species	Na, K, Ca	K	Na		
Mod.-salinity type					
Th		134±7	200 - 220		
Salinity		7 - 17	7 - 16		
Cation Species		Ca	Na		
High-salinity type					
Th					120±20
Salinity					13 - 30
Cation Species					Na, Ca (& CO2/CH4)
CO2-rich type					
Th	270			130	
Salinity		8		4	
Other Gas Species	CH4/N2	CH4/N2		CO2/CH4	

These fluids show a wide range of homogenisation temperatures, and first melting temperatures suggest a variety of dissolved salt species (mainly NaCl, KCl, $CaCl_2$ and $MgCl_2$) in the fluids. The most commonly reported gas species in the CO_2-rich fluid inclusions are (in addition to CO_2), CH_4 and lesser amounts of C_2H_6, H_2S, N_2, H_2 and Ar (Boer *et al.*, 1995; Drennan *et al.*, 1995). The variation in composition of the post-depositional fluid inclusions suggests a complex history of metasomatic events which have affected the rocks of the Witwatersrand Basin.

3. Geological Setting of Vaal Reefs No.10 Shaft

3.1 Stratigraphy

The stratigraphy of the rocks at Vaal Reefs No.10 Shaft is shown in Fig.3.1. The strike of the rocks is north-easterly and they dip at approximately 20 - 30^0 towards the north-west. The rocks which are intersected at the bottom of the shaft at c. 1770 m below surface belong to the Commonage Formation (Johannesburg Subgroup) (Antrobus *et al.*, 1986). These quartzites are grey-brown, medium to coarse grained argillaceous quartzites which contain few scattered medium to large polymictic pebbles. Thin (usually <20 cm thick) dark brown fine grained argillites are occasionally intercalated with the quartzites. A minimum stratigraphic thickness of 250 m is inferred from underground exposure.

At the base of the quartzites belonging to the Stilfontein Quartzite Formation lies the Livingstone Reef. This reef is <50 cm thick and varies from a matrix- to a pebble-supported, usually polymictic conglomerate. It contains small to medium, often dark-rimmed, quartz pebbles and up to 5 vol% polymictic (mainly igneous) pebbles. The reef is often poorly mineralised (<5 vol% sulphides).

The Livingstone Reef is overlain by yellow-brown argillaceous quartzites which contain numerous thin (<40 cm thick) colourful polymictic pebble bands and/or scattered polymictic pebbles. Small amounts of pyrite mineralisation (<2 vol% sulphides) are present in several of these pebble bands. The quartzites also contain thin, typically <20 cm thick, argillites similar to the quartzites from the underlying Commonage Formation. The rocks belonging to the Stilfontein Quartzite Formation attain their maximum thickness in the east of the lease area (see Fig.1.1), where they probably exceed 150 m.

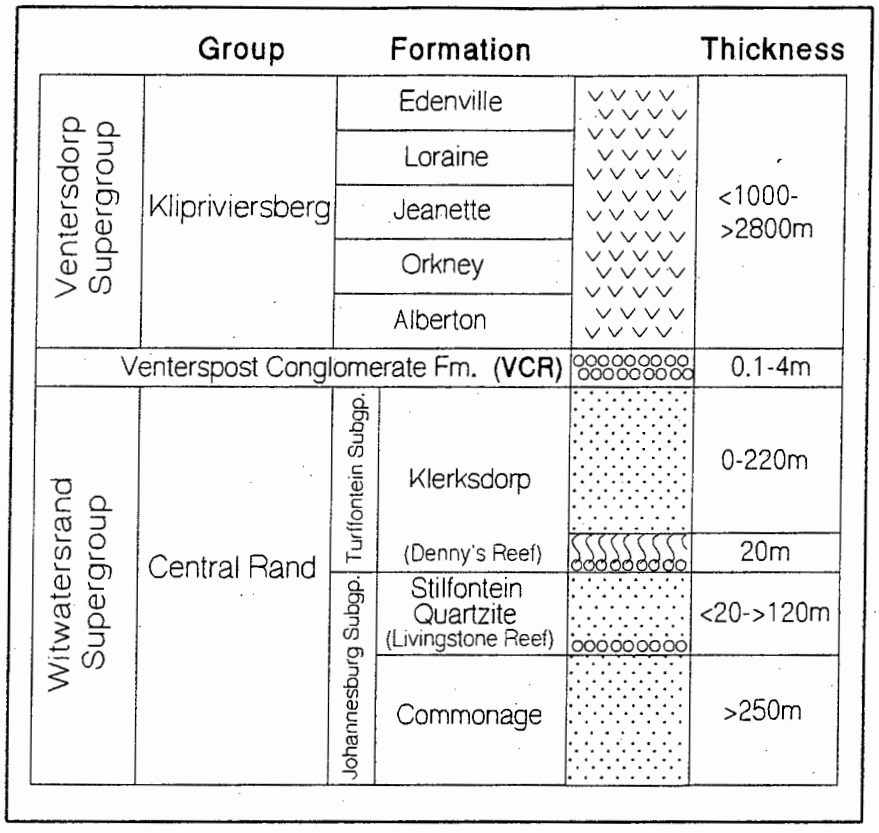

Fig.3.1: Lithostratigraphy at Vaal Reefs No.10 Shaft.

These quartzites are directly overlain by the Denny's Reef, which lies at the base of the Klerksdorp Formation (Turffontein Subgroup). Further to the east, the Stilfontein Quartzite Formation is considerably thicker and is overlain by the Strathmore and Gold Estates Formations (Antrobus *et al.*, 1986). At Vaal Reefs No.10 Shaft, these latter two formations are missing because of erosional removal prior to the deposition of the rocks of the Klerksdorp Formation. This has led to the formation of marked unconformable stratigraphic relationships which exist at Vaal Reefs No.10 Shaft (Fig.3.2). As much as 350 m of quartzites belonging to the Stilfontein Quartzite Formation are inferred to have been removed from the stratigraphic sequence at Vaal Reefs No.10 Shaft.

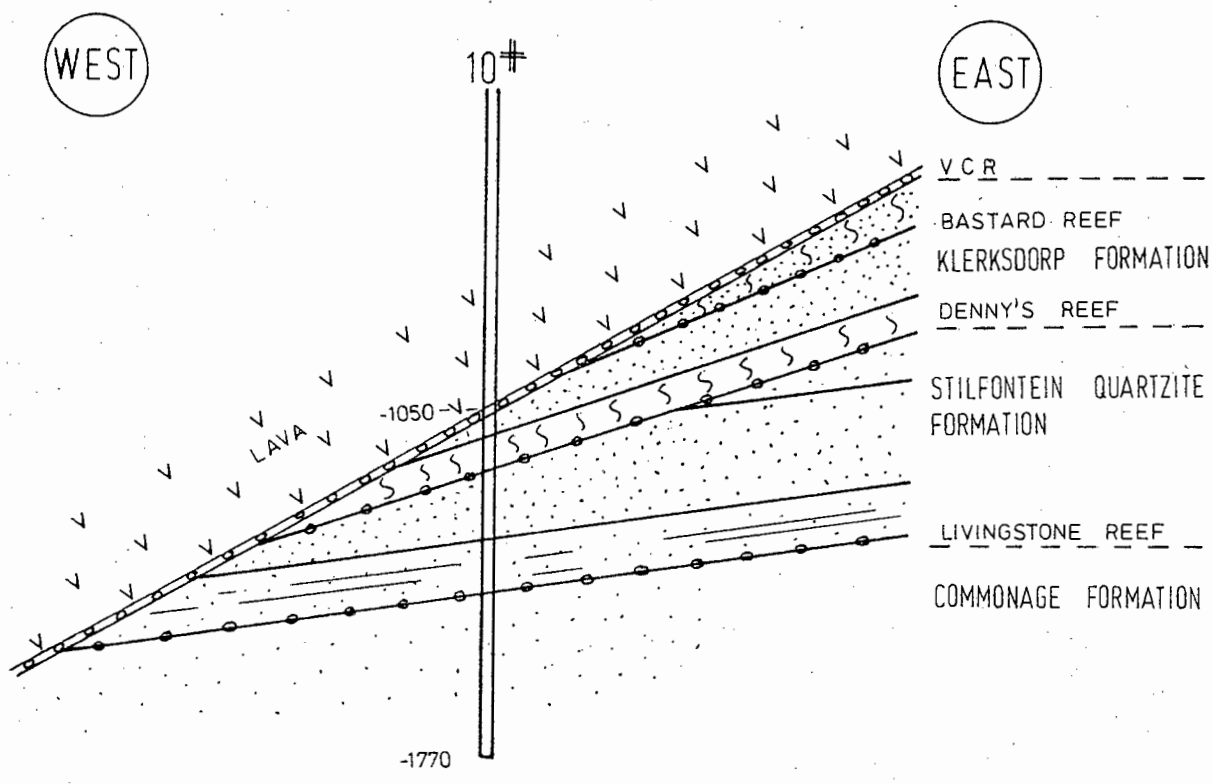

Fig.3.2: Schematic east-west cross section at Vaal Reefs No.10 Shaft, illustrating the unconformable relationship between the rocks.

The Denny's Reef rests unconformably on the quartzites of the Stilfontein Quartzite Formation. Most of the current Denny's Reef exposure indicates the presence of a poorly developed pebble lag. In some places, however, this reef is highly channelised and forms narrow channels several metres wide and <2 m deep. The Denny's Reef is an oligomictic, often pebble supported, typically large pebble to medium cobble conglomerate. The quartz clasts frequently exhibit a dark rim towards the clast margins. Rounded pyrite grains of up to centimetre size have been observed in the better channelised reef facies, where sulphide mineralisation may attain c. 5 vol%.

Overlying the Denny's Reef is a 15 - 20 m thick, dark grey, highly siliceous quartzite unit which is also referred to as the Denny's Quartzite (Antrobus *et al.*, 1986). It is a very persistent quartzite bar which can be correlated over most of the Klerksdorp goldfield. The Denny's Quartzite changes abruptly to argillaceous quartzites, which form the upper part of the Klerksdorp Formation. These quartzites are medium grained and have a homogeneous grey-brown colour. Occasional gritty zones are present,

and towards the eastern half of the lease area, several siliceous units varying in thickness from 1 - 12 m are intercalated with the quartzites. Thin argillites are interbedded with the argillaceous quartzites.

The decrease in the stratigraphic thickness of these quartzites from c. 220 m on the eastern side of the lease area to 0 m on the western side is due to the erosion of the quartzites prior to the deposition of the VCR. Apart from the removal of >200 m of quartzites from the upper Klerksdorp Formation, c. 100 m of quartzites and conglomerates belonging to the overlying Elsburg Formation have also been removed in the Vaal Reefs No.10 Shaft lease area prior to deposition of the VCR.

The average angle of unconformity between the VCR and the underlying footwall rocks is c. 7^0. Stratigraphically, the VCR has been grouped into the Venterspost Conglomerate Formation (Fig.3.1) (SACS, 1980). A quartzite- and a conglomerate-dominated facies and a thin reef facies can be distinguished within the VCR at Vaal Reefs No.10 Shaft. The quartzite-dominated facies consists predominantly of fine to medium grained grey siliceous quartzite, with channel widths of up to several metres. Sulphide mineralisation is generally low (<2 vol%) and occurs in the form of pyrite-bearing foresets and/or as secondary pyrite (typically towards the top of the VCR).

The conglomerate-dominated facies consists of an oligomictic matrix- to pebble-supported, generally small pebble to small cobble conglomerate. More than 95 vol% of the detrital clast population consists of quartz and <5 vol% of chert. Polymictic pebbles are very rare. The pebbles are typically rounded, except towards the top of the VCR where they are smaller in size and subangular. Thin lenticular quartzite lenses are often developed within the conglomerate. Channel widths are lower than in the quartzite-dominated facies and are typically <1.5 m. In the better mineralised portions, up to 15 vol% pyrite occur.

The thin VCR reef facies is characterised by a single pebble lag (often <5 cm thick) which consists of medium to large oligomictic pebbles. The sulphide mineralisation of this reef facies is poor (<2 vol%).

The VCR is overlain by fine to medium grained, green-grey metabasaltic rocks belonging to the Klipriviersberg Group (Ventersdorp Supergroup). These rocks contain various proportions of quartz-, chlorite-, calcite- and epidote-filled amygdales an d veins. Amygdales range in size from <5 mm to tens of centimetres, but are usually absent close to the VCR (i.e. within 20 m). Close towards the VCR a characteristic porphyritic marker zone (consisting of plagioclase phenocrysts and corresponding to the lower porphyritic marker of the Alberton Formation) can be identified over virtually the whole study area. The rocks of the Ventersdorp Supergroup have a maximum thickness of c. 2800 m in the west, although it is likely that the true thickness was greater prior to the erosion of these rocks.

3.2 Structure

The structure at Vaal Reefs No.10 Shaft is dominated by several north and north-easterly striking, east- and westwards dipping normal faults. They are, from east to west, the Buffelsdoorn Fault, the Nooitdegacht Fault and the Schoonspruit Fault (see Map 1 in Appendix A). These faults, which vary in dip from 45 - 75^0, have displacements of up to several hundred metres and are attributed to block faulting in an extensional tectonic setting. Their strike orientation implies that the extensional stresses were orientated east-west to south-east/north-west. Underground exposure of the Nooitgedacht and Buffelsdoorn Faults indicates that they displace the Klipriviersberg lavas, i.e. they are probably of late Ventersdorp or Transvaal age. The fault rock typically consists of quartz and/or calcite veins and cataclasite and/or fault rock breccia.

In addition to these extensional faults, several fault transfer systems have been recognised (e.g. the New Year's Fault zone, see Map1 in Appendix A) which probably developed in response to the stresses imposed during block faulting. These transfer structures comprise a fault zone with displacements ranging from c. 100 m to <1 m. The strike of these fault zones is in a westerly direction and they generally dip steeply (>70^0) towards the south.

Low-angle thrust faults, resulting either in reef duplication or in reef elimination, are frequently observed underground. The presence of ultramylonite along these low-angle, approximately bedding-parallel faults suggests ductile or brittle-ductile deformation. Slickenside lineations along the thrust faults and along bedding planes in the footwall quartzites indicate a westerly direction of displacement, although an eastwards displacement has also been identified in places. A more detailed description of mesoscale structures follows in Chapter 5..

4. Petrography and Mineralogy

4.1 Introduction

The textures and mineralogy of the following rocks were examined: footwall quartzites, hangingwall metabasalts, pseudotachylite, ultramylonite, quartz/calcite veins, dykes and the VCR. In addition to optical petrography (discussed in this chapter), confirmation of phyllosilicate minerals present in the footwall quartzites was done through X-ray diffraction (XRD) analysis.

4.2 Footwall Quartzites

A total of 21 thin and polished sections of the footwall rocks were examined, ranging from the immediate contact with the VCR to a depth of 60 m below the VCR. The footwall rocks usually consist of grey-brown argillaceous quartzites interlayered with thin (usually <15 cm thick) finer grained argillites. A noticeable foliation approximately parallel to bedding is sometimes present in the quartzites. In thin section this is defined by the subparallel alignment of phyllosilicate minerals and occasionally of elongate anhedral quartz grains. Modal mineral proportions of the footwall quartzites are presented in Table 4.1.

The *detrital quartz* grains in the quartzites vary from highly strained to virtually strain-free grains. The lack of complete recrystallisation indicates that the peak metamorphic temperature did not exceed 350^{0}C (Voll, 1976; Buggisch and Kleinschmidt, 1991). Only limited amounts of secondary quartz overgrowths around detrital quartz grains have been observed using cathodoluminescence imaging (CLI). Quartz grains range in size from <0.1 - 2.5 mm and typically have irregular serrated grain margins. The grain shape suggests that silica was partially consumed during metamorphism/metasomatic alteration. In the argillites, the modal proportion of quartz may be less than 50 vol% of the rock, although within the quartzites, quartz typically amounts to >80 vol% of the rock.

Table 4.1: Modal Mineral Proportions in Footwall Quartzite Rocks

Lithology	Pyrophyllitised Quartzite	Sericitised Quartzite	Chloritised Quartzite	Ultrachloritised Quartzite
Depth below VCR	60m	2m	<0.2m	<0.2m
Quartz	55	87	83	12
Pyrophyllite	44	-	-	-
Mica I	1	1	*	*
Mica II	-	12	12	3
Chlorite I	*	*	*	*
Chlorite II	-	-	5	85
Amphibole	*	*	-	-
Chloritoid	*	*	-	-
Zircon	*	*	*	*
Rutile/Leucoxene	*	*	*	*
Pyrite	*	*	*	*
Chromite	*	*	*	*
Chalcopyrite	-	*	*	*
Sphalerite/Galena	-	-	-	*

* trace amounts - not observed

Texturally, two types of *white mica* can be identified in the quartzites and argillites. Minor amounts (up to 1 - 2 vol%) of large (0.3 - 2 mm) kink-banded muscovite flakes, here termed mica I, are characteristically interstratified with chlorite and are present throughout the quartzites and argillites. Texturally this muscovite is similar to the mica I described by Sutton *et al.* (1990) and Zhao *et al.* (1994). Based on the relatively high Ti, Fe and Mg contents, a detrital origin for this mica type has been proposed by these authors. The kink-banded texture of mica I is interpreted to be the result of deformation during burial/regional metamorphic conditions.

The dominant mica type, here termed mica II, is a very fine grained sericitic white mica which occurs within c. 3 m of the VCR. XRD and electron microprobe (EMP) analyses indicate that this mica is muscovite. Mica II is undeformed and occurs as anhedral aggregates with no preferred orientation. EMP analyses of mica I and mica II are shown in Fig.4.1 below and, by analogy with Sutton *et al.* (1990) and Frimmel *et al.* (1993), the low Ti, Fe and Mg contents of the latter mica type suggest a metamorphic/metasomatic origin. Although Sutton *et al.* (1990) infer a metamorphic origin for their mica II, evidence presented in this study suggests that the mica II

which is present in the footwall quartzites immediately below the VCR is a product of K^+ metasomatic alteration (see Chapter 6.).

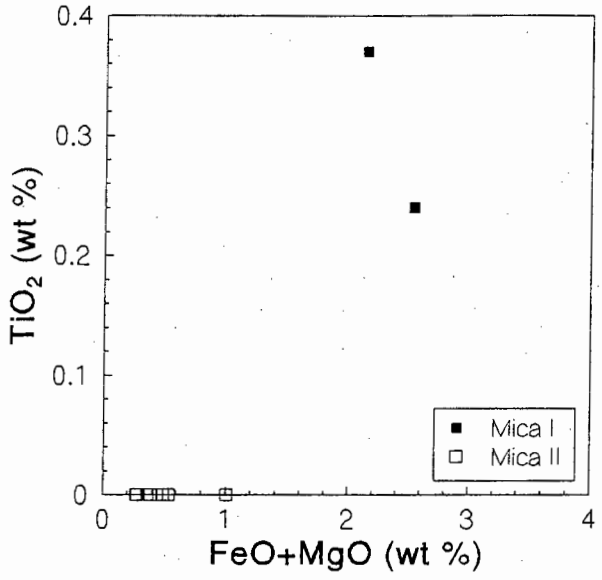

Fig.4.1: Plot of FeO+MgO vs TiO_2 contents of footwall quartzite mica types I and II.

Pyrophyllite is present in the bulk of the footwall quartzites and was confirmed by XRD to be present to a depth of at least 30 m below the VCR. Studies done by Phillips (1988) have shown that pyrophyllite extends for hundreds and even thousands of metres into the Witwatersrand quartzites. However, pyrophyllite is typically absent <3 m below the VCR, which coincides with the appearance of muscovite. Pyrophyllite forms fine grained masses which have grown at the expense of some of the detrital quartz grains. The pyrophyllite appears to be undeformed and shows no preferred orientation. The fine grained nature and lack of deformation of the pyrophyllite are interpreted to indicate its metamorphic origin.

Tiny anhedral pleochroic grains of *amphibole* are rarely present in the quartzites and the texture suggests that the amphibole grains are of detrital origin.

Compact rounded *pyrite* grains are either concentrated along bedding foresets or occur as isolated grains within the quartzites. No porous or concentrically zoned rounded pyrite grains (using the classification adopted by Hallbauer, 1986) have been observed in the footwall quartzites. The

common occurrence of anhedral rounded *zircon, chromite* and *rutile* grains along pyrite-rich foresets are interpreted to indicate a detrital origin of these minerals.

Angular to euhedral pyrite cubes are indicative of a secondary origin and are scattered throughout the quartzites. The presence of small inclusions of chalcopyrite and pyrrhotite within secondary pyrite grains is interpreted to reflect the secondary origin for the former two sulphide minerals.

Chlorite is rare in the deeper footwall rocks and occurs only where it is intergrown/interstratified with the kink-banded mica I variety. The interstratified relationship indicates that this chlorite type (termed chlorite I) is probably a product of the alteration of original biotite intergrowths with mica I.

Chloritoid was identified in two quartzite samples (VHG056 and VHG090) as randomly orientated clusters consisting of subidioblastic laths. The habit and the occurrence together with pyrophyllite in the deeper footwall quartzite samples suggests that chloritoid is of metamorphic origin. Although no textural equilibrium with chlorite can be demonstrated in this study, Frimmel (1994) has identified the coexistence of chlorite with chloritoid in quartzites at the base of the Central Rand Group.

Tiny acicular *rutile* needles are concentrated in the chloritised footwall zone immediately below the VCR. They were probably derived from the alteration of original biotite and/or titanomagnetite grains during the chloritisation of the immediate footwall quartzite. They are, in contrast to the rounded rutile grains, interpreted to be of metamorphic/metasomatic origin. Few anhedral *leucoxene* grains (possibly alteration products of originally detrital titanomagnetite grains) were observed throughout the quartzites.

The contact of the footwall quartzites with the overlying VCR can be sharp or gradational. Typically, the colour of the quartzites is grey-brown but at various localities immediately below the VCR (e.g. samples VHG017, 063(B), 091(B), 104, 170) the footwall quartzites have a dark grey colour and the argillaceous appearance of the quartzites has been destroyed. The extent of the darkened quartzites is laterally variable over metres to tens of metres and vertically the

darkening may extend to a depth of 0.1 - 1.0 m below the VCR. In general terms, the darkening of the quartzites attains its maximum thickness where the VCR is thinnest. No visible control on the lateral distribution of the darkening has, as yet, been identified.

Mineralogically, the gradual colour change in the quartzites is associated with the appearance of fine grained randomly orientated and undeformed aggregates/clusters of *chlorite* of up to 15 vol% (Table 4.1). Based on its texture and morphology, this chlorite is referred to as type II chlorite and is interpreted to be a product of metamorphic/metasomatic alteration (see Chapter 6.). Type II chlorite is intergrown with sericitic muscovite (mica II) close to (<1 m below) the VCR and sometimes hosts base metal sulphide mineralisation.

The presence of base metal sulphide mineralisation (*galena* and *sphalerite*) is limited to (at most) several centimetres into the chloritised footwall quartzites. Very similar observations on the distribution of galena, sphalerite and chalcopyrite in the quartzites below the VCR have also been made at the Western Deep Levels Gold Mine in the Carletonville goldfield (Zhao *et al.*, 1994). These authors attribute the base metal sulphides to a sulphidisation event.

Occasionally the immediate footwall rock (i.e. <0.2 m below the VCR) is fine grained and almost completely chloritised ("ultrachloritised") and consists of >80 vol% chlorite (Table 4.1) (e.g. sample VHG125). This probably represents a more extreme form of alteration of the darkened chloritised quartzite described above. Minute *calcite* inclusions and subordinate sericite laths are present in secondary quartz overgrowths around detrital quartz grains within this ultrachloritised zone. With progressive depth below the VCR the mineralogy of the ultrachloritised footwall quartzites gradually changes and the quartzites become lighter grey/brown in colour. The calcite inclusions within the quartz grains and the chlorite in the quartzites disappear, whereas the amount of fine grained muscovite increases over the same interval.

4.3 Hangingwall Metabasalts

13 thin and polished sections of the hangingwall metabasalts, ranging from the immediate contact with the VCR to a distance of >50 m above the VCR, were examined. The mineral assemblage in the *higher hangingwall metabasalt* (i.e. >30 m above the VCR) is a typical greenschist facies assemblage and consists of plagioclase, actinolite, chlorite, epidote/clinozoisite, quartz, calcite, ± sericite ± sulphide phases (Table 4.2). This metabasalt has a green to olive-green colour and an aphanitic microlitic texture. The amygdales which are sometimes present in the metabasalt vary in size from <1 mm to several centimetres and contain quartz, chlorite and/or epidote/clinozoisite.

Table 4.2: Modal Mineral Proportions in Less Altered Hangingwall Metabasalt Rocks

Lithology	Aphanitic Metabasalt	White Phenocryst Zone	Dark Phenocryst Zone
Distance above VCR	50m	15m	5m
Plagioclase	58	41	-
Actinolite	18	15	-
Chlorite	13	19	10
Quartz	5	-	1
Epidote/Zoisite	4	4	-
Calcite	2	19	47
Sericite	*	2	41
Rutile	-	-	*
Pyrite	*	*	*
Pyrrhotite	-	-	*
Chalcopyrite	*	*	*
Ilmenite	-	-	*
Magnetite	-	-	1

* trace amounts - not observed

A characteristic phenocryst zone, which may extend up to 25 m above the VCR, is almost always present in the metabasalt unit immediately overlying the VCR. At a distance of >5 - 10 m above the VCR, up to 8 cm large and sometimes bowtie shaped, white plagioclase phenocrysts are common. This zone is referred to as the *white phenocryst zone*. Partial carbonatisation and minor sericitisation of the plagioclase phenocrysts and of the groundmass are evident in this light grey-green metabasalt zone. Chalcopyrite and very small amounts of over- and intergrown secondary pyrite are present.

The colour of the phenocrysts changes usually gradually from white to light greenish-white to apple green with increasing proximity to the VCR. The metabasalt zone approximately 1 - 5 m above the VCR is termed the *dark phenocryst zone* because of the dark green to almost black colour of the phenocrysts. The metabasalt has a light grey/green colour and a cryptocrystalline texture. The groundmass as well as the phenocrysts are intensely sericitised and/or carbonatised. Fine grained chlorite is present in the matrix. Up to 1 vol% of fine grained, octahedral magnetite crystals and tabular ilmenite grains are disseminated throughout this zone. The magnetite grains sometimes become increasingly finer grained towards the VCR. Chalcopyrite is present in small amounts and only rarely contains intergrown pyrite.

The *"contact" metabasalt zone* (i.e. <1 m from the VCR) often has a mottled light yellow/grey-green colour and a "bleached" appearance. In addition to the intense chloritisation and/or sericitisation, which are typical for this zone, the small grain size of this altered rock does not permit meaningful modal proportions from point counting to be obtained. Pyrite cubes can be locally very abundant but generally pyrite occurs as small disseminated grains. Chalcopyrite occurs either as inclusions within pyrite or as scattered finely disseminated grains. Either one of these two sulphides may be dominant. Locally, rutile needles are common and galena has only rarely been noted in the contact zone. No magnetite or ilmenite are present in the contact zone metabasalt.

Rare pillow lava structures and toes of pahoehoe lava flows (resulting in reef deformation) and partial ingestion of VCR into the metabasalt have been observed in the hangingwall in contact with the VCR. Similar observations have been made on the hangingwall to the VCR in the Carletonville goldfield, where pillow lavas and volatile escape structures in the inter-reef metabasalt and in the overlying metabasalt have been recorded (Tankard *et al.*, 1982). These features in the immediate hangingwall metabasalt suggest that the VCR was semiconsolidated and was subaerially and/or subaqueously exposed.

4.4 Pseudotachylites, Ultramylonites and Quartz/Calcite Veins

Four of the five *pseudotachylites* which were examined come from the VCR-footwall contact while one pseudotachylite sample and two ultramylonite samples examined come from the VCR-hangingwall contact. The pseudotachylite typically contains between 10 - 50 vol% relics of the original country rock, which vary in size from <0.01 mm up to several centimetres. These relics are subrounded to angular in shape and usually consist of quartz grains or aggregates of country rock. The pseudotachylite matrix is partially devitrified and contains minor amounts of chlorite and calcite and accessory amounts of anhedral zircon and opaques.

Opaque minerals are anhedral subangular and generally very fine grained (≤0.2 mm). Pyrite is the main ore mineral, although small amounts of pyrrhotite, chalcopyrite, galena and sphalerite are also present. Underground mine sampling indicates that locally, the pseudotachylite may also be enriched in gold. Elevated Au, P and S contents in VCR-associated pseudotachylites from the Carletonville goldfield have also been observed by Killick (1994). This author tentatively suggests that a S-bearing fluid (which could have contained dissolved Au and Pb) might have been present prior to or at the time of pseudotachylite formation.

The *ultramylonite* is characterised by the complete absence of country rock relics. It is completely recrystallised/altered to very fine grained chlorite and sericite in approximately equal proportions, the former mineral as rounded to subrounded irregular aggregates and the latter mineral as very small laths. A dense anastomosing network of rutile needles is often associated with the more sericite-rich portions. Accessory amounts of quartz, calcite, epidote and opaques are also present. A macroscopically visible foliation is defined by chlorite- and sericite-rich zones in thin section. Chlorite veinlets which cut across both the sericite and the chlorite aggregates are evidence for multiple chlorite formation events.

Up to 2 vol% of ore minerals are present in the ultramylonite. Euhedral to subhedral secondary, finely disseminated pyrite grains and/or aggregates are frequently associated with the chlorite-rich areas. Small amounts of anhedral chalcopyrite and pyrrhotite may be associated with the pyrite. Very finely disseminated rutile grains are concentrated parallel to the fabric of the rock.

The bedding-parallel *quartz veins* consist of small to large (up to 7 mm) quartz grains and fine grained quartz zones, minor to major amounts of calcite and accessory amounts of chlorite, bitumen nodules and opaques. In places where quartz veins occur at the basal contact or along the top contact of the VCR, calcite is a major constituent. Quartz veins within the VCR, however, either contain no calcite or only minute calcite inclusions within quartz grains. Pseudohexagonal pyrrhotite platelets are the most common Fe-sulphide mineral in the quartz veins (e.g. samples VHG163(A)-(C), 166, 181). Anhedral irregular chalcopyrite, which appears to be more common in bedding-parallel as opposed to bedding-perpendicular quartz veins, is intergrown with quartz and calcite. Healed microfractures with bedding-parallel and/or bedding-perpendicular orientations (the former orientation usually being dominant) are present in virtually all of the quartz veins.

Underground observation indicate that the bedding-parallel quartz veins pre-date the formation of the pseudotachylite. One such quartz vein (sample VHG169) contains two compositionally different chlorite varieties (one of syn- to post-quartz vein and the other of post-pseudotachylite age).

Two approximately bedding-parallel quartz veins, characterised by fine grained quartz breccia zones, are present in VCR samples VHG048 and VHG165. The presence of abundant minute calcite inclusions (<0.02 mm in size) within the fine grained quartz zone suggests that a Ca^{2+}-rich fluid was introduced during a brittle deformation event (possibly related to the pseudotachylite event). Subhedral secondary pyrite grains and very small amounts of pyrrhotite (subhedral laths in calcite grains), galena, chalcopyrite and gold are present in this quartz vein. The ore minerals are essentially confined to the calcite-inclusion rich fine grained quartz zone.

Although the bedding-perpendicular quartz veins are often restricted to the VCR, they may extend into the hangingwall metabasalt and rarely also into the footwall quartzite. Calcite is generally absent from these quartz veins, but several of them contain bitumen nodules and sulphide minerals.

An unusual mineral assemblage consisting of an unidentified mineral (with a fibrous habit), sericite, baryte, bitumen nodules and sulphide minerals is present in vugs in a bedding-

perpendicular quartz vein within the VCR (sample VHG181). The paragenetic sequence, based on textural relationships, is baryte - sulphides - bitumen nodules + sericite + unidentified mineral. A complex paragenetic history is also revealed by CLI of euhedral hydrothermal quartz crystals in that sample.

Other textural features within quartz veins are 120^0 triple junctions and deformation lamellae. The latter are the result of the deformation of the quartz vein by dislocation creep (White and Treagus, 1975) and the presence of the deformation lamellae indicates that the temperature did not exceed c. 300^0C subsequent to the formation of the lamellae.

One quartz vein which is of particular interest cuts at an angle of c. 30^0 from the hangingwall into the VCR. In places where this <7 cm wide quartz vein (samples VHG163(A)-(C)) transects the VCR, macroscopically visible gold, base metal sulphides and bitumen nodules are present within vugs in the quartz vein. This quartz vein, which will be referred to in the following as **the** auriferous quartz vein, contains accessory amounts of chlorite (pseudohexagonal stacks within quartz grains), calcite (minute inclusions in the core zone of euhedral quartz crystals) and apatite (euhedral elongate grains intergrown with quartz grains).

Two distinct zones with different textural, mineralogical and fluid inclusion characteristics are present in the auriferous quartz vein. The zone in contact with the VCR is referred to as the marginal zone and is characterised by large (<6 mm) anhedral quartz grains. The quartz grains show strong undulose extinction and are transected by fine grained brecciated quartz zones containing minute anhedral grains of pyrite and chlorite. Numerous fluid inclusion trails cross-cut the quartz grains and this zone contains both a high- and a low-temperature fluid inclusion population (see Chapter 8.).

In contrast, the central zone occurs towards the middle of the quartz vein and is typically vuggy and contains euhedral undeformed quartz crystals up to several millimetres in size. These quartz crystals contain abundant minute calcite and low-temperature fluid inclusions in their cores and CLI indicates a complex growth history of these quartz crystals. Galena is the major ore mineral and forms irregular intergrowths with gold and bravoite (?). Gold, sphalerite and chalcopyrite are

also intergrown with chlorite. All of these minerals, as well as euhedral pyrrhotite platelets and bitumen nodules (<5 mm in size), have crystallised in the vugs together with quartz crystals. Limited replacement of euhedral pyrite by pyrrhotite is evident.

4.5 Dykes

Samples from five different dykes, ranging in thickness from 0.2 m to c. 10 m, were collected. Some of the dykes are highly sericitised and carbonatised (VHG133), whereas others are intensely serpentinised and chloritised (VHG134). Less altered dykes contain actinolite, plagioclase, chlorite, quartz and calcite ± epidote ± rutile/sphene. Opaque minerals consist of sub- to euhedral pyrite grains and anhedral chalcopyrite grains.

4.6 Ventersdorp Contact Reef

A total of 58 thin and polished sections from the VCR, which included quartzite and metaconglomerate samples, footwall and hangingwall contact samples and reef profiles across the VCR, were examined.

Predominantly monocrystalline *quartz pebbles* constitute >95 vol% of the clasts in the VCR, the remaining portion comprising chert, shale, quartzite and rare igneous lithic fragments. The quartz grains (which generally exceed 85 vol% of the VCR quartzite fraction) are commonly anhedral rounded to angular and often have serrated/embayed grain margins. They are heterogranular and range in size from <0.02 - c. 3 mm. Although the quartz grains exhibit variable degrees of strain (both undulose and straight extinction) and frequent formation of subgrain boundaries, only limited recrystallisation and formation of secondary quartz has occurred. Visual estimation as well as CLI (see Chapter 9.) indicate that secondary quartz overgrowths contribute <5 vol% of the total quartz volume.

The VCR quartzite has a medium grey colour, but this may change to a dark grey to almost black colour close towards the top contact with the overlying metabasalt. Far less common are irregular light yellow-green alteration zones in the VCR quartzite (Plate 7.1.1). Examination of two samples from such a zone indicates the presence of abundant siderite (c. 5 vol%) as well as Fe-rich chlorite (X_{Fe} = 0.8).

Chlorite, which is the major phyllosilicate mineral in the VCR in the study area, has also been documented in the VCR in the Carletonville goldfield (Stefan and Martin, 1993; Smits, 1994). Only trace amounts of sericite and no pyrophyllite were found in the VCR. Five different textural types of chlorite can be recognised. Rare, large (0.4 - 0.7 mm) chlorite flakes, often with a brownish pleochroism, are interpreted to be pseudomorphs (probably formed during burial metamorphism) of originally detrital biotite/amphiboles. They are therefore paragenetically the earliest chlorite type (type I chlorite).

The second and most abundant "matrix" chlorite type is termed type II chlorite and varies from c. 1 - 10 vol% in the VCR. Type II chlorite occurs as randomly orientated, undeformed anhedral clusters/aggregates interstitially between the quartz grains (Plate 4.1) and also forms narrow vein-like chlorite-rich zones. This chlorite approximates ripidolite in composition and has a light to dark green pleochroism and a purplish-blue interference colour. Microprobe analyses have shown that the type II chlorite is sometimes interstratified with sericite. In places, type II chlorite also partially replaces rounded and secondary pyrite grains and quartz grains.

Type III chlorite is relatively rare and can best be described as chlorite "twirls" within quartz grains (samples VHG062, 063(A), 125). Base metal sulphides and gold often occur at the termination of a chlorite twirl (Plate 4.2). CLI of this chlorite type has revealed that the quartz immediately surrounding the chlorite (and the gold) has a metamorphic/hydrothermal signature (Plate 9.7, Chapter 9.), whereas the remainder of the quartz grain may retain a detrital signature. Compositionally this chlorite type does not differ from type II chlorite.

A fourth and morphologically very distinct chlorite type forms pressure shadows partially surrounding rounded pyrite grains. This type IV chlorite is only rarely developed around

secondary pyrite grains and detrital quartz grains (e.g. in samples VHG062 and VHG063(A)). Secondary quartz (containing minute calcite inclusions) and showing a lamellar texture, is occasionally intergrown with the chlorite in the pressure shadow zones. Type IV chlorite has a more restricted, Mg-rich composition compared to the other chlorite types and is paragenetically later than the type II chlorite and the chloritic alteration zones (illustrated in Plate 4.1).

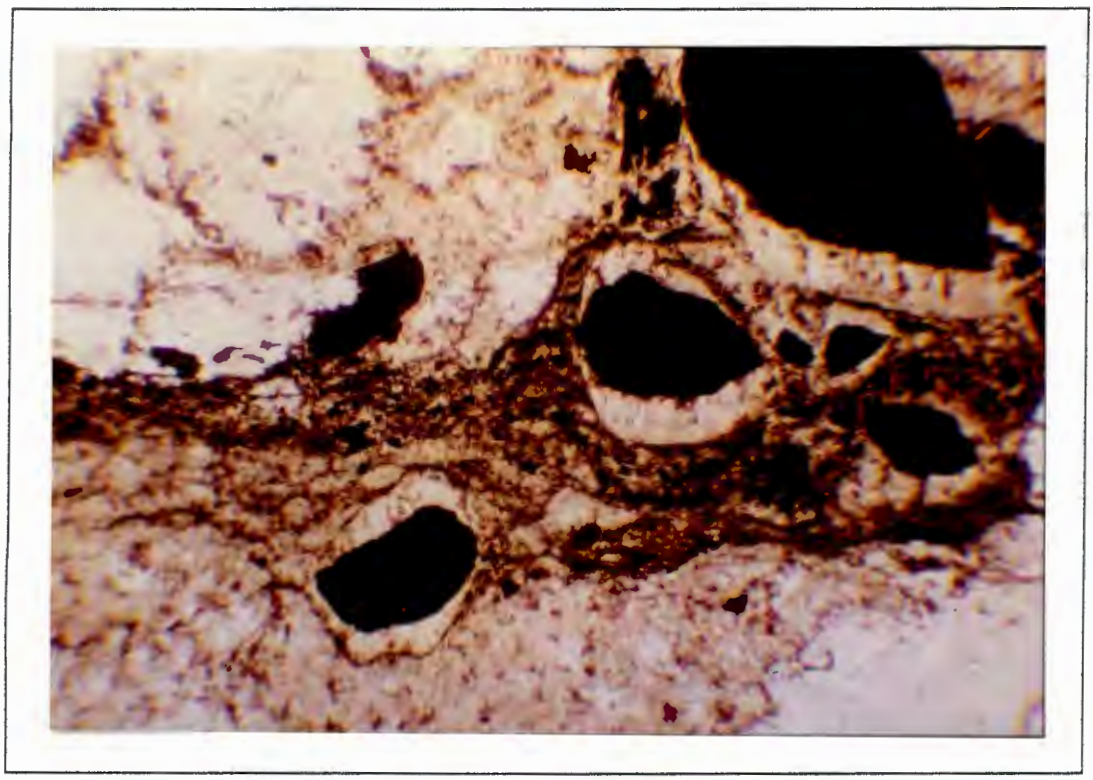

Plate 4.1: Bedding-perpendicular orientated type IV chlorite post-dating a chloritic zone (type II chlorite) close to the base of the VCR. (sample VHG093(A), PPL, length of photo = 3.5 mm).

Type IV chlorite is often developed close to the basal contact of the VCR. It occurs particularly in those samples which contain abundant rounded pyrite grains and where quartz recrystallisation has commenced (samples VHG062, 063(A), 074, 091(B), 093(A), 103, 125). The orientation of type IV chlorite at right angles to the basal contact of the VCR indicates that $\sigma 1$ was orientated parallel to bedding at the time of formation of the pressure shadows. This implies that bedding-parallel fluid pressures exceeded the lithostatic pressure. An accompanying feature is that some of the largest rounded pyrite grains are fractured and forced apart in an approximately bedding-perpendicular sense by the chlorite/quartz intergrowths during the associated fluid infiltration event.

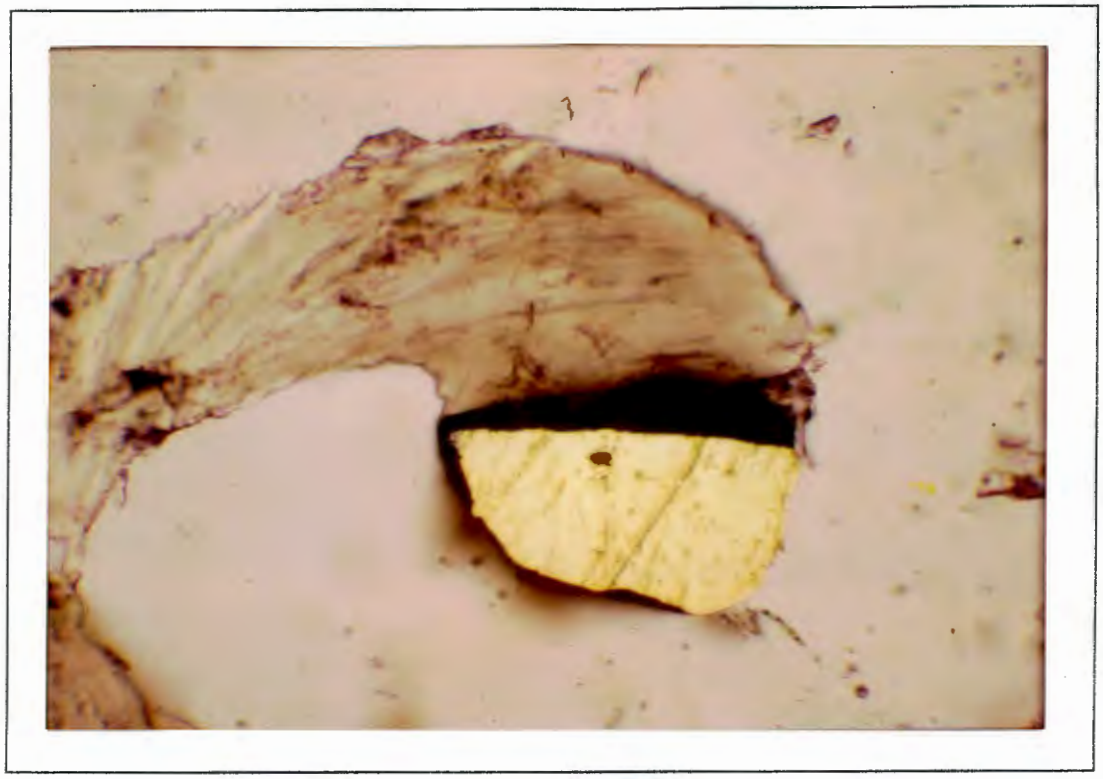

Plate 4.2: 120 µm Gold particle attached to the end of a chlorite "twirl" (type III chlorite) within a quartz grain. (sample VHG125, PPL & RL, length of photo = 0.4 mm).

Chlorite veins (type V chlorite) sometimes contain calcite or pyrite (e.g. samples VHG162 and VHG164) and probably represent the paragenetically latest chlorite type. Compositionally, however, type V chlorite is similar to type II chlorite.

Tiny *sericite* laths (mica II) are present in secondary quartz overgrowths in several of the VCR samples, particularly in those samples in close contact with the hangingwall or footwall (samples VHG093(B), 102, 105, 114, 150(B)). EMP analyses confirm that this mica is fine grained muscovite, small amounts of which are sometimes present in the chloritic matrix (e.g. in samples VHG043 and VHG062). Petrographically, coarser-grained mica II has only been identified in 3 VCR samples (VHG055(B), 148(B), 156) where it forms narrow rims around secondary pyrite grains and is overgrown with chlorite.

Calcite almost always occurs as an accessory mineral which may be intergrown with type II chlorite (e.g. samples VHG024, 046, 088).The presence of chlorite-calcite veins has already been

mentioned and in sample VHG088, pyrrhotite ± gold are present in association with such a vein where calcite and chlorite occur in textural equilibrium. Minute calcite inclusions (<0.05 mm in size) are concentrated in secondary quartz overgrowths around detrital quartz grains and are also present in the chlorite/quartz pressure shadows. Euhedral *siderite* crystals are present in several VCR samples (VHG153(A), 158(B), 164). The euhedral grain morphology of the siderite is interpreted to indicate its secondary origin.

Zircons are often concentrated along heavy mineral-rich foresets. The foresets are defined by high concentrations of rounded pyrite, chromite, titanomagnetite grains (<0.5 mm in size) and rare uraninite grains. Rounded *rutile/leucoxene* grains in the VCR, the rutile grains sometimes exhibiting lamellar twinning, are interpreted to represent the alteration product of originally detrital titanomagnetite. Very small *rutile needles* of secondary origin are present in type II chlorite and in secondary quartz overgrowths.

Rare subhedral *apatite* grains (<0.4 mm) are present adjacent to chlorite/quartz pressure shadows (e.g. sample VHG074) and are probably related to metasomatic fluid infiltration event(s).

Bitumen nodules occur in accessory amounts in virtually all of the VCR samples. They are opaque, have a "spongy" texture, an irregular rounded shape and range in size from 0.3 - 1.5 mm. A radial fracture pattern penetrating surrounding quartz grains is a common feature and the bitumen nodules sometimes embay quartz grains and quartz pebbles. The partial replacement and fracturing of secondary pyrite grains by the bitumen nodules (Plate 4.3) indicates that the latter post-date a pyrite crystallisation event and are paragenetically relatively late stage. Similar observation of the cross-cutting nature of bitumen across pyrrhotite veinlets has lead Robb and Meyer (1991) to suggest that hydrocarbon formation was the final event in the post-burial history of the Witwatersrand Basin.

A total of 12 identified and 4 unidentified ore minerals (the latter intergrown with an anhedral gold grain in sample VHG103) have been observed in the VCR in decreasing order of abundance: pyrite, pyrrhotite, galena, gold, nickel-arsenosulphide, chalcopyrite, sphalerite, chromite, uraninite, titanomagnetite, pentlandite, brannerite, 4 unidentified ore minerals.

Pyrite is by far the most abundant Fe-sulphide in the VCR at Vaal Reefs No.10 Shaft (constituting >95 vol% of the ore minerals), in contrast to the VCR in the Carletonville goldfield where pyrrhotite may be the dominant Fe-sulphide (e.g. at Elandsrand Gold Mine, Henckel and Schweitzer, 1994). Elsewhere in the Carletonville goldfield (e.g. at Western Deep Levels South Gold Mine), both pyrite and pyrrhotite occur in major amounts (Zhao *et al.*, 1994).

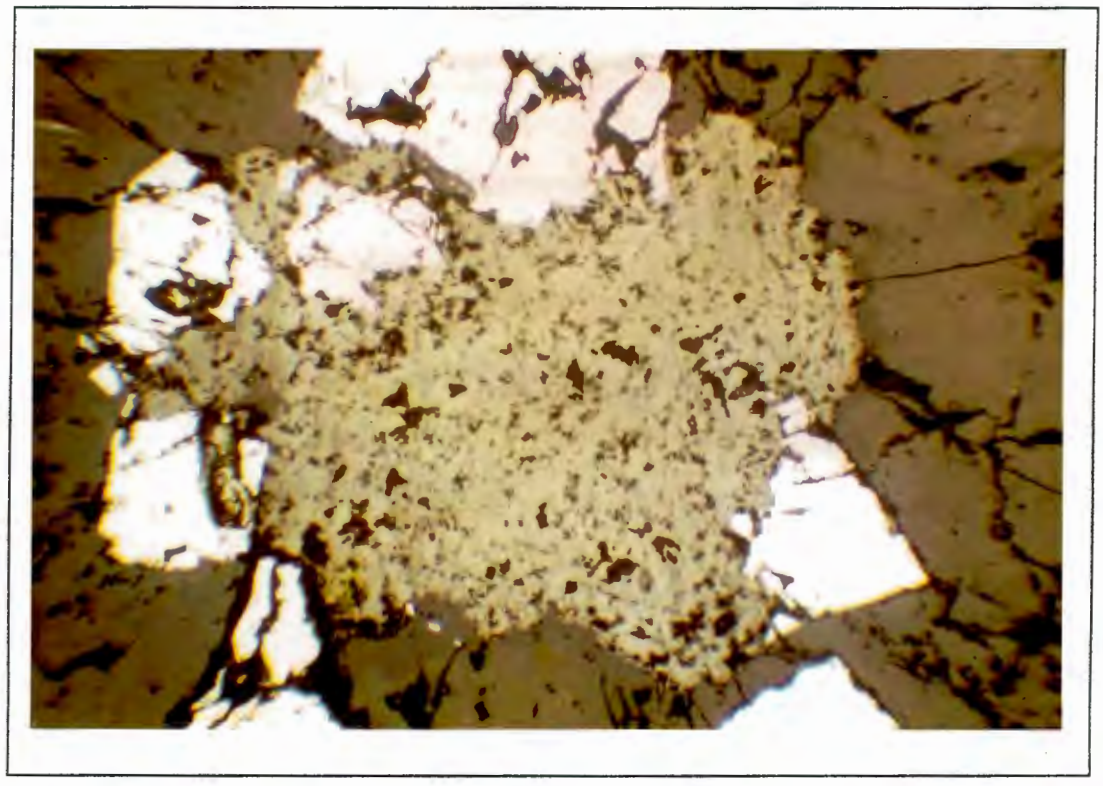

Plate 4.3: Anhedral bitumen nodule (light grey) replacing secondary pyrite (white). (sample VHG120, RL, length of photo = 1.2 mm).

Only limited textural evidence for the replacement of rounded and secondary pyrite by chlorite and very rarely by pyrrhotite exists (e.g. samples VHG062, 064, 125, 156).

Euhedral to subhedral secondary pyrite grains (type II pyrite) dominate over rounded pyrite grains, except in samples VHG063(A), 102, 131, 135. Rounded pyrite varieties include compact, porous/pitted and concentrically zoned pyrite types (using the classification adopted by Hallbauer, 1986), with the proportions of the two former types being highly variable (5 - 95%) and the latter being very scarce. Rounded pyrite grains vary from <0.5 mm - c. 10 mm in size and are

occasionally overgrown by secondary pyrite (e.g. Plate 4.4). Small anhedral subrounded inclusions of other ore minerals (chalcopyrite, galena, pyrrhotite and gold) are found in all three rounded pyrite varieties. The fractured nature of some of the rounded pyrite grains as a result of the formation of the chlorite/quartz pressure shadows has already been described above.

Secondary pyrite grains in the VCR range from <0.1 mm - c. 15 mm in size. They usually form discrete anhedral angular to euhedral cubes and sometimes contain inclusions of chalcopyrite, galena, pyrrhotite and gold. Bedding-perpendicular hydrothermal pyrite veinlets are also present in the VCR and textural relationships indicate that some of the secondary pyrite grains and veinlets are coeval or post-date the quartz veins (see Plate 5.-). Secondary pyrite grains are occasionally partially replaced by bitumen nodules (Plate 4.3).

Pyrrhotite is the second most abundant opaque phase in the VCR. It usually occurs as small inclusions within, or as secondary sub- to euhedral needles around, rounded pyrite grains and (occasionally together with gold) also intergrown with the chlorite (± quartz) matrix. Pyrrhotite grains occasionally occur around, or as inclusions in, bitumen nodules. Pyrrhotite very rarely contains *pentlandite* exsolution lamellae (sample VHG095). A pyrrhotite-gold veinlet cross-cutting a bedding-perpendicular quartz vein (sample VHG093(A)), and the association of pyrrhotite with calcite veins in the VCR (sample VHG025) both support a relatively late, syn- to post-quartz vein age of pyrrhotite ± gold mineralisation in the VCR.

Galena and *sphalerite* are intergrown with type II chlorite and also occur as inclusions in secondary pyrite. Galena is also present as fracture-filling in rounded pyrite grains and as tiny inclusions in bitumen nodules, the latter possibly as a result of radioactive decay of uraninite, remnants of which are present in the bitumen nodules.

Chalcopyrite forms anhedral grains within the quartz/chlorite matrix and is present as anhedral inclusions in secondary pyrite, where it may be intergrown with galena, nickel-arsenosulphide or gold. Less common are chalcopyrite intergrowths with bitumen nodules (sample VHG028) and the occurrence at the termination of type III chlorite (sample VHG125) (similar to the gold - type III chlorite association).

Nickel-arsenosulphide occurs as anhedral (and often fractured) grains, as inclusions within secondary pyrite and as anhedral grains intergrown with gold (e.g. samples VHG075, 093(B), 103) and/or attached to the surface of secondary pyrite grains. It also sometimes forms anhedral subrounded "grains" which are attached to the surface of secondary pyrite grains. This texture is very similar to that described by Knipe *et al.* (1992) and Foster (1993) as "cling-ons". These authors tentatively attribute this morphology to physical and chemical adsorption of nickel-arsenosulphide, gold and other sulphides onto a pyrite substrate. Less common are nickel-arsenosulphide grains which occur as fracture-filling in secondary pyrite and as small anhedral inclusions in bitumen nodules.

Anhedral *uraninite* inclusions (sometimes together with galena) within bitumen nodules are relatively rare, especially when compared to the Vaal Reef where uraninite is a common component of bitumen nodules (Zumberge *et al.*, 1978). *Brannerite* is rarely present as an alteration product after uraninite.

4.7 Gold Textures and Mineral Associations

Routine underground mine sampling indicates that gold is present in the footwall quartzites, hangingwall metabasalts as well as in quartz veins and pseudotachylites. The gold particles in this study are present in 26 out of the 58 VCR samples examined and in two quartz vein samples. The gold particles in the VCR range in size from <1 μm to c. 500 μm, with an average of about 10 μm. In the auriferous quartz vein (samples VHG163(A)-(B)) the gold particles are ≤2 mm in size and are visible macroscopically. The two dimensional grain shape of the VCR gold particles is anhedral irregular and in the auriferous quartz vein rare euhedral gold crystals are present.

The frequency of gold association with other minerals in the VCR and in the auriferous quartz vein is presented in Table 4.3. Only mineral associations of those gold grains which were analysed with the electron microprobe are listed in Table 4.3. Gold in the VCR is commonly associated with type II chlorite and quartz, and to a lesser extent with (predominantly secondary) pyrite.

Table 4.3: Gold Association with Other Minerals

Sample No.	Quartz Grain	Qtz Grain Margin	Quartz Vein	Chlorite/ Quartz	Chlorite Type II/III	Chlorite Type V	Pyrite	Pyrrhotite	Galena	Chalco-pyrite	Gersdorffite	Bitumen Nodule	Siderite	TOTAL No. GRAINS
VHG 021					2									2
VHG 046					1		1					1		3
VHG 062	9			2	4	1	6			1				23
VHG 063(A)	4				14		12							30
VHG 074	4			7	8		4		1					24
VHG 088					2		1							3
VHG 091(B)				5				1						6
VHG 093(A)	8			5	10		5	1 (vein)						29
VHG 093(B)	25			16	7		9	1		1				59
VHG 095							3	1						4
VHG 103	10				9		4				1			24
VHG 105	1				7		1					1		10
VHG 107	10	8			4		4							26
VHG 120							8							8
VHG 125	3				10		3	1						17
VHG 130	3				3		2	1						9
VHG 131	3	1		1	5		2		1	1				14
VHG 150(B)	3				1									4
VHG 163(B)			3											3
VHG 163(C)			27											27
VHG 164	1				2	1						9	11	24
TOTAL	84	9	30	36	89	2	65	6	2	3	1	11	11	349

Gold particles associated with *type II chlorite*, *quartz grains* and with *quartz grain margins* generally have an anhedral irregular to (sub)rounded shape. Similarly, the gold particles at the termination of *type III chlorite* (chlorite "twirls") have a subrounded shape (see Plate 4.2) and may be surrounded by a c. 5 μm partial halo of minute (<1 μm) gold 'globules' within the quartz grain. The quartz which surrounds these gold particles has a metamorphic/hydrothermal CL signature (see Chapter 9.).

Gold particles which are associated with *pyrite* commonly occur as anhedral inclusions within secondary pyrite and occasionally in rounded pyrite grains, sometimes together with chalcopyrite or pyrrhotite (Plate 4.4). More rarely, gold was also found in the form of fracture filling within secondary pyrite grains. Gold and *nickel-arsenosulphide* grains occasionally occur intergrown together in type II chlorite. Less common are anhedral gold/nickel-arsenosulphide "cling-ons" which are attached to anhedral secondary pyrite grains.

Intergrowths of anhedral gold and *pyrrhotite* grains in type II chlorite are present in several samples. No pyrite-gold veins have been observed, but a pyrrhotite-gold vein was noted in samples VHG088 and VHG093(A).

The association of gold particles (as inclusions within or attached to the surface of) *bitumen nodules* occurs more often than what is reflected in Table 4.3. However, these gold particles are usually too small (<3 μm in diameter) to permit analysis with the EMP. Only in sample VHG164, which contains c. 5 vol% bitumen nodules, is the gold-bitumen nodule association predominant. In this sample, gold particles also form irregular intergrowths with anhedral *siderite* grains.

Gold-*galena* intergrowths in type II chlorite are anhedral and irregular. Small inclusions of gold together with galena and *chalcopyrite* also occur within secondary pyrite grains. Only one gold-*rutile* association and one gold-*leucoxene* association have been observed.

The gold, which is present in the fine grained brecciated *quartz vein* zone in sample VHG165, occurs as finely disseminated particles together with very small calcite inclusions (c. 2 μm) in and around margins of sheared and fractured quartz grains. Within the auriferous quartz vein, gold forms anhedral irregular intergrowths predominantly with galena and quartz and less commonly

with bravoite (?), sphalerite and chlorite. The presence of gold particles within vugs and on euhedral galena crystals suggests that the base metal sulphide and gold mineralisation occurred at a relatively late stage in the paragenetic sequence.

Plate 4.4: Anhedral gold particles (bright yellow) intergrown with galena (dull grey) and pyrite (yellow) in type II chlorite (greenish) and inclusions of gold particles and other sulphides in secondary pyrite.
(sample VHG074, PPL & RL, length of photo = 0.8 mm).

5. Meso- and Microscale Structural Features

Fault Rocks Related to Brittle and Ductile Deformation

Pseudotachylite and highly altered ultramylonite fault rocks with an approximately bedding-parallel orientation occur in close proximity to the VCR. These fault rocks have distinct macro- as well as microscopic characteristics.

Pseudotachylite usually occurs at the base of, or several metres below the base of, the VCR in the footwall quartzites. Pseudotachylite veins have sharp contacts and can be highly variable in thickness and in structure. They range from bedding-parallel, several centimetre thick veins, to anastomosing networks of injection melt material up to tens of centimetres thick. The pseudotachylite has a blue-grey colour, shows a very well developed complex flow-banded texture and contains rotated country rock clasts up to several centimetres in size.

The fault rock which is usually present along the VCR - metabasalt contact has, in accordance with the description of Heitzmann (1985), been classified as an ultramylonite. This rock is extremely well foliated, fine grained and lacks any relic clasts. The ultramylonite is interpreted to be a product of ductile or brittle/ductile deformation and at least two generations can be identified. The ultramylonite generally is <5 cm thick, has a yellow-brown colour and a "banded" appearance. Underground observations indicate that some secondary pyrite crystallisation post-dates the formation of the ultramylonite.

Bedding-parallel displacements of tens of metres in an east-westerly direction have been noted along the bedding-parallel ultramylonite fault planes, resulting in reef elimination or in reef duplication. In contrast, no lateral displacement could be observed along the pseudotachylites.

Quartz Veins

Two dominant orientations of quartz veins are present in vicinity to the VCR. Quartz veins with a bedding-parallel or near bedding-parallel orientation commonly occur in the immediate footwall quartzites, in the VCR and/or in the hangingwall metabasalts. Locally these quartz veins can form vein networks in the VCR which may branch off either into the footwall or the hangingwall rocks at a slightly oblique angle (Plate 5.1). The bedding-parallel quartz veins vary in width from <1 cm up to tens of centimetres, particularly where they occur in the hangingwall metabasalts. They are laterally continuous for tens, and possibly hundreds, of metres.

Plate 5.1: Bedding-parallel quartz vein in the VCR quartzite branching off into the hangingwall and cross-cutting the yellow ultramylonite present along the VCR-metabasalt contact. The cross-cutting relationship between several thin bedding-perpendicular quartz veins and the bedding-parallel quartz vein in the VCR suggests the approximately coeval formation of these two sets of quartz veins.
(locality 1130 N1A Raise 13, P7, scale bar in inches).

Being of an approximately bedding-parallel nature, the orientation of these quartz veins is similar to that of the VCR. The dip direction/amount of 33 of these quartz veins were measured and are represented by their poles on a lower hemisphere stereographic projection (Fig.5.1). The π- axis of the best fit great circle for these quartz veins has an azimuth/plunge of 225/12 and the mean azimuth/plunge of the poles to the quartz veins is 99/71. This gives a strike and dip of 189/19NW of the bedding-parallel quartz veins, which is similar to the strike/dip of the VCR of 205/27NW.

Although the second set of quartz veins, which have an approximately bedding-perpendicular orientation, are usually restricted to the VCR, they may sometimes extend for several tens of centimetres into the hangingwall and/or the footwall rocks. These quartz veins range in thickness from <0.5 cm to c. 5 cm and are spaced between 0.5 m up to tens of metres apart.

The poles of the dip direction/amount of 147 bedding-perpendicular quartz veins indicate that the majority of the quartz veins dip steeply (c. 80^0) towards the east (Fig.5.2). The mean azimuth/plunge of the poles to the bedding-perpendicular quartz veins is 269/18, and the π- axis to the best fit great circle has an azimuth/plunge of 130/78. The mean strike/dip of 179/72E of these quartz veins is similar to the orientation of the Nooitgedacht Fault (with a strike/dip of 197/45E).

The coeval nature of these two sets of quartz veins is indicated by their cross-cutting relationship and is also supported by fluid inclusion data (Chapter 8.). The frequency of both sets of quartz veins appears to be fairly consistent throughout the study area and is independent of the proximity to major structural features. Nevertheless, the orientation of the bedding-perpendicular quartz veins suggests that they were formed in response to a dilational (i.e. extensional) deformation phase with σ^3 orientated north-west/south-east. The orientation of the bedding-parallel quartz veins suggests that they utilised pre-existing zones of weakness such as bedding planes and lithological contacts.

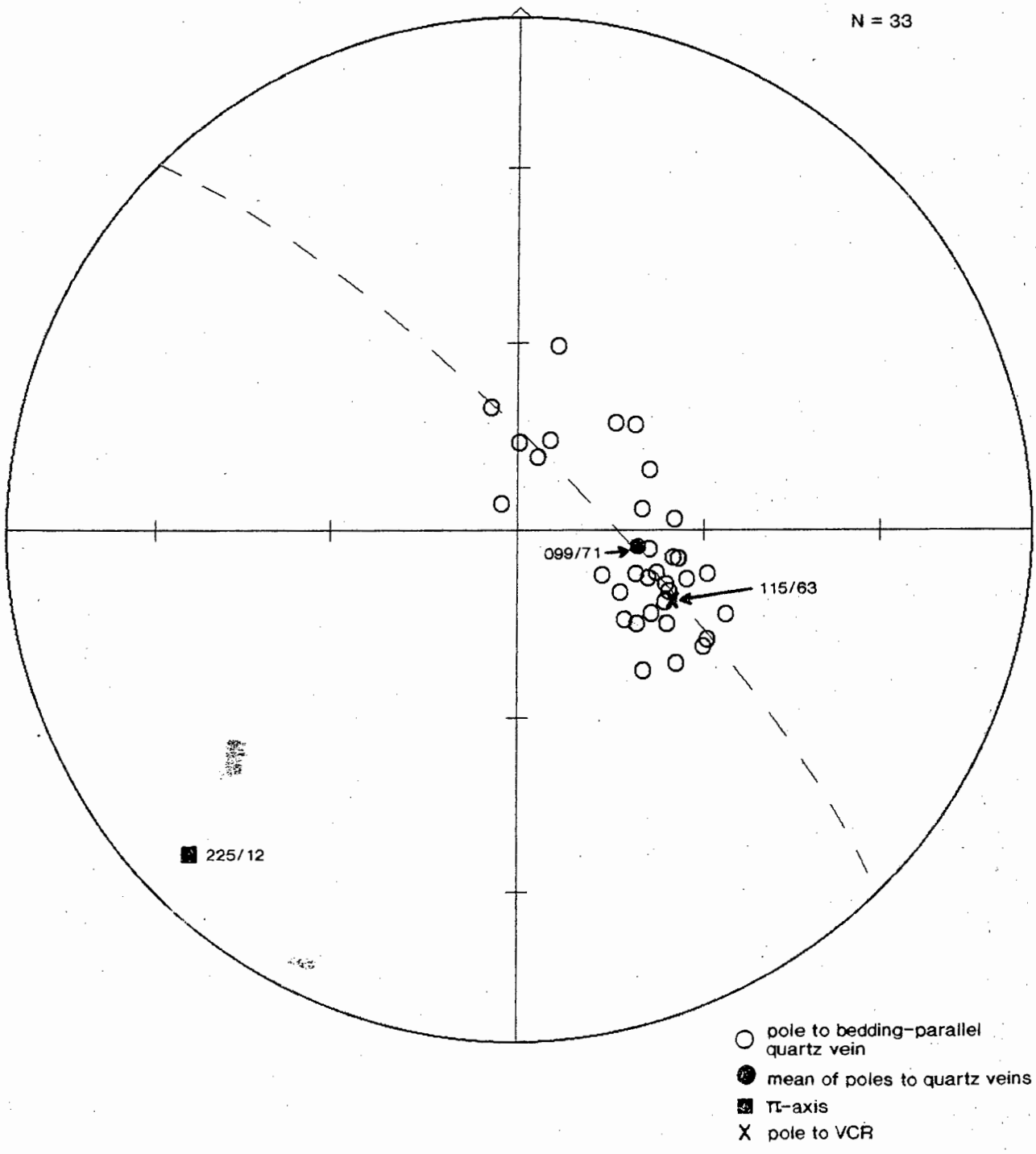

Fig.5.1: Stereographic projection of poles to dip direction/amount of 33 bedding-parallel quartz veins. Also shown are the mean azimuth/plunge of the quartz vein poles, the best fit great circle and its corresponding π- axis and the pole to the dip direction/amount of the VCR.

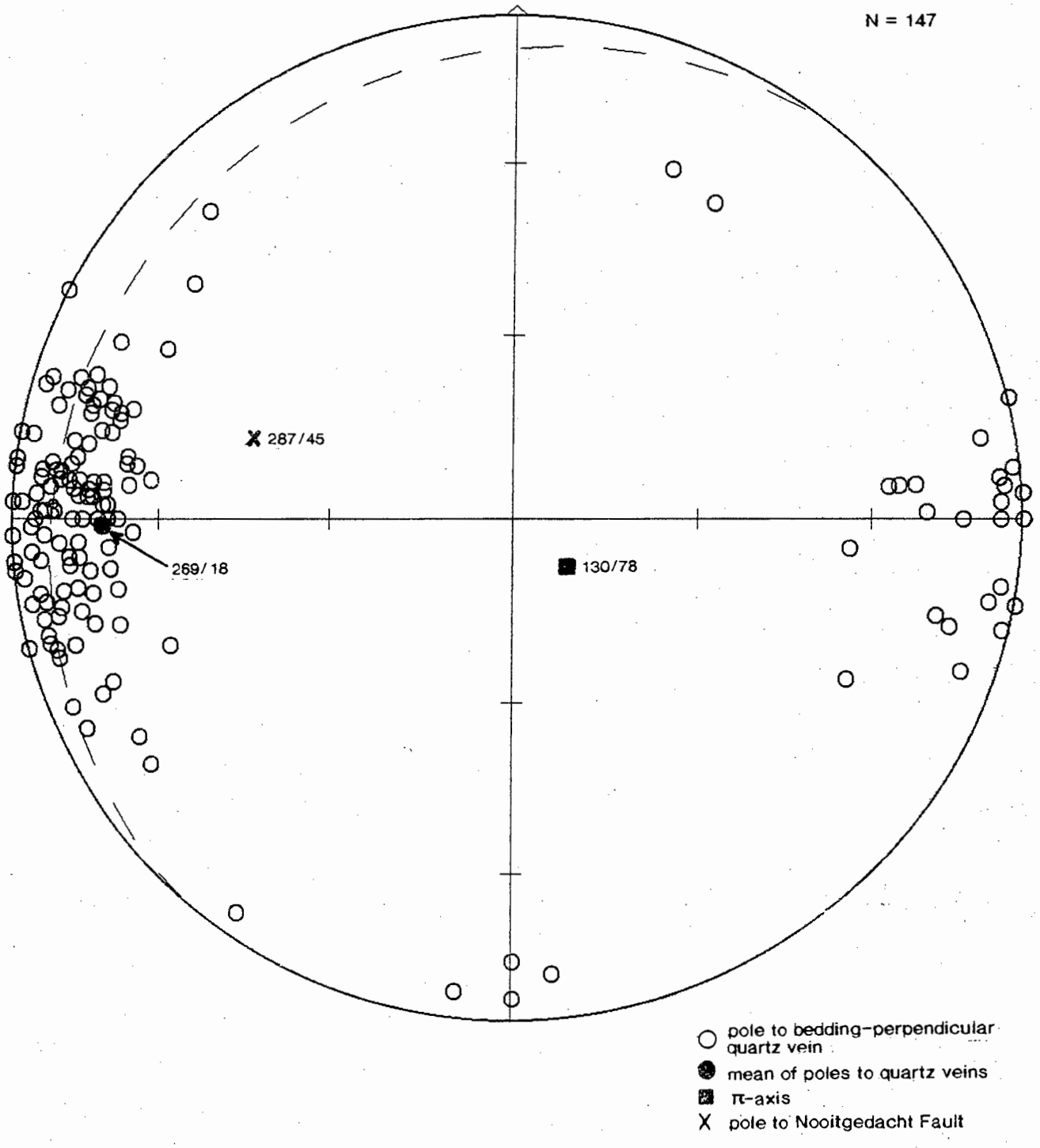

Fig.5.2: Stereographic projection of poles to dip direction/amount of 147 bedding-perpendicular quartz veins. Also shown are the mean of the poles, the best fit great circle and its corresponding π- axis, and the pole to the dip direction/ amount of the Nooitgedacht Fault.

Bedding-perpendicular quartz veins sometimes terminate at the ultramylonite along the top contact of the VCR. At other localities, however, both sets of quartz veins cross-cut the ultramylonite (Plate 5.1). This supports other observations which suggest the presence of more than one ultramylonite-forming deformation event. In contrast, the cross-cutting nature of the footwall pseudotachylite across a bedding-parallel quartz vein (sample VHG169) indicates that the pseudotachylite post-dates the bedding-parallel quartz vein.

Microscale and Other Structures

Lineations along the ultramylonite and along bedding planes in the footwall quartzites are relatively common. They have also been observed along thrust planes which result in reef duplication. The direction of observed reef duplication and the east-westerly trend of the lineations both support a general westwards thrusting event towards the basin margin. In one area, however, a lateral displacement of c. 15 m of a sliver of VCR (measuring approximately 10 m x 20 m) **towards the north-east** has been observed, suggesting more than one phase of thrusting. The steeply plunging lineations which are sometimes observed along fault planes indicate that fault displacements were generally of a dip-slip nature.

Microstructural features such as fractures and chlorite and pyrite veinlets in the VCR have similar orientations as mesoscale structural features (e.g. quartz veins and fault rocks). Microscale displacements in the order of <10 μm up to 0.5 mm of bedding-parallel and bedding-perpendicular fractures have been identified. The mutual displacement of these fracture sets supports previous interpretations that the two fracture orientations are related to the same tectonic event.

An example of bedding-parallel silicified fracture zones which are offset by a series of bedding-perpendicular fractures is shown in Plate 5.2. Secondary pyrite which grows within the bedding-parallel fracture indicates that pyrite crystallisation post-dates the bedding-parallel fracturing event. The microscale fractures usually consist of fine grained silicified quartz vein breccia and occasionally contain chlorite, sericite, calcite or fine grained siderite (e.g. in samples VHG153(A) and VHG158(B)).

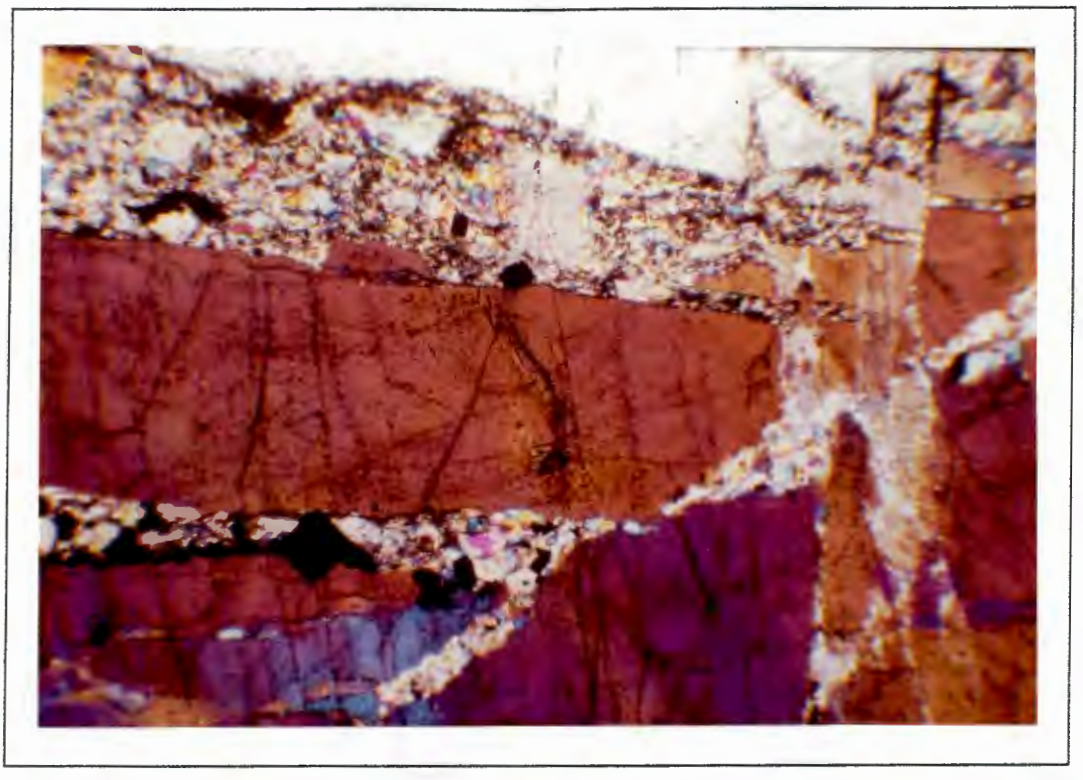

Plate 5.2: Detrital VCR quartz grain (purplish) showing bedding-parallel silicified fracture zones offset by bedding-perpendicular fractures. The formation of secondary pyrite (black cubes) post-dates the bedding-parallel fracture event. Note the abundant fluid inclusion trails parallel to the bedding-perpendicular fracture orientation in the quartz grain.
(sample VHG170, XPL, length of photo = 2.3 mm).

6. Bulk Rock Geochemistry

6.1 Introduction

Macroscopic and mineralogical changes are evident in the metabasalts and quartzites with increasing proximity to the VCR (see Chapter 4.), indicating that metasomatic/metamorphic alteration processes must have affected these rocks (as well as the VCR itself). In order to determine the extent to which major elements were mobile during post-depositional alteration, hangingwall metabasalt and footwall quartzite bulk rock samples were analysed by X-ray fluorescence spectrometry (XRF). In addition, rare earth elements of selected metabasalt and quartzite samples were analysed by ion chromatography.

The mineralogy and homogeneous nature of the basalt make this rock particularly useful in recording progressive alteration effects. The changes which have occurred in the bulk rock composition with increasing proximity to the VCR permit a calculation of net losses or gains of elements which have taken place during the alteration process(es).

6.2 Sample Locality and Study Material

A traverse along 1200 S2 cross-cut 7 (for locality, see Map 1 in Appendix A) was chosen so as to cover as much as possible of the hangingwall above and a portion of the footwall below the VCR (Fig.6.1). Eight metabasalt samples from 0.1 - 16 m stratigraphically above the VCR and six footwall quartzite samples from 0.1 - 5.5 m stratigraphically below the VCR were collected and their major elements analysed on a Siemens XRF spectrometer at the University of Cape Town. A more detailed outline of the sample preparation and of the instrumental analytical precision are given in Appendix B.

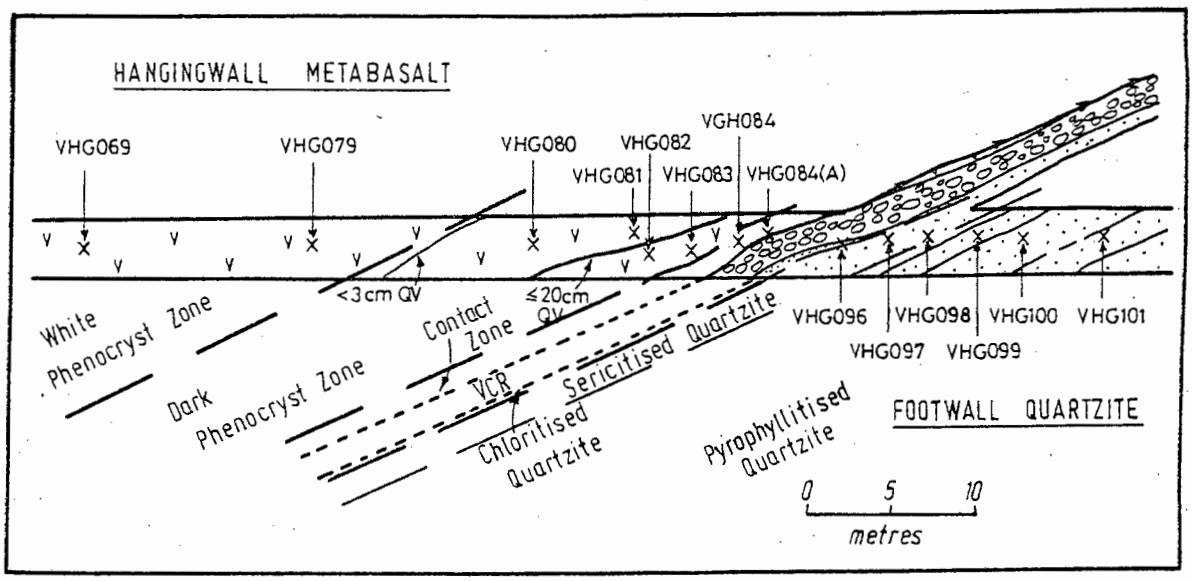

Fig.6.1: North-facing section along 1200 S2 cross-cut 7 showing XRF sample localities.

The footwall quartzite samples which were analysed come from the dark grey chloritised footwall quartzite (<0.2 m below the VCR at this locality), the grey-brown muscovite-rich quartzite (0.2 - 3 m below the VCR) and from the pyrophyllitised quartzite (>3 m below the VCR). The metabasalt samples include samples from the "white phenocryst" zone (approximately >8 m above the VCR at this locality), the "dark phenocryst" zone (1 - 8 m above the VCR) and the "contact" zone (<1 m above the VCR). Care was taken in choosing only such quartzite and metabasalt samples that were free of excessively high concentrations of pyrite and any visible phenocrysts, amygdales and quartz veins, respectively.

6.3 Composition-Volume Relationships during Metamorphic Processes

Progressive metasomatic/metamorphic alteration which affects a rock can be considered as a combination of chemical and volume changes. This has been applied by, for instance, Gresens (1967), Babcock (1973) and Kerrich *et al.* (1977) in the calculation of the net gains/losses of elements involved during metamorphic reactions. The following equation represents the metasomatic replacement reaction of mineral/rock A by mineral/rock B:

$$aA + \uparrow (X) \downarrow \rightleftharpoons bB$$

where a and b are the amounts (in g) of mineral/rock A and B, respectively, and (X) is the total amount of material lost or gained (in g). The following equation (Gresens, 1967) also takes into account the change in volume of the mineral/rock during the alteration process:

$$100 \times [F_v \times (g_B/g_A) \times c_n^B - c_n^A] = x_n$$

where F_v = volume factor
g_A and g_B = specific gravity of mineral/rock A (initial) and B (final)
c_n^A and c_n^B = weight fraction of component n in mineral/rock A (initial) and B (final) (known from the chemical analysis)
x_n = total amount of material lost or gained (in g per 100 g initial reactants).

For $F_v = 1$, the reaction proceeds isovolumetrically, whereas if $F_v > 1$ or $F_v < 1$ the alteration is associated with a volume gain or a volume loss, respectively. By making certain assumptions regarding the immobility of some elements, the change in volume and the loss or gain of other elements during the reaction can be calculated.

6.4 Major Element Distribution

The results of the XRF bulk rock analyses of the major elements as well as selected rare earth elements are given in Table 6.1. In the footwall quartzites, Al_2O_3 and TiO_2 decrease progressively towards the VCR, with a sharp decrease in Al_2O_3 within 0.2 m of the VCR (Fig.6.2). This is balanced by a corresponding increase in Fe_2O_3 and MgO (and MnO). This compositional variation in the bulk rock can be directly related to the change from a pyrophyllite- and muscovite-rich rock at >0.2 m below the VCR to a chlorite-rich rock at <0.2 m below the VCR.

The gradual increase in K_2O from >5 m below the VCR up to a maximum at 0.6 m below the VCR is directly related to the mineralogical change from a pyrophyllite-rich rock to a muscovite-rich rock at c. 2.5 m below the VCR. The subsequent sharp decrease in K_2O which is observed between the sericitised and the chloritised quartzite at 0.2 - 0.6 m below the VCR is due to a decrease and increase in the modal proportions of muscovite and chlorite, respectively, over that interval.

Table 6.1: Bulk Rock Metabasalt and Quartzite Compositions

		METABASALT								QUARTZITE					
Sample No. VHG....		069	079	080	081	082	083	084	084(A)	096	097	098	099	100	101
Zone		White Phenocryst		Dark Phenocryst				Contact		Chloritised	Sericitised			Pyrophyllitised	
Distance from VCR (m)		+16	+10.5	+5.5	+3.5	+2.5	+1.5	+0.6	+0.1	-0.1	-0.6	-1.5	-2.5	-3.5	-5.5
SiO2	(wt %)	53.08	50.58	50.78	47.66	50.13	50.02	47.22	51.38	86.77	87.15	89.52	89.3	88.58	88.23
TiO2		1.01	0.97	0.94	0.95	0.94	0.95	1.01	1.09	0.12	0.15	0.14	0.15	0.17	0.20
Al2O3		13.52	13.08	12.43	12.75	12.69	12.67	13.91	16.03	4.72	7.53	6.34	7.36	7.45	8.36
Fe2O3*		10.74	10.38	9.92	9.86	9.55	10.01	15.49	13.04	4.54	0.84	0.85	0.65	0.68	0.75
MnO		0.13	0.13	0.12	0.14	0.13	0.15	0.19	0.16	0.03	bd	bd	bd	bd	bd
MgO		5.19	5.57	5.23	5.08	5.16	5.23	6.29	5.42	1.51	0.10	0.02	bd	0.02	0.02
CaO		7.57	7.42	8.28	8.98	8.81	8.38	5.15	3.41	0.01	0.04	0.09	0.05	0.01	0.01
Na2O		2.96	2.24	0.44	0.03	0.04	0.05	0.02	0.08	0.06	0.49	0.85	0.52	0.17	0.09
K2O		0.08	0.14	1.30	1.51	1.40	1.36	0.64	1.80	0.37	1.62	0.88	0.66	0.46	0.26
P2O5		0.14	0.12	0.13	0.13	0.13	0.13	0.09	0.16	0.01	bd	0.01	0.01	0.01	0.01
H2O-		0.07	0.07	0.07	0.07	0.06	0.03	0.01	bd	bd	bd	0.30	0.17	0.11	0.07
LOI		4.29	8.53	9.83	11.17	10.73	10.52	8.90	7.18	1.43	1.10	0.87	1.12	1.33	1.58
TOTAL		98.78	99.23	99.47	98.33	99.77	99.5	98.92	99.75	99.57	99.02	99.87	99.99	98.99	99.58
La	(ppm)	9.70	nd	nd	11.70	nd	nd	13.80	3.87	13.70	nd	nd	nd	nd	21.00
Ce		21.90	nd	nd	26.20	nd	nd	27.20	9.55	22.80	nd	nd	nd	nd	38.20
Pr		2.66	nd	nd	3.17	nd	nd	3.17	1.23	1.91	nd	nd	nd	nd	3.71
Nd		11.60	nd	nd	14.00	nd	nd	13.50	6.49	7.49	nd	nd	nd	nd	12.70
Sm		2.93	nd	nd	3.28	nd	nd	2.67	1.97	1.45	nd	nd	nd	nd	2.30
Eu		1.13	nd	nd	1.08	nd	nd	1.30	0.76	0.34	nd	nd	nd	nd	0.44
Gd		3.03	nd	nd	3.21	nd	nd	2.85	2.25	1.09	nd	nd	nd	nd	1.35
Tb		0.49	nd	nd	0.50	nd	nd	0.43	0.36	0.12	nd	nd	nd	nd	0.15
Dy		2.93	nd	nd	2.90	nd	nd	2.73	2.22	0.64	nd	nd	nd	nd	0.90
Er		1.68	nd	nd	1.52	nd	nd	1.51	1.41	0.36	nd	nd	nd	nd	0.48
Yb		1.34	nd	nd	1.31	nd	nd	1.14	1.36	0.38	nd	nd	nd	nd	0.45
S.G.		2.81	2.75	2.81	2.87	2.85	2.77	2.80	2.90	2.76	2.80	2.67	2.83	2.67	2.75

LOI: Loss on Ignition bd : below detection nd : not determined

* total Fe S.G.: Specific Gravity

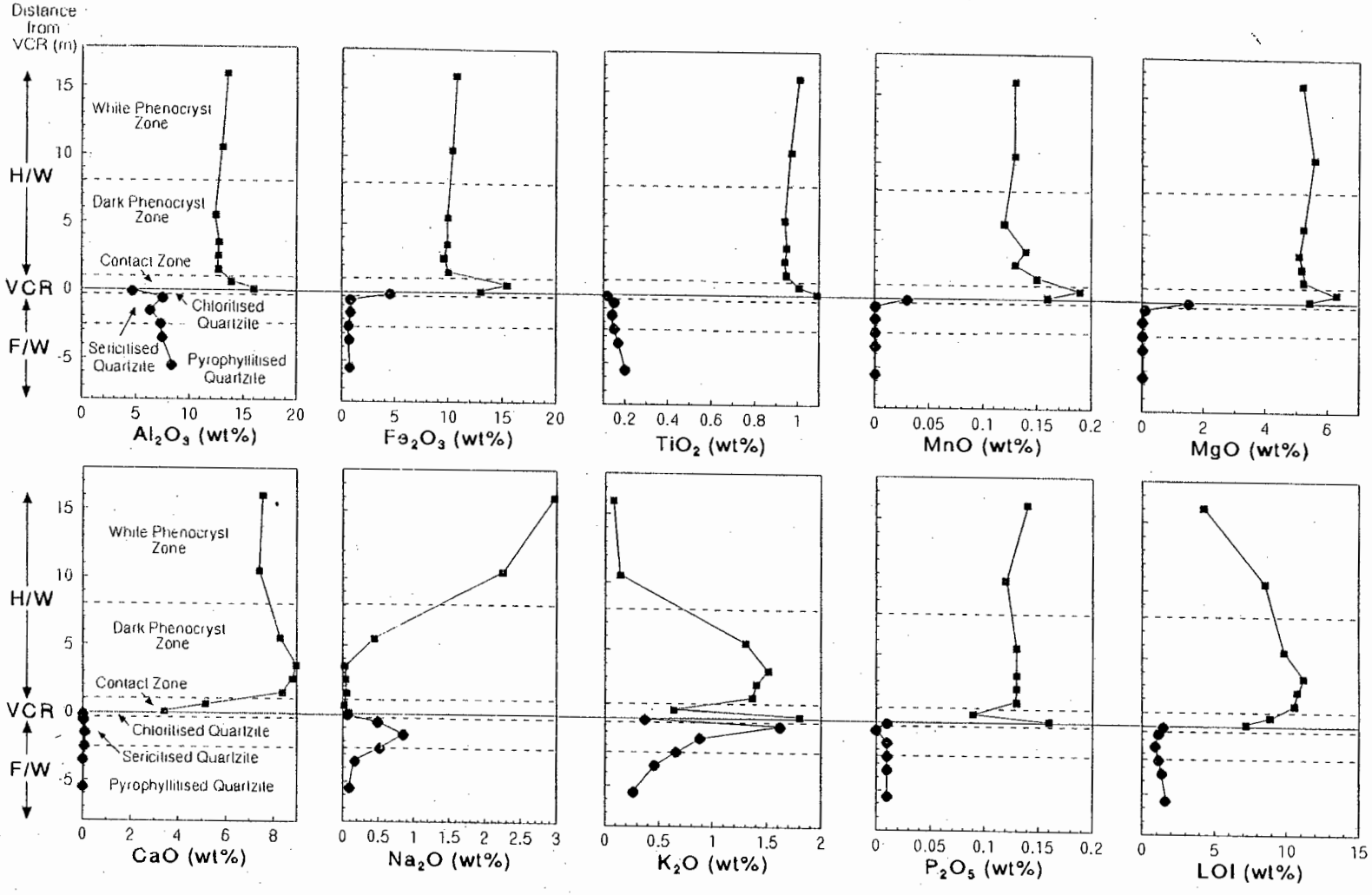

Fig. 6.2: Variation of selected element oxides from metabasalt and quartzite samples with increasing proximity to the VCR.

Variations in some major element ratios in the quartzites are shown in Fig.6.3. An antithetic relationship exists between the Al:Fe and Al:Si ratios (Fig.6.3(a)). The sharp decrease in the Al:Fe ratio and the corresponding increase in the Al:Si ratio in the footwall quartzites towards the VCR suggests strong enrichment in Fe and depletion in Si in the chloritised quartzite zone (assuming Al immobility). The sharp decrease in the Al:Mg ratio which is observed between the sericitised and the chloritised footwall quartzite (Fig.6.3(b)) indicates the introduction of substantial amounts of Mg (assuming Al immobility).

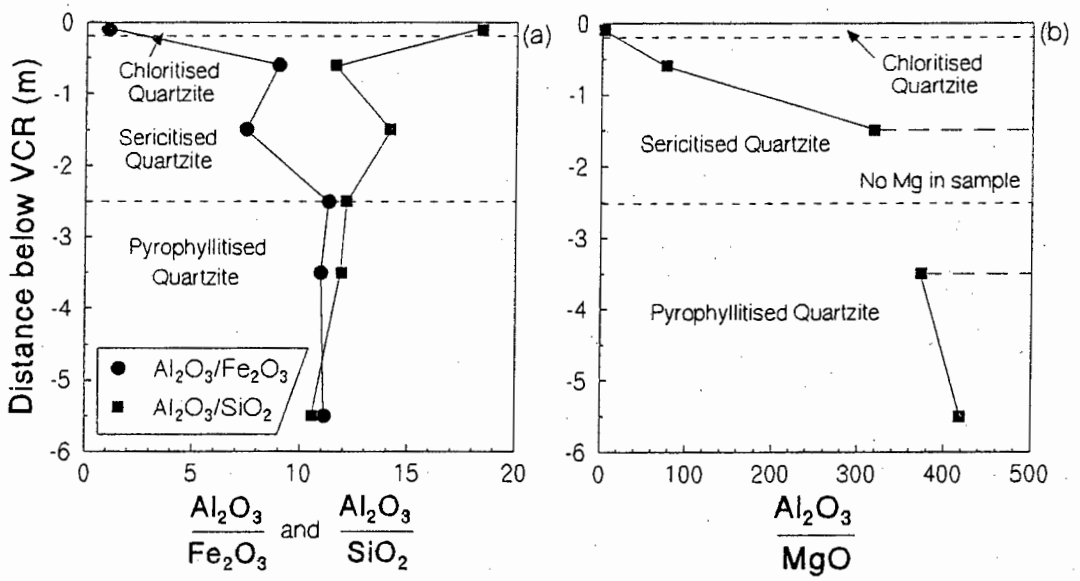

Fig.6.3: Variations in selected major element ratios in the footwall quartzites with increasing proximity to the VCR.

No significant changes in Al_2O_3, Fe_2O_3, TiO_2, MnO and MgO contents occur between the white and the dark phenocryst zones in the metabasalt (Fig.6.2). However, significant changes in Na_2O and K_2O, and to a lesser extent in CaO and the volatile content (LOI), occur over the same interval. The change from the dark phenocryst zone to the contact zone is associated with significant changes in Al_2O_3, Fe_2O_3, CaO, K_2O and LOI content.

Petrographic investigation of the white phenocryst zone indicates that the plagioclase phenocrysts and matrix are partially replaced by sericite, calcite and chlorite. The breakdown of plagioclase in the metabasalt released Ca which became available for the formation of calcite in veins,

amygdales and as individual grains in the metabasalt matrix. The significant decrease in Na_2O and increase in K_2O from the white to the dark phenocryst zone is explained by the progressive alteration of plagioclase and the increase in sericitisation (of muscovite composition) of the rock with increasing proximity to the VCR.

The increase of Al_2O_3, Fe_2O_3, TiO_2 and MgO in the metabasalt in the contact zone (Fig.6.2) is balanced by a loss of CaO and LOI. CaO is present mainly in the form of calcite in the dark phenocryst zone and as plagioclase further away from the VCR. A sharp decrease of CaO and LOI from the dark phenocryst to the contact zone is reflected by a corresponding decrease of modal calcite towards the contact zone.

Selected element oxide ratios of the metabasalts have been plotted against each other (Fig.6.4) to compare the change in concentration of one element with another. The sharp increase of the Al:Ca ratio in the contact zone (Fig.6.4(a)) indicates that Ca is severely depleted within this zone. A similar trend to that of the Al:Ca ratio is shown by the Al:Si ratio, which suggests that both Si and Ca were removed from the metabasalt contact zone, assuming Al to have been immobile.

The decrease in the Al:Fe ratio between the dark phenocryst and parts of the the contact zone (Fig.6.4(a)) suggest that enrichment in Fe in the contact zone occurred. This is further supported by the sharp increase in the bulk rock X_{Fe} from 0.66 to 0.71 between the dark phenocryst and the contact zones (Fig.6.4(c)). Similarly, the chlorite X_{Fe} increases over the same interval from 0.49 to 0.57, suggesting that the chlorite composition was, in part, controlled by the bulk rock composition.

The increase in the Al:Na ratio and the decrease in the Al:K ratio from the white to the dark phenocryst zone (Fig.6.4(d)) indicates that Na was removed from and K was added to the rock. The highly variable Al:Na ratios which are encountered within the dark phenocryst and contact zones suggest that, due to the great mobility of the alkaline earth elements, local variations of these may have occurred on a scale of centimetres and metres.

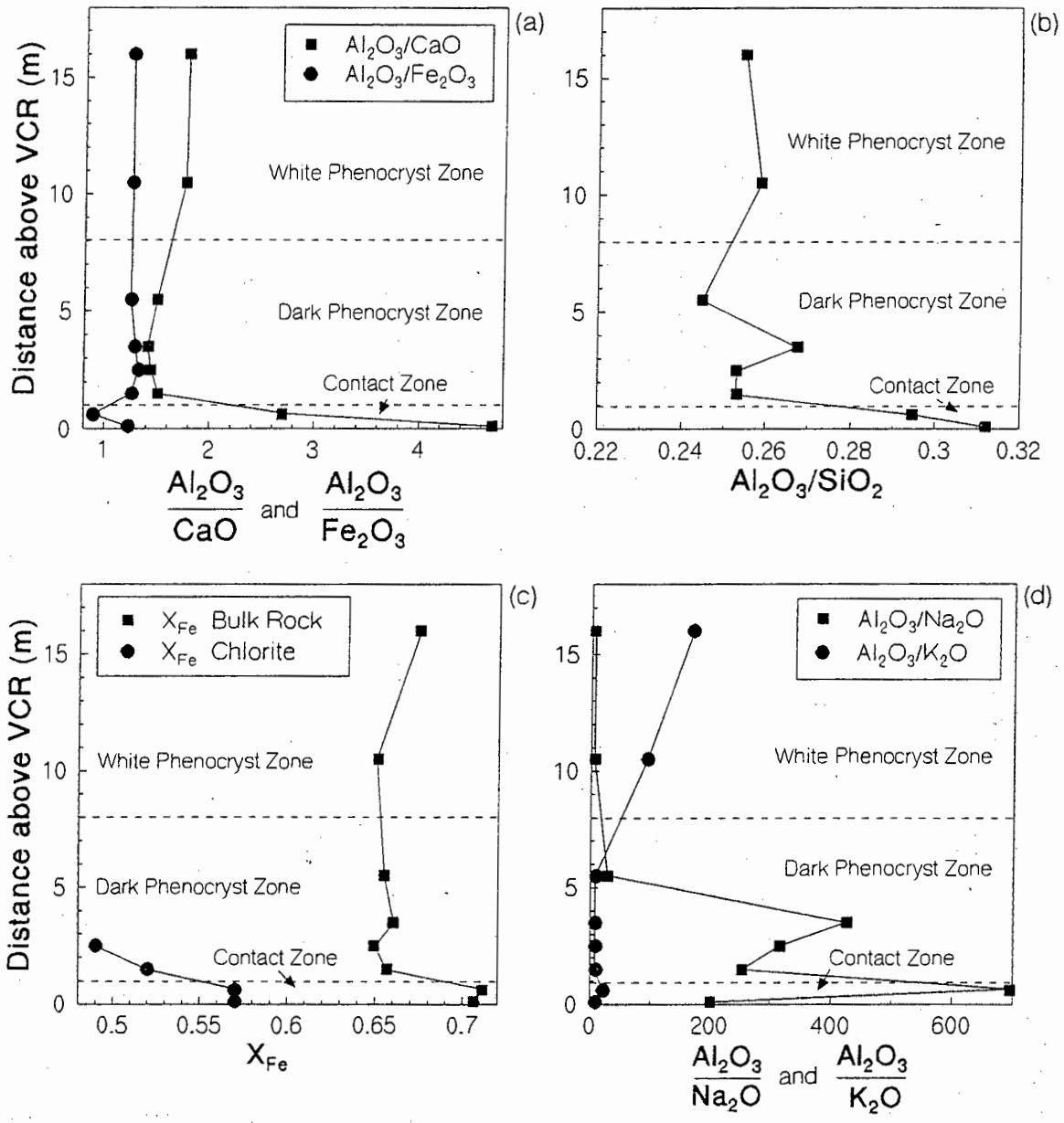

Fig.6.4: Variation in selected major element ratios in the metabasalt with increasing proximity to the VCR.

Composition-volume diagrams are used to compare different quartzite and metabasalt samples with each other. Certain assumptions regarding the immobility of some elements have to be made. Al_2O_3 is commonly regarded as being relatively immobile and is used in the chemical alteration index (CIA) as a measure to determine the amount of loss/gain of mobile elements such as Na, K and Ca (Nesbitt and Young, 1982). For the successful application of composition-volume diagrams, F_v has to be known or estimated. This can be done by determining F of immobile

elements and using this as a reference against which more mobile elements are measured. An alternative method is to examine the clustering of F_v's of the less mobile elements on a composition-volume diagram. It is very difficult, if not impossible, to determine volume changes in the quartzites and metabasalts by routine optical examination and in this study therefore, F_v was determined using the "cluster" method.

As will be demonstrated below, two completely different metasomatic alteration events, during which different elements were added to and removed from the rock, are documented in the footwall quartzites as well as in the hangingwall metabasalts.

The composition-volume diagrams for the alteration of a pyrophyllitised quartzite sample VHG101 to a muscovite-rich quartzite sample VHG097, and the alteration of the latter sample (VHG097) to the chlorite-rich quartzite sample VHG096 are shown in Fig.6.5. The calculated net gains/losses of elements during these alteration processes are given in Table 6.2. Two different calculations are presented, one for Al immobility and the other for isovolumetric alteration ($F_v = 1$).

Table 6.2: Net Gains/Losses (g per 100g Parent Rock) During Muscovite- and Chlorite-forming Alteration Processes

Lithology	Quartzite Alteration *		Quartzite Alteration **		Metabasalt Alteration *	
Initial ---> Final Alteration Event	101 ----> 097 Potassic Altn.	097 ----> 096 Chloritic Altn.	101 ----> 097 Potassic Altn.	097 ----> 096 Chloritic Altn.	069 ----> 081 Potassic Altn.	081 ----> 084 Chloritic Altn.
Fv	1.09	1.62	1.00	1.00	1.04	0.94
SiO2	+8.62	+51.30	+0.38	-1.53	-2.51	-4.38
TiO2	-0.03	+0.04	-0.05	-0.03	0	-0.02
Al2O3	0	0	-0.70	-2.87	0	0
Fe2O3	+0.18	+6.40	+0.10	+3.64	-0.28	+4.34
MnO	0	+0.05	0	+0.03	+0.02	+0.03
MgO	+0.09	+2.31	+0.08	+1.39	+0.20	+0.69
CaO	+0.03	-0.02	+0.03	-0.03	+1.96	-4.25
Na2O	+0.45	-0.39	+0.41	-0.43	-2.93	-0.01
K2O	+1.54	-1.03	+1.39	-1.25	+1.52	-0.92
LOI	-0.36	+1.19	-0.46	+0.30	+7.56	-3.00

* - assuming Al immobility
** - assuming constant volume

An examination of the changes in SiO_2 which are predicted to occur in the quartzites during K^+ alteration reveals that significant amounts (8.6 g SiO_2 per 100 g parent rock) of SiO_2 must be added to the original pyrophyllite-bearing rock as a reactant for $F_v = 1.09$ (i.e. 9% volume increase for the case of Al immobility). However, the potassic alteration of a pyrophyllite- to a muscovite-rich quartzite produces SiO_2, and therefore the assumption of $F_v = 1.09$ cannot be

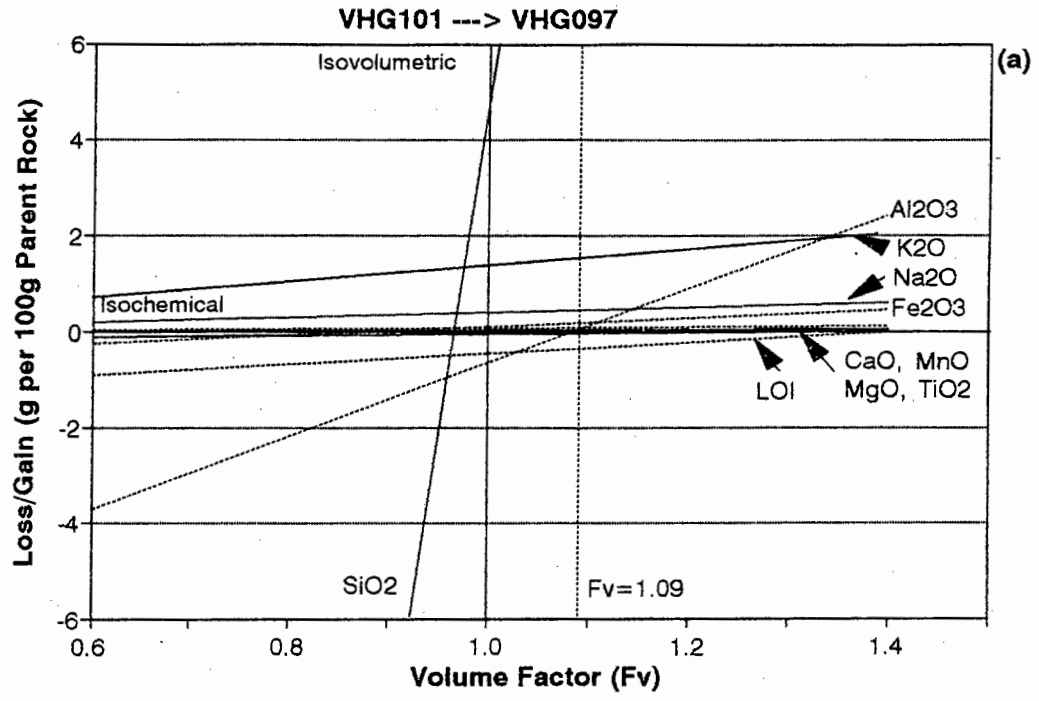

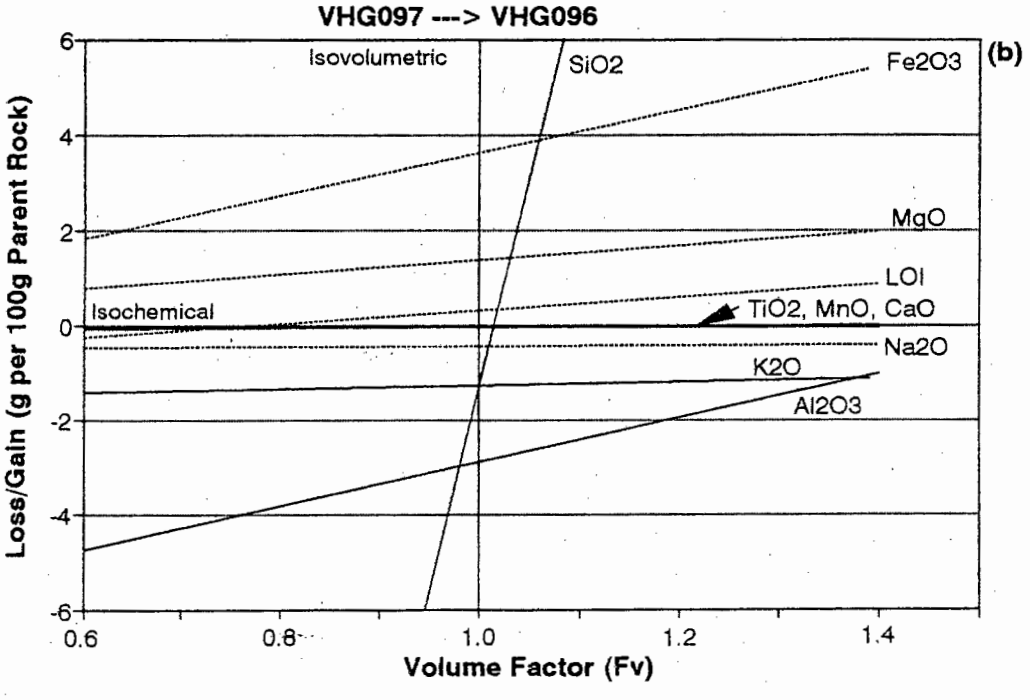

Fig.6.5: Composition-volume diagrams comparing (a) pyrophyllite-rich quartzite sample VHG101 to muscovite-rich sample VHG097, and (b) sample VHG097 to chlorite-rich quartzite sample VHG096.

correct. The lack of large variations in the Al:Si ratio (Fig.6.3(a)) during the muscovite-forming alteration event indicates that no net gain or loss of Al and Si has occurred. In order to obtain a fairly constant Al:Si ratio, the assumption is made that during the muscovite-forming alteration event of the quartzites, $F_v = 1$. The steep slope of the SiO_2 component line in Fig.6.5, however, means that even small variations of F_v will result in apparently large predicted gains or losses of the SiO_2 component.

The balanced reaction for the alteration process of the pyrophyllite-bearing quartzite sample to the muscovite-bearing sample is

$$100g\ (VHG101) + 0.4g\ SiO2 + 0.1g\ Fe_2O_3 + 0.1g\ MgO + 0.4g\ Na_2O + 1.4g\ K_2O = 102g\ (VHG097) + 0.7g\ Al_2O_3 + 0.5g\ LOI \quad \text{---------- (1)}$$

Ignoring the apparent gains/losses in SiO_2 and Al_2O_3, the only other significant change is the addition of substantial amounts of K to the rock (as is expected).

A volume increase of 62% (Table 6.2) as predicted for the chlorite-forming alteration event of sample VHG097 to sample VHG096, assuming Al immobility, is clearly unrealistic. Instead, the assumption is made that no volume change occurred (i.e. $F_v = 1$). Based on this assumption, the following reaction gives the net gain/losses of elements which occurred during chlorite metasomatism:

$$100g\ (VHG097) + 3.6g\ Fe_2O_3 + 1.4g\ MgO + 0.3g\ LOI = 99g\ (VHG096) + 1.5g\ SiO_2 + 2.9g\ Al_2O_3 + 0.4g\ Na_2O + 1.3g\ K_2O \quad \text{---------- (2)}$$

The addition of Fe and Mg during the chlorite-forming alteration event of sample VHG097 to sample VHG096 is thus predicted and also expected, based on the mineralogy. Significant amounts of Si, Al and K are also predicted to have been lost from the rock. This implies that Al was, to a certain extent, mobile during this chloritisation event of the footwall quartzite. The sharp increase in the Al:Si ratio in Fig.6.3(a), however, suggests that far more Si relative to Al was lost. If this is the case, the amount of Al lost from the rock as calculated from reaction (2) above is an overestimation.

In order to compute the alteration effects on the metabasalt, a sample from the white phenocryst zone (sample VHG069) is compared with a sample from the dark phenocryst zone (sample VHG081) (Fig.6.6(a)) and sample VHG081 is, in turn, compared with a metabasalt sample from the contact zone (sample VHG084) (Fig.6.6(b)).

Comparing sample VHG069 with VHG081, the F_v of Al_2O_3, Fe_2O_3, TiO_2 and MgO all plot between 0.98 and 1.07 (Fig.6.6(a)) and an average F_v value of 1.04 (corresponding to Al immobility) is therefore used. For the case of $F_v = 1.04$, the compositional gains/losses (in g per 100 g of parent rock) of each element oxide during the progressive muscovite-forming alteration event of metabasalt sample VHG069 to VHG081 is given in Table 6.2. The K^+ alteration event can be expressed by the following equation:

$$100g\ (VHG069) + 0.2g\ MgO + 2.0g\ CaO + 1.5g\ K_2O + 7.6g\ LOI = 106g\ (VHG081) + 2.5g\ SiO_2 + 0.3g\ Fe_2O_3 + 2.9g\ Na_2O \quad (3)$$

Similarly, the net changes in elements during the chloritic alteration of sample VHG081 to sample VHG084 (for $F_v = 0.94$, which corresponds to Al immobility) can be expressed by the reaction

$$100g\ (VHG081) + 4.3g\ Fe_2O_3 + 0.7g\ MgO = 92g\ (VHG084) + 4.4g\ SiO_2 + 4.3g\ CaO + 0.9g\ K_2O + 3.0g\ LOI \quad (4)$$

The similar F_v values, which correspond to Al immobility, suggest that the muscovite- and chlorite-forming alteration events which affected the metabasalt were accompanied by a negligible volume increase, i.e. both metasomatic alterations proceeded essentially isovolumetrically. Reaction (3) shows that significant amounts of Ca and K and especially volatiles (i.e. H_2O and CO_2) were added to the rock and that Si and Na were removed from the rock during K^+ alteration. The introduction of substantial amounts of Fe and lesser Mg and the removal of Si, Ca and LOI during chloritic alteration is shown by reaction (4).

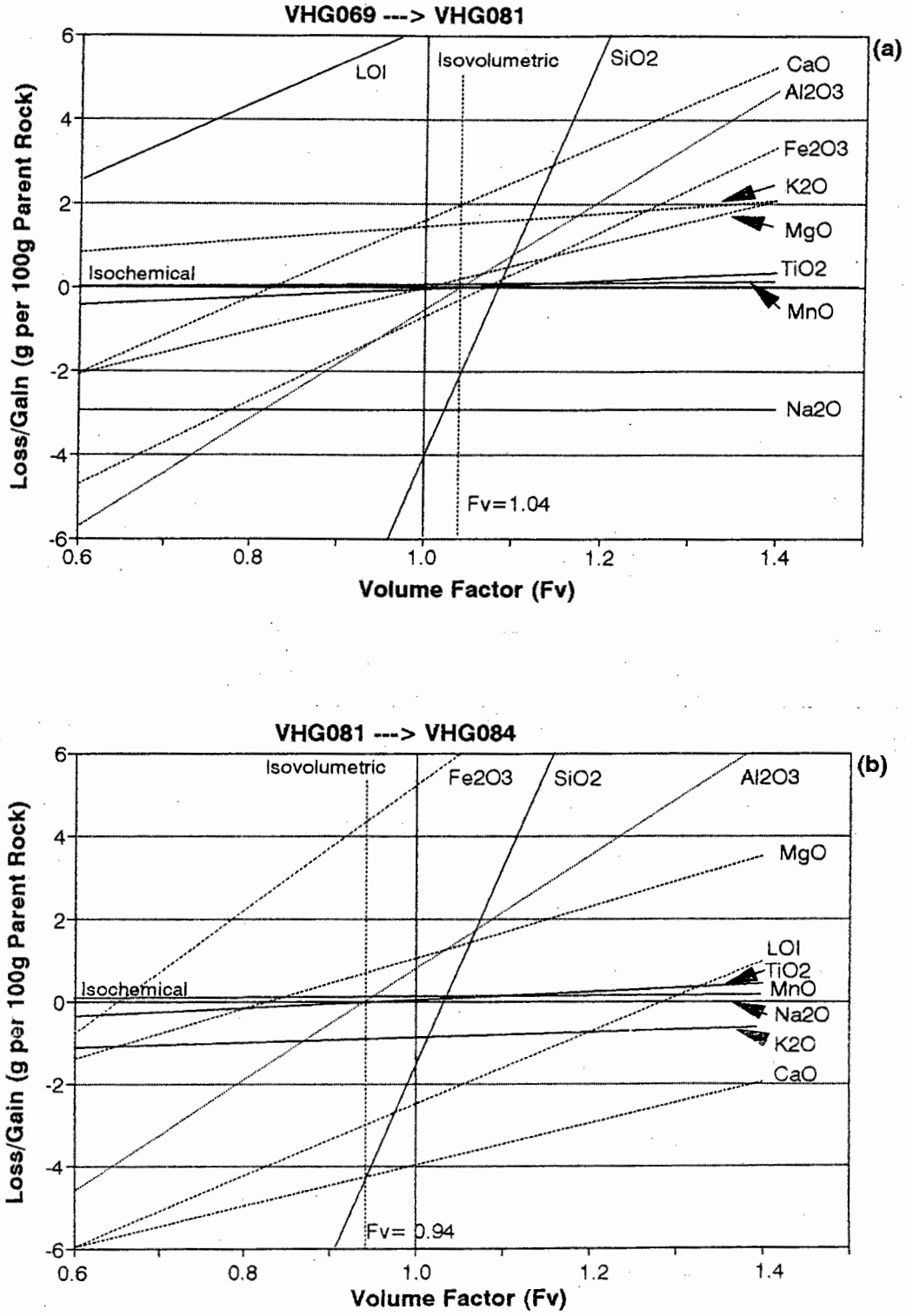

Fig.6.6: Composition-volume diagrams comparing (a) white phenocryst sample VHG069 to dark phenocryst sample VHG081, and (b) sample VHG081 to contact zone sample VHG084.

A further method of investigating the potassic alteration event in the footwall quartzites is the use of the chemical index of alteration (CIA). The CIA was originally used to determine the extent of alteration of sedimentary rocks (Nesbitt and Young, 1982) and is calculated, using mole fractions, as follows:

$$CIA = Al_2O_3/(Al_2O_3+CaO+Na_2O+K_2O).$$

The CIA has been applied to the Witwatersrand quartzites in an attempt to show that palaeosol formation at major erosional unconformities is associated with an increase in the CIA value. Sutton *et al.* (1990), in their investigation of quartzites from the Central Rand and West Rand Groups in the Klerksdorp goldfield, found that the CIA increased upwards within individual formations and in the section as a whole. Ritger (1990) found that for some reefs (e.g. the Vaal Reef), the footwall has a much higher CIA compared to the hangingwall rocks.

All of these authors interpret the upward increase in CIA within formations as the result of weathering and palaeosol formation. Furthermore, Sutton *et al.* (1990) imply that, due to the (apparent) absence of noticeable alteration halos around the major erosional unconformities, the upward increase in K over a vertical distance of 2300 m reflects K enrichment by groundwaters and/or diagenetic fluids.

Muscovite is the only K-bearing mineral in the footwall quartzites and Na- and Ca-bearing mineral phases are absent from most of the Central Rand Group quartzites. Al_2O_3 is regarded as a relatively immobile component (Nesbitt and Young, 1982) and therefore variations in the CIA reflect the change in muscovite content in the footwall quartzites.

A plot of the CIA (normalised to SiO_2) of the footwall quartzites (Fig.6.7) with increasing proximity to the VCR indicates two trends. Firstly, a marked *decrease* in the CIA index occurs with increasing proximity to the VCR up to c. 1.5 m below the VCR. Secondly, a very sharp *increase* in the CIA occurs in the transition into the chloritised footwall zone.

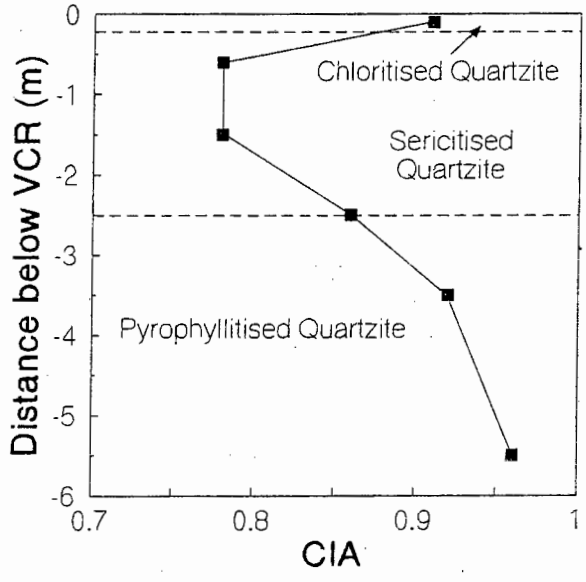

Fig.6.7: Variation of CIA in footwall quartzites with increasing proximity to the VCR.

The decreasing trend in the CIA over 4 m towards the VCR is contrary to what would be expected if weathering of the footwall rocks and leaching of mobile elements had occurred. The decreasing CIA trend implies that either a significant enrichment of K (and potentially Na and Ca) must have taken place or that a net loss of Al from the quartzites has occurred. From XRD analyses it is known that the change from a pyrophyllite-bearing quartzite to a muscovite-bearing quartzite occurs between 3.5 m and 1.5 m below the VCR. This coincides with the decreasing CIA trend, which can therefore directly be attributed to the formation of muscovite through K^+ metasomatic alteration.

The sharp increase in the CIA within 0.2 m below the VCR coincides with the chloritised footwall zone. Data presented above shows that this chloritisation can be related to a metasomatic alteration event during which both Al and K were lost from the chloritised footwall zone. The mobility of Al, documented for this event, precludes a meaningful application of the CIA index, and the increasing CIA merely reflects the loss in K.

Summarising, two alteration events can be identified in the quartzites and in the metabasalts, and the diagnostic alteration mineral assemblages are represented in Table 6.3. Bulk rock modelling supports petrographic observations (see Chapter 4.) which show that a K^+ metasomatic alteration

event has affected the footwall as well as the hangingwall rocks up to several metres from the VCR. A second, chlorite-forming, alteration event affected the quartzites and the metabasalts up to a distance of c. 1 m from the VCR. The muscovite-forming alteration event was associated with a change from a pyrophyllite-rich to a muscovite-rich rock in the footwall quartzites. In the hangingwall metabasalts, the same event resulted in the formation of sericitic muscovite in addition to the regional greenschist facies mineral assemblage (which includes chlorite, actinolite and calcite).

Table 6.3: Alteration Mineral Assemblages Around the VCR

Lithology	Zone	Typical Distance from VCR (m)	Colour	Indicator Mineral	Diagnostic Alteration Mineral Assemblage
Hangingwall Metabasalt	Aphanitic	>20	olive green	Chlorite	Act > Chl > Ep = Cc
	White Phenocryst	8 - 20	medium grey/green	Calcite	Chl = Cc > Act > Ep >> Ms (carbonatisation/sericitisation of plag.)
	Dark Phenocryst	1 - 9	light grey/green	Sericitic Muscovite	Ms = Cc > Chl (intense sericitisation/carbonatisation/ chloritisation of plagioclase)
	Contact	<1	light yellow/ grey-green	Chlorite	Chl > Ms = Cc ("bleached" appearance)
VCR			light to dark grey	Chlorite	Chl >> Ms
Footwall Quartzite	Chloritised	<0.2	dark grey	Chlorite	Ms> Chl (partial chloritisation of quartzite)
	Sericitised	0.2 - 3	grey/brown	Sericitic Muscovite	Ms
	Pyrophyllitised	>3	grey/brown	Pyrophyllite	Prl >> Cld

Act - Actinolite, Chl - Chlorite, Ep - Epidote, Ms - Muscovite, Cc - Calcite, Prl - Pyrophyllite, Cld - Chloritoid

During the muscovite-forming alteration event, which took place essentially isovolumetrically, significant amounts of K were introduced into the quartzites and metabasalts. The change in the quartzite bulk rock composition is represented on an A'KF diagram (Fig.6.8(a)), on which the large increase in the potassic component of the rock is evident.

According to reaction (3), significant amounts of Ca and volatiles were added to the metabasalts in addition to K during K^+ alteration. This implies that the alteration from white to dark phenocryst zone (i.e. extending c. 10 m into the metabasalt) was the result of the infiltration by a Ca/K-rich fluid. At the same time, the loss of Si and Na from the rock indicates the breakdown of plagioclase during this sericitic alteration event. An increase in the Ca and K content of the bulk rock are also indicated on the ACF diagram (Fig.6.8(b)).

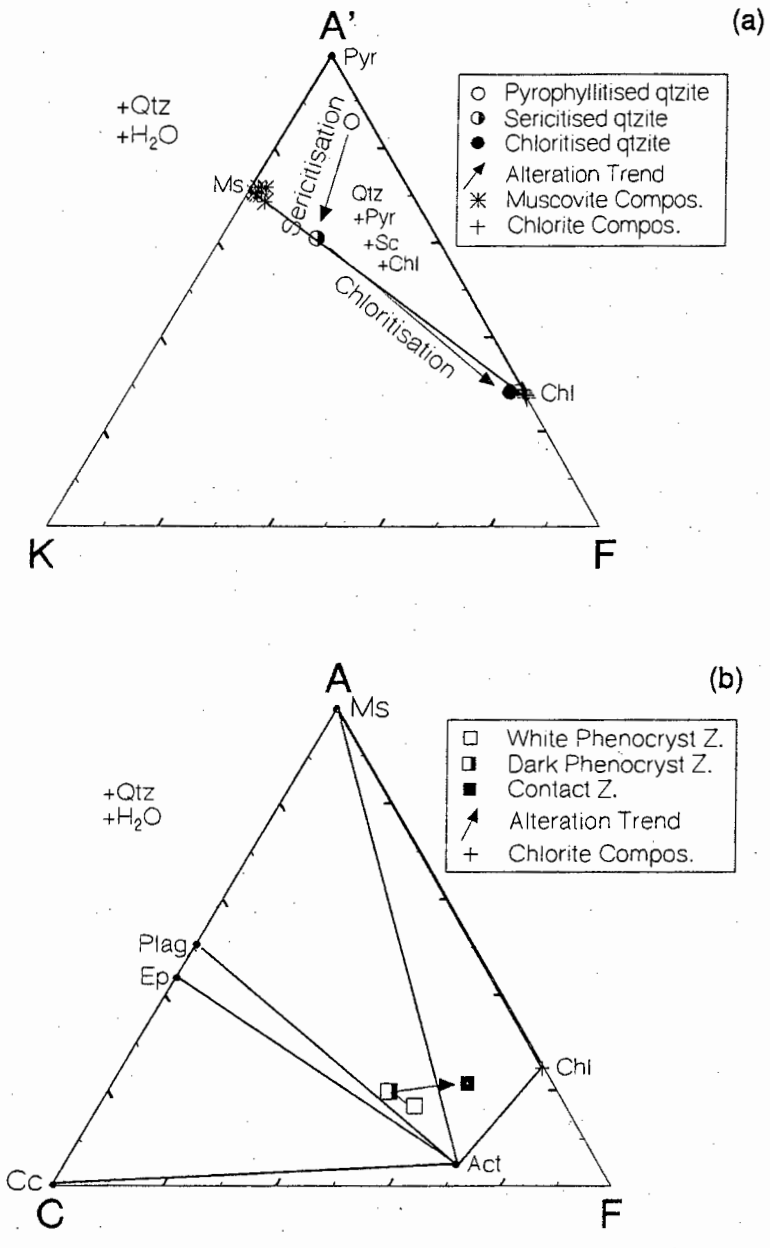

Fig.6.8: Bulk rock alteration trends in (a) the footwall quartzites and (b) hangingwall metabasalts as indicated on A'KF and ACF diagrams, respectively.

The chlorite-forming alteration process was associated with the introduction of significant amounts of Fe and Mg into the footwall and hangingwall rocks, which is reflected by the increase in the alteration trend towards the FeO+MgO component in the A'KF and ACF diagrams (Fig.6.8). Si, K and Al were removed from the footwall quartzites during the chloritic alteration, indicating the mobility of Al under the chlorite-forming conditions. In the hangingwall

metabasalts, significant amounts of Si, Ca and volatiles were lost during this alteration event.

The addition of Fe to the metabasalt during the chlorite-forming alteration event as calculated from reaction (4) supports underground observations which indicate locally abundant secondary pyrite cubes in the contact zone metabasalt immediately above the VCR. A common feature of the metabasalt within tens of metres of the VCR is the presence of massive quartz veins up to 50 cm thick as well as smaller calcite veins and amygdales. This suggests that Si and Ca, which were released during the chlorite-forming metasomatic alteration event, reprecipitated locally in the form of these veins and amygdales.

6.5 Rare Earth Element Distribution

Rare earth elements (REE) of selected footwall quartzite and hangingwall metabasalt samples were analysed by ion chromatography at the University of Cape Town (see Appendix B). REE's in the footwall quartzites are present chiefly in zircon and rutile, and in the hangingwall metabasalts probably occur in rutile, sphene and possibly apatite.

The four hangingwall metabasalt samples which are compared to each other are from the contact zone (samples VHG084(A) and VHG084), the dark phenocryst zone (sample VHG081) and from the white phenocryst zone (sample VHG069). The analytical results, which are shown in Table 6.2, were normalised against primitive mantle composition.

A noticeable depletion of light REE's from the metabasalt sample closest to the VCR (sample VHG084(A)) is evident (Fig.6.9). However, no change in REE distribution is apparent in any of the other three metabasalt samples, which lie between 0.6 - 16 m above the VCR. This indicates that the chloritisation event was capable of remobilising the REE's only within c. 0.5 m of the VCR, probably because of the higher fluid:rock ratios experienced closer towards the VCR.

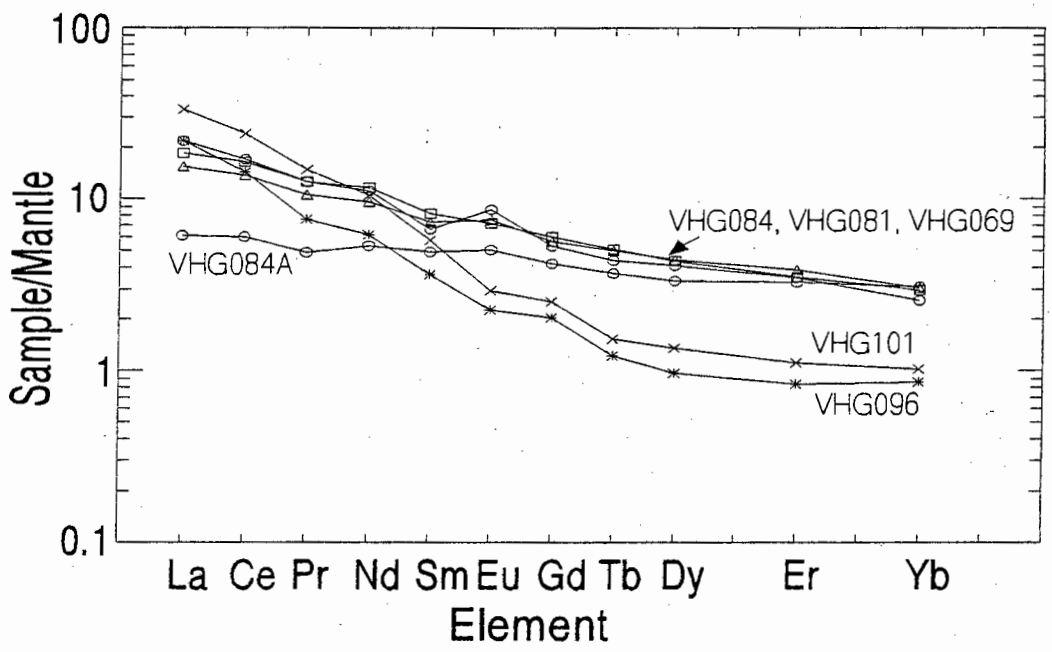

Fig.6.9: Primitive mantle-normalised REE abundances in four hangingwall meta-basalt samples (samples VHG084(A),VHG084, VHG081 and VHG069) and in two footwall quartzite samples (VHG096 and VHG101).

The REE distribution in the chloritised footwall quartzite sample VHG096 was compared to that in the pyrophyllitised footwall quartzite sample VHG101 (Fig.6.9). Although the actual trend itself means very little (because normalisation is based on primitive mantle composition), the consistency in the ratio of REE's between these two quartzite samples suggests that there was virtually no REE mobility in these rocks.

7. Mineral Chemistry

7.1 Chlorite

7.1.1 Introduction

Chlorite is an important metamorphic/metasomatic mineral in the VCR, the immediate footwall quartzites and the hangingwall metabasalt. It also occurs in dykes, pseudotachylites/ultramylonites and in somequartz veins. Electron microprobe (EMP) analysis of the chlorites was done in order to characterise and compare their composition within and between different rock types.

The non-stoichiometry of chlorite not only makes it a potentially useful geothermometer, but it also allows an estimate of the chemical properties, such as $f(O_2)$ and $f(S_2)$, of the chlorite-forming fluid(s) to be made (Bryndzia and Scott, 1987). Bulk rock composition can also influence the Al content of chlorites, as illustrated in Laird *et al.* (1988).

7.1.2 Chlorite Analyses and Normalisation

Chlorite analyses were made using a Cameca (Camebax) electron microprobe at the Department of Geological Sciences at the University of Cape Town. An outline of the operating conditions and of the standards used is given in Appendix C. All chlorite analyses quoted are anhydrous and are normalised to 14 oxygens (half-formula). Initial analyses for fluorine and chlorine in the chlorite indicated that these were present below the lower limit of detection (LLD = 0.01 wt%) and were subsequently not analysed for further.

The differentiation between Fe^{2+} and Fe^{3+} is not possible with the electron microprobe. There is neither haematite nor magnetite in any of the samples analysed (except in a few hangingwall metabasalt samples from the dark phenocryst zone) and all iron is calculated as Fe^{2+}.

The following chemical parameters are derived from the chlorite analyses: interlayer cations (Na+K+Ca), non-interlayer cations (Si+Al+Cr+Fe+Mg+Mn) and chlorite content X_{Chl}. The

chlorite content can range from 0 (for smectite which has 8.91 half-formula non-interlayer cations) to 1 (for the trioctahedral chlorite end-member with a total of 10 non-interlayer cations) (Robinson *et al.*, 1993).

7.1.3 Chlorite Geothermometry

Numerous authors have investigated the variation in chlorite composition as a function of temperature (e.g. Kranidiotis and MacLean, 1987; Cathelineau, 1988; Zang and Fyfe, 1995) and some of their results are reviewed in Caritat *et al.* (1993). Cathelineau (1988) related the chlorite formation temperature only to the Al^{IV} content because he found only a very weak correlation between Al^{IV} and Fe/Mg content. Contrary to this, other authors (e.g. Kranidiotis and MacLean, 1987; Zang and Fyfe, 1995) found a fairly strong positive correlation between X_{Fe} (=Fe/(Fe+Mg)) and Al^{IV} in the chlorite. Each of these authors, although taking into account the X_{Fe} and Al^{IV} content of the chlorite, derived slightly different empirical calibrations for chlorite formation temperature.

When applying Cathelineau's (1988) calibration to the chlorites in this study, the calculated temperatures of chlorite formation lie between 350 - 450°C. This is considered to be an over-estimation in view of pressure-corrected fluid inclusion microthermometric results from several chlorite-bearing hydrothermal quartz veins. When applying the calibration of Kranidiotis and MacLean (1987), the calculated temperatures are around 220°C. For the majority of samples in this study there is a positive correlation between Al^{IV} and X_{Fe} (e.g. see Fig.'s 7.1.8 and 7.1.9). This relationship is taken into account by the chlorite calibration of Zang and Fyfe (1995), which is therefore used in this study. The Al^{IV} correction is calculated on the basis of 14 (O+OH) as follows

$$Al^{IV}_c = 2 \times Al^{IV} - 0.88 \times (X_{Fe} - 0.34),$$

and the temperature calibration is calculated from

$$T(^0C) = 106.2 \times Al^{IV}_c + 18.$$

Applying this calibration to the chlorites in this study yields temperatures of chlorite formation of around 300°C, which is similar to the temperature obtained by other researchers (e.g. Meyer *et al.*, 1990; Meyer, 1991) from VCR chlorites in the Carletonville goldfield.

7.1.4 Analytical Results

Average chlorite compositions from the footwall quartzites, hangingwall metabasalts, pseudotachylites/ultramylonites, quartz veins and from dykes are presented in Table 7.1.1.

The chlorite end-member compositions are shown in a plot of total Al content versus the sum of non-interlayer cations (Fig.7.1.1). The chlorite compositions from the footwall quartzite, hangingwall metabasalt, pseudotachylite/ultramylonites, quartz vein and dyke samples in the enlarged portion in Fig.7.1.1 indicate that the majority of chlorites from the different rock types are very similar to each other. Compositionally the chlorites lie between the clinochlore and the sudoite end-members, but they show a greater similarity to the trioctahedral clinochlore end-member as indicated by most of the chlorites having close to 10 non-interlayer cations. Several chlorites (notably from pseudotachylite/ultramylonite samples) tend towards the sudoite end-member composition (identified by as few as 9.3 non-interlayer cations). This implies that these chlorites deviate from the trioctahedral chlorite structure.

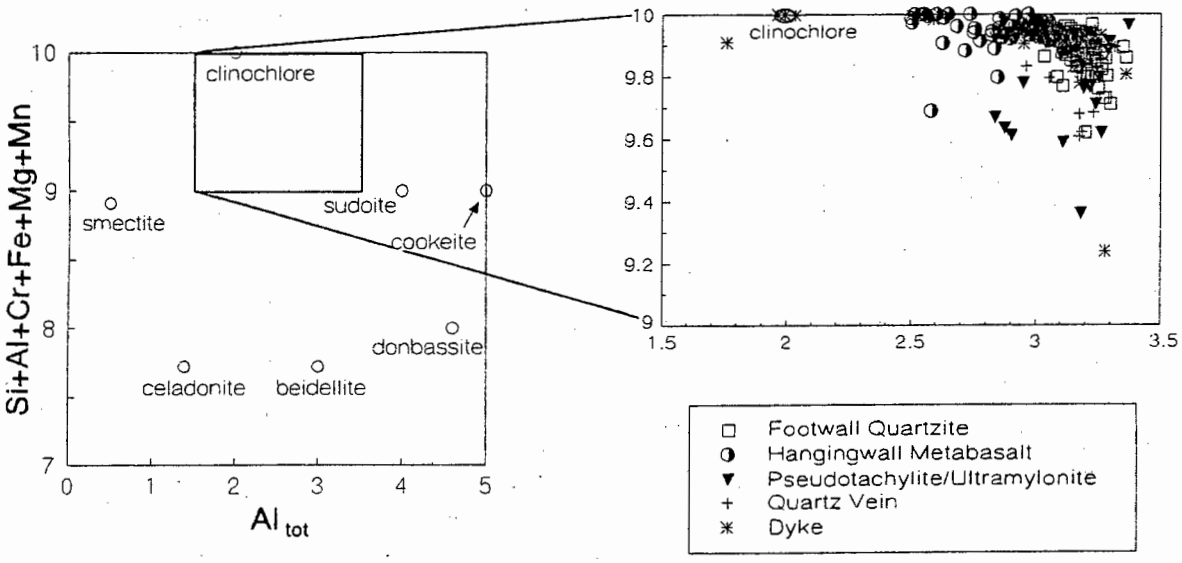

Fig.7.1.1: Plot of the sum of non-interlayer cations vs total Al content illustrating chlorite end-member compositions (after Robinson *et al.*, 1993). Enlarged portion shows the chlorite compositions of different rock types (excluding the VCR).

7.1.4 Analytical Results

Average chlorite compositions from the footwall quartzites, hangingwall metabasalts, pseudotachylites/ultramylonites, quartz veins and from dykes are presented in Table 7.1.1.

The chlorite end-member compositions are shown in a plot of total Al content versus the sum of non-interlayer cations (Fig.7.1.1). The chlorite compositions from the footwall quartzite, hangingwall metabasalt, pseudotachylite/ultramylonites, quartz vein and dyke samples in the enlarged portion in Fig.7.1.1 indicate that the majority of chlorites from the different rock types are very similar to each other. Compositionally the chlorites lie between the clinochlore and the sudoite end-members, but they show a greater similarity to the trioctahedral clinochlore end-member as indicated by most of the chlorites having close to 10 non-interlayer cations. Several chlorites (notably from pseudotachylite/ultramylonite samples) tend towards the sudoite end-member composition (identified by as few as 9.3 non-interlayer cations). This implies that these chlorites deviate from the trioctahedral chlorite structure.

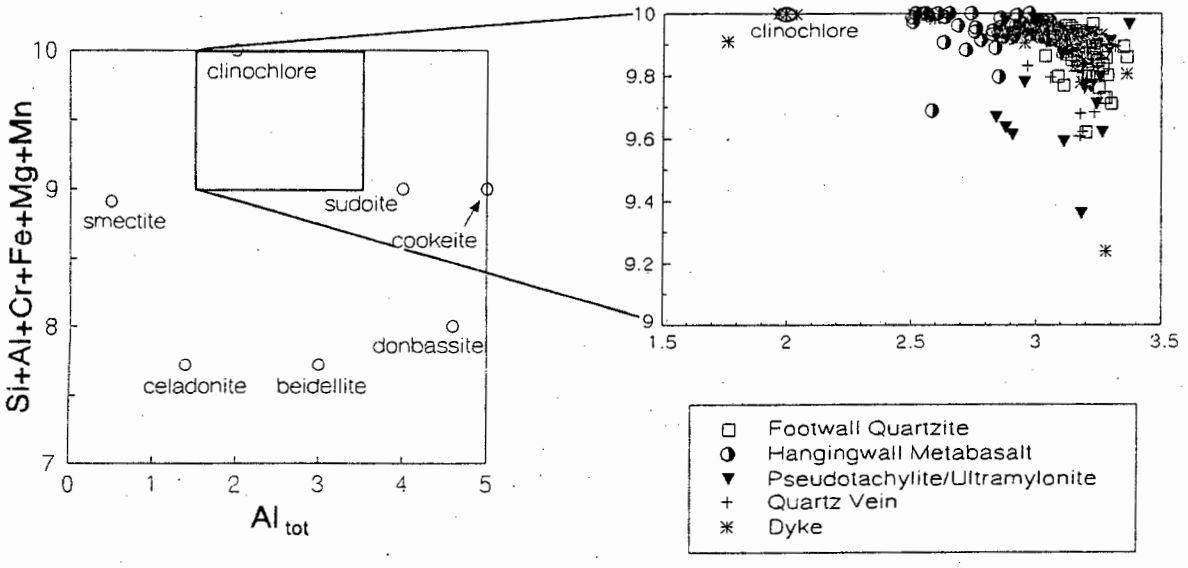

Fig.7.1.1: Plot of the sum of non-interlayer cations vs total Al content illustrating chlorite end-member compositions (after Robinson *et al.*, 1993). Enlarged portion shows the chlorite compositions of different rock types (excluding the VCR).

Table 7.1.1: Average Chlorite Compositions of Different Rock Types (wt%)

Lithology	Footwall Quartzite			Hangingwall Metabasalt		Mylonite Pseudotach.		Quartz Vein			Dyke	
Sample	VHG063(B)	VHG170	VHG125	VHG171	VHG183	VHG027	VHG129	VHG137	VHG163(A)	VHG182	VHG023	VHG134
No. Analyses	(5)	(5)	(5)	(6)	(5)	(8)	(6)	(7)	(10)	(6)	(7)	(5)
SiO2	25.57	23.57	24.53	23.82	25.99	24.21	23.85	24.13	23.96	24.42	24.19	29.36
TiO2	bd	bd	bd	bd	bd	0.01	0.21	bd	bd	bd	bd	bd
Al2O3	27.03	25.83	26.07	25.30	20.54	24.28	25.69	23.74	26.28	24.59	24.32	16.63
Cr2O3	0.09	bd	0.04	0.03	bd	0.05	0.05	bd	bd	bd	0.79	0.35
FeO*	22.77	31.26	26.57	28.89	28.52	29.26	31.79	31.13	27.33	29.31	27.11	24.48
MnO	0.20	0.13	0.23	0.22	0.28	0.10	0.14	0.16	0.20	0.15	0.18	bd
MgO	14.3	8.81	13.37	10.93	14.01	11.74	8.32	10.71	12.16	11.51	12.51	19.42
CaO	0.07	0.01	bd	0.01	0.01	bd	0.05	0.04	bd	0.02	0.01	0.03
Na2O	0.05	bd	bd	bd	bd	bd	0.01	bd	bd	0.02	bd	bd
K2O	0.10	0.03	0.03	0.03	bd	0.01	0.04	bd	bd	0.03	bd	bd
Total	90.18	89.64	90.84	89.23	89.35	89.66	90.15	89.91	89.93	90.05	89.11	90.27
Si(IV)	2.56	2.50	2.50	2.51	2.73	2.54	2.52	2.55	2.47	2.55	2.53	2.98
Al(IV)	1.44	1.50	1.50	1.49	1.27	1.46	1.48	1.45	1.53	1.45	1.47	1.02
Al(VI)	1.75	1.72	1.62	1.64	1.27	1.54	1.71	1.51	1.67	1.57	1.53	0.97
Ti	0.00	0.00	0.00	0.00	0.00	0.00	0.02	0.00	0.00	0.00	0.00	0.00
Cr3+	0.01	0.00	0.00	0.00	0.00	0.00	0.00	0.00	0.00	0.00	0.07	0.03
Fe2+	1.91	2.77	2.26	2.54	2.51	2.57	2.81	2.75	2.36	2.56	2.37	2.08
Mn2+	0.02	0.01	0.02	0.02	0.02	0.01	0.01	0.01	0.02	0.01	0.02	0.00
Mg	2.13	1.39	2.03	1.71	2.19	1.83	1.31	1.69	1.87	1.79	1.95	2.94
Ca	0.01	0.00	0.00	0.00	0.00	0.00	0.01	0.00	0.00	0.00	0.00	0.00
Na	0.01	0.00	0.00	0.00	0.00	0.00	0.00	0.00	0.00	0.00	0.00	0.00
K	0.01	0.00	0.00	0.00	0.00	0.00	0.01	0.00	0.00	0.00	0.00	0.00
Fe/(Fe+Mg)	0.47	0.67	0.53	0.60	0.53	0.58	0.68	0.62	0.56	0.59	0.55	0.41
Al/(Al+Fe+Mg)	0.44	0.44	0.42	0.42	0.35	0.41	0.44	0.40	0.43	0.41	0.41	0.28
T (°C) **	311	307	320	311	270	306	301	299	322	303	310	228
XChl	0.83	0.90	0.94	0.93	1.00	0.96	0.87	0.97	0.93	0.94	0.94	1.00
i/l cat	0.03	0.01	0.00	0.01	0.00	0.00	0.01	0.00	0.00	0.01	0.00	0.00
non-i/l	9.82	9.89	9.94	9.92	10.00	9.96	9.86	9.97	9.93	9.93	9.94	10.01

bd: below detection XChl: chlorite content i/l cat: interlayer cations non i/l: non-interlayer cations

* all Fe as FeO ** temperature calculated after Zang and Fyfe (1995)

The completely different bulk rock compositions of the footwall quartzites and the hangingwall metabasalts are probably the reason that the type II chlorites in the footwall quartzites have slightly higher Al/(Al+Fe+Mg) ratios than the hangingwall metabasalt samples (Fig.7.1.2). However, the chlorites from all the rock types show a similar range in X_{Fe} ratios (except chlorites from one dyke sample). The wide range in X_{Fe} of the chlorites suggests that the factors controlling chlorite composition (e.g. $f(O_2)$, $f(S_2)$, pH, fluid:rock ratio) were locally variable. The control which bulk rock composition has on the chlorite composition, is also illustrated in Fig.6.4(c). This shows that there is a positive relationship between increasing bulk rock X_{Fe} and chlorite X_{Fe} in the hangingwall metabasalt.

Chlorites from two high hangingwall metabasalt samples (150 - 200 m above the VCR) have lower Al/(Al+Fe+Mg) contents compared to the chlorites from the metabasalt samples close to (i.e. <20 m above) the VCR (Fig.7.1.2). The reason that the metabasalt samples close to the VCR have a higher Al content is probably the result of leaching of mobile elements during metasomatic alteration (see Chapter 6.).

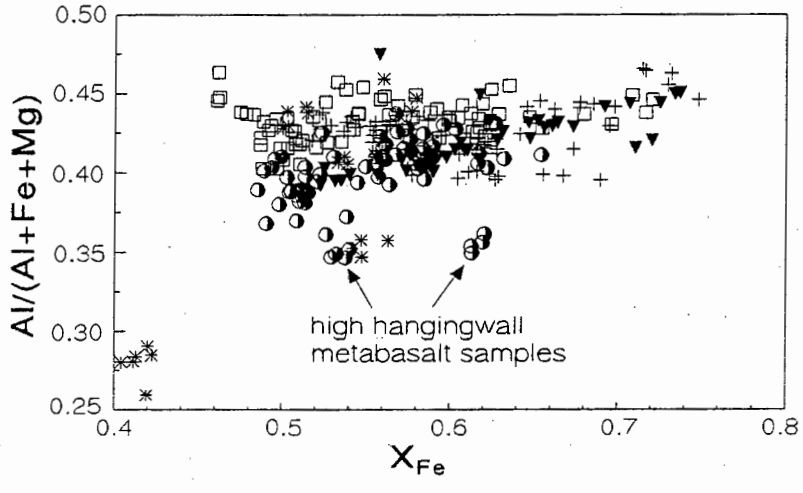

Fig.7.1.2: Plot of Al/(Al+Fe+Mg) vs X_{Fe} ratios of chlorites from different rock types. For symbols see Fig.7.1.1.

The chlorite compositions from five dyke samples were analysed and their differences are reflected in the different groupings of the chlorites (Fig.7.1.2). The chlorite compositions in one dyke sample in particular are significantly different (X_{Fe} = 0.42 and low Al/(Al+Fe+Mg)) from those in the other dyke samples.

Most of the chlorites plotted in Fig.7.1.3 have X_{Chl} contents >0.8, which indicates the tendency towards a trioctahedral chlorite structure. Chlorites with X_{Chl} <0.8 are present in all the rock types (especially in the pseudotachylites), which is probably due to varying amounts of mixed-layer clays within those chlorites. This is supported by the elevated K_2O contents of some of the footwall chlorite analyses, which suggests contamination with small amounts of intergrown muscovite. The low X_{Chl} contents of these chlorites therefore indicate that the chlorites did not equilibrate completely with the chlorite-forming fluid. This also explains the apparently low temperatures of 215 - 250°C, which should not mistakenly be identified for a lower-temperature group of chlorites. The majority of the chlorites have a calculated temperature of chlorite formation of 260 - 340°C, with a mean temperature of 307°C.

The trend of increasing X_{Chl} with increasing temperature (as described by Schiffman and Fridleifsson (1991) in interlayered chlorite/smectite clays in Icelandic metabasalts) is shown by the chlorites from the pseudotachylite/ultramylonite and the quartz vein samples. It is unlikely that chlorites from, for example, different pseudotachylite samples were formed under significantly different temperatures. This suggests that the large range in temperatures shown by these chlorites is probably due to incomplete equilibration between the chlorite and the fluid.

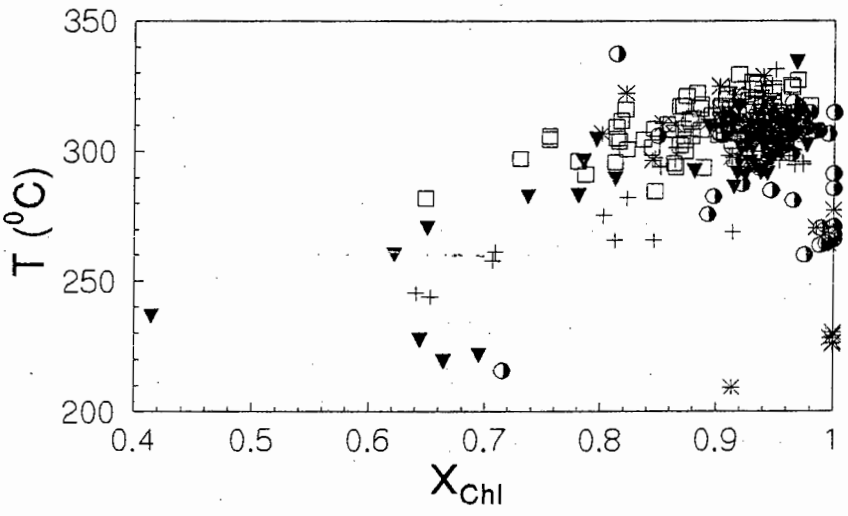

Fig.7.1.3: Plot of calculated temperature of chlorite formation (after Zang and Fyfe, 1995) vs chlorite content X_{Chl} (after Robinson *et al.*, 1993). For symbols see Fig.7.1.1.

The range in X_{Fe} of chlorites within and between three chloritised footwall quartzite samples, collected several hundreds of metres apart, is shown in Fig.7.1.4. In samples VHG058 and VHG096 the chlorites show a relatively narrow range of X_{Fe} ratios, but a considerable range in X_{Fe} of between 0.63 - 0.72 is shown by the chlorites in sample VHG170. The wide range in X_{Fe} of chlorites in the latter sample suggests that the factors determining Fe-Mg substitution in chlorite were locally controlled on a thin section scale.

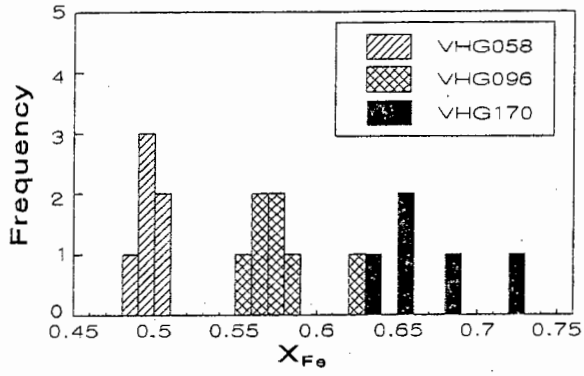

Fig.7.1.4: Histogram of X_{Fe} of chlorite analyses from three different chloritised footwall quartzite samples, showing the range in X_{Fe} within and between samples.

Two petrographically distinct chlorite populations with bluish and brownish interference colours, respectively, have been identified in a bedding-parallel quartz vein at the VCR-footwall contact (sample VHG169) (Fig.7.1.5). The mean X_{Fe} of these two chlorite populations are not significantly different (X_{Fe} = 0.67 and 0.71) (Table 7.1.2). However, the 'blue' and the 'brown' chlorite populations have very different Al^{IV} contents, which suggests that the Al^{IV} content, rather than the X_{Fe} ratio, is related to the interference colours shown by these chlorites. Furthermore, it also implies that the two chlorite populations were formed at different temperatures but under similar $f(O_2)$ and $f(S_2)$. A mean X_{Fe} of 0.69 was used to calculate the temperatures at given Al^{IV} contents in Table 7.1.2.

Table 7.1.2: Average XFe, Al(IV) and T of Chlorites in Sample VHG169

	XFe	Al(IV)	T (°C)
'Brown' Chlorite (n=8)	0.71±0.03	1.31±0.05	261±11
'Blue' Chlorite (n=7)	0.67±0.02	1.47±0.04	299±10

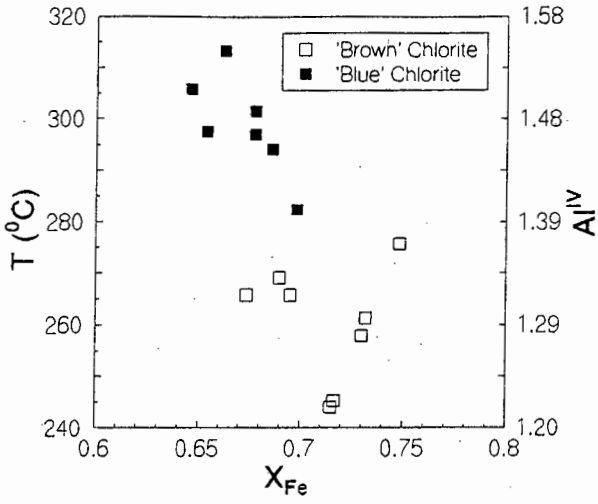

Fig.7.1.5: Plot of calculated temperature of chlorite formation (after Zang and Fyfe, 1995) and Al^{IV} content vs X_{Fe} of two, petrographically distinct, chlorite populations in bedding-parallel quartz vein sample VHG169.

The chlorite compositions in 46 VCR metaconglomerate and quartzite samples were also examined. In the data presentation below, however, only the most important textural and mineralogical associations, namely type II and type IV chlorites, as well as gold- and pyrite-associated chlorites, are illustrated. Average analyses of these chlorites are given in Table 7.1.3. Types III and V chlorites do not differ significantly in compositions from type II chlorites.

All except two of the VCR chlorites have >9.8 non-interlayer cations (Fig.7.1.6) which implies that the VCR chlorites, irrespective of mineralogical or textural association, are virtually ideal trioctahedral chlorites without any clay interlayers. The VCR chlorites show a very similar range in composition as the chlorites from the other rock types (compare with Fig.7.1.1).

Table 7.1.3: Average VCR Chlorite Compositions with Different Mineral/Textural Associations (wt%)

Chlorite Type	Type II			Type IV		Type V		Pyrite Chlorite		Gold Chlorite	
Sample	VHG041	VHG062	VHG070	VHG062	VHG103	VHG088	VHG162	VHG046	VHG062	VHG062	VHG091(B)
No. Analyses	(6)	(5)	(6)	(5)	(5)	(2)	(4)	(5)	(4)	(6)	(5)
SiO2	23.82	25.29	24.04	24.72	24.40	24.19	23.42	23.25	25.03	24.76	24.69
TiO2	bd	0.06	bd	bd	bd	bd	bd	bd	0.02	bd	0.23
Al2O3	22.51	25.76	24.65	26.90	25.78	24.28	24.82	22.42	25.65	26.20	25.50
Cr2O3	bd	bd	0.04	bd	bd	bd	bd	0.21	0.16	0.13	0.05
FeO*	35.09	24.10	31.15	24.55	24.85	29.14	35.62	37.70	24.68	24.30	25.84
MnO	0.19	0.21	0.14	0.20	0.20	0.15	0.13	0.13	0.17	0.24	0.30
MgO	8.13	14.11	10.72	14.06	13.89	11.93	7.37	6.50	14.12	14.23	11.69
CaO	0.02	0.09	0.03	0.05	bd	bd	0.01	0.02	bd	0.02	0.03
Na2O	0.02	0.04	bd	0.04	bd	bd	bd	bd	bd	0.02	0.02
K2O	bd	bd	bd	bd	0.01	bd	bd	bd	bd	bd	bd
Total	89.78	89.66	90.77	90.52	89.13	89.69	91.37	90.23	89.83	89.90	88.35
Si(IV)	2.58	2.57	2.51	2.49	2.51	2.53	2.49	2.55	2.55	2.52	2.58
Al(IV)	1.42	1.43	1.49	1.51	1.49	1.47	1.51	1.45	1.45	1.48	1.42
Al(VI)	1.46	1.66	1.55	1.69	1.64	1.53	1.60	1.45	1.63	1.65	1.71
Ti	0.00	0.00	0.00	0.00	0.00	0.00	0.00	0.00	0.00	0.00	0.02
Cr3+	0.00	0.00	0.00	0.00	0.00	0.00	0.00	0.02	0.01	0.01	0.00
Fe2+	3.18	2.05	2.72	2.07	2.14	2.55	3.17	3.46	2.10	2.07	2.25
Mn2+	0.02	0.02	0.01	0.02	0.02	0.01	0.01	0.01	0.01	0.02	0.03
Mg	1.31	2.14	1.67	2.11	2.13	1.86	1.17	1.06	2.14	2.16	1.82
Ca	0.00	0.01	0.00	0.01	0.00	0.00	0.00	0.00	0.00	0.00	0.00
Na	0.00	0.01	0.00	0.01	0.00	0.00	0.00	0.00	0.00	0.00	0.00
K	0.00	0.00	0.00	0.00	0.00	0.00	0.00	0.00	0.00	0.00	0.00
Fe/(Fe+Mg)	0.71	0.49	0.62	0.49	0.50	0.58	0.73	0.76	0.50	0.49	0.55
Al/(Al+Fe+Mg)	0.39	0.42	0.41	0.43	0.42	0.40	0.42	0.39	0.42	0.43	0.44
T (°C) **	285	307	308	323	319	307	302	287	312	319	301
XChl	0.98	0.88	0.97	0.91	0.93	0.97	1.00	0.99	0.91	0.91	0.85
i/l cat	0.01	0.02	0.00	0.01	0.00	0.00	0.00	0.00	0.00	0.01	0.01
non-i/l	9.97	9.87	9.96	9.90	9.92	9.97	9.95	9.99	9.90	9.91	9.83

bd: below detection XChl: chlorite content i/l cat: interlayer cations non i/l: non-interlayer cations

* all Fe as FeO ** temperature calculated after Zang and Fyfe (1995)

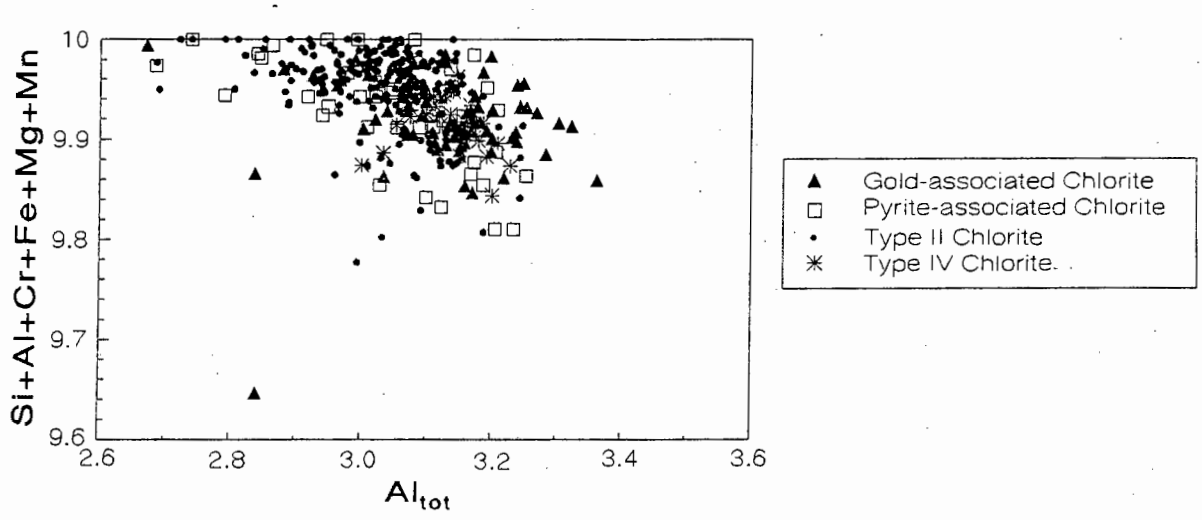

Fig.7.1.6: Plot of the sum of non-interlayer cations vs total Al content for selected VCR chlorites.

The large range in X_{Fe} which is present in type II chlorites and in the pyrite- and gold-associated chlorites is illustrated in Fig.7.1.7. Both type II chlorites and pyrite-associated chlorites show the same range in composition, and textural evidence supports the coeval formation of these chlorites. Although the majority of the gold-associated chlorites are Mg-rich (X_{Fe} <0.55), some of them have X_{Fe} ratios as high as 0.71. No distinction can be made either texturally or chemically between type II, pyrite- or gold-associated chlorites, which suggests that all these chlorites were formed at the same time. In contrast, type IV chlorites are younger than type II chlorites and grew in a different stress field. Their compositional range is more restricted (Mg-rich) (X_{Fe} = 0.43 - 0.55) than that of the other VCR chlorites.

The Al/(Al+Fe+Mg) ratios of the VCR chlorites are similar to those from the footwall quartzites and the hangingwall metabasalts (Fig.7.1.2). It is interesting to note, however, that the X_{Fe} and Al/(Al+Fe+Mg) ratios show a negative correlation in the VCR chlorites but a positive correlation in the other rock types (Fig.7.1.2).

All except two of the VCR chlorites have X_{Chl}>0.8 and show a temperature range of 260 - 340°C with a mean of 307 ± 14°C (Fig.7.1.8). This temperature is the same as that of the chlorites from the other rock types (Fig.7.1.3). In contrast to the wide range in X_{Chl} of the pseudotachylite-chlorites (Fig.7.1.3), the narrow range in X_{Chl} in the VCR chlorites implies that these latter chlorites contain only very small, if any, amounts of interlayered clays.

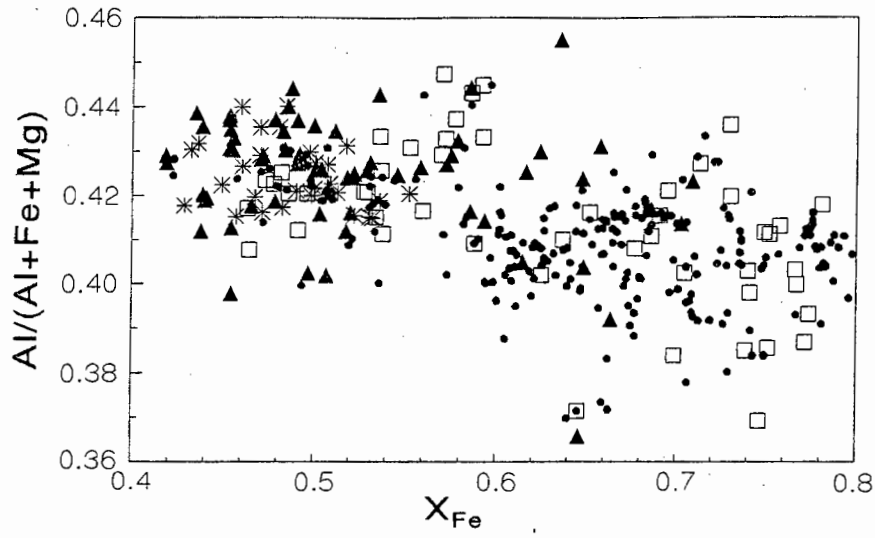

Fig.7.1.7: Plot of Al/(Al+Fe+Mg) vs X_{Fe} of selected VCR chlorites. For symbols see Fig.7.1.6.

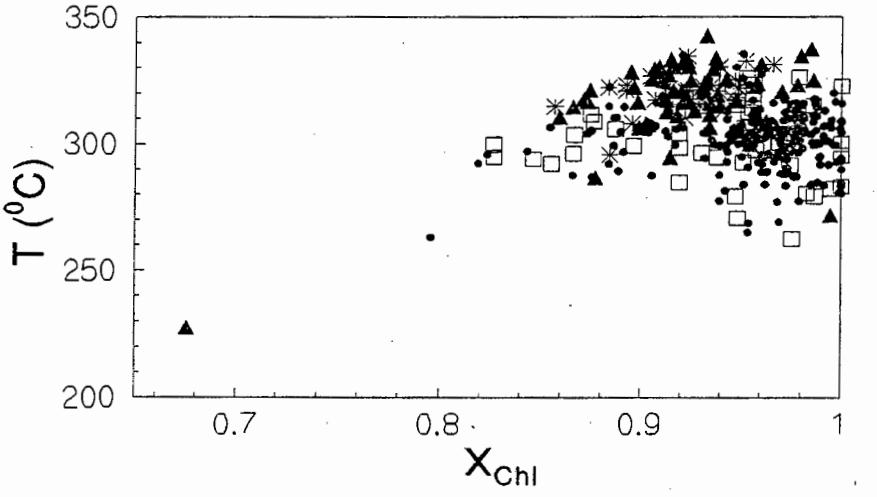

Fig.7.1.8: Plot of calculated temperature of chlorite formation (after Zang and Fyfe, 1995) vs chlorite content X_{Chl} (after Robinson *et al.*, 1993).
For symbols see Fig.7.1.6.

The compositional range in Al^{IV} and X_{Fe} of chlorites with different mineral/textural associations in VCR sample VHG074 illustrates a positive correlation between these two parameters (Fig.7.1.9). The compositional similarity between the gold-associated chlorites and type II

chlorites on a thin section scale supports evidence given in Chapter 4. of these two chlorite types having been formed during the same alteration event. However, the large range in X_{Fe} ratios shown by the chlorites in this sample implies that the factors controlling Fe-Mg substitution in the chlorites (i.e. $f(O_2)$, $f(S_2)$) were highly localised.

The four chlorites from a portion of footwall quartzite in contact with the VCR have X_{Fe} ratios which overlap with those of the VCR chlorites. This suggests that the chlorites in the chloritised footwall quartzite and those in the VCR were formed under the same $f(O_2)$ and $f(S_2)$ conditions, as both are in textural equilibrium with pyrite.

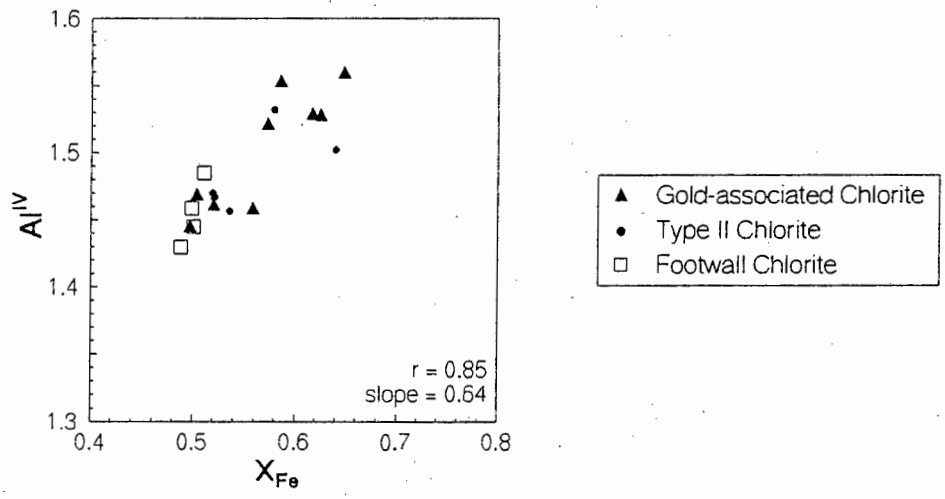

Fig.7.1.9: Plot of Al^{IV} vs X_{Fe} content of VCR and footwall quartzite chlorites (of presumably the same generation) in sample VHG074, showing a positive correlation between Al^{IV} and Fe/Mg contents.

The range in X_{Fe} and Al^{IV} in four gold-bearing VCR samples is shown in Fig.7.1.10. Chlorites from some samples show large ranges in both X_{Fe} and Al^{IV} (e.g. samples VHG062 and VHG125), whereas chlorites in other samples vary either only in their X_{Fe} or in their Al^{IV} contents (e.g. samples VHG088 and VHG164, respectively). The variable X_{Fe} ratios within and between samples are similar to those observed in the footwall quartzites (Fig.7.1.4) and can best be explained by locally variable chemical conditions of the fluid.

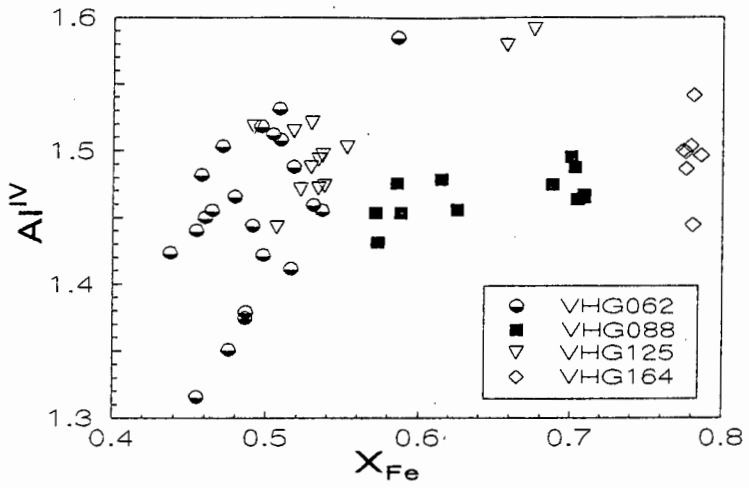

Fig.7.1.10: Plot of Al^{IV} vs X_{Fe} illustrating the wide range in Al^{IV} and/or X_{Fe} present in chlorites in four VCR samples.

A plot of Al^{IV} versus X_{Fe} of chlorite analyses from four samples across a VCR channel, illustrated in Plate 7.1.1, is shown in Fig.7.1.11. At this locality (1350 N1 Raise 8 North Ledging), an irregular yellow-green Fe-metasomatised zone extended laterally for a distance of metres to tens of metres within the VCR metaconglomerate/quartzite.

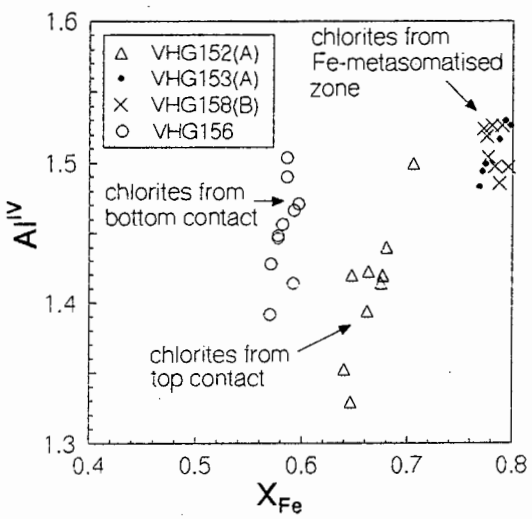

Fig.7.1.11: Plot of Al^{IV} vs X_{Fe} of chlorite analyses from 4 samples of Fe-metasomatised VCR shown in Plate 7.1.1. Note the small compositional range in the Fe-rich chlorites compared to the larger range in the more magnesian VCR type II chlorites.

Plate 7.1.1: 2m thick VCR channel showing an irregular yellow-greenish Fe-metasomatised alteration zone. Samples for chlorite EMP analyses are as indicated. Minor channelling into the f ootwall quartzite is visible on the right hand side, as is a dark grey/ black angular quartzite boulder in the middle-lower left hand side of the VCR. The darkened top contact with the hangingwall metabasalt and the lowermost 1 m of dark grey VCR quartzite towards the bottom contact with the footwall are also visible. (locality: 1350 N1 Raise 8 North Ledging, scale rule = 1m).

The chlorites in the Fe-metasomatised zone (which contains 5 vol% siderite) are Fe-enriched (X_{Fe} = 0.78 - 0.80) compared to the the chlorites from the top and bottom VCR contacts (X_{Fe} = 0.56 - 0.70). These Fe-rich chlorites are compositionally more restricted in their Al^{IV} contents and X_{Fe} ratios when compared to the "normal" VCR type II chlorites, the latter showing large variations especially in Al^{IV} content. Underground observations suggest that these Fe-metasomatised zones occur sporadically within the VCR.

7.2 Carbonates

7.2.1 Introduction

The composition of carbonates was determined by EMP analysis (for operating conditions and standards used see Appendix C). The samples which were investigated included three Fe-metasomatised, siderite-rich VCR samples, two hangingwall metabasalt samples, two quartz/calcite veins, two pseudotachylite ± calcite vein samples and two fault-associated quartz/calcite veins from two major extensional faults (with displacements of up to 200 m).

7.2.2 Analytical Results

The mean compositions of carbonates from different rock types are given in Table 7.2.1. Except for the carbonates in the Fe-metasomatised sample VHG164, no significant intra-sample compositional variation exists between the carbonates (see below). The carbonate compositions from the samples, except those from the VCR, are shown in Fig.7.2.1. Irrespective of the different bulk rock compositions, all the carbonates in metabasalt, quartz/calcite vein, pseudotachylite and in the fault rock samples are calcitic in composition (Fig.7.2.1). The calcite contains minor to trace amounts of Fe, Mg and Mn, the contents of these being slightly higher in the metabasalts.

Table 7.2.1: Average Carbonate Analyses from Different Rock Types (wt%)

Lithology	Metabasalt	Quartz Vein	Fault Zone	Fe-metas. VCR	Fe-metasomatised VCR		
Sample No.	VHG045	VHG137	VHG178(A)	VHG158(B)	VHG164		
No. Analyses	(n=7)	(n=6)	(n=8)	(n=6)	Cc Vein (n=3)	Ankerite (n=4)	Siderite (n=15)
CaCO3	94.15	96.72	97.93	0.38	95.56	49.75	0.55
FeCO3	2.73	1.26	0.39	97.93	1.34	31.88	95.36
MgCO3	1.43	0.70	0.24	0.46	0.00	16.05	2.49
MnCO3	1.46	0.67	1.10	0.98	2.88	2.78	1.34
Total	99.77	99.35	99.66	99.75	99.78	100.46	99.74

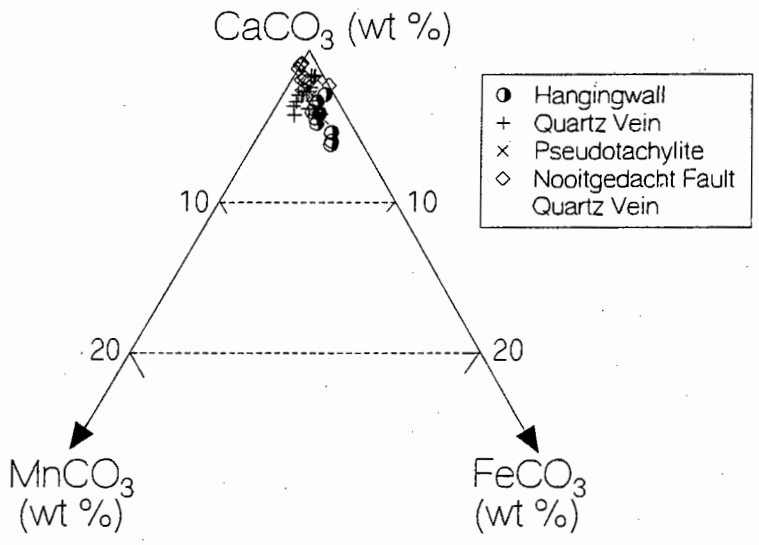

Fig.7.2.1: Ternary $CaCO_3$-$FeCO_3$-$MnCO_3$ compositional plot of calcite from different rock types.

The compositional range of siderite in samples VHG153(A) and VHG158(B), both from the Fe-metasomatised VCR profile (Plate 7.1.1), indicates the presence of nearly pure siderite with only very small amounts of Mg, Mn and Ca (Fig.7.2.2). In contrast, both ankerite and siderite occur together in Fe-metasomatised sample VHG164 (see Table 7.2.1 for mean compositions).

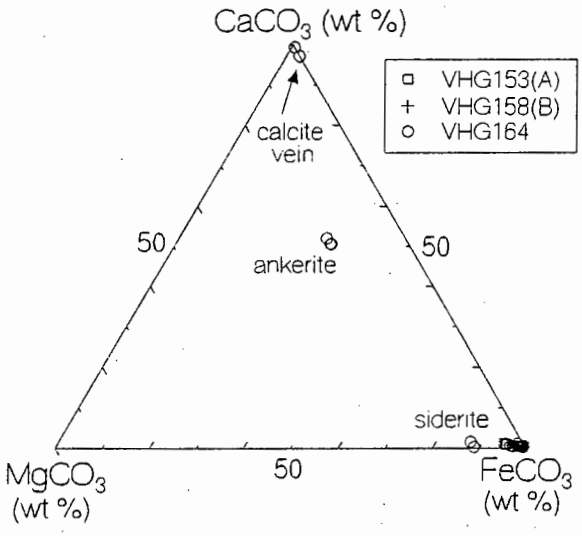

Fig.7.2.2: Ternary $CaCO_3$-$FeCO_3$-$MgCO_3$ compositional plot of carbonates from three Fe-metasomatised VCR samples.

Calcitic veins/shear zones occur in addition to the siderite and ankerite grains in sample VHG164. The presence of this later calcite generation indicates that a Ca-metasomatic event has affected this sample. Further evidence for this is also found by the presence of ankerite grains (interpreted to represent partially calcitised siderite grains) and the zonation of siderite grains. One siderite grain in particular in this sample shows a sharp increase in Mg and Ca towards the rim and a decrease in Fe and Mn over the same interval (Fig.7.2.3), thereby supporting partial calcitisation by a localised metasomatic event.

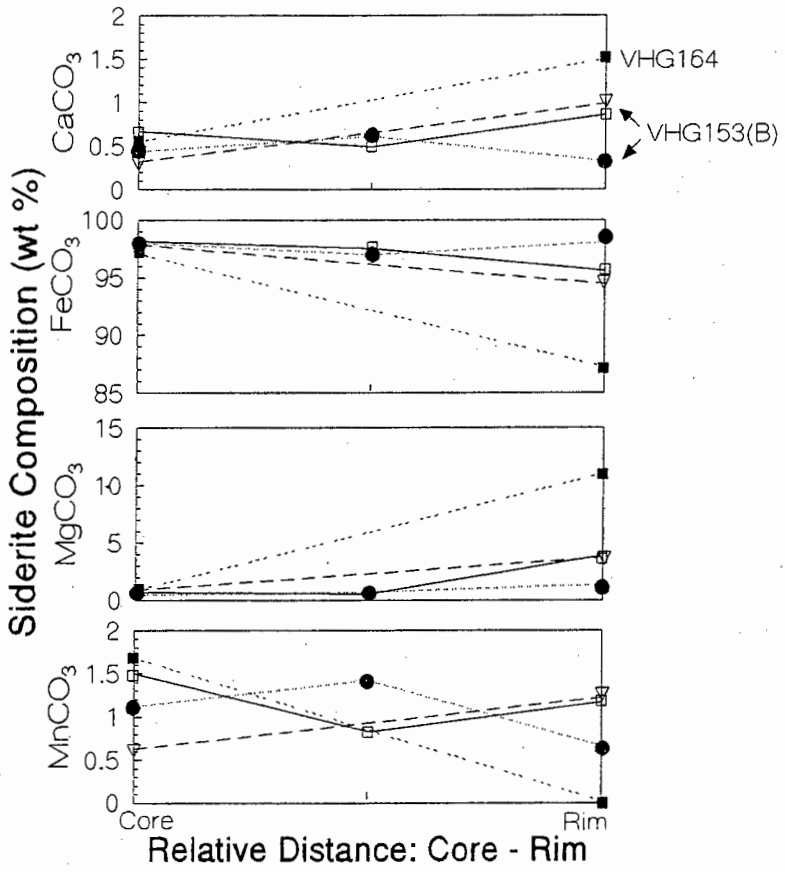

Fig.7.2.3: Compositional core-rim zonation of four siderite grains.

The core-rim zonations of three siderite grains from sample VHG153(A) in Fig.7.2.3 indicate that Fe generally decreases slightly and Mg increases slightly towards the rim. Ca and Mn, although showing a positive correlation with each other, have variable trends from core to rim. Overall, however, the rims of these siderite grains are not as Mg/Ca-enriched as that of the grain in sample VHG164, suggesting that Ca-metasomatism has not affected sample VHG153(A).

7.3 Gold

7.3.1 Previous Studies

Several workers have analysed the composition of Witwatersrand gold particles over the past decades (e.g. Saager, 1969; Utter, 1979; von Gehlen, 1983; Oberthür and Saager, 1986; Reid *et al.*; 1988; Frimmel *et al.*, 1993) using various preparation and analytical techniques. The reported Ag and Hg concentrations in gold particles range from 3 - 32 wt% Ag and 0.3 - 6.0 wt% Hg (von Gehlen, 1983; Hallbauer, 1986; Reid *et al.*, 1988). No element impurities except for Ag and Hg have been detected in Witwatersrand gold particles, despite the analysis of gold particles with a proton microprobe (Frimmel, 1994). The semi-quantitative identification of trace amounts of other elements (e.g. Cu, Ni, Co, Mn, Fe, Mo, Bi, Pb, As, Sb) in some gold particles (Feather and Koen, 1975) is probably due to the presence of tiny mineral inclusions within these gold particles and does not necessarily reflect compositional variations of the gold particles.

No core-rim zonation (as has been described for gold particles from modern-day placer deposits, e.g. Groen *et al.*, 1990; Santosch *et al.*, 1992) has yet been detected in Witwatersrand gold particles. Instead, individual gold particles are homogeneous within the precision of the analytical technique (analytical error = ± 0.2 wt% for EMP analysis) (e.g. Frimmel *et al.*, 1993). However, a variation in gold fineness between gold particles has been identified by several researchers. Gold fineness (or silver content) is calculated by F = Au x 1000/(Au+Ag) (elements in wt%). Oberthür and Saager (1986) found that the fineness of gold particles from the Carbon Leader Reef (Carletonville goldfield) remained relatively constant over tens of metres, but that significant variations existed on a larger (hundreds of metres) scale. Similarly, Utter (1979) reported large variations of gold fineness in gold particles from different reefs in the Klerksdorp goldfield. Reid *et al.* (1988) also reported significant variations in fineness between gold particles from different Vaal Reef samples (Klerksdorp goldfield).

7.3.2 Analyses of Gold Particles from the VCR

The variation in composition of gold particles was examined on three scales, namely (i) intra-grain variation (micrometre scale), (ii) intra-sample variation (centimetre scale) and (iii) between samples (scale of tens to hundreds of metres).

A total of 349 gold particles from 19 polished sections from the VCR quartzite/ metaconglomerate and 2 polished sections from an auriferous quartz vein were analysed for Au, Ag and Hg using a Cameca (Camebax) electron microprobe at the Department of Geological Sciences at the University of Cape Town. The maximum size of the gold particles analysed was 1.5 mm (from the auriferous quartz vein), but the average VCR gold particle size was 5 - 10 µm. The analytical procedure employed is the same as that described by Reid *et al.* (1988) and the operating conditions and standards used are outlined in Appendix C.

7.3.3 Analytical Results

Gold particles from the VCR vary in composition from 82.51 - 92.88 wt% Au, 6.03 - 11.16 wt% Ag and 0.64 - 5.82 wt% Hg (Fig.7.3.1). The average compositions of gold particles from 94 Vaal Reef samples (after Reid *et al.*, 1988) are given as a comparison to the VCR samples. This was done so that a comparison could be made between the composition of gold particles which come from different conglomerates horizons within the same goldfield. Gold particles from the VCR have a lower mean Au content (and therefore a lower fineness) than the Vaal Reef gold particles. The Ag content of the gold particles in both reefs is similar, although the Ag content in the Vaal Reef samples is skewed more towards the right.

A significant difference between the gold particles from these two reefs, however, is the Hg content. The VCR gold particles contain, on average, twice as much Hg as the Vaal Reef gold particles.

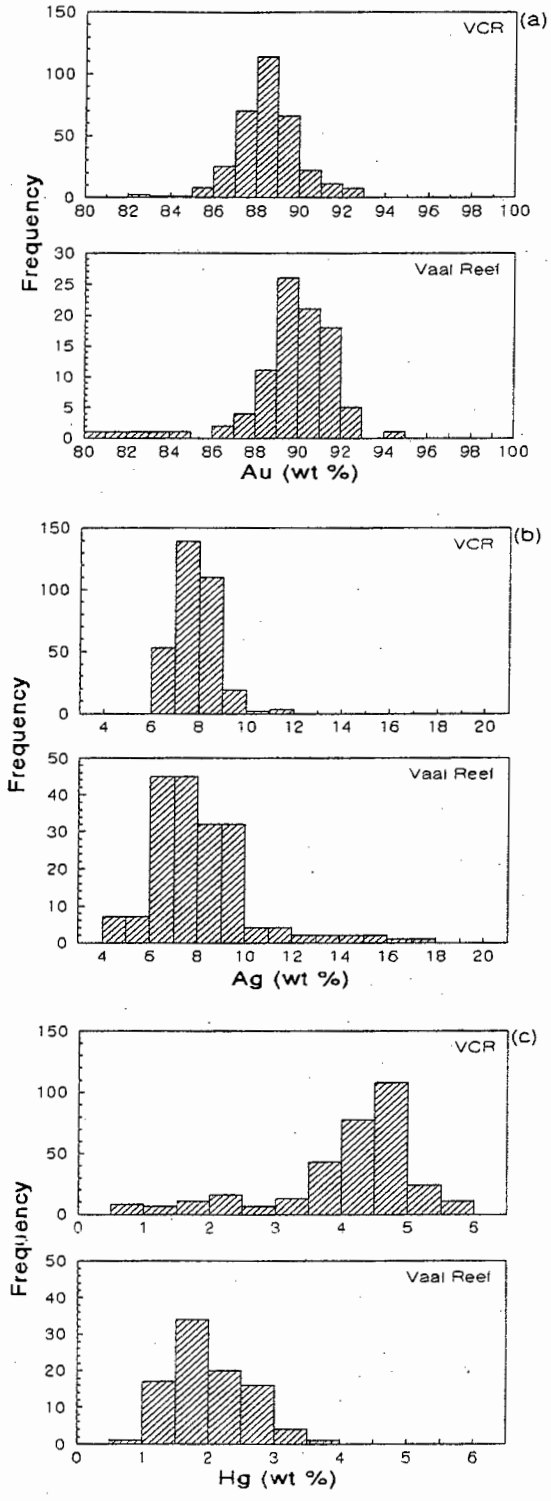

Fig.7.3.1: Histogram of weight per cent composition of (a) Au, (b) Ag and (c) Hg of 349 individual gold particles from the VCR (this study) and the average of gold particles from 94 Vaal Reef samples (after Reid *et al.*, 1988) from the Klerksdorp goldfield.

Unlike the wide range in gold fineness of gold particles from the VCR, as reported by Utter (1979), gold particles from the VCR at Vaal Reefs No.10 Shaft appear to have a very restricted range in fineness of 881 - 939 (Fig.7.3.2). Unfortunately it is not reported exactly where the gold particles for Utter's study were collected.

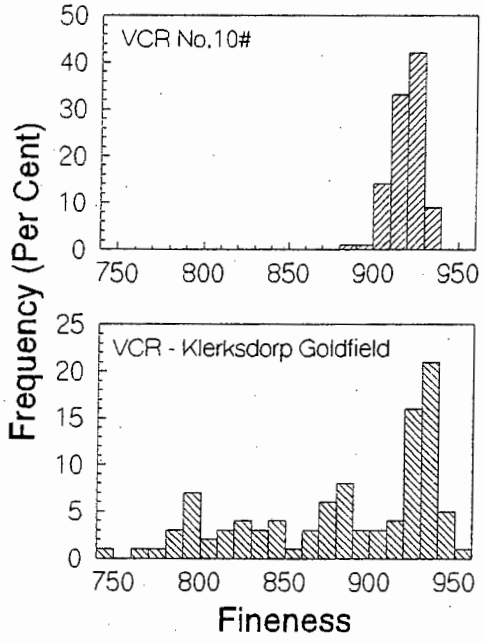

Fig.7.3.2: Histogram comparison of gold fineness from the VCR No.10 Shaft (this study) and VCR from other localities in the Klerksdorp goldfield (after Utter, 1979).

Although no distinct compositional zonation of individual gold particles was detected, two gold particles from the auriferous quartz vein (sample VHG163(B)) are compositionally inhomogeneous with respect to Au and Ag (Table 7.3.1) and the intra-grain compositional variation is shown in Fig.7.3.3. These findings contrast with previous results published by Reid *et al.* (1988) and Frimmel *et al.* (1993) who found individual gold particles to be homogeneous on a grain scale.

Table 7.3.1: Intra-grain Compositional Inhomogeneity of Two Gold Particles (Sample VHG163(B))

	Grain 1			Grain 2		
Analysis	1.	2.	3.	1.	2.	3.
Au	88.15	84.38	84.44	87.74	85.40	86.66
Ag	8.23	10.18	10.09	9.21	10.55	8.73
Hg	4.14	4.27	4.32	3.91	4.33	3.85
Total	100.52	98.83	98.85	100.86	100.28	99.24
Fineness	915	892	893	905	890	908

Analyses in wt %

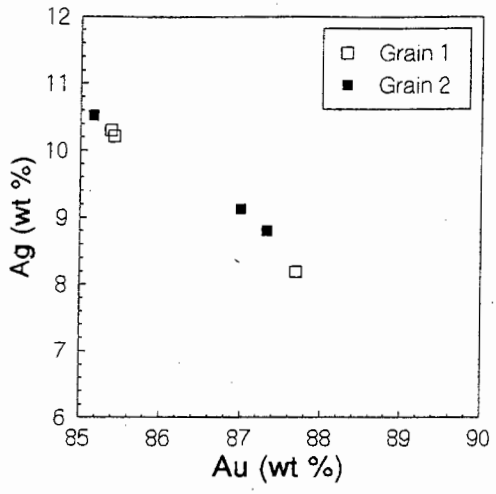

Fig.7.3.3: Plot of Au vs Ag contents (wt%) illustrating the inhomogeneous composition of two gold particles from the auriferous quartz vein (sample VHG163(B)). (analytical totals normalised to 100 wt%).

The variation in composition of gold particles within and between four VCR samples is shown in Fig.7.3.4. A relatively narrow compositional range of Ag and Hg is shown by gold particles from sample VHG062 (Fig.7.3.4(a)), except for one quartz grain-associated gold particle with significantly lower Hg and higher Ag contents. Analyses of gold particles from the Fe-metasomatised VCR sample VHG164 (Fig.7.3.4(b)) indicate that these gold particles have a higher Ag content than the gold particles in sample VHG062 (Fig.7.3.4(a)). On a thin section scale in sample VHG164, the siderite-associated gold particles (Fig.7.3.4(b)) contain, on average, 1 wt% more Hg than the bitumen nodule-associated gold particles.

The extremely large compositional variation in Ag and Hg of gold particles from a VCR basal contact sample VHG074 is shown in Fig.7.3.4(c). A comparison between the compositions of gold particles associated with different minerals in that sample reveals that considerable variations exist in the composition of gold associated with both quartz and chlorite (Table 7.3.2).

Table 7.3.2: Composition of Gold Particles Associated with Different Minerals (Sample VHG074)

Gold Assoc.	Analysis	Mean	Min	Max
Quartz Grain (n=4)	Au	88.84	87.06	91.64
	Ag	6.73	6.49	7.02
	Hg	4.48	1.66	5.59
	Total	100.05	99.26	100.70
	Fineness	930	925	934
Type II Chlorite (n=8)	Au	84.93	82.51	87.38
	Ag	9.64	7.70	11.16
	Hg	5.40	5.06	5.77
	Total	99.96	99.00	101.31
	Fineness	898	881	919
Chlorite/ Quartz (n=7)	Au	88.14	87.23	89.83
	Ag	7.26	6.51	7.88
	Hg	5.20	4.28	5.58
	Total	100.60	100.07	101.19
	Fineness	924	917	932
Pyrite (n=4)	Au	90.82	89.45	92.88
	Ag	7.38	6.03	8.38
	Hg	1.52	0.83	2.12
	Total	99.71	98.86	100.11
	Fineness	925	914	939

Analyses in wt%

The two samples VHG062 and VHG093(B) (documented in Fig.'s 7.3.4(a) and (d), respectively) were collected c. 40 m apart from each other. A comparison of these two samples illustrates that the mean compositions of gold particles can change significantly over tens of metres. The large range in both Ag and Hg contents of the quartz- and undifferentiated chlorite/quartz-associated gold particles in sample VHG093(B) suggests that very little, if any, inter-grain homogenisation occurred after deposition/precipitation.

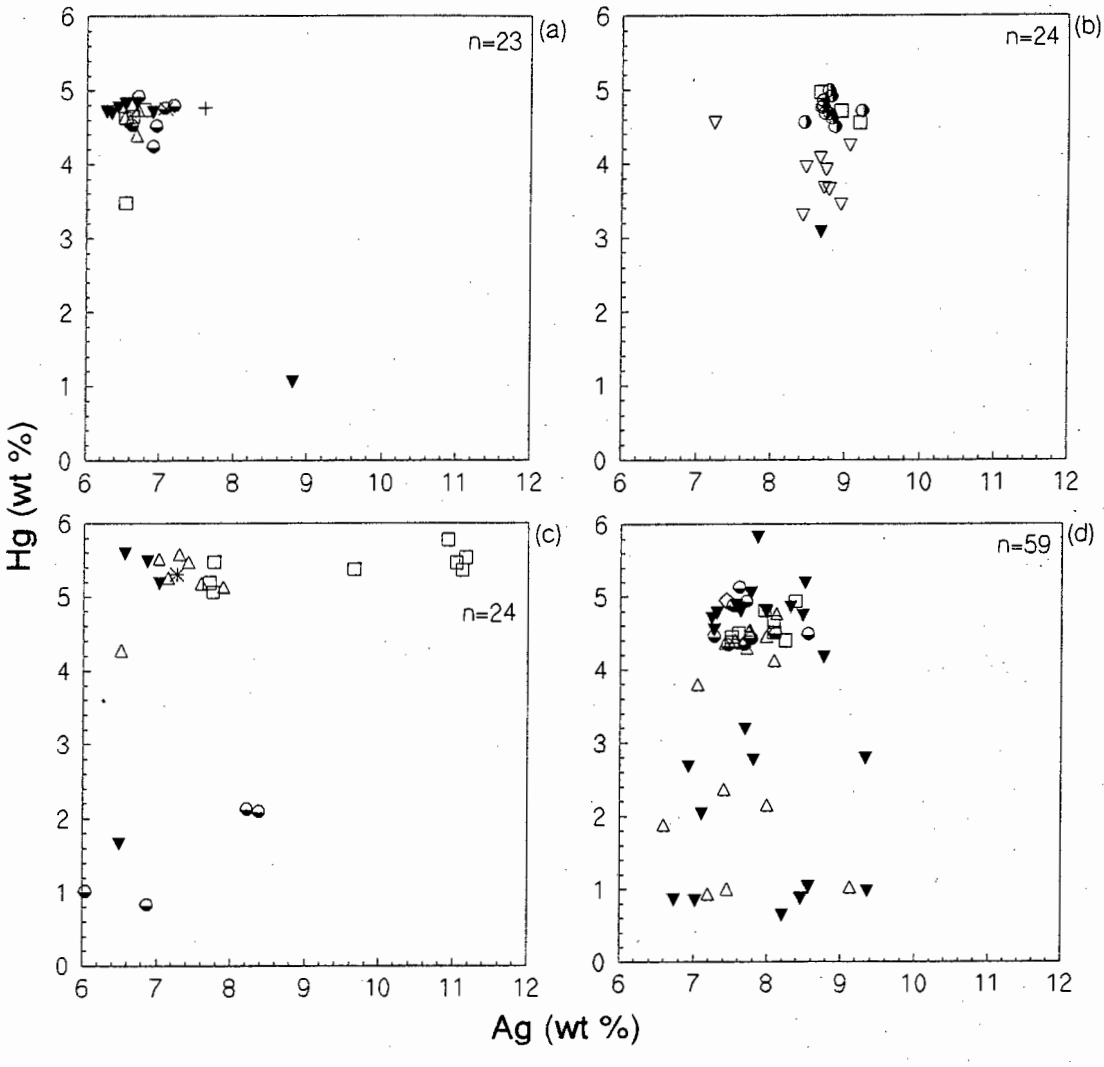

Fig.7.3.4: Plot of Ag vs Hg contents (wt%) of gold particles in samples (a) VHG062, (b) VHG164, (c) VHG074 and (d) VHG093(B).

The following symbols for gold-associations are used:

▼ Gold with Quartz	◒ Gold with Pyrite
□ Gold with Chlorite II	✳ Gold with Galena
+ Gold in Chlorite Vein	× Gold with Chalcopyrite
△ Gold in Chlorite/Quartz	◇ Gold in Pyrrhotite Vein
○ Gold along Quartz Grain Margin	◑ Gold with Siderite
	▽ Gold in Bitumen Nodule

Disregarding the one VCR sample showing the greatest compositional variability (sample VHG074, Fig.7.3.4(c)), the gold particles which are associated with type II chlorite and pyrite have very similar compositional ranges (Fig.7.3.5). Quartz grain-associated gold particles have Ag contents similar to those of chlorite- and pyrite-associated gold particles. However, some quartz grain-associated gold particles have as little as 0.6 wt% Hg. Average compositions for gold particles associated with quartz grains, type II chlorite and with pyrite are given in Table 7.3.3.

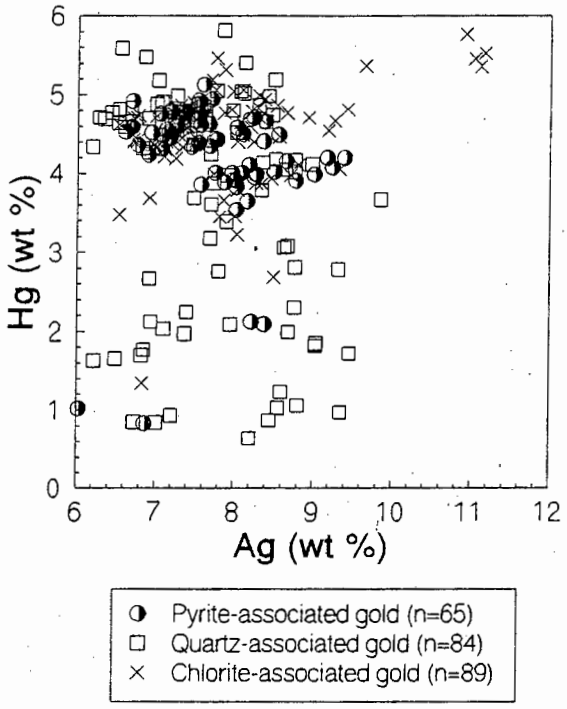

Fig.7.3.5: Plot of Ag vs Hg contents (wt%) of all quartz-, chlorite- and pyrite-associated gold particles in the VCR samples.

The compositional variation of 30 gold particles from two samples from the auriferous quartz vein is illustrated in Fig.7.3.6. The gold particles in sample VHG163(B) (mean compositions of multiple grain analyses are given) are associated with sphalerite/galena ± chlorite. In contrast, the gold particles in sample VHG163(C), collected approximately 40 cm away, are predominantly associated with galena and quartz. The distinctly different Ag contents of the

Table 7.3.3: Composition of Gold Particles Associated with Different Minerals

Gold Assoc.	Analysis	Mean	Min	Max	St. D.
Quartz (n=84)	Au	88.96	85.98	92.63	1.53
	Ag	7.73	6.19	9.85	0.87
	Hg	3.62	0.64	5.82	1.45
	Total	100.30	98.52	101.46	0.68
	Fineness	920	899	936	9
Type II Chlorite (n=89)	Au	87.99	82.51	91.71	1.52
	Ag	7.86	6.53	11.16	0.99
	Hg	4.51	1.35	5.77	0.61
	Total	100.36	98.60	101.49	0.71
	Fineness	918	881	932	11
Pyrite (n=65)	Au	88.41	86.07	92.88	1.19
	Ag	7.72	6.03	9.39	0.68
	Hg	4.23	0.83	5.13	0.8
	Total	100.36	98.52	101.47	0.74
	Fineness	920	902	939	7

Analyses in wt%

hydrothermal gold particles from these two samples suggests that the gold composition was locally controlled during gold precipitation and/or post-precipitation alteration processes and that very little inter-grain homogenisation has occurred after gold precipitation.

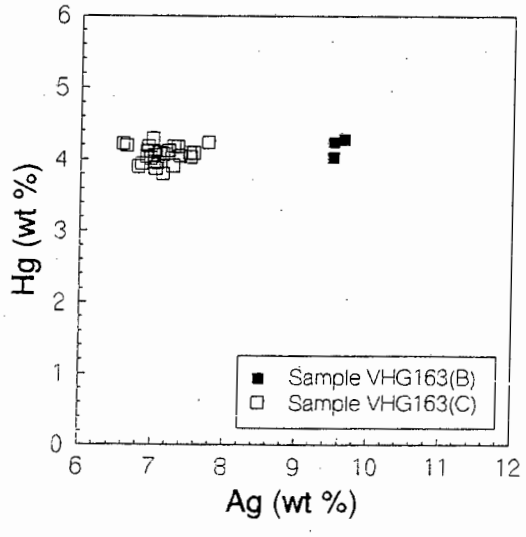

Fig.7.3.6: Plot of Ag vs Hg contents (wt%) of gold particles from samples VHG163(B) and VHG163(C) from the auriferous quartz vein.

8. Fluid Inclusion Study

8.1 Petrography

The focus of this part of the study was on the composition of the post-depositional fluids trapped in quartz (± calcite) veins and in the quartzite fraction of the VCR. Quartz-hosted fluid inclusions from six bedding-parallel, five bedding-perpendicular, from one auriferous quartz vein, from the Nooitgedacht Fault zone quartz vein as well as from seven VCR metaconglomerate/quartzite samples were examined. Some primary but mostly secondary fluid inclusions were identified.

Four distinct types of post-depositional fluid inclusions can be recognised (Fig.8.1(a)). Type I inclusions are monophase, liquid- or vapour-filled fluid inclusions. Most of these are probably the result of necking down, but some (such as several dark brownish fluid inclusions lying along a microfracture) have been observed in the auriferous quartz vein sample (VHG163(A)). No further work has been done on the type I fluid inclusions.

Type II fluid inclusions are the most abundant and consist of aqueous two-phase, liquid-rich fluid inclusions. They are present in hydrothermal quartz veins and occur either isolated, loosely grouped or along healed microfractures/fluid inclusion trails (Fig.8.1(d)). Although type II inclusions have variable liquid:vapour (L/V) ratios (<5 - >30 vol% by area), these are interpreted to reflect post-entrapment changes. The type II inclusions which were measured have L/V ratios of c. 5 - 15 vol% (as estimated at room temperature). Apart from the auriferous quartz vein sample where a second group of type II inclusions with L/V ratios >15 vol% was observed, no other type II inclusions with consistent L/V ratios with greater than c. 15 vol% were noted.

Secondary type II inclusions which occur isolated or in groups range in size from c. 2 μm to >15 μm (average of 5 - 6 μm). Type II fluid inclusions occurring along microfractures are commonly <5 μm in size and are slightly smaller than the isolated or grouped type II inclusions within the same sample. Type II inclusions vary in shape from anhedral rounded to subhedral angular to euhedral.

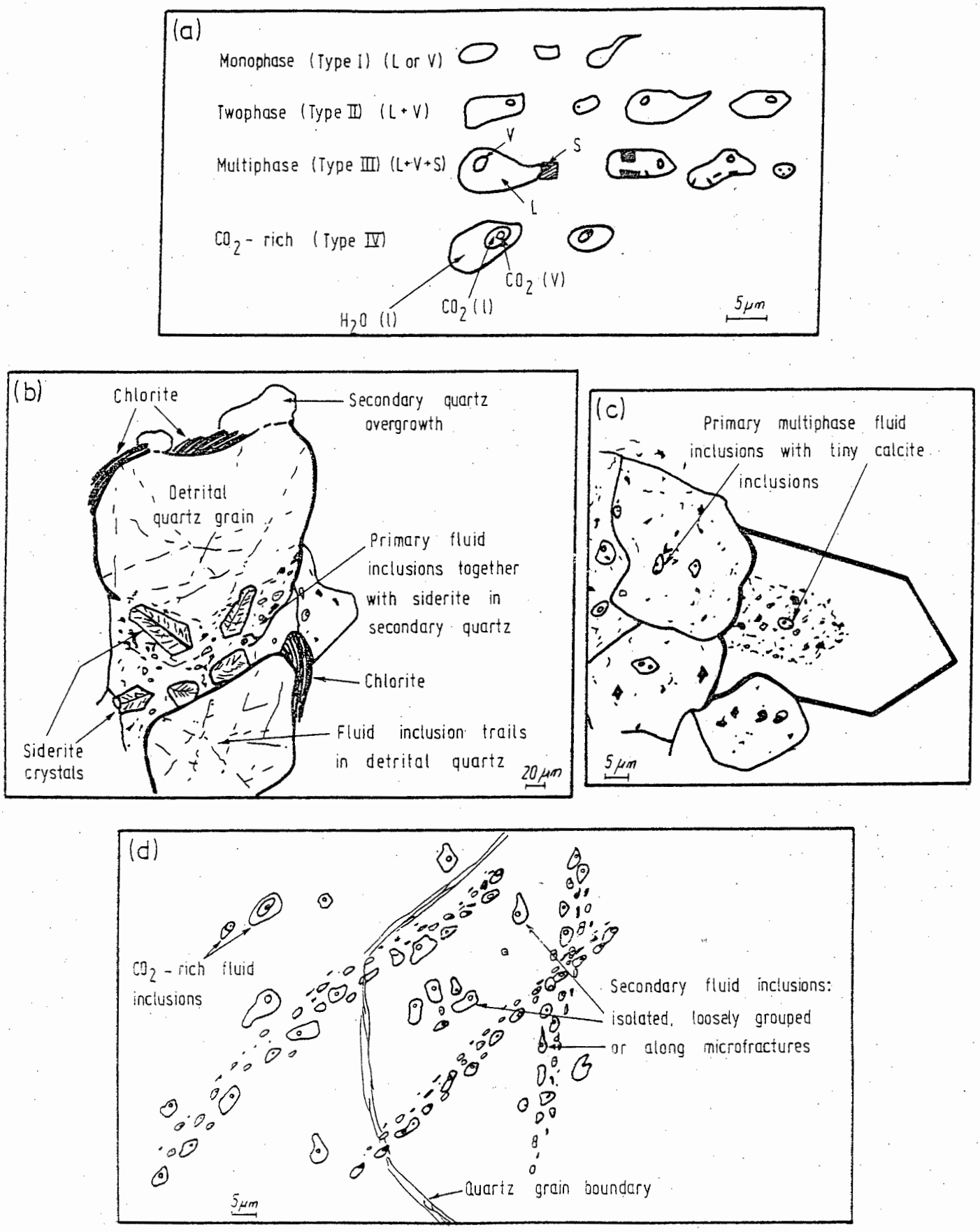

Fig.8.1: Fluid inclusion types and inclusion morphology.

Type III inclusions have been observed in several quartz vein and VCR samples together with type II inclusions. Type III inclusions differ from type II inclusions in that the former contain one or more solid inclusions. Apart from the solid inclusions, however, they have similar sizes, shapes and L/V ratios as type II inclusions. The solid inclusions are usually anisotropic, sometimes isotropic and very rarely opaque. They can be up to 3 μm in size and, based on the solid inclusion characteristics (e.g. birefringence, shape, habit), most of the solid inclusions are interpreted to be carbonate, white mica or chlorite. No true daughter crystals have been identified in any of the fluid inclusions.

Type IV fluid inclusions are CO_2 -rich inclusions which occur together with aqueous fluid inclusions in hydrothermal quartz veins (Fig.8.1(d)) and along quartz grain margins and/or as fluid inclusion trails within quartz grains in the VCR quartzite. Type IV fluid inclusions commonly have an elongate rounded shape and consist either of two or three phases (liquid H_2O, CO_2 -rich vapour ± liquid CO_2) at room temperature. They range in size from 3 - 15 μm and have variable CO_2/H_2O proportions. Type IV inclusions from the Nooitgedacht Fault zone (sample VHG178(B)) contain 60 - 85 vol% (by area) CO_2 and those from a bedding perpendicular quartz vein (sample VHG180) and VCR quartzite (sample VHG055(B)) contain 8 - 18 vol% CO_2.

Primary fluid inclusions can be subdivided into types II and III and were identified in authigenic/metamorphic quartz in VCR sample VHG158(B) and in the auriferous hydrothermal quartz vein (sample VHG163(A)). In VCR sample VHG158(B) the primary fluid inclusions occur together with metamorphic/metasomatic siderite crystals and tiny siderite inclusions in secondary quartz overgrowths around detrital quartz grains (Fig.8.1(b)).

In the auriferous quartz vein the primary type II and type III fluid inclusions occur in the central zone of euhedral quartz crystals and in associated fine grained anhedral quartz (Fig.8.1(c)). The primary type III inclusions contain one or more small (<2 μm), anisotropic, anhedral (rarely rhombohedral shaped) solid inclusions which are interpreted to be calcite (the latter being present as larger solid inclusions within the quartz grains). These solid inclusions do not dissolve on heating, which supports similar observations made by Robert and Kelly (1987) on the non-dissolution of carbonate crystals within fluid inclusions during heating.

8.2 Microthermometry

Investigations were carried out on a United States Geological Survey (U.S.G.S.) heating-freezing stage and experimental procedures are described in more detail in Appendix D. It has been shown that both the physical and the chemical character of a fluid inclusion may be changed after entrapment (e.g. Hall *et al.*, 1991). In order to avoid the influence of necking and other post-entrapment alteration, only those inclusions were taken into account which show constant L/V ratios along a given microfracture. Data was accepted only if their homogenisation temperature (T_h) and the final melting temperature (T_m) did not differ by more than 10^0C and 0.5^0C, respectively.

Due to the small size of some of the fluid inclusions along microfractures, isolated or loosely grouped fluid inclusions were also measured. No significant differences between isolated type II inclusions and type II inclusions occurring along microfractures within a sample were found. However, the isolated fluid inclusions generally showed a slightly greater range in T_m and T_h, possibly reflecting the influence of necking.

Duplicate temperature measurements of T_m, T_h and T_e (the eutectic, or first melting, temperature) were obtained on each measured fluid inclusion where possible. The salinity of the fluid was calculated from the revised equation of Bodnar (1993):

$$\text{salinity (wt\%)} = 1.78 \times T - 0.0442 \times T^2 + 0.000557 \times T^3,$$

where T is the depression of the freezing point (T_m) in degrees Celsius, and the salinity is expressed as weight per cent $NaCl_{equivalent}$.

The range in salinity and T_h of fluid inclusions from quartz veins and from the VCR are shown in Fig. 8.2. Little variation exists between fluid inclusions from the different quartz veins and the VCR and, in general, the fluid inclusions can be characterised as having a low salinity (generally <9 wt% $NaCl_{eq}$) (see Table 8.1). The T_h and salinity of individual aqueous fluid inclusions range from 80 - 256^0C and 1.05 - 13.72 wt% $NaCl_{eq}$, respectively. Some of the differences in T_h can be

attributed to variations in L/V ratios and the differences in salinity are (partly) accounted for by the accuracy of T_m measurements of $\pm 0.5^0$C (equivalent to ± 0.9 wt% $NaCl_{eq}$).

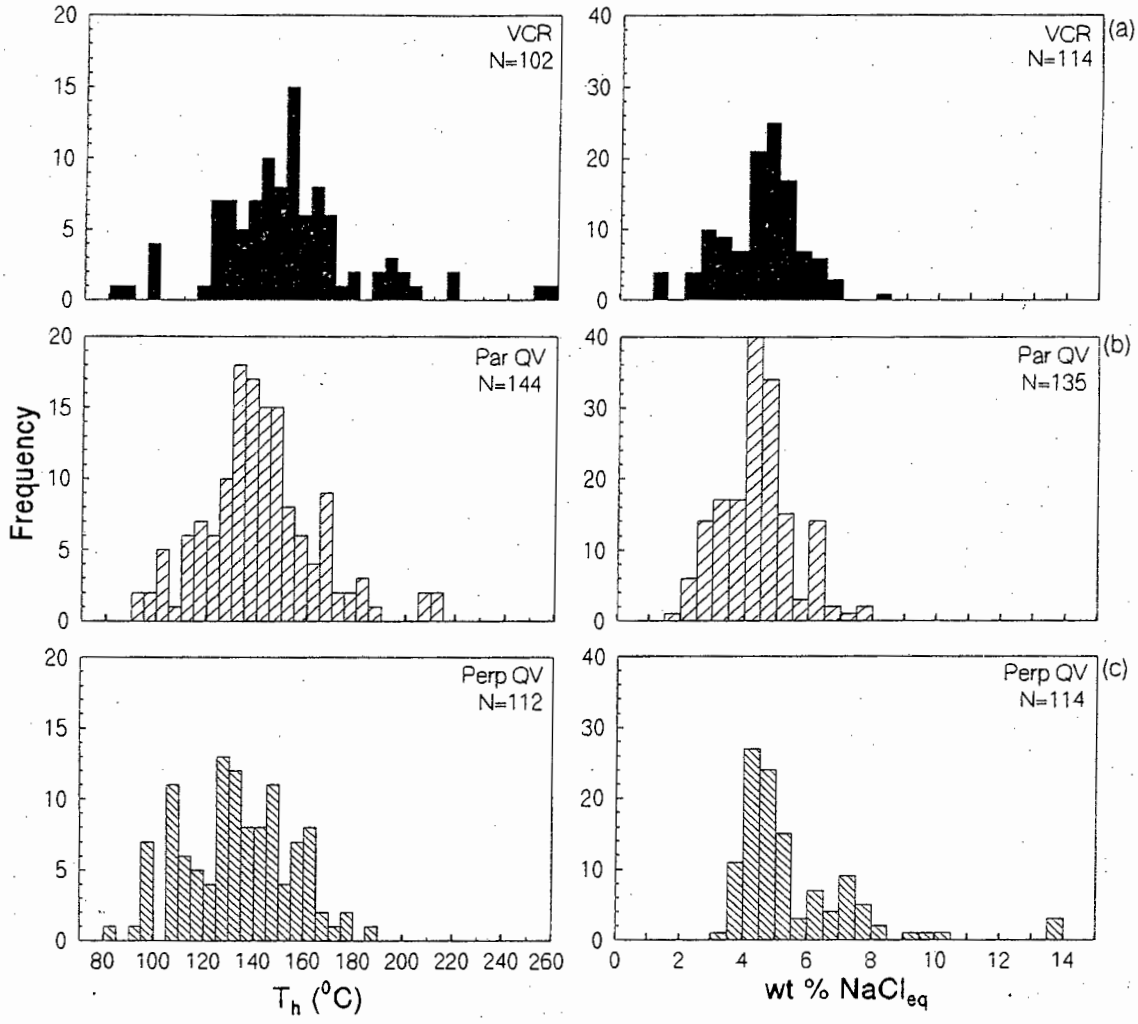

Fig.8.2: Histograms of T_h and salinity of (a) VCR quartzite, (b) bedding-parallel (Par QV) and (c) bedding-perpendicular (Perp QV) quartz vein hosted aqueous fluid inclusions.

The mean composition of these (predominantly secondary) fluid inclusions is similar to the type II fluid inclusions identified by Boer *et al.* (1995) in the VCR from the Elandsrand and Vaal Reefs gold mines. These authors measured a T_h of 115 - 190^{0}C and a salinity of <9 wt% $NaCl_{eq}$ for their type II inclusions.

The microthermometric results of type II, type III and type IV fluid inclusions for this study are given in Table 8.1. Inclusion types II and III have been grouped together because no significant difference between the measured temperatures exists. Similar temperature ranges also exist between primary and secondary type II and type III fluid inclusions. However, variations in T_h and/or salinity are present in primary as well as in secondary fluid inclusions within several of the samples.

Table 8.1: Microthermometric Results of Quartz-hosted Fluid Inclusions

Fluid Inclusion Host	Inclusion Type	Sample	wt% NaCleq	Th (°C)
Bedding-parallel Quartz Vein	Type II	VHG038	4.70±0.90 (N=18)	120±17 (N=28)
	Type II & III	VHG055(B)	4.29±1.94 (N=4)	155±44 (N=4)
	Type IV		-	23± 2 (N=3)
	Type II	VHG087	2.88±0.49 (N=26)	140± 7 (N=28)
	Type II		6.66±0.95 (N=7)	208± 4 (N=2)
	Type II	VHG137	3.95±0.36 (N=21)	145±14 (N=25)
	Type II	VHG166	4.71±0.94 (N=28)	128±15 (N=24)
	Type II		5.25±1.03 (N=7)	178±16 (N=7)
	Type II	VHG172	4.17±0.94 (N=24)	155±16 (N=26)
Bedding-perpendicular Quartz Vein	Type II & III	VHG016	7.63±1.08 (N=20)	115±15 (N=19)
	Type II & III		13.65±0.06 (N=3)	104± 6 (N=3)
	Type II	VHG039	4.67±0.41 (N=23)	150±18 (N=24)
	Type II		6.74±0.32 (N=5)	125±26 (N=5)
	Type II	VHG093(A)	4.61±0.32 (N=8)	124±17 (N=8)
	Type II	VHG174	5.02±0.88 (N=33)	129±18 (N=31)
	Type II & III	VHG180	4.23±0.49 (N=22)	146±19 (N=22)
	Type IV		-	35± 4 (N=5)
Auriferous Quartz Vein	Type II & III *	VHG163(A)	6.17±1.27 (N=48)	127±15 (N=40)
	Type II & III		5.71±1.35 (N=20)	207±18 (N=23)
Nooitgedacht Fault Zone QV	Type II & III	VHG178(B)	5.92±0.78 (N=15)	167±28 (N=15)
	Type IV		-	14± 4 (N=5)
VCR	Type II & III	VHG055(B)	4.62±0.70 (N=29)	155±13 (N=19)
	Type II & III		5.38±0.71 (N=6)	125±26 (N=8)
	Type II & III	VHG063(A)	4.74±1.06 (N=10)	121±11 (N=7)
	Type II & III	VHG074	5.21±0.53 (N=3)	142±17 (N=4)
	Type II & III	VHG093(A)	4.86±0.35 (N=8)	135±29 (N=6)
	Type II & III		6.30±0.39 (N=3)	182±18 (N=3)
	Type II & III	VHG093(B)	5.16±1.23 (N=20)	130±23 (N=19)
	Type II & III	VHG131	3.43±0.77 (N=10)	140±11 (N=11)
	Type II & III *	VHG158(B)	2.97±1.02 (N=25)	156±15 (N=25)

* Primary Fluid Inclusions

Nearly all of the fluid inclusions measured have T_e of $\leq$-25°C. The true T_e is lower because of the difficulties in observing the first melting in small, low-salinity fluid inclusions. The lowest T_e

measured was -44.5°C, which was obtained from a primary fluid inclusion in the auriferous quartz vein (sample VHG163(A)). This temperature, together with slow to moderate initial melting rates, indicates the presence of $CaCl_2/MgCl_2$ in addition to NaCl (Crawford, 1981). Only one fluid inclusion which differed significantly by having a T_e of -10°C, was found in a bedding-perpendicular quartz vein (sample VHG016). The very rapid melting of ice observed in this fluid inclusion suggests the presence of KCl (Crawford, 1981).

The results of primary type II and type III fluid inclusions from the Fe-metasomatised VCR sample VHG158(B) are shown Fig.8.3. Only one type of fluid is interpreted to be present. The occurrence of siderite within the fluid inclusions in sample VHG158(B) and the lack of pyrite and pyrrhotite indicates the presence of CO_2, a relatively low sulphur fugacity and a relatively high pH for this fluid.

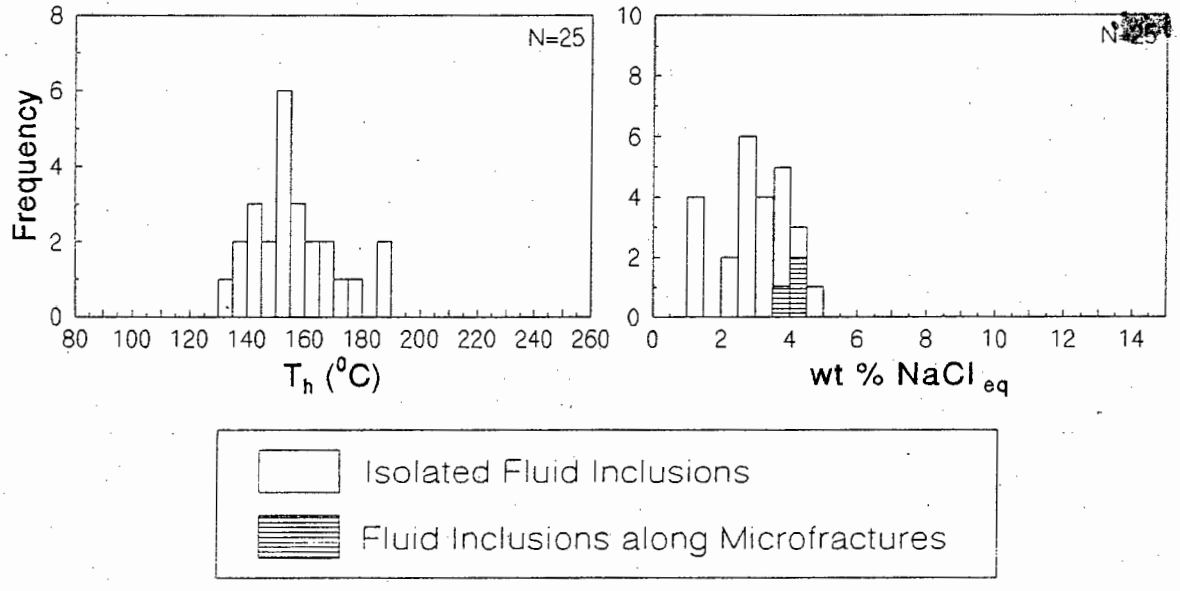

Fig.8.3: Histograms of T_h and salinity of primary type II and type III fluid inclusions from an Fe-metasomatised, siderite-rich VCR quartzite (sample VHG158(B)).

Two distinct groups of fluid inclusions are defined in the T_h salinity histogram of primary and secondary type II and type III fluid inclusions from the auriferous quartz vein sample VHG163(A) (Fig.8.4). The two fluid inclusion populations from the central and the marginal zones have very similar salinities but differ in the T_h. The absence of a higher-T_h group of inclusions from the

central zone supports textural observations which indicate that the formation of the central zone post-dates that of the marginal zone. The lower-temperature group of inclusions could reflect a second pulse of the fluid which was introduced as temperatures decreased.

The presence of calcite as solid inclusions in quartz grains/crystals in both the central and the marginal zones and T_e values as low as -44.5^{0}C, are strong indications that the fluid was $CaCl_2$ -rich throughout the infiltration event. Gold is closely associated with base metal sulphides in predominantly the central zone. It therefore appears that the presence of gold in this quartz vein is associated with a Ca-rich fluid and sulphides.

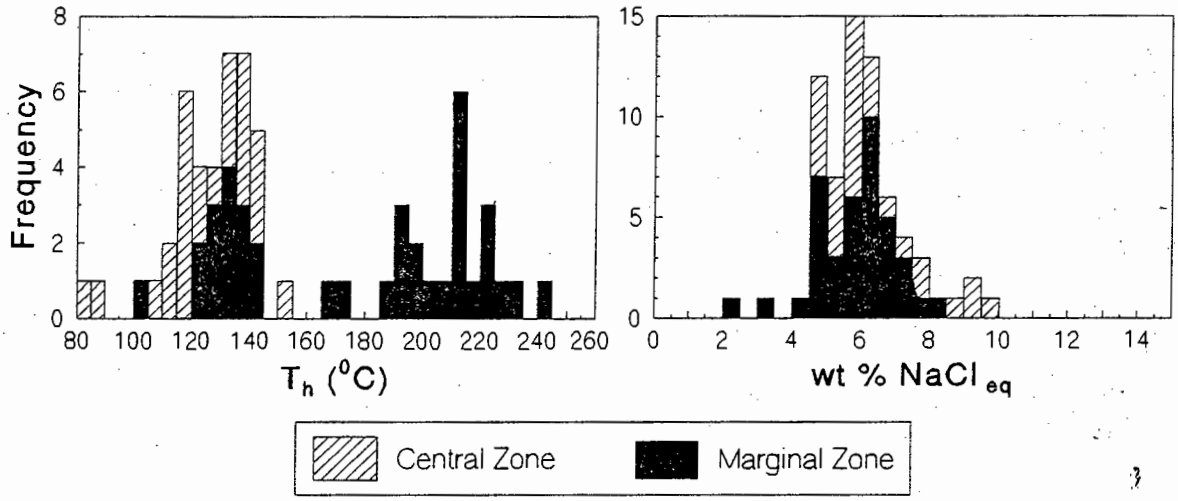

Fig.8.4: Histograms of T_h and salinity of primary and secondary type II and type III fluid inclusions from the auriferous quartz vein (sample VHG163(A)). Although the salinities of all the fluid inclusions are similar, two groups of fluid inclusions with distinctly different T_h are present in the central and marginal zones.

Secondary, predominantly type II fluid inclusions from another bitumen-bearing, bedding-perpendicular quartz vein (sample VHG180) have slightly higher T_h and c. 2 wt% $NaCl_{eq}$ lower salinity than the lower-temperature group of fluid inclusions in sample VHG163(A) (see Table 8.1). However, in addition to type II and type III fluid inclusions in sample VHG180, this quartz vein also contains type IV inclusions. This quartz vein does not contain any visible calcite grains or gold mineralisation. It does, however, contain pyrrhotite and baryte.

The three isolated fluid inclusions in sample VHG016 (Fig.8.5(a)) which have a salinity of c. 13.6 wt% $NaCl_{eq}$ are the highest salinity fluid inclusions observed in this study. A second, lower-salinity group of inclusions is also present in the same quartz vein. First melting temperatures of all except one of these inclusions indicate the presence of a mixture of NaCl-$CaCl_2$-$MgCl_2$ in the fluid. The T_e of one of the fluid inclusions indicates the presence of dissolved KCl in addition to NaCl. The fluid inclusions can be grouped into low- to moderately saline, Na/Ca/Mg/(K)-rich fluid inclusions.

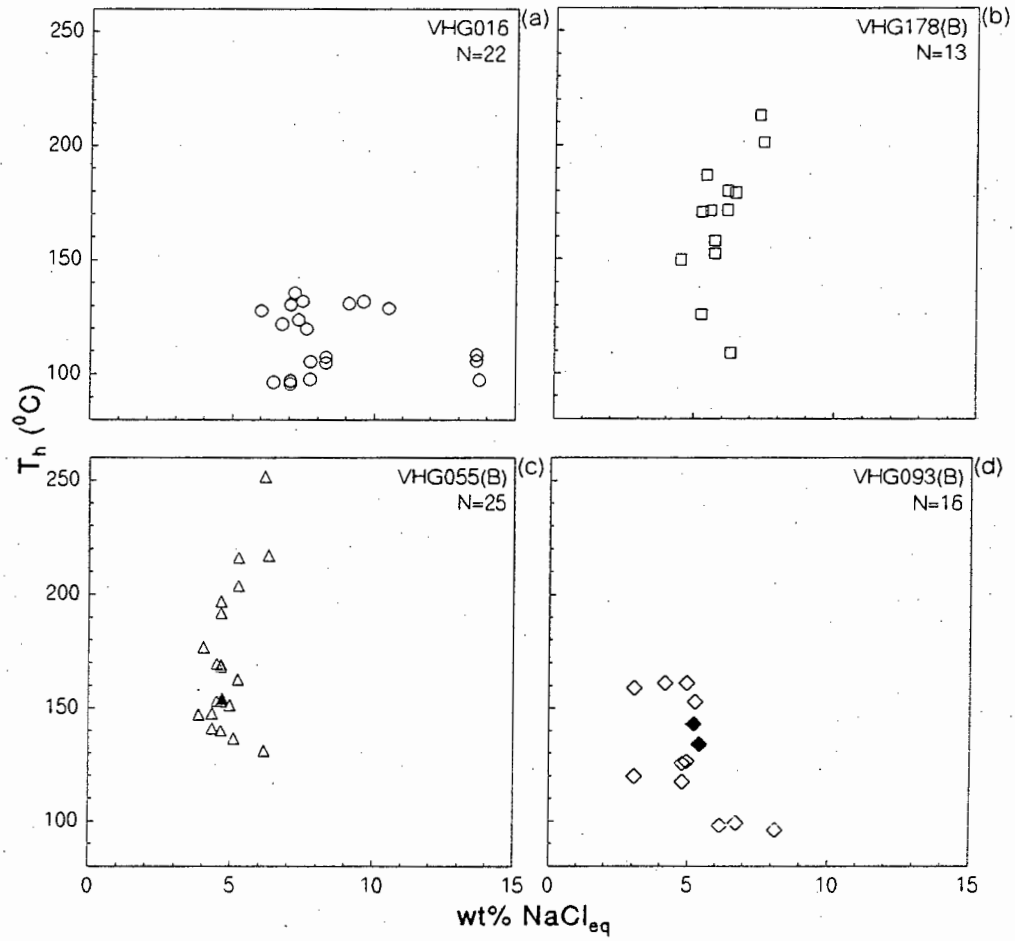

Fig.8.5: Examples of salinity (wt% $NaCl_{eq}$) vs T_h plots of secondary type II and type III fluid inclusions from (a) a bedding-perpendicular quartz vein, (b) the Nooitgedacht Fault zone quartz vein and (c)-(d) VCR quartzite. Open symbols: individual fluid inclusions; Filled symbols: mean of 3 or more fluid inclusions from a microfracture.

The secondary fluid inclusions from a quartz vein associated with the Nooitgedacht Fault (Fig.8.5(b)) have salinities which are indistinguishable from VCR- and hydrothermal quartz vein-

hosted fluid inclusions. The fairly large range in T_h of 109 - 213°C is due to variations in L/V ratios of 10 - 20 vol%. This range in L/V ratios could be due to post-entrapment changes (e.g. necking down), or it could be the result of trapping of different pulses of a single evolving fluid. First melting temperatures of <-33°C indicate the presence of $CaCl_2/MgCl_2$ in addition to NaCl in the fluid. Although the range in T_h of the fluid inclusions in sample VHG178(B) varies considerably, the salinity of type II and type III inclusions remains fairly constant.

Two examples of type II/type III fluid inclusions from the VCR quartzite fraction (samples VHG055(B) and VHG093(B)) are shown in Fig.8.5(c)-(d). The fluid inclusions in samples VHG055(B) and VHG093(B) have similar ranges in T_h and/or salinity as the secondary fluid inclusions from quartz veins (e.g. Fig.8.5(a)-(b)). Overall, the fluid inclusions from the VCR are indistinguishable from the fluid inclusions in hydrothermal quartz veins.

Two secondary type II fluid inclusion populations with distinctly different T_h and salinities are present in a bedding-parallel quartz vein sample VHG087 (Fig.8.6). These two fluid inclusion populations come from two differently orientated microfractures. The presence of different fluids within differently orientated microfractures suggests that, with changing orientation of the stress field, the composition of the prevailing fluid also changed.

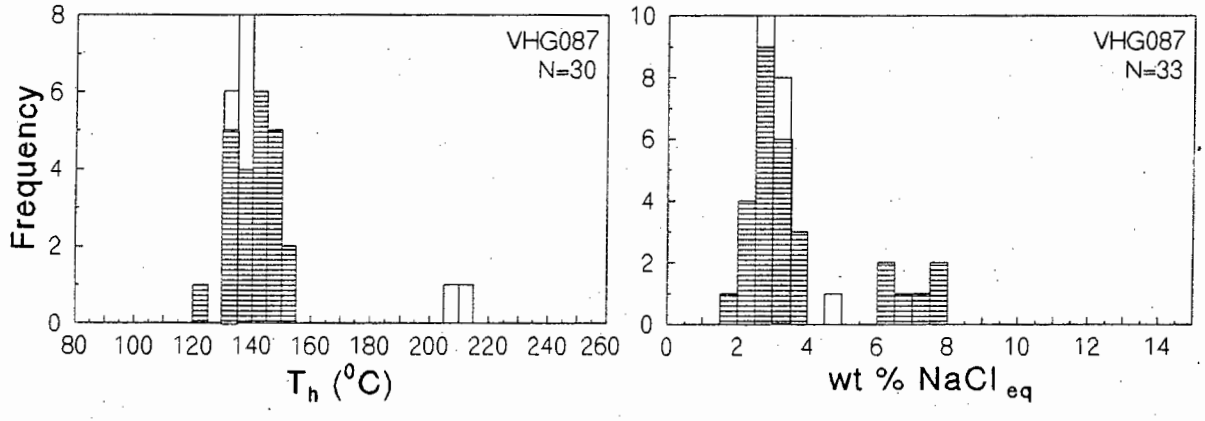

Fig.8.6: Histograms of T_h and salinity of secondary fluid inclusions from a bedding-parallel quartz vein (sample VHG087). Two distinct groups of fluid inclusions are present in this sample. For legend see Fig.8.3.

The fluid inclusion composition from a bedding-parallel quartz/calcite vein along the VCR/footwall contact is shown in Fig.8.7. This quartz vein is <7 cm wide and is well mineralised with chalcopyrite. The T_h and salinity of these type II inclusions are typical of the low-salinity group of inclusions found in the other quartz veins and in the VCR.

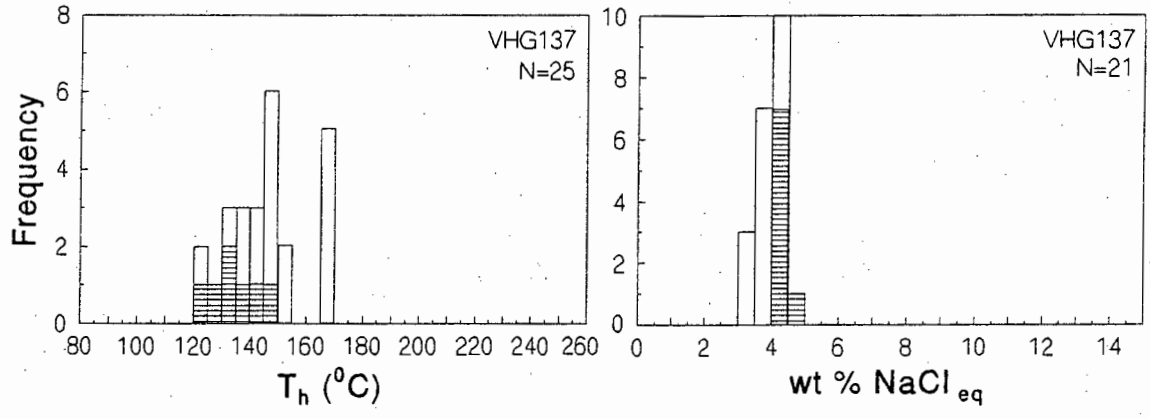

Fig.8.7: Histograms of T_h and salinity of secondary fluid inclusions from a bedding-parallel quartz/calcite vein (sample VHG137). For legend see Fig.8.3.

The presence of type IV (CO_2-rich) fluid inclusions in quartz veins and VCR quartzite has previously been described by Boer *et al.* (1995) from the VCR at Vaal Reefs No.10 Shaft. With the help of quadrupole mass spectrometry, these authors analysed the gases within the carbonic-rich fluid inclusions. They found that H_2O, CO_2 and CH_4 constitute more than 99 mol% of the gas composition. The fluids also have variable CO_2/H_2O ratios and a mean T_h and salinity of 130°C and 4 wt% $NaCl_{eq}$, respectively.

The type IV fluid inclusions in each of the samples in this study can be distinguished from each other on the basis of different $T_h(CO_2)$ which varies from 14 - 35°C (see Table 8.1). No clathrate melting temperatures for the CO_2-rich fluid inclusions could be obtained. The depression of T_e from -56.6°C to as low as -62.6 C in the quartz vein sample VHG180 indicates significant amounts (up to 30 mol%) of other gaseous species (e.g. CH_4 , H_2S , N_2) in the fluid (Hall and Bodnar, 1990).

9. Cathodoluminescence Study of Quartz

9.1 Introduction

Cathodoluminescence (CL) is the process whereby rays in and near the visible part of the electromagnetic spectrum are emitted from a sample when the sample surface is irradiated with a beam of electrons. CL is believed to be generated at depths of 2 - 8 μm below the sample surface (Grant and White, 1978; Marshall, 1988).

The CL imaging (CLI) in this study was carried out using a Cambridge Stereoscan S440 scanning electron microscope (SEM) and a more detailed description of the instrument and of the operating conditions are given in Appendix E. A feature of SEM-CL is that with the additional use of a monochromator, CL spectra can be collected. This allows the CL emission patterns to be quantified in terms of monochromatic light intensity versus wavelength. The method of recording SEM-CL information is through digitally stored panchromatic CL images and by the acquisition of monochromatic spectral CL emissions.

The causes of CL in quartz are attributed to intrinsic effects (i.e. structural defects), extrinsic effects (i.e. trace element impurities) and the state of crystal water. Although numerous studies of the CL of quartz have been made over the past decades (e.g. Grant and White, 1978; Sprunt *et al.*, 1978; Sprunt, 1981; Ramseyer *et al.*, 1988; Behr *et al.*, 1989; Houseknecht, 1991; Vollbrecht *et al.*, in press), the origin of CL of crystalline quartz is thought to be very complex and no unique explanation has yet emerged (Remond *et al.*, 1992). Some of the more commonly observed CL colours and/or peak wavelength emissions of quartz as well as possible causes for quartz CL are listed in Table 9.1.

The aim of CLI was not to investigate the possible causes of CL in quartz but (i) to determine textural features of Witwatersrand quartz not previously identified, (ii) to identify the presence of different genetic types of quartz (i.e. detrital, authigenic/metamorphic and hydrothermal) and (iii) to quantify the CL emissions with the help of spectra.

With the use of CLI it was hoped that a better understanding of the relationship between quartz and the other minerals in the VCR (particularly gold and chlorite) and of changing fluid composition (as indicated by quartz solution/precipitation textures) would be gained. Furthermore, a limited investigation was carried out on the effect that the instrument set-up conditions (e.g. scan area, irradiation time etc.) have on the reproducibility of spectra.

Table 9.1: Previously Reported Results of the CL Colour, Wavelengths and Possible Causes of Quartz CL

Author	Optical CL Colour of Quartz	Quartz Peak (nm)	Type of Quartz	Possible Cause of CL
Grant and White (1978)		400-500		Al replacing Si
		400-500 (major) 620 (minor)		Al replacing Si ?
		400-500 (major) 620 (major)		Al replacing Si ?
Sprunt et al. (1978)	red	?	Secondary quartz overgrowths	Low T deformation
	blue	?		High T deformation
Zinkernagel (1978)	non-luminescent	-	Hydrothermal and authigenic quartz (T< 300 C)	
	orange/ brown	450 (minor) 620 (major)	Low to high grade metam. rocks (T= 300-573 C)	Slow cooling
	violet/ blue	450 (major) 620 (major)	High grade metam. or igneous rocks (T> 573 C)	Fast cooling
Sprunt (1981)	red	645 (major) 725 (major)		Low [Ti] + high [Fe3+]
	blue	?		High [Ti] + low [Fe3+]
Kearsley and Wright (1988)	blue/brown	400 (minor) 425 (major) 580 (major)	Authigenic quartz cement	
	blue	400 (minor) 415 (major)	Quartz core	
Meunier et al. (1988)	non-luminescent		Quartz overgrowths	
	reddish to violet/ blue		Cores of detrital quartz	
	pale reddish to pale violet/blue		Rims around quartz	Damage by α particles
Ramseyer et al. (1988)	non-luminescent			
	brown (long-lived)	515 (minor) 650-670 (major)		Lattice defects (due to particle bombardment ?)
	blue/green/yellow (short-lived)	440 500	Authigenic Quartz Authigenic Quartz	Cation impurities Cation impurities
Behr et al. (1989)	orange-red	420 (minor) 620 (major)	Hydrothermal vein quartz	Activators and presence of OH and H2O in SiO2 lattice
	red-brown	425 (major) 600 (major)	Hydrothermal vein quartz	Activators and presence of OH and H2O in SiO2 lattice
	blue/green	485 (major) 600 (minor)	Hydrothermal vein quartz	Activators and presence of OH and H2O in SiO2 lattice
	violet/blue	430 (major)		Activators and presence of OH and H2O in SiO2 lattice
Remond et al. (1992)		380		Varies as function of electron dose
		440-470		Lattice defect ?
		510-570		
		650		Impurities (Na, H+, OH) or oxygen vacancies in lattice

9.2 CL Imaging

The types of quartz which were investigated include detrital quartz grains, authigenic/ metamorphic quartz overgrowths and fracture-fillings and hydrothermal vein quartz. Eight samples from the VCR, two samples from the VCR-footwall contact, four samples from different types of quartz veins and one synthetic KEVEX quartz sample were examined.

One common feature exhibited by the VCR and footwall quartzite samples is that detrital quartz grains show a large range in CL intensities from brightly luminescent to dark grey (Plate 9.2). Similar observations have been made by Vollbrecht *et al.* (in press) of Carbon Leader Reef samples from the Carletonville goldfield using optical CL. These differences in CL intensities (i.e. CL colours) of quartz pebbles and quartz grains are interpreted to reflect different origins (e.g. plutonic, metamorphic, hydrothermal) of the detrital quartz grains.

Some of the VCR quartz grains are irregularly fractured with dark grey (weakly luminescent) authigenic/metamorphic quartz filling the fractures or cementing the broken quartz fragments. The fractured nature of some of the quartz grains is not visible under the optical microscope (compare Plates 9.1 and 9.2, taken under XPL and CL, respectively). This textures is probably the result of brittle fracturing as a result of lithostatic pressure during burial metamorphism. Furthermore, detrital quartz grains have embayed grain margins (indicating quartz dissolution) and are sometimes surrounded by an irregular rim of weakly luminescent authigenic/metamorphic quartz (Plate 9.3). The amount of authigenic/metamorphic quartz present as rims, cement and fracture-fillings in all of the samples examined is estimated at ≤ 5 vol%.

Dickinson and Milliken (1995) utilised SEM-CL to study the 100 m thick pile of porous Etjo Sandstone in northern Namibia, which are estimated to have been overlain by a 1 - 2 km thick sequence of lava flows. The authors found that during compaction and burial, brittle deformation was the dominant process which resulted in fracturing and the modification of original detrital quartz grain shapes. This process was syn- and post-dated by the formation of "significant" amounts of authigenic cement. Quartz dissolution and pressure solution apparently played only a minor role in the formation of the arcuate quartz grain shapes.

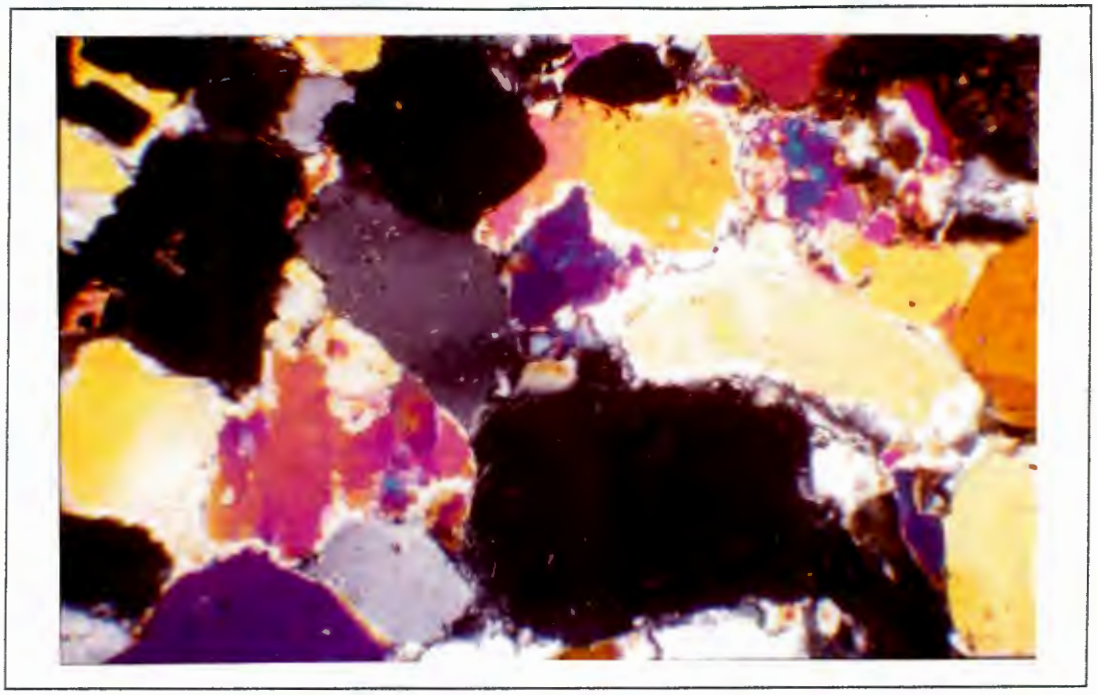

Plate 9.1: Detrital quartz grains and rounded pyrite (black). (sample VHG136, XPL, length of photo = 2.3 mm).

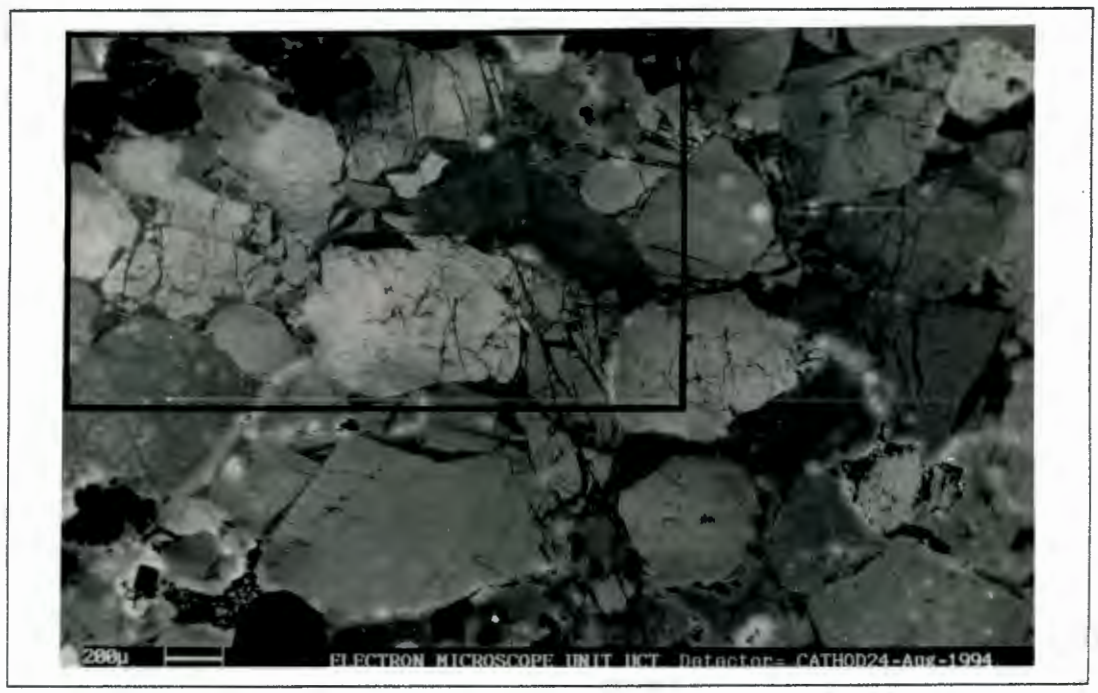

Plate 9.2: Subangular, fractured detrital quartz grains showing varying degrees of CL intensity. Note dark grey authigenic/metamorphic quartz cement and fracture-filling quartz. Pyrite and chlorite are black. (sample VHG136, CL, length of photo = 3.4 mm; area of Plate 9.1 is outlined).

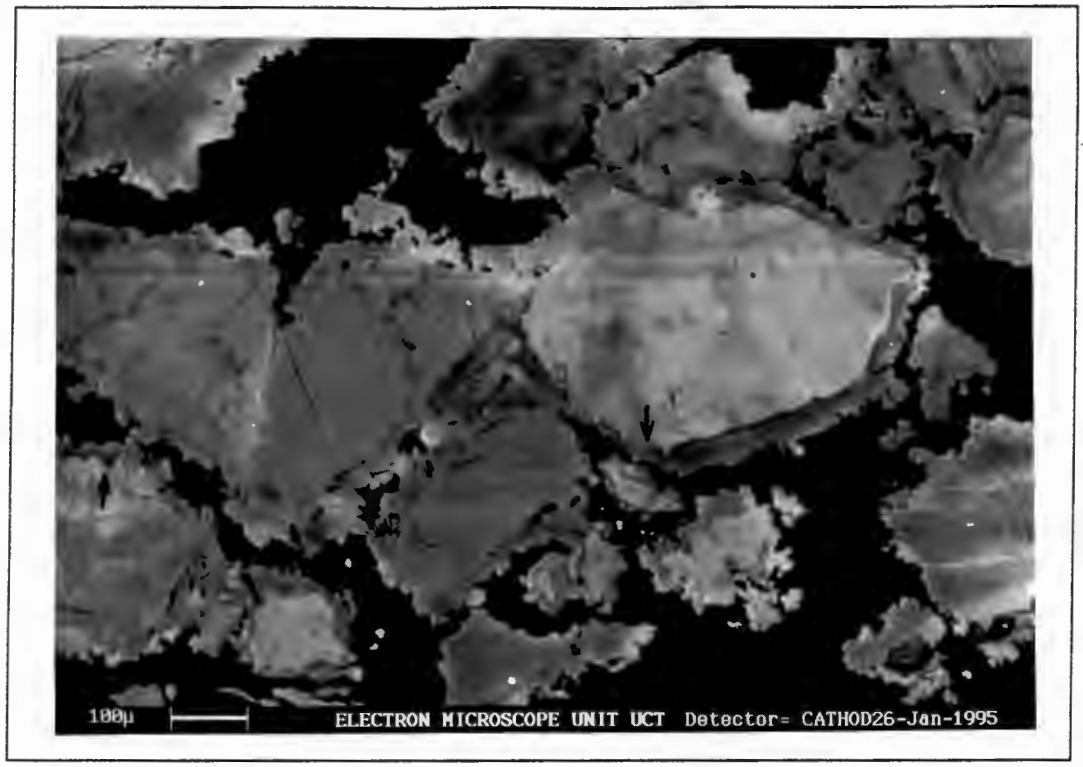

Plate 9.3: Detrital quartz grains surrounded by dark grey authigenic/ metamorphic quartz overgrowth rims. Note embayed grain margins (arrows) of detrital quartz grains.
(sample VHG093(A), CL, length of photo = 1.3 mm).

A brightly luminescent rim was observed around quartz grains immediately adjacent to bitumen nodules in several samples (e.g. sample VHG063(A)). This texture has been described by Meunier *et al.* (1988) and Behr *et al.* (1989) in uranium-bearing sandstones and by Vollbrecht *et al.* (in press) in the quartzite fraction of Carbon Leader Reef samples. The cause of these brightly luminescent zones, along which increased U concentrations have been observed by SEM-EDS element mapping (Frimmel, pers. comm.), is attributed to damage of the quartz lattice by α-particles. The presence of uraninite and its (very commonly) close association with bitumen nodules in the Witwatersrand conglomerates has been well documented (e.g. Feather and Koen, 1975; Hallbauer, 1986; Landais *et al.*, 1990).

Although bitumen nodules (but no visible uraninite) are present in trace amounts in VCR sample VHG131, virtually all of the quartz grains in that sample have very irregular "serrated" grain outlines and are surrounded by a similarly strongly luminescent rim described above. The rim is present irrespective of the CL intensity or the size of the individual detrital grains. This suggests

that locally within the VCR, chemical conditions were favourable for the redistribution of uranium in solution, which subsequently resulted in the radioactive damage of the detrital quartz grains.

With the help of CLI it becomes apparent that most of the chlorite in the VCR (irrespective of morphology or mineralogical association) is partially or completely surrounded by dark grey authigenic/metamorphic quartz. The CL investigation also reveals that not only chlorite, but also all of the gold particles within the quartz grains (in those samples examined using CLI) are embedded in authigenic/metamorphic quartz (as illustrated in Plate 9.7).

CLI of hydrothermal quartz from several quartz veins revealed that some of the euhedral quartz crystals, which have grown into open space in fractures, show an intense zonation, with zones of almost black to very bright CL intensities. Towards the crystal margin there is often a distinct zone of brecciation or quartz resorption (e.g. as shown in Plate 9.9), indicating partial quartz dissolution at some stage during the period of crystal growth. These textures, which are not visible during optical examination (compare Plates 9.4 and 9.5, taken under XPL and CL, respectively), suggest a change in fluid conditions during hydrothermal quartz growth.

9.3 CL Spectra

The wavelength range over which quartz CL spectra were acquired was 400 - 700 nm. Representative examples of detrital quartz, authigenic/metamorphic quartz and hydrothermal quartz spectra which illustrate the characteristic wavelength spectra of each of these genetic types of quartz are shown in Fig.9.1.

A dominant peak maximum around 400 nm (corresponding to violet light) is a common feature of all the quartz CL spectra. The differences in the CL emission spectra between the three genetic types of quartz are apparent at the higher end of the visible light spectrum, i.e. in the yellow/orange wavelength range. The detrital quartz spectra (Fig.9.1(a)) usually have a subordinate orange peak around 630 nm with a violet:orange peak ratio of approximately 6:1 to 3:1.

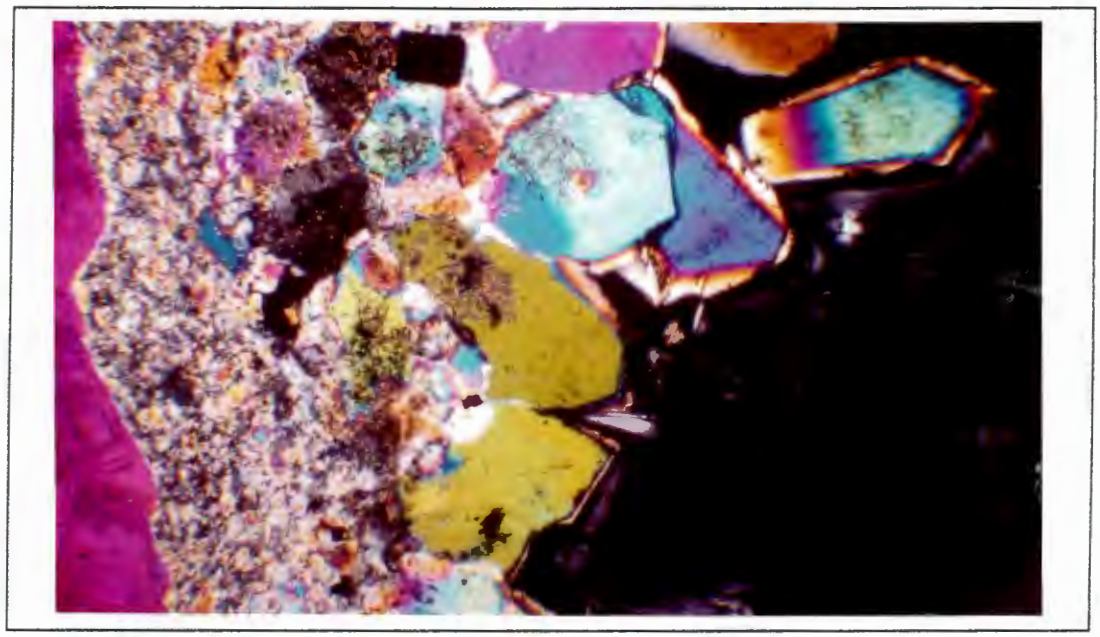

Plate 9.4: Hydrothermal auriferous quartz vein showing euhedral quartz crystals (on right hand side), a fine grained anhedral quartz (towards left hand side) and a large anhedral hydrothermal quartz grain (purple) on the extreme left hand side.
(sample VHG163(A), XPL, length of photo = 2.3 mm)

Plate 9.5: Approximately the same field of view as in Plate 9.4. The zonation of the euhedral quartz crystals is clearly visible under CL, as is the fine grained quartz towards the left hand side.
(sample VHG163(A), CL, length of photo = 3 mm)

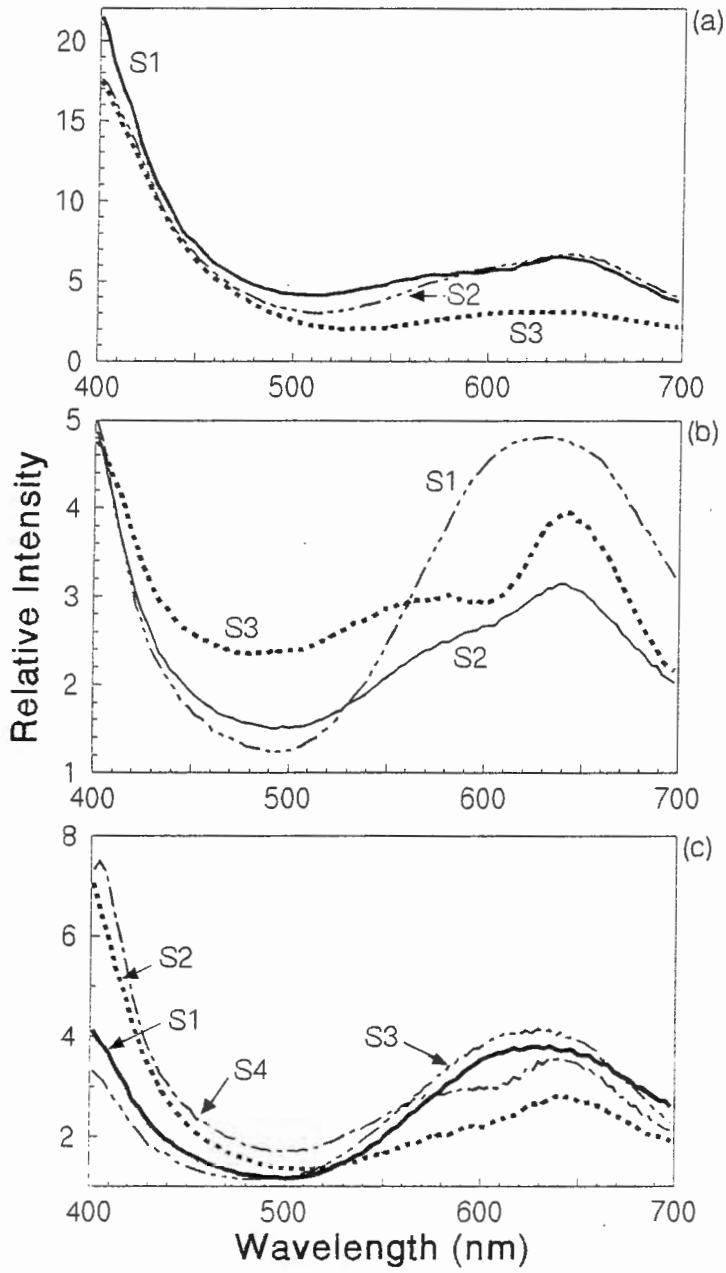

Fig.9.1: Typical quartz CL spectra of (a) detrital quartz (spectrum S1 is from VCR sample VHG063(A) and spectra S2/S3 are from sample VHG158(B)), (b) authigenic/ metamorphic quartz (spectra S1/S2 are from footwall quartzite sample VHG173(B), spectrum S3 is from quartz immediately adjacent to the gold particle shown in Plate 9.7 (sample VHG063(A)) and (c) hydrothermal quartz (spectra S1/S2 are from a zoned euhedral quartz crystal from quartz vein sample VHG181; spectra S3 and S4 are from a quartz/calcite vein at the VCR-footwall contact (sample VHG172) and the auriferous quartz vein (sample VHG163(A), respectively).

The spectra from the authigenic/metamorphic quartz and the hydrothermal quartz are very similar to each other. In contrast to the detrital quartz spectra, these secondary quartz spectra have an orange peak of nearly the same magnitude as the violet peak.

In all three genetic types of quartz the orange peak occasionally has an asymmetric shape (e.g. spectrum S1 in Fig.9.1(b)). Depending on the instrument set-up (e.g. probe current, acceleration

voltage), this single peak can sometimes be resolved into two individual peaks, one at approximately 575 nm and the other at 635 nm.

Plate 9.6 (sample VHG093(A)) shows the scan areas where the spectra S1-S4 (shown in Fig.9.2) were acquired. Spectra S1 and S2 (Fig.9.2(a)) come from two different (medium grey) detrital quartz grains and have violet:orange peak ratios of approximately 4:1 to 3:1. The two quartz grains are separated from each other by a zone of (dark grey) authigenic/metamorphic quartz (spectrum S4). Spectrum S3 (Fig.9.2(b)) was acquired in what appears to be a dark grey brecciated and re-cemented detrital quartz grain. The CL spectrum of this quartz grain has an authigenic/metamorphic signature.

Plate 9.6: Areas of spectra acquisition S1-S4 shown in Fig.9.2.
Spectra S1 and S2 are from two adjacent detrital quartz grains. Spectrum S3 comes from a brecciated and re-cemented dark grey detrital quartz grain with an authigenic/metamorphic signature. Spectrum S4 is from the dark grey authigenic/metamorphic quartz overgrowth rim separating the two detrital quartz grains. Note the lighter grey rectangular boxes (radiation damaged areas) caused by electron bombardment during acquisition of CL spectra.
(sample VHG093(A), CL, length of photo = 0.4 mm).

No significant difference can be observed between the CL emission spectra of hydrothermal quartz (spectrum S5 in Fig.9.2(b)) and those of the authigenic metamorphic quartz (see spectra S3 and S4 in Fig.9.2(b)).

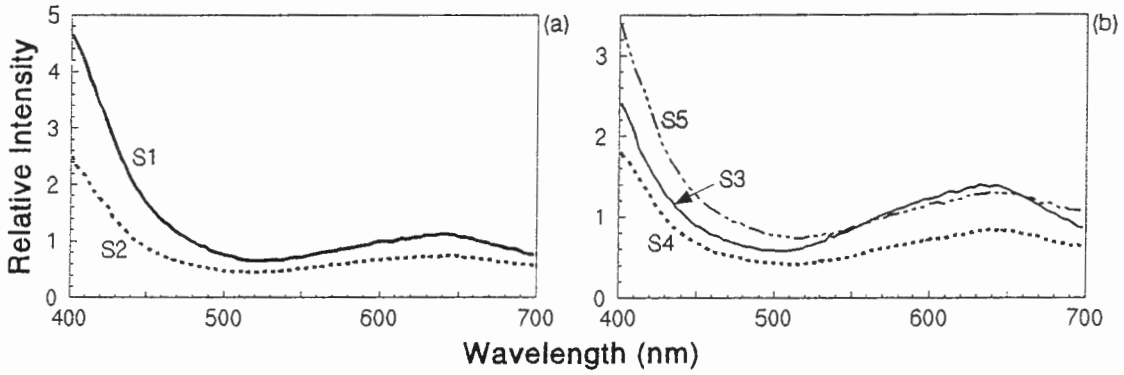

Fig.9.2: Quartz CL spectra, the areas of acquisition are shown in Plate 9.6.
Note the asymmetry of the orange peak in some of the spectra.
S1/S2: detrital quartz grains
S3: fractured detrital grain with authigenic/metamorphic signature
S4: authigenic/metamorphic quartz rim
S5: hydrothermal quartz from a quartz vein in the same sample.

Two quartz grains containing a pseudohexagonal chlorite flake and two gold particles (one of them attached to a chlorite "twirl") are shown in a backscatter electron and a CL image in Plate 9.7. The left hand quartz grain has an authigenic/metamorphic signature (see spectrum S3 in Fig.9.3) and the right hand quartz grain has a detrital signature (spectrum S1 in Fig. 9.3). Both the CL image and the CL spectra indicate that the gold particles and the chlorite which are contained within the quartz grains are enclosed by authigenic/metamorphic quartz. The CL image and the CL spectra readily allow the distinction between the different genetic types of quartz in this sample.

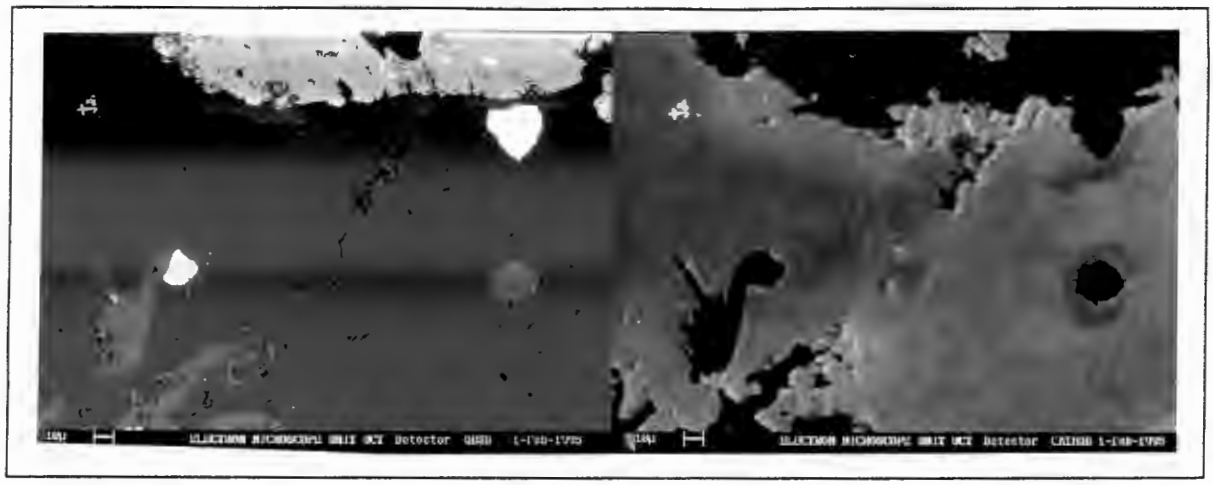

Plate 9.7: Comparison of backscatter electron image (left) and CL image (right) of VCR sample VHG063(A). Two very brightly reflectant grains in the backscatter image are gold grains, one of them is attached to type III chlorite (in the left hand quartz grain) and the other one adjacent to chlorite/pyrite (medium grey grain along top edge of backscatter image). A pseudohexagonal chlorite flake is present in the right hand quartz grain. (sample VHG063(A), backscatter and CL image; length of each photo = 0.3 mm).

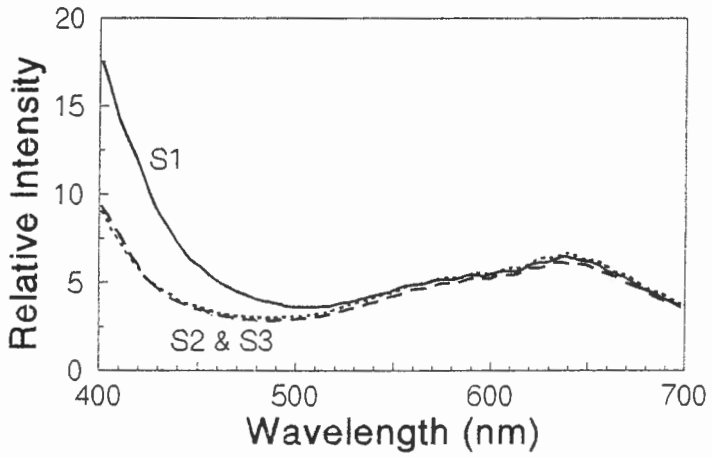

Fig.9.3: Quartz CL spectra from gold- and chlorite-bearing quartz grains from VCR sample VHG063(A).
Spectrum S1 was acquired in the medium grey detrital quartz grain next to the pseudohexagonal chlorite flake in the right hand quartz grain, and spectra S2 and S3 are from the authigenic/metamorphic quartz rim surrounding the pseudohexagonal chlorite flake, and from immediately adjacent to the gold particle in the left hand quartz grain, respectively (see CL image of Plate 9.7).

A brightly luminescent, slightly fractured detrital quartz grain from a footwall quartzite sample (VHG173(B)) <5 cm below the VCR is surrounded by dark grey authigenic/metamorphic quartz and chlorite (Plate 9.8). The CL spectra of the detrital quartz grain (spectrum S1) and those from the authigenic/metamorphic quartz surrounding the detrital quartz grain (spectra S2-4) are shown in Fig.9.4. The very close association between chlorite (medium/dark grey) and galena (Gn) with secondary quartz suggests that the former two minerals were precipitated during formation of the secondary quartz.

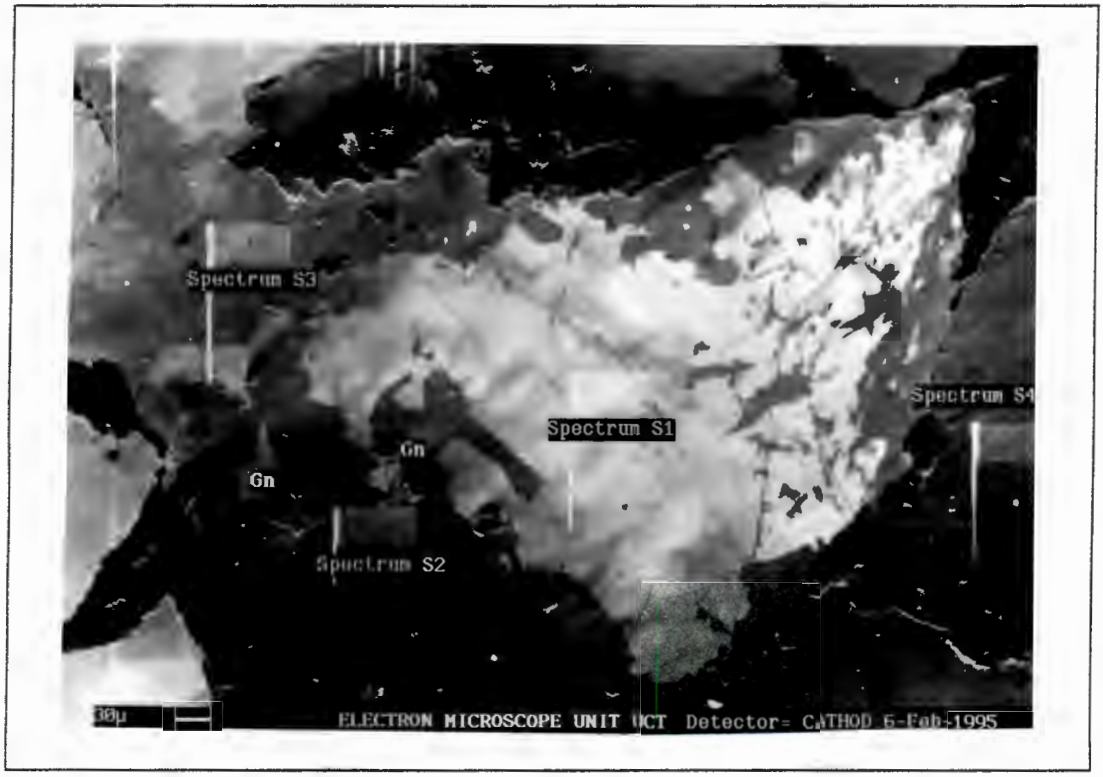

Plate 9.8: Detrital quartz grain from footwall quartzite (showing very bright CL intensity) surrounded by authigenic/metamorphic quartz with very low (dark grey) CL intensity. Galena (Gn) and chlorite (black) are closely associated with the latter. Areas of spectra acquisition S1-S4 (shown in Fig.9.4) are as indicated.
(sample VHG173(B), CL, length of photo = 0.8 mm).

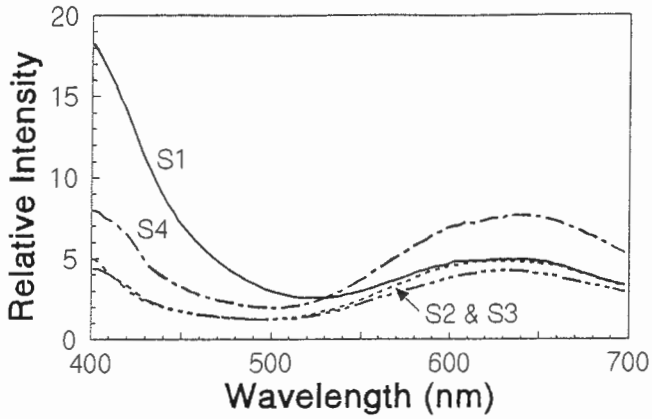

Fig.9.4: Quartz CL spectra from footwall quartzite sample VHG173(B) (areas of spectra acquisition are shown in Plate 9.8).
S1: detrital quartz grain
S2/S3/S4: authigenic/metamorphic quartz surrounding the detrital quartz grain and enclosing galena and chlorite.

The complex zonation of a euhedral quartz crystal (from the auriferous quartz vein, sample VHG163(A)) is shown in Plate 9.9 and the respective spectra are illustrated in Fig.9.5. The core zone of the euhedral quartz crystal, from which spectra S1 and S2 were collected, contains abundant minute calcite and fluid inclusions. Spectra S1 and S2 are very similar to each other except for a small peak around 485 nm in S1. These spectra show a basic hydrothermal signature on which other peaks at 568 nm and 660 nm are superimposed. Spectra S3 (from the dominantly dark grey/black zone) and S4 (from the outer "dissolution" zone) differ from spectra S1 and S2 in that the former lack these other peaks.

Several examples illustrating the effects which instrument set-up/operating conditions can have on the CL spectra are shown in Fig.9.6. The two detrital quartz spectra in Fig.9.6 are nearly identical, despite a four-fold difference in the size of the scan area between the two. In the synthetic quartz spectra, however, the orange peak intensities of the two spectra differ from each other. In this study it was found that the acquisition of spectra at higher rather than lower magnification (i.e. smaller rather than larger scan areas) usually yielded more detailed spectra.

Plate 9.9: CL image of a euhedral quartz crystal from the auriferous quartz vein showing complex growth zonation. The jagged nature of the outer zone indicates a quartz dissolution and subsequent precipitation event. Areas of acquisition of spectra S1-S4 (shown in Fig.9.5) are as indicated. (sample VHG163(A), CL, length of photo = 0.3 mm).

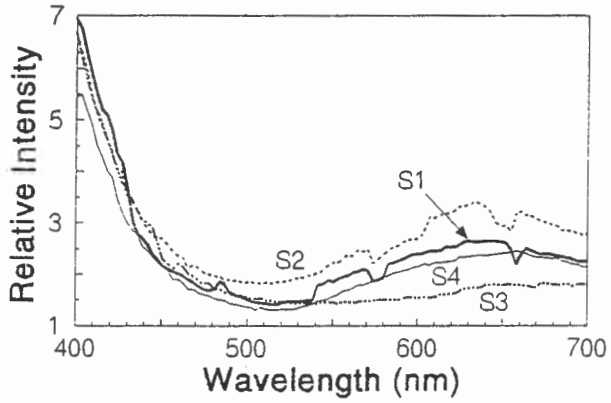

Fig.9.5: Hydrothermal quartz CL spectra from the euhedral quartz crystal (sample VHG163(A)) shown in Plate 9.9.
S1/S2: core zone containing minute calcite and fluid inclusions
S3: intermediate dark grey/black CL zone
S4: dissolution zone towards the margin of the quartz crystal

Fig.9.6(b) (sample VHG163(A)) illustrates that an increase in the irradiation time and/or the probe current results in a greater intensity and a slightly more detailed wavelength emission spectrum. The reproducibility of a spectrum from a particular scan area is illustrated by the two pairs of spectra in Fig.9.6(c). Spectrum S2 is a re-scan of the identical area of spectrum S1 (sample VHG063(A)) after it had been irradiated for 155 seconds. Although the CL intensity decreases slightly with the second irradiation, the "peakedness" of the orange peak around 635 nm is improved. Even more dramatic is the difference between spectra S3 (first acquisition) and S4 (second acquisition after 130 seconds) (sample VHG062) over the identical area. The peakedness of the orange peak is again improved during the second irradiation, but none of the peaks which were detected with S3 are present in S4.

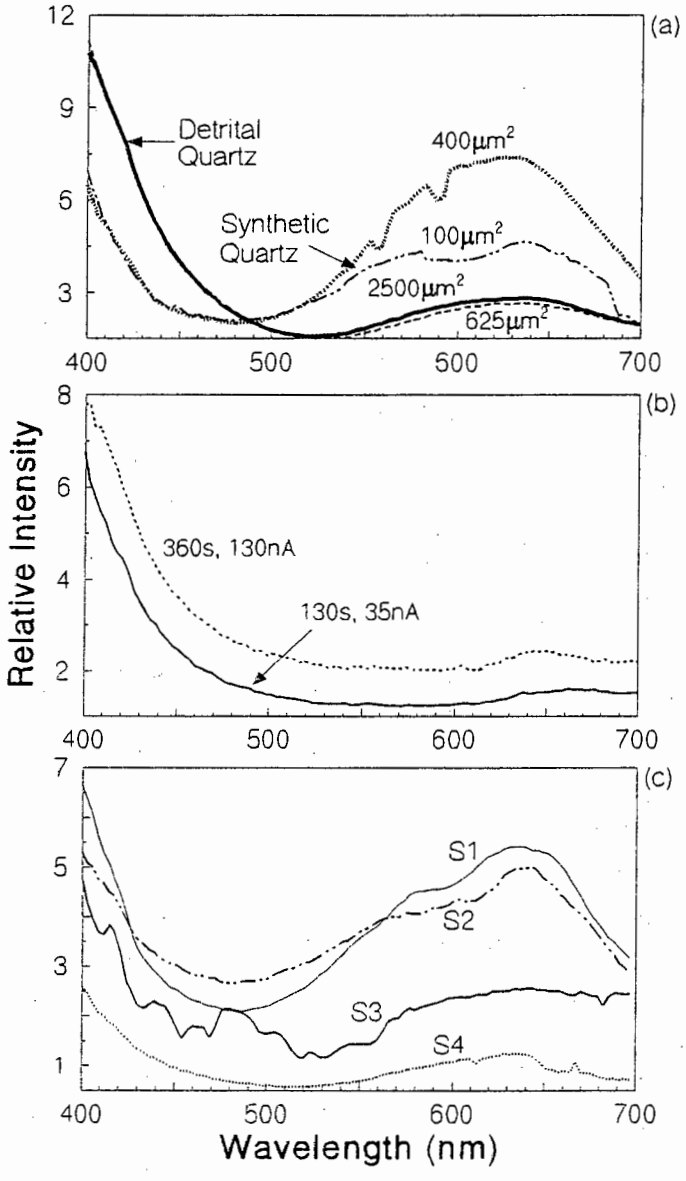

Fig.9.6: Effects of instrument set-up/operating conditions on CL spectra. (a) shows the effect of changing the scan area, (b) the effect of increasing scan time and probe current and (c) the acquisition of spectra after rescanning an area after 155 seconds (S1 and S2) and another area after 130 seconds (S3 and S4).

10. Estimation of P-T Conditions

10.1 P-T Conditions of Metamorphism

The following metamorphic equilibrium assemblages were found in the footwall quartzites and hangingwall metabasalts:

Ab - Act - Chl - Qtz - Ep - Cc	hangingwall metabasalt
Qtz - Prl - Cld	footwall quartzites
Qtz - Prl	

The occurrence of fine grained muscovite in the footwall quartzite and hangingwall metabasalt rocks within 3 - 10 m of the VCR is interpreted to be a product of K^+ metasomatic alteration (Chapter 6.) and therefore is not included in the peak metamorphic mineral assemblage. Similarly, the matrix minerals found in the VCR can all be explained by later metasomatic events, and as such do not reveal anything about metamorphic conditions which were attained during burial.

Peak metamorphic conditions for the VCR in the Klerksdorp goldfield were probably reached during post-Transvaal times, by which stage a total estimated thickness of c. 2800 m of Ventersdorp Supergroup rocks and c. 3700 m of Transvaal Supergroup rocks had been deposited above the VCR (SACS, 1980; Antrobus *et al.*, 1986; Bowen *et al.*, 1986). Assuming a specific gravity of 2.85 and an estimated overburden of 6.5 km of Ventersdorp and Transvaal Supergroup rocks, a peak pressure of c. 2 kbar is calculated for the VCR.

The equilibrium mineral assemblage present in the hangingwall metabasalts can be represented by a seven phase (including a fluid phase), eight component system. Applying Gibbs's phase rule $F = C - P + 2$ to this system, the resultant three degrees of freedom do not allow constraints to be placed on the P-T conditions. However, this mineral assemblage is of lower greenschist facies, implying that pressures did not exceed c. 3 kbar and temperatures ranged from 200 - 600^{0}C. Additional information about the peak metamorphic temperature comes from chlorite

geothermometry of two high hangingwall metabasalt samples (>150 m above the VCR). The calculated temperature of these chlorites is 269 ± 7°C (Fig.10.1), which suggests that the regional metamorphic temperature attained by the Ventersdorp Supergroup lavas was <300°C. The effect of pressure on the chlorite composition and on the calculated temperature of formation is believed to be only small (Cathelineau, 1988; Bryndzia and Scott, 1987).

The difference in temperature between this calculated temperature of chlorite formation and the previously interpreted regional metamorphic temperature of 350 ± 50°C (Phillips, 1987; Wallmach and Meyer, 1990) can be explained by the fact that the Ventersdorp Supergroup metabasalts were not buried to the same depths as the Witwatersrand quartzites. These P-T conditions are therefore considered to be in good agreement with estimates for peak metamorphic conditions experienced by the Witwatersrand Supergroup.

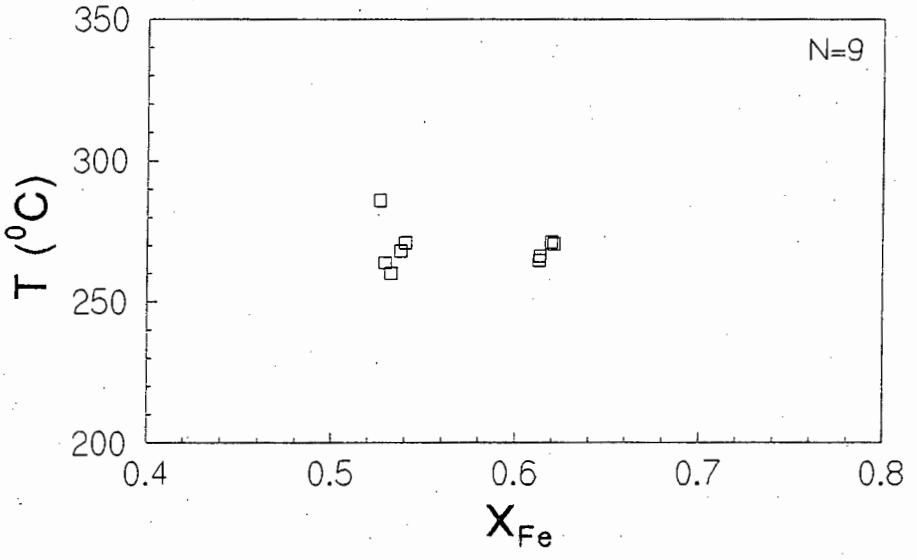

Fig.10.1: Calculated temperature of chlorite formation (after Zang and Fyfe, 1995) vs X_{Fe} of regionally metamorphosed hangingwall metabasalt samples VHG126 and VHG183.

The minerals present in the footwall quartzites can be described by a four-phase assemblage, consisting of quartz, pyrophyllite and chloritoid and a fluid phase. These can be represented by the five components SiO_2, Al_2O_3, FeO, MgO and H_2O in the F(M)ASH system (Fig.10.2). The

bulk rock composition of a pyrophyllitised footwall quartzite sample plots close towards the SiO_2 apex in Fig.10.2 and lies nearly on the Al - Si tie line. This indicates that the pyrophyllitised quartzite consists mainly of quartz and pyrophyllite and that an Fe-Mg phase (in this case chloritoid) is practically absent. These findings are also supported by modal mineral proportions of the footwall quartzites (see Chapter 4.).

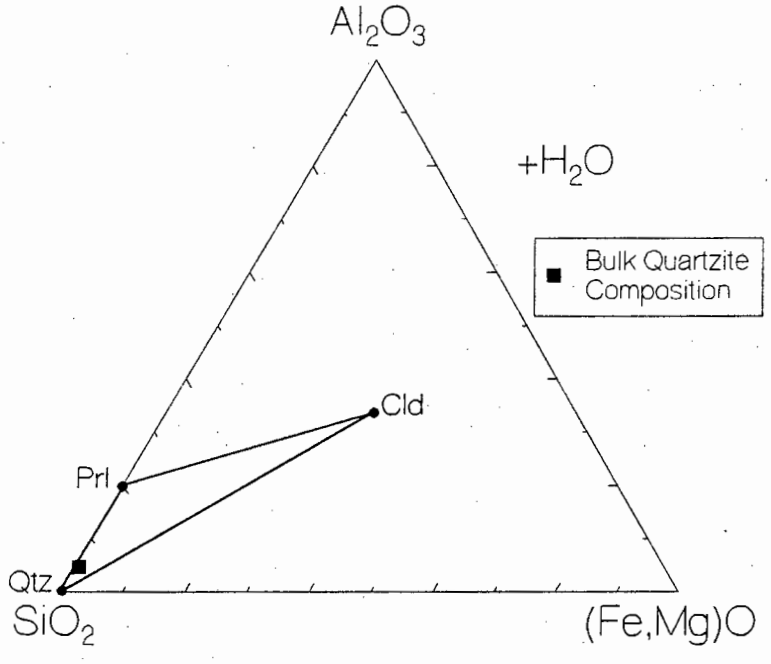

Fig.10.2: F(M)ASH system for the footwall quartzites is defined by the phases quartz (Qtz), pyrophyllite (Prl) and chloritoid (Cld) (H_2O in excess).

Mineral reactions which occurred in the quartzites during prograde metamorphism are limited by the mineral assemblage which is present. Several of these dehydration reactions are shown in Fig.10.3, and the steep slope in P-T space indicates that they are relatively insensitive to pressure. Better constraints on the peak metamorphic temperature are provided by the temperature range over which pyrophyllite is stable. The first pyrophyllite-forming reaction is given by

$$\underset{\text{kaolinite}}{Al_2Si_2O_5(OH)_4} + 2\underset{\text{quartz}}{SiO_2} = \underset{\text{pyrophylllite}}{Al_2Si_4O_{10}(OH)_2} + H_2O$$

and this reaction, assuming a pressure of 2 kbar, occurs at a temperature of c. 290°C (reaction (2) in Fig. 10.3). This provides a minimum temperature which was attained by the rocks. The anhedral embayed texture exhibited by the quartz grains in the footwall quartzites supports the formation of pyrophyllite through the consumption of quartz. Although the stability of pyrophyllite with respect to temperature is, especially at low pressures (<4 kbar), very dependent on $a(H_2O)$ (Frey, 1987), the absence of significant amounts of carbonates in the rocks precludes a significant reduction of $a(H_2O)$.

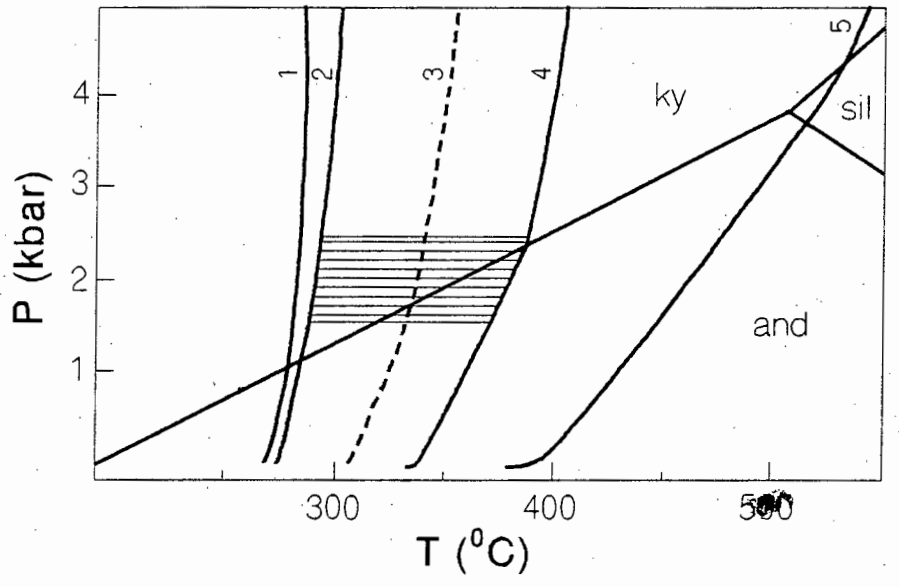

Fig.10.3: P-T diagram (after Frimmel, 1994) showing several metamorphic reactions in the FASH system. Solid lines represent stable mineral reactions involving the phases quartz (qtz), kaolinite (kln), pyrophyllite (prl), chlorite (chl), chloritoid (cld) and kyanite (ky) (H_2O in excess). Dashed line represents mineral reaction in the absence of quartz. Shaded area outlines the approximate P-T conditions of regional metamorphism as interpreted for the VCR in the study area.

The upper limit of pyrophyllite stability is given by the breakdown to form kyanite (or andalusite at lower pressures), quartz and a fluid phase. At a pressure of 2 kbar, the pyrophyllite breakdown

reaction occurs at T = c. 380^{0}C (reaction (4) in Fig.10.3). Kyanite has only been reported locally in quartz veins and fault zones in rocks of the Witwatersrand Basin, and has been interpreted to represent pyrophyllite breakdown (Schreyer and Bisschoff, 1982). The complete absence of kyanite from the footwall quartzites (and from the sedimentary rocks of the Witwatersrand Basin in general) therefore indicates that the peak metamorphic temperature which was attained was <380^{0}C. Based on pyrophyllite stability reactions, the peak metamorphic temperature which was attained in the study area is therefore interpreted to be 335 ± 45^{0}C at P = 2 kbar and assuming $a(H_2O) = 1$.

Other potential reactions in the F(M)ASH system are the formation of chloritoid during the reaction of chlorite and kaolinite (reaction (1) in Fig.10.3). However, the equilibrium chlorite/chloritoid mineral assemblage was not found in the footwall quartzites and therefore this reaction cannot be applied to the quartzites. The breakdown of kaolinite to produce pyrophyllite and kyanite and fluid (reaction (3) in Fig.10.3) is only stable in the absence of quartz. The presence of quartz as the major phase in the footwall quartzites therefore means that this reaction cannot be used to constrain peak metamorphic temperatures.

10.2 P-T Conditions of Metasomatism

No absolute constraints can be placed on the pressure which prevailed during metasomatic alteration processes. However, given the fairly late stage (around 2.0 Ga) at which the muscovite- and the chlorite-forming alteration events occurred (see Chapter 13.), similar pressures as for the peak regional metamorphism are inferred, i.e. c. 2 kbar. The limited occurrence of type IV chlorite at several localities in the VCR implies that the maximum lithostatic pressure of c. 2 kbar was, in places, slightly exceeded by horizontally focused fluid overpressure during the chlorite-forming metasomatic event.

A plot of the calculated temperature of chlorite formation versus X_{Fe} for chlorites from the footwall quartzites, hangingwall metabasalts and from the VCR is shown in Fig.10.4. The mean calculated temperature of formation of the chlorites is 306 ± 15^{0}C (1σ). Chlorites with calculated

temperatures as low as 215°C are also present. No textural evidence, however, exists which indicates that these lower-temperature chlorites belong to a different generation. Furthermore, no significant difference in the calculated temperature exists between chlorite types II, III, IV and V from the VCR, suggesting that they were all formed during the same event. The lower-temperature chlorites are therefore interpreted to be the result of incomplete equilibration between the infiltrating fluid and the rock.

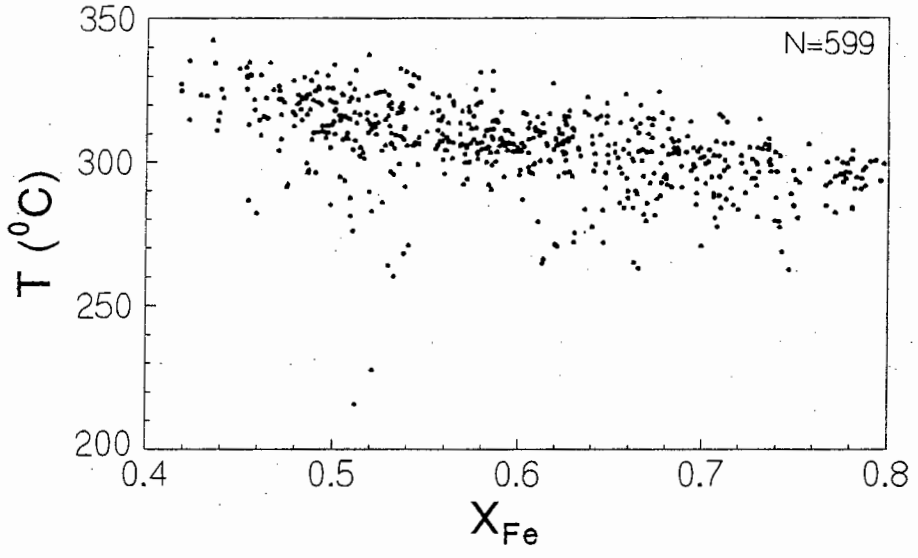

Fig.10.4: Calculated temperature of chlorite formation (after Zang and Fyfe, 1995) vs X_{Fe} of chlorites.

Using a prevailing pressure of 2 kbar at the time of entrapment of the quartz-hosted fluid inclusions, fluid inclusion data can be used to obtain estimates of the temperature during entrapment (Fig. 10.5). Two groups of isochores are present, the main one indicating a temperature of entrapment T_{trap} of c. 250°C and the other indicating T_{trap} of 330°C (for P = 2 kbar). The presence of both these T_{trap} populations in fluid inclusions in the auriferous quartz vein suggests that temperature fluctuations in the order of 80 - 100°C occurred during the same event. This is further supported by fluid inclusions from sample VHG087 which, although yielding different T_{trap} along differently orientated microfractures, are interpreted to have been trapped during the same event. The higher T_{trap} is similar to the mean temperature obtained from chlorite thermometry.

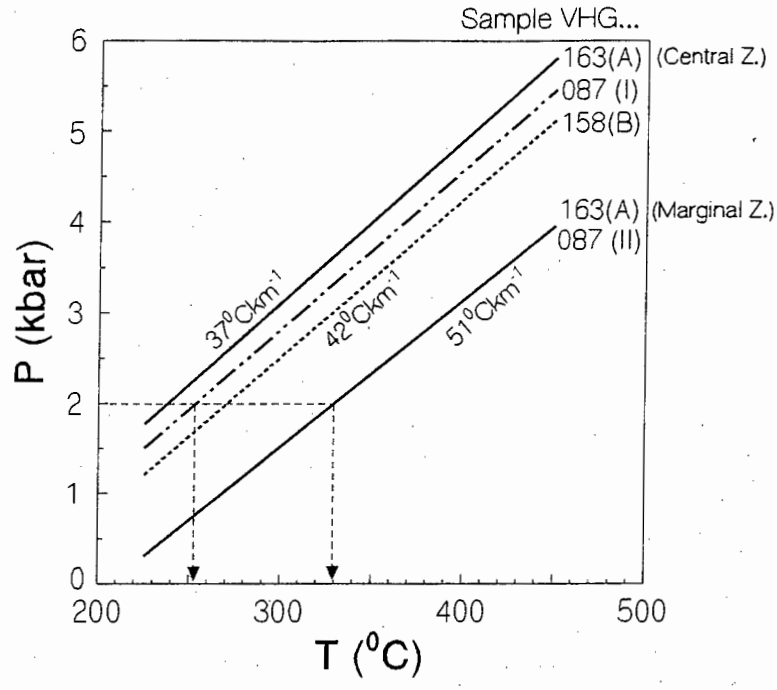

Fig.10.5: Isochores calculated for primary fluid inclusions (samples VHG158(B) and VHG163(A)) and secondary fluid inclusions along microfractures in hydrothermal vein quartz (sample VHG087), using the equation of state of Brown and Lamb (1989). Calculated geothermal gradients (based on the different isochores) are also shown.

Geothermal gradients of between 37 - 51°C/km are calculated from the isochores. Although these geothermal gradients are much higher than what would normally be expected for stable cratonic areas, they reflect post-depositional metasomatic alteration processes and as such do not indicate a true burial metamorphic geotherm.

11. Fluid Characterisation and Evolution

Both pre-depositional as well as post-depositional fluids are preserved in the rocks of the VCR. Pre-depositional fluids in form of fluid inclusion trails which terminate at quartz grain boundaries, can be found in quartz grains and quartz clasts of the quartzites and metaconglomerates of the VCR. Different generations of pre-depositional fluids can be distinguished on the basis of differently orientated fluid inclusion trails. This study, however, is concerned with the post-depositional fluids and therefore no further consideration will be given to the composition of the pre-depositional fluids.

11.1 Diagenesis

The progressive burial of the sediments which were deposited in a coastal/offshore marine environment in the Witwatersrand Basin resulted in the expulsion of substantial volumes of intergranular pore fluid. This was a gradual process, spanning a considerable period of time from syn-Witwatersrand deposition and culminating in the regional metamorphic event which probably reached its peak during Transvaal times (c. <2300 Ma).

Direct evidence for the composition of this pore fluid is absent. However, indirect evidence permits an estimation of hydrospheric and atmospheric conditions at the time during sediment deposition. The ubiquitous presence of rounded pyrite grains together with other heavy minerals (e.g. chromite and uraninite) and the absence of iron-titanium oxides (e.g. haematite, magnetite and ilmenite) and detrital feldspars (probably due to their breakdown to kaolinite) have been used to infer relatively low $f(O_2)$ and high f_2S) atmospheric conditions during the Archaean (Schidlowski and Junge, 1973; Holland, 1984). In addition, Krupp *et al.* (1994) concluded that fairly high atmospheric CO_2 partial pressures of c. 1 bar prevailed, which would conceivably have resulted in low pH meteoric waters.

11.2 Contact Metamorphism

Underground observations indicate that at the time of basalt eruption, the VCR was semi-consolidated and, by implication, close to or completely water saturated. The interaction of basalt at a temperature of c. 1100^{0}C with a water-saturated rock with an ambient temperature would probably have resulted in the explosive degassing and an almost instantaneous decrease in the temperature of the basalt to about 60 % of its original temperature (Jaeger, 1957).

The total cumulative thickness of Ventersdorp lavas which were extruded above the VCR in the Klerksdorp goldfield was c. 2800 m (Antrobus *et al.*, 1986; Bowen *et al.*, 1986). Ages of 2714 Ma and 2708 Ma for metabasalts from the Klipriviersberg and Platberg Groups, respectively (Armstrong *et al.*, 1991), suggest that the lavas were probably erupted over a relatively short period of time. Ritger (1990) modelled the heat generated by the extrusion of numerous basalt flows and concluded that a rise in temperature of 300 - 400^{0}C only in the upper-most 100 m of the Witwatersrand succession would have occurred. A rise in temperature to >300^{0}C that may have affected the footwall quartzites could have resulted in the formation of pyrophyllite. This would therefore make it difficult to distinguish between regional and contact metamorphic effects in this upper-most section. Pyrophyllite in the upper-most 100 m of quartzites could therefore be the result of either contact metamorphism or regional metamorphism or both.

However, pyrophyllite has been identified over a much larger stratigraphic range than in the first few hundred metres below the Ventersdorp lavas (e.g. Phillips, 1988). In the quartzites in the lower portion of the Witwatersrand Supergroup, the presence of pyrophyllite has been attributed to regional prograde metamorphism of a quartz-kaolinite mineral assemblage (Phillips, 1987; Wallmach and Meyer, 1990). Similarly, the presence of pyrophyllite in the footwall quartzites at Vaal Reefs No.10 Shaft may be the result of regional metamorphism. If this is the case, the implication is that subsequent metamorphic/metasomatic alteration events have eliminated any traces of possible contact metamorphism.

11.3 Regional Metamorphism

Regional metamorphic P-T conditions affected the footwall quartzites and hangingwall basalts to a similar extent. Detrital feldspars are absent from the VCR and the underlying footwall rocks. This may either be due to the weathering of the feldspars under acidic atmospheric conditions prior to the deposition in the Witwatersrand Basin, or it may indicate that a metamorphic fluid with a low pH prevailed during the *in situ* breakdown of feldspars within the Witwatersrand sediments. The absence of metamorphic muscovite and the predominance of pyrophyllite in the footwall quartzites constrains the pH to less than 3.9 at $a(K^+) = 0.1$ *m*.

The absence of carbonate rocks from the VCR and footwall quartzites suggests that $a(H_2O)$ of the fluid was close to unity. The presence of CO_2-rich fluid inclusions as well as calcite in quartz veins, however, indicates that $a(H_2O)$ of the fluid varied with time.

11.4 K^+ Metasomatic Alteration Event

Two metasomatic alteration events can be identified in the VCR and surrounding footwall and hangingwall rocks. The first of these was a potassic alteration event during which fine grained muscovite (mica II) was formed, probably at the expense of pyrophyllite. Where muscovite is present in the footwall quartzites (within 3 m of the VCR), pyrophyllite is virtually absent. The pH of the potassic metasomatic fluid is constrained by the stability of muscovite and the absence of pyrophyllite and K-feldspar to between 3.9 and 5.5 at an assumed $a(K^+)$ of 0.1 *m* and T = 300^{0}C.

Fluid inclusion microthermometry of aqueous secondary fluid inclusions hosted in quartz veins and in the VCR quartzite has not, however, permitted the satisfactory identification of fluid inclusions which are related exclusively to the muscovite-forming alteration event. Only a single fluid inclusion with $T_e = -10^0$C (indicating an NaCl/KCl-rich fluid) was observed. Most of the fluid inclusion data in this study comes from quartz veins and the apparent absence of K-bearing fluid inclusions may indicate that the muscovite-forming alteration event occurred prior to the

formation of these quartz veins.

In the Welkom goldfield, Frimmel *et al.* (1993) were able to identify a low salinity (<4 wt% $NaCl_{eq}$) K-rich fluid with T_h = 130 - 140°C within secondary quartz. The authors attribute this fluid to the potassic alteration event, and tentatively relate this to the formation of the Vredefort Dome and/or intrusion of the Bushveld Igneous Complex.

11.5 Chlorite-forming Alteration Event

A chlorite-forming metasomatic alteration event post-dates the K^+ metasomatic event. As mentioned above, the clear distinction between the fluids which resulted in each of these alteration events is difficult. However, several quartz veins which contain euhedral pseudohexagonal chlorite grains (indicating that chlorite grew in equilibrium with the fluid) have been observed. Fluid inclusion measurements from such quartz veins yield temperatures and salinities which do not differ significantly from those of non-chlorite bearing quartz veins. The fluid inclusion data is interpreted to reflect the conditions of chlorite formation in those quartz veins.

An aqueous fluid containing a mixture of $NaCl\text{-}CaCl_2\text{-}MgCl_2\text{-}(KCl)$ (based on first melting temperatures) is present in secondary fluid inclusions. This fluid is of low salinity (<9 wt% $NaCl_{eq}$) and homogenisation temperatures indicate a range of 250 - 330°C during trapping (corrected for 2 kbar pressure). The density of these fluids ranges from 0.9 - 1.0 gcm^{-3}. In addition, chlorite thermometry of chlorite grains within several quartz veins yield a calculated temperature of formation of 260 - 330°C.

The ambient oxygen and sulphur fugacities during the chlorite-forming metasomatic alteration event can be estimated from the composition of chlorite that coexists with Fe-sulphide phases (Bryndzia and Scott, 1987). The wide-spread distribution of pyrite in the VCR and the local presence of pyrrhotite suggests that $f(S_2)$ and $f(O_2)$ conditions in the VCR were close to the pyrite-pyrrhotite phase boundary (Fig. 11.1). A minimum value for $f(S_2)$ of 10^{-11} bars (for the VCR) was calculated using the GEO-CALC program of Brown *et al.* (1989). A realistic upper

limit of sulphur fugacity is difficult to constrain from the information available. A value of around 10^{-38} - 10^{-40} bars is suggested for $f(O_2)$, based on the assumption that conditions were close to the pyrite-pyrrhotite boundary.

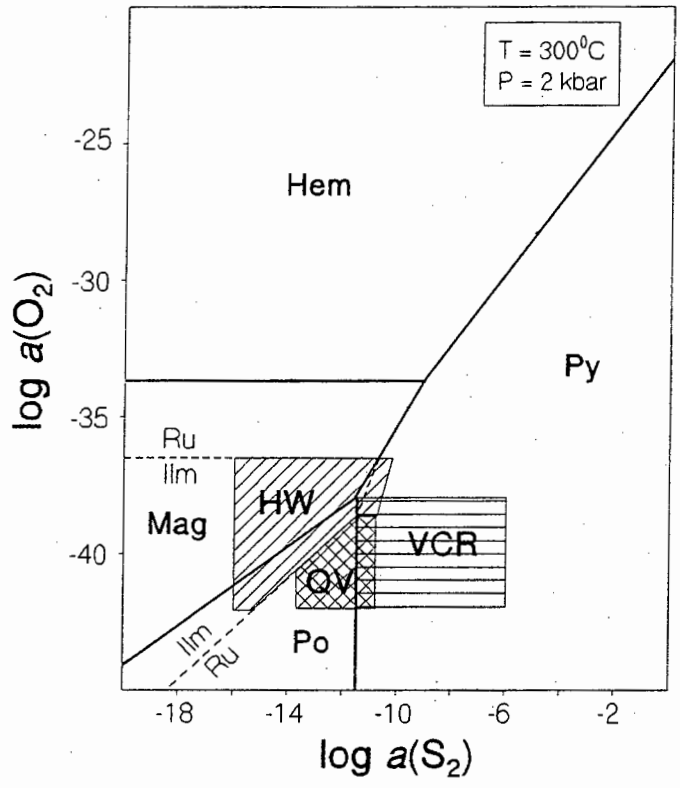

Fig.11.1: Sulphur vs oxygen fugacity diagram showing the stability fields for pyrite (Py), pyrrhotite (Po), magnetite (Mag), haematite (Hem), rutile (Ru) and ilmenite (Ilm) at T = 300°C, P = 2 kbar. Differently hatched areas indicate the possible ranges in fugacities which may have existed in the VCR, the metabasalts (HW) and in quartz veins (QV). Phase boundaries were calculated using the GEO-CALC program of Brown *et al.* (1989).

The large ranges in chlorite X_{Fe} which occur between VCR samples (0.4 - 0.8) as well as within samples (0.44 - 0.59) indicate fluctuations in $f(O_2)$ and $f(S_2)$ of the chlorite-forming fluid on a centimetre scale. The presence of euhedral pyrrhotite platelets in several quartz veins and the occasional presence of pyrite indicate that $f(S_2)$ conditions in the quartz veins were generally slightly lower than in the VCR. In addition, the presence of pyrite as the stable Fe-sulphide phase

in the contact zone of the hangingwall metabasalt and the presence of magnetite and ilmenite in the dark phenocryst zone indicate that the $f(S_2)$ in the metabasalts was several orders of magnitude lower than in the VCR.

The identification of localised Fe-metasomatised zones (characterised by Fe-rich chlorites and the presence of siderite) in the VCR are interpreted to reflect infiltration by a (fairly late-stage) Ca^{2+}-rich fluid. The limited distribution of these Fe-metasomatised zones indicate that during this event, which post-dates the main chlorite-forming alteration event, relatively low fluid:rock ratios existed. This implies that the chlorite composition was largely controlled by the bulk rock composition.

12. Metamorphism and Mobility of Gold

12.1 Introduction

The extent of gold mobility in a hydrothermal system does not only depend on P, T and fluid chemistry, but also on (i) the presence of suitable conduits for the fluid, (ii) the quantity of fluid available for transport and (iii) changes in any one of the independent parameters that can lead to the precipitation of the gold. The VCR can be considered as part of a hydrothermal system in the sense that it has experienced the effects of muscovite- and chlorite-forming metasomatic alteration events.

Within the context of the metamorphosed placer theory, the presence of conduits is not critical because gold mobilisation on a local scale only is predicted (Frimmel *et al.*, 1993). However, if the hydrothermal model of gold origin in the Witwatersrand is considered, the presence of suitable fluid conduits becomes very important. The relatively porous and coarse grained nature of the Witwatersrand conglomerate horizons compared to the quartzites makes the conglomerates potential zones of fluid flow. The VCR in particular would have been very suitable, because it is capped by denser, less permeable basalts, which would have lead to a very focused fluid flow. The major extensional normal faults and thrust faults which have been documented along the margin of the Witwatersrand Basin (e.g. Myers *et al.*, 1992) may have acted as additional conduits for metamorphic/metasomatic fluids.

Evidence for large amounts of fluids which allegedly have percolated through the rocks of the Witwatersrand Basin during its post-depositional history has been presented by Phillips *et al.* (1990). Large fluid:rock ratios do not, however, automatically imply extensive gold mobility. Gold solubility is strongly dependent on a series of chemical parameters, such as pH, $f(O_2)$, $f(S_2)$, $a(H_20)$, temperature and pressure (e.g. Fyfe and Kerrich, 1984; Seward, 1984; Shenberger and Barnes, 1989; Bowers, 1991; Hayashi and Ohmoto, 1991). The most critical of these factors, which probably influenced the mobility of the gold in the VCR, are discussed below.

12.2 Fluid Characteristics during Gold Mobilisation

The close spatial association of gold with chlorite types II and III and with (predominantly secondary) pyrite suggests that gold was mobilised during the chlorite-forming metasomatic alteration event. The coexistence of pyrite together with type II chlorite, the presence of small secondary rutile needles with this chlorite type and the local presence of pyrrhotite in the VCR indicate that $f(S_2)$ conditions of the fluid were probably close to the pyrite-pyrrhotite phase boundary. This allows $f(S_2)$ to be calculated as $>10^{-11}$ bars (see Fig.11.1). At conditions close to the pyrite-pyrrhotite boundary, $f(O_2)$ conditions can be roughly constrained as $<10^{-38}$ bars. Boer *et al.* (1995), using quadrupole mass spectrometric fluid inclusion data, calculated $\log f(H_2S) = 0.6$.

Based on chlorite thermometry, the temperature which prevailed during gold mobilisation in the VCR is constrained at 307 ± 14^0C (see Chapter 7.1) and the pressure is estimated at c. 2 kbar (see Chapter 10.). Data from this study precludes the determination of the pH of the chlorite-forming (and gold mobilising) fluid. Boer *et al.* (1995), however, determined a pH of around 3 for carbonic-rich fluid inclusions, which they relate to gold mobilisation in the VCR at Vaal Reefs No.10 Shaft.

Two groups of primary fluid inclusions of similar salinity (c. 6 wt% $NaCl_{eq}$) but with different temperatures of entrapment of around 250^0C and 330^0C were found in the auriferous quartz vein (samples VHG163(A)-(C)). The low first melting temperatures of between -35 - -44^0C which were observed in the majority of these fluid inclusions suggest a Ca-rich nature of these fluids, the $a(Ca^{2+})$ of which is estimated at c. 0.1 *m*. Both of these fluids are interpreted to have had the potential to carry gold in solution (see below).

The composition of the fluid as discussed above is very similar to a fluid described by Frimmel *et al.* (1993) from authigenic, gold-bearing quartz. These authors describe that fluid as Ca-rich with a salinity of c. 12 wt% $NaCl_{eq}$ (corresponding to 0.1 *m* Ca^{2+}) and $T_h = 134^0$C. They interpreted this fluid as being responsible for the post-depositional mobilisation of the gold in the Basal Reef.

Other occurrences of gold-bearing quartz veins have been described by Hallbauer (1983) who noted that the T_h of the fluid inclusions within the sample studied was 340 - 360°C. A gold-bearing quartz vein from the C Reef from the Klerksdorp goldfield has been described by Phillips *et al.* (1988), but the exact composition of this fluid is not given. Instead, the composition is quoted together with other quartz vein-hosted fluid inclusions as having a salinity of 6 - 18 wt% $NaCl_{eq}$ and $T_h = 155 \pm 30^0C$.

Gold chloride complexing seems to be more important in low $f(S_2)$, high temperature systems (>400°C) (Seward, 1984), whereas gold bisulphide complexes are important under lower temperatures (<350°C) within a S-rich system (Hayashi and Ohmoto, 1991). Meyer *et al.* (1991) suggest that the solubility of gold in the conglomerates of the Witwatersrand Basin in form of the $Au(HS)_2^-$ complex at T = 300 - 350°C was about three orders of magnitude less than that of the $AuCl_2^-$ complex at T > 350°C (using concentrations of S = 0.01 mole, K^+ = 0.3 mole and Cl^- = 2.0 moles). The importance of both the chloride and the bisulphide gold complexes in the VCR at Vaal Reefs No.10 Shaft has been discussed by Boer *et al.* (1995). These authors suggested that gold was equally soluble as either of these two complexes, assuming a temperature of 350°C. The temperature determined in this study for chlorite formation and associated gold precipitation is, however, lower (c. 310°C) and therefore, the Au-S complex is believed to have been dominant.

Solubility contours of the $AuCl_2^-$ and $Au(HS)_2^-$ complexes are superimposed on a sulphur versus oxygen fugacity diagram, together with the stability fields of pyrite, pyrrhotite, magnetite and haematite (Fig.12.1) (after Romberger, 1991).

Although the conditions during gold mobilisation in the VCR were different to those used to calculate the gold solubilities and stability field boundaries in Fig.12.1 (and therefore the gold solubilities as shown in Fig.12.1 cannot directly be applied to the VCR), the figure illustrates how gold mobility in the VCR may have been controlled. For a gold bisulphide complex, a decrease in $f(S_2)$ by one order of magnitude would have reduced the gold solubility by more than one order of magnitude (at constant $f(O_2)$). Reduction in $f(S_2)$ is an efficient mechanism for the precipitation of gold (Hayashi and Ohmoto, 1991). A decrease in $f(O_2)$ (at constant $f(S_2)$) will, however, result in an increase in gold solubility. This suggests that fluctuations in $f(S_2)$ and $f(O_2)$ in the VCR may

have been two very important factors in controlling gold mobility. Support for such fluctuations comes from the range in chlorite X_{Fe} of 0.4 - 0.8, by the association of gold with bitumen nodules and by the rare association of gold with pyrrhotite in veins. These associations imply that variations in $f(S_2)$ and/or $f(O_2)$ may have played an important role in determining gold (and pyrite) solubilities in the VCR.

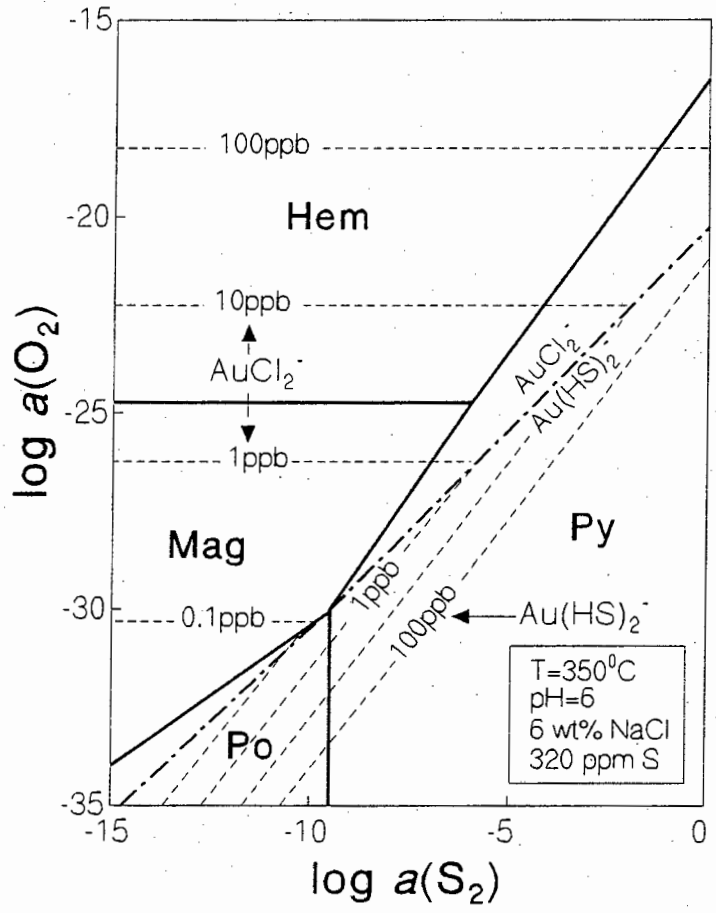

Fig.12.1: Gold solubility of $Au(HS)_2^-$ and $AuCl_2^-$ complexes as a function of $f(O_2)$ and $f(S_2)$ in a solution at T = 350°C, pH = 6, salinity = 6 wt% NaCl and 320 ppm S (after Romberger, 1991). Also shown are the stability fields of pyrite (Py), pyrrhotite (Po), magnetite (Mag) and haematite (Hem).

The close association of gold with sulphides (e.g. galena, sphalerite and bravoite (?)) in the auriferous quartz vein implies that precipitation mechanisms for these minerals were related to each other. A possible mechanism that could have resulted in the precipitation of these minerals

was the interaction of a sulphide-enriched fluid with the country rock, thereby leading to a decrease in $f(S_2)$, which in turn would have reduced the gold solubility.

A positive correlation between gold content and elevated volatile content (mainly CH_4) in fluid inclusions from a set of VCR samples has been recognised by Boer *et al.* (1995). Gold is also associated with bitumen nodules in the VCR matrix and in quartz veins, although bitumen-bearing quartz veins, which are free of any visible gold, have also been observed.

Another mechanism which has the potential to precipitate gold may be the adsorption of Au_{aq} by sulphide minerals as determined experimentally by Bancroft and Jean (1982). The occurrence of gold and other precious metal complexes in form of subrounded particles on a pyrite substrate has been described as "cling-ons" (Knipe *et al.*, 1992; Foster, 1993) and is attributed to the process of gold adsorption. Textures found in this study, that are similar to those described by Knipe *et al.* (1992) and Foster (1993), suggest that adsorption might have played some role in the precipitation of gold.

12.3 Homogenisation of Gold Particles

Witwatersrand gold particles contain Ag and Hg as impurities. Intra- and inter-grain post-depositional diffusion will tend to homogenise the gold particles. The time required for such homogenisation to occur through the process of intracrystalline diffusion can be calculated from the following formula (from Czamanske *et al.*, 1973):

$$t = \left(\frac{-\int_0^{c'} x\,dc}{2\,(dc/dx)_{c'}}\right)/D_{c'}$$

where t = time in sec
$D_{c'}$ = diffusion coefficient in cm^2/s at concentration c'
x = distance in cm
dc = change in composition; if homogeneous, dc = detection limit (= 0.2 wt%)
dx = area, i.e. integral (given by 1/2 x diameter x change in concentration (wt%)).

The analysis of gold particles which precipitated from the auriferous hydrothermal quartz vein indicates that individual gold particles are inhomogeneous with respect to Ag and Au (see Chapter 7.3). This is perhaps surprising, because the time required for the homogenisation of a 30 μm gold particle (which is the approximate size of the two inhomogeneous gold particles in the auriferous quartz vein) at T = 300°C, and assuming an initial variation in Ag content of 10 wt%, is calculated to be only c. 180000 years (Fig.12.2). At a temperature of 200°C, the time required for the homogenisation of the same gold particles would have been c. 100 million years (i.e. an increase of three orders of magnitude). The diffusion and homogenisation of gold particles with respect to Hg would have occurred approximately two orders of magnitude faster. The lack of homogenisation with respect to Ag implies that the temperature within the auriferous quartz vein decreased fairly rapidly to well below 300°C soon after gold precipitation had occurred.

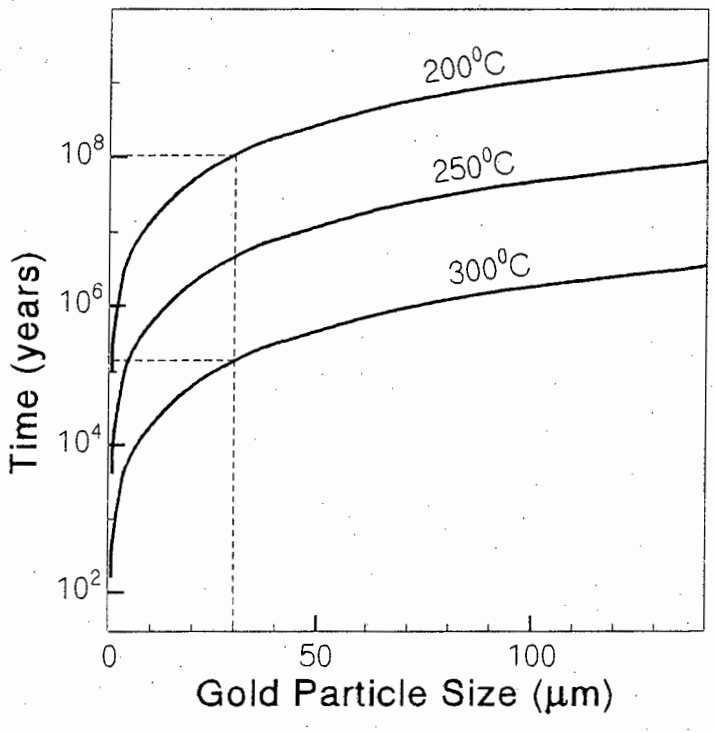

Fig.12.2: Diagram illustrating the time required to homogenise a gold particle with respect to Ag at different temperatures, assuming an initial variation of 10 wt% Ag. Diffusion coefficients are from Askill (1989).

Chlorite thermometry suggests that gold mobilisation in the VCR occurred at $T = 307 \pm 14^{0}C$. Although individual gold particles in the VCR are homogeneous, a large inter- and intra-sample compositional variation of gold particles exists. This implies that the conditions during chlorite formation (and gold mobilisation) were such that inter-particle homogenisation with respect to Ag and Hg could not occur. Such conditions may have been caused by a rapid drop in temperature or by very low fluid:rock ratios after gold precipitation.

13. Conclusions

13.1 Post-depositional Alteration Events

At Vaal Reefs No.10 Shaft in the Klerksdorp goldfield, a metamorphic/metasomatic alteration halo can be identified surrounding the VCR. The scale of this alteration halo, which macroscopically is identifiable by the discolouration of footwall quartzite and hangingwall metabasalt rocks, extends for tens of centimetres to several metres into the footwall and hangingwall rocks. Three important alteration events which have affected the footwall quartzites, the hangingwall metabasalts and the VCR can be documented on the basis of mineralogical and bulk rock compositional changes. Two of these events are interpreted to be the result of metasomatic alteration. A schematic representation of the metamorphic/metasomatic alteration events which have affected the VCR, together with the mineral paragenesis and development of structural features, are shown in Table 13.1.

Contact metamorphism during the extrusion of the Ventersdorp lavas at c. 2714 Ma (Armstrong *et al.*, 1991) was undoubtedly the first important metamorphic event to affect the VCR. A likely reason that no evidence for this event could be found is that the effects of contact metamorphism were masked by later metamorphic/metasomatic overprints.

The first product of progressive metamorphism of the footwall quartzites is pyrophyllite. The fine grained nature and lack of preferred orientation of the pyrophyllite and the fact that its occurrence is unrelated to faults, shear zones or veins, suggests that it is a product of burial metamorphism. The embayed texture exhibited by quartz grains and the absence of kaolinite from the quartzites indicate that pyrophyllite probably formed by *in situ* recrystallisation of the matrix at the expense of quartz and kaolinite during a quartz-consuming dehydration reaction. Pyrophyllite stability in the footwall quartzites indicates low pH conditions of <4 and implies that leaching of alkalis occurred. This is supported by a fairly high CIA of >0.9 in the pyrophyllitised quartzites. In places, pyrophyllite is associated with chloritoid, both of which are attributed to peak metamorphism.

Table 13.1: Paragenetic Sequence Associated with Metamorphic/Metasomatic Alteration Events

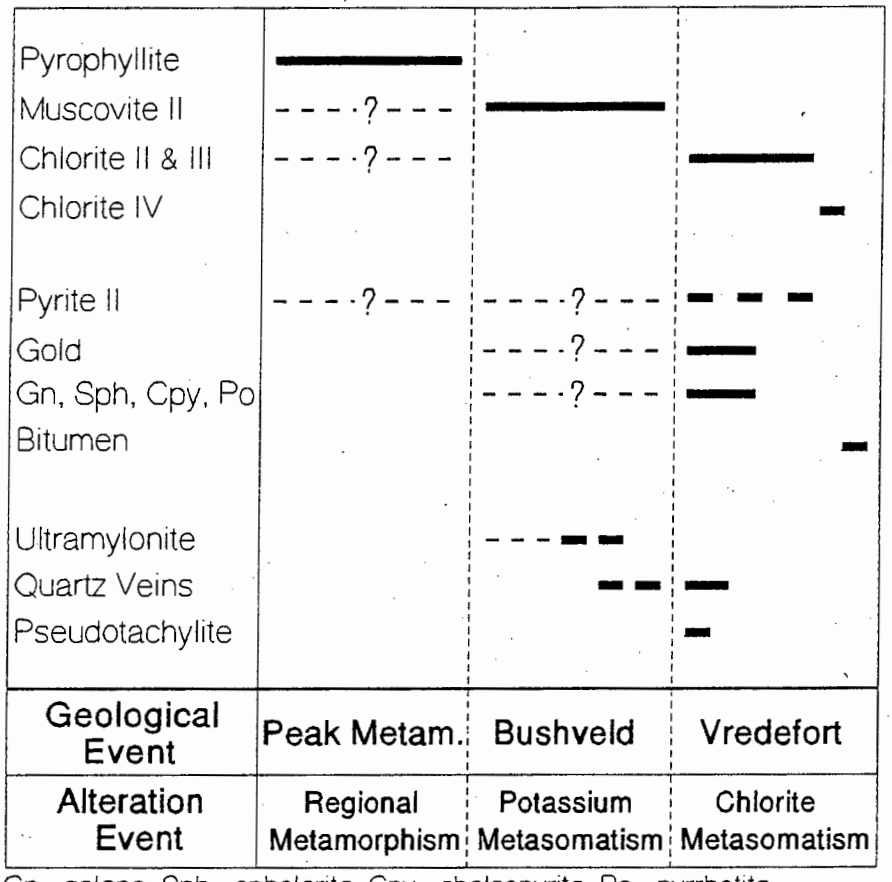

Gn - galena, Sph - sphalerite, Cpy - chalcopyrite, Po - pyrrhotite

In the higher hangingwall metabasalts (> c. 30 m above the VCR) a mineral assemblage consisting of plagioclase, actinolite, epidote/clinozoisite, quartz, chlorite, calcite ± sulphides is observed. This mineralogy is attributed to lower greenschist facies conditions which were attained during regional metamorphism of the basalts.

Based on the presence of pyrophyllite and the absence of kaolinite and kyanite in the footwall quartzites, and an estimated overburden of c. 6500 m (combined thickness of the Ventersdorp and Transvaal Supergroups in the Klerksdorp goldfield) towards the end of Transvaal depositional times, peak metamorphic P-T conditions of c. 2 kbar and 335 ± 45^{0}C are inferred for the VCR and footwall quartzites in the Klerksdorp goldfield. These conditions were probably reached towards the end of the deposition of the Transvaal Supergroup around 2200 Ma.

The second prominent alteration event can be described as a K^+-metasomatic alteration which was focused along the VCR. This resulted in the formation of fine grained muscovite (mica type II) in the footwall quartzites and hangingwall metabasalts within c. 5 - 10 m of the VCR. This potassium metasomatic alteration event is attributed to the interaction of a K^+-rich fluid with the regionally metamorphosed, pyrophyllite-bearing quartzites and plagioclase-rich metabasalts. Major elements that were particularly mobile during this alteration event are K, Na, Ca and Si.

The K^+-forming reaction also involved the formation of secondary quartz, which is interpreted to have reprecipitated locally as secondary quartz overgrowths (in the quartzites) and in amygdales and quartz veins (in the metabasalt). Optical petrography and CLI confirm the presence of authigenic/metamorphic quartz overgrowths around detrital quartz grains in the VCR and in the footwall quartzites. This event also resulted in a marked decrease in the CIA in the footwall quartzites from >0.9 in the pyrophyllite-bearing quartzites to <0.8 in the muscovite-bearing quartzites.

An alternative explanation for the sericitisation could be K-enrichment as a result of percolating groundwater (e.g. Sutton *et al.*, 1991). However, in view of the greater vertical extent of K^+-alteration experienced by the hangingwall metabasalts, this alternative is considered very unlikely. The almost complete absence of muscovite from the VCR can be explained by the overprinting of a subsequent alteration event which was also focused along the VCR.

The third (and in the VCR the latest identifiable) alteration event is a chlorite-forming metasomatic event. This alteration event is characterised by the formation of predominantly type II chlorite in and immediately around the VCR. Chloritisation occurred up to a maximum distance of c. 1 m into the footwall quartzites and up to c. 5 m into the hangingwall metabasalts. This indicates that the chlorite-forming event was less intense than the previous muscovite-forming alteration event, possibly because of lower fluid:rock ratios. The chlorite-forming event, which was identified over the whole study area (i.e. covering at least 4 km^2), was associated with the introduction of significant amounts of Fe and Mg into the VCR and surrounding rocks. In addition, modelling of the bulk rock composition indicates the removal of Si, K and Al from the footwall quartzites and Si, K and Ca from the hangingwall metabasalts.

The pervasive chloritisation of the VCR, during which only traces of muscovite remained, suggests that the VCR acted as a fluid pathway for these Fe- and Mg-rich fluids. The fact that conglomerate- and quartzite-dominated reef facies contain approximately equal amounts of chlorite implies that the chlorite-forming fluid was able to move through the VCR irrespective of the grain/clast size. This is also supported by underground observations which show that the greatest extent of chloritisation of the footwall quartzites occurs where the VCR is thinnest, implying that the greatest fluid:rock ratios existed where the VCR was poorly developed.

The presence of relatively Mg-rich type IV chlorites which post-date type II chlorites implies that more than one fluid pulse occurred during the chlorite-forming event. However, no difference in the calculated temperature of chlorite formation between these two chlorite types exists, suggesting that type II and IV chlorites were formed under similar temperature conditions, possibly during the same event.

The vertically more extensive nature of the K^+ metasomatism and the fact that this event pre-dates the pseudotachylite event are strong indications that the K^+ alteration event is related to the earlier Bushveld emplacement (dated at 2054 ± 2 Ma, Walraven and Hattingh, 1993). This may be supported by K-Ar ages of c. 1900 - 2000 Ma of detrital muscovite and metamorphic white mica from the VCR from Western Deep Levels South gold mine, which are interpreted by Zhao *et al.* (1995) as evidence of a major isotope resetting event. A possible source of K for this metasomatic event could have been the magmatic fluids which were associated with the intrusion of the felsic Bushveld magmas.

Underground observations indicate that the chlorite metasomatic alteration event post-dates the formation of the pseudotachylite (dated at 2006 ± 17 Ma, Trieloff *et al.*, 1994). Pseudotachylite formation has been related to the Vredefort event (Trieloff *et al.*, 1994) and by analogy, chlorite formation is related to the same event (dated at 2024 Ma, Kamo *et al.*, 1995). In addition, the bedding-perpendicular orientation of type IV chlorites in the VCR indicates that locally, the horizontally focused fluid pressure exceeded the lithostatic pressure of c. 2 kbar during some stage of the chlorite-forming alteration event.

Two sets of quartz veins (a bedding-perpendicular and an approximately bedding-parallel set) are present in close proximity to the VCR. Based on underground cross-cutting relationships and fluid inclusion microthermometric data, these two sets of quartz-filled fractures are coeval in age. Similar fracture orientations are also visible on a microscopic scale.

The orientation of the bedding-perpendicular fractures/quartz veins are interpreted to be related to extension tectonics with s^3 orientated north-east/south-west. The approximately bedding-parallel quartz veins utilised pre-existing zones of weakness (e.g. bedding planes), and are interpreted to be related to local fluid pressures exceeding the lithostatic pressure.

13.2 Conditions and Timing of Gold Mobilisation

Gold in the VCR is commonly associated with secondary quartz, with a textural type II chlorite (which is interpreted to be a product of metasomatic alteration) and with sulphides (mainly secondary pyrite). The sulphide grain morphology and the association of pyrite (and other sulphides) with metasomatic chlorite suggest that most of the sulphides are of secondary origin, possibly related to the chloritisation event. The replacement of secondary pyrite by bitumen nodules also indicates that the bitumen is of hydrothermal origin and that it is a relatively late-stage mineral in the paragenetic sequence.

The close association of gold with chlorite types II and III implies that physico-chemical conditions of the chlorite-forming fluid were suitable for the mobilisation of the gold in the VCR. Chlorite types II, III and IV in the VCR are interpreted to be products of chlorite metasomatism. Chlorite thermometry indicates a temperature of 307 ± 14^0C for this event.

Based on the close mineralogical association of metasomatic chlorite with secondary gold, the timing of the latest gold mobilising event in the VCR is therefore given by the age of the Vredefort event at 2024 Ma. However, considering the protracted and complex metamorphic and fluid history of the Witwatersrand Basin, it is likely that conditions suitable for gold mobilisation occurred more frequently. Supporting evidence for this comes from the age of secondary zircon

which is present together with gold in secondary quartz in a Basal Reef sample, Welkom goldfield (Frimmel, 1994). The zircon age which has been obtained is 2.5 Ga, which by implication is also the time of gold mobilisation in the Basal Reef sample. The age of this gold mobilisation event therefore pre-dates that of the latest VCR gold mobilisation by c. 500 Ma.

Physico-chemical conditions in and around the VCR must have controlled gold solubility. Variations in fluid:rock ratios are indicated by the extent to which the rocks around the VCR were first sericitised and at a later stage chloritised. Gold dissolution would have been favoured by the interaction of a metasomatic fluid with pyrite-rich zones within the VCR, which conceivably would have lead to an increase in the $f(S_2)$ of this fluid. Given that a temperature of c. 300°C prevailed during gold mobilisation, the gold complex which was most likely to be formed was a bisulphide complex (Shenberger and Barnes, 1989; Hayashi and Ohmoto, 1991).

Based on the stability of pyrite in the VCR over virtually the whole study area and only the rare presence of pyrrhotite, $f(O_2)$ and $f(S_2)$ conditions can be constrained as being within the pyrite stability field. The equilibrium coexistence of pyrite with type II chlorite, and the presence of secondary rutile needles in type II chlorite, indicates that $f(S_2)$ conditions were probably close to the pyrite-pyrrhotite boundary. This sets a lower limit of $f(S_2) > 10^{-11}$ bars at T = 300°C. A lower limit of $f(O_2)$ is more difficult to constrain, but based on the presence of rutile together with chlorite within the pyrite stability field, a minimum value for $f(O_2)$ of between 10^{-35} and 10^{-40} bars is inferred.

Evidence that fluctuations in $f(S_2)$ and/or $f(O_2)$ of the fluid were important in determining the solubility of gold and sulphides is provided by the mineralogy in the auriferous quartz vein. The close association of gold with galena, bravoite (?) and sphalerite in this quartz vein suggests that a decrease in $f(S_2)$ and/or $f(O_2)$ (e.g. as a result of changes in the fluid:rock ratio) resulted in the precipitation of sulphides, which in turn lead to the precipitation of gold. Marked fluctuations in quartz solubility in this quartz vein, as indicated by CLI, may be related to changes in the pH and/or temperature of the fluid. An increase in T or a decrease in pH would have lead to quartz precipitation.

Significant variations in the inter- and intra-sample gold particle compositions are present in the majority of the VCR samples examined. A compositional variation in Ag and Hg of up to 5 wt% exists on a thin section scale in the VCR samples. Furthermore, two gold particles from the auriferous quartz vein are inhomogeneous with respect to Ag and Au on an intra-particle scale of 30 μm. The time required to homogenise these gold particles with respect to Ag, assuming an initial variation in Ag of 10 wt% and T = 300^{0}C, is c. 180,000 years. If the temperature had dropped to 200^{0}C shortly after gold precipitation, then the time required to homogenise the same gold particles would be just over 100 million years. The lack of homogenisation of these hydrothermal gold particles suggests that the temperature must have dropped rapidly after gold mobilisation, thus making the homogenisation of gold particles by diffusion exceedingly slow.

The temperature of c. 310^{0}C which was attained during the chlorite-forming metasomatic event does not differ significantly from the regional peak metamorphic temperature achieved during burial and possibly during the Bushveld event. The fact that gold particles are inhomogeneous on an inter- and intra-sample scale as well as on an intra-grain scale implies that the temperature of the gold mobilising event decreased to well below 300^{0}C (and possibly to below 200^{0}C) fairly quickly after gold precipitation. An event of a sufficiently short-lived nature to satisfy this requirement could be the Vredefort impact event.

REFERENCES

Antrobus, E.S.A., Brink, W.C.J., Brink, M.C., Caulkin, J., Hutchinson, R.I., Thomas, D.E., Van Graan, J.A. and Viljoen, J.J., 1986. The Klerksdorp Goldfield. *In:* Anhaeusser, C.R. and Maske, S. (Eds). Mineral Deposits of Southern Africa. **1**, Geol. Soc. S. Afr., 549-598.

Armstrong, R.A., Compston, W., Retief, E.A., Williams, I.S. and Welke, H.J., 1991. Zircon ion microprobe studies bearing on the age and evolution of the Witwatersrand triad. Precambr. Res., **53**, 243-266.

Armstrong, R.A., Fanning, C.M. and Eldridge, C.S., 1995. Geochronological and isotopic constraints on provenance and post-depositional alteration of the Witwatersrand Supergroup. Abstr. Centennial Geocongress (1995), Geol. Soc. S. Afr., Johannesburg, 1083.

Askill, J., 1989. Radioactive tracer diffusion data for pure metals. *In:* Weast, R.C., (Ed.). CRC Handbook of Chemistry and Physics, 70th edition, Boca Raton, Florida, CRC Press, F54-F60.

Babcock, R.S. 1973. Computational models of metasomatic processes. Lithos, **6**, 179-190.

Bancroft, G.M. and Jean, G., 1982. Gold deposition at low temperature on sulphide minerals. Nature, **298**, 657.

Behr, H., Fyfe, W.S., Hoefs, J., Johannes, W. and Touret, J.L.R., 1989. Der Nachweis von Paläoporosität, Paläopermeabilität und Paläofluidfluss im subsedimentären Basement mit Kathodolumineszenz. Abstract: Gesteinsfluide: Ihre Herkunft und Bedeutung für geologische Prozesse. Nds. Akad. Geowiss. Veröfftl., Hannover, 27-42.

Bisschoff, A.A., 1982. Thermal metamorphism in the Vredefort Dome. Trans. Geol. Soc. S. Afr., **85**, 43-57.

Bodnar, R.J., 1993. Revised equation and table for determining the freezing point depression of H_2O-NaCl solutions. Geochim. et Cosmochim. Acta, **57**, 683-684.

Boer, R.H., Reimold, W.U. and Kesler, S.E., 1995. Conditions of gold remobilization in the Ventersdorp Contact Reef, Witwatersrand Basin. Extended abstr. Geol. Soc. S. Afr.: The Economic Significance of Metamorphism and Fluid Movement within the Witwatersrand Basin, 26 October 1995, Western Deep Levels, 1-4.

Bowen, T.B., Marsh, J.S., Bowen, M.P. and Eales, H.V., 1986. Volcanic rocks of the Witwatersrand Triad, South Africa. I: Description, classification and geochemical stratigraphy. Precambr. Res., **31**, 297-324.

Bowers, T.S., 1991. The deposition of gold and other metals: Pressure-induced fluid immiscibility and associated stable isotope signatures. Geochim. et Cosmochim. Acta, **55**, 2417-2434.

Brown, P.E. and Lamb, W.M., 1989. P-V-T properties of fluids in the system H_2O±CO_2±NaCl: New graphical presentations and implications for fluid inclusion studies. Geochim. et Cosmochim. Acta, **53**, 1209-1221.

Brown, T.H., Berman, R.G. and Perkins, R.G., 1989. GEO-CALC: Software package for calculation and display of pressure-temperature-composition phase diagrams using an IBM or compatible personal computer. Computer & Geoscience, **14**, 279-289.

Bryndzia, L.T. and Scott, S.D., 1987. The composition of chlorite as a function of sulphur and oxygen fugacity: an experimental study. Am. J. Science, **287**, 50-76.

Burke, K., Kidd, W.S.F. and Kusky, T.M., 1986. Archaean foreland basin tectonics in the Witwatersrand Supergroup, South Africa. Tectonics, **5**, 439-456.

Buggisch, W. and Kleinschmidt, G., 1991. Recovery and recrystallisation of quartz and "crystallinity" of illite in the Bowers and Robertson Bay Terranes, Northern Victoria Land, Antarctica. *In:* Thomson, M.R.A., Crame, J.A. and Thomson, J.W. (Eds.). Geological Evolution of Antarctica. Cambridge University Press, Cambridge, 155-159.

Cathelineau, M., 1988. Cation site occupancy in chlorites and illites as a function of temperature. Clay Minerals, **23**, 471-485.

Crawford, M.L., 1981. Phase equilibria in aqueous fluid inclusions. *In:* Hollister, L.S. and Crawford, M.L. (Eds.). Short Course in Fluid Inclusions: Applications to Petrology. Mineral. Assoc. Canada, **6**, 75-100.

Czamanske, G.K., Desborough, G.A. and Goff, F.E., 1973. Annealing history limits for inhomogeneous, native gold grains as determined from Au-Ag diffusion rates. Econ. Geol., **68**, 1275-1288.

Davidson, C.F., 1955. The mineralisation of the Witwatersrand. Mining Mag., **92**, 152-156.

De Caritat, P., Hutcheon, I. and Walshe, J.L., 1993. Chlorite geothermometry: A review. Clays and Clay Minerals, **41**, 219-239.

Dickinson, W. and Milliken, K.L., (in press). The diagenetic role of brittle deformation in compaction and pressure solution of quartzose sandstones. J. Geol.

Drennan, G.R., Cathelineau, M., Boiron, M.-C., Landais, P. and Robb, L.J., 1995. Characteristics of post-depositional fluids in the Witwatersrand Basin, with emphasis on hydrocarbon-bearing fluids. Extended abstr. Geol. Soc. S. Afr.: The Economic Significance of Metamorphism and Fluid Movement within the Witwatersrand Basin, 26 October 1995, Western Deep Levels, 5-9.

Eldridge, C.S., Phillips, G.N. and Myers, R.E., 1993. Sulfides in the Witwatersrand gold fields: New perspectives on old sediments via SHRIMP. Geol. Soc America, Abstracts with program, **25**, A278.

Eriksson, K.A., Turner, B.R. and Vos, R.G., 1981. Evidence of tidal processes from the lower part of the Witwatersrand Supergroup, South Africa. Sediment. Geol., **29**, 309-325.

Feather, C.E. and Koen, G.M., 1975. The mineralogy of the Witwatersrand reefs. Minerals Sci. Engng., **7**, 189-224.

Foster, R.P., 1993. Chemical evolution of fluids and the precipitation of gold in mesothermal lode gold deposits. Extended abstr. Geofluids '93, 378-382.

Frey, M., 1987. Low temperature metamorphism. Blackie, Glasgow, 351pp.

Frimmel, H.E., Le Roex, A.P., Knight, J. and Minter, W.E.L., 1993. A case study of the postdepositional alteration of the Witwatersrand Basal Reef gold placer. Econ. Geol., **88**, 249-265.

Frimmel, H.E., 1994. Metamorphism of Witwatersrand gold. Explor. Mining Geol., **3**, 357-370.

Fuller, A.O., 1958. A contribution to the petrology of the Witwatersrand System. Trans. Geol. Soc. S. Afr., **61**, 19-50.

Fyfe, W.S. and Kerrich, R., 1984. Gold: natural concentration processes. *In:* Foster, R.P. (Ed.). 1984. Gold '82: The Geology, Geochemistry and Genesis of Gold Deposits. Balkema, Rotterdam, 99-127.

Germs, G.J.B. and Schweitzer, J.K., 1994. A provisional model for the regional morphostratigraphy of the Venterspost Conglomerate Formation in the West Rand and Carletonville goldfields. S. Afr. J. Geol., **97**, 279-287.

Gibson, R. and Stevens, G., 1995. Regional metamorphism in the Witwatersrand Basin: The Bushveld-Vredefort connection. Extended abstr. Geol. Soc. S. Afr.: The Economic Significance of Metamorphism and Fluid Movement within the Witwatersrand Basin, 26 October 1995, Western Deep Levels, 13-16.

Grant, P.R. and White, S.H., 1978. Cathodoluminescence and microstructure of quartz overgrowths on quartz. Scan. Electr. Micr., **1**, 789-794.

Graton, L.C., 1930. Hydrothermal origin of the Rand gold deposits. Part I. Testimony of the conglomerates. Econ. Geol., **25**, Suppl. to No.3, 1-185.

Gresens, R.L., 1967. Composition-volume relationships of metasomatism. Chem. Geol., **2**, 47-65.

Groen, J.C., Craig, J.R. and Rimstidt, J.D., 1990. Gold-rich rim formation on electrum grains in placers. Canad. Mineralogist, **28**, 207-228.

Guilbert, J.M. and Park, C.F., Jr., 1986. The Geology of Ore Deposits. Freeman and Company, New York, 985pp.

Hall, D.L. and Bodnar, R.J., 1990. Presence of methane in fluid inclusions from granulites. Geochim. et Cosmochim. Acta, **54**, 641-651.

Hall, D.L., Bodnar, R.J. and Craig, J.R., 1991. Evidence for postentrapment diffusion of hydrogen into peak metamorphic fluid inclusions from massive sulfide deposits at Ducktown, Tennessee. Am. Mineral., **76**, 1344-1355.

Hall, R.C.B., 1993. A general overview of the inter-reef lavas on Kloof Gold Mine and their stratigraphic setting. Extended abstr., VCR Mini Symposium - The VCR revisited. Geol. Soc. S. Afr., 25-26 August 1993, Carletonville, 42-45.

Hall, R.C.B., 1994. Supporting evidence for the placement of the inter-reef Lavas and associated sediments within the Venterspost Conglomerate Formation: Kloof Gold Mine. S. Afr. J. Geol., **97**, 297-307.

Hallbauer, D.K., 1983. Geochemistry and fluid inclusions in detrital minerals as guides to their provenance and distribution. Proceedings 1st Internat. Congress on Appl. Mineral., Johannesburg, Geol. Soc. S. Afr., Spec. Publ., **7**, 39-57.

Hallbauer, D.K. and Kable, E.J.D., 1982. Fluid inclusions and trace element content of quartz and pyrite pebbles from Witwatersrand conglomerates: their significance with respect to the genesis of primary deposits. 742-752. *In:* Amstutz *et al.*, 1982. Ore Genesis - The State of the Art. Springer Verlag, Berlin, 742-752.

Hallbauer, D.K., 1986. The mineralogy and geochemistry of Witwatersrand pyrite, gold, uranium and carbonaceous matter. *In:* Anhaeusser, C.R. and Maske, S. (Eds). Mineral Deposits of Southern Africa, **1**, Geol. Soc. S. Afr., 731-752.

Hayashi, K.-I. and Ohmoto, H., 1991. Solubility of gold in NaCl- and H_2S-bearing aqueous solutions at 250-350^{0}C. Geochim. et Cosmochim. Acta, **55**, 2111-2126.

Heitzmann, P., 1985. Kakirite, Kataklasite, Mylonite - Zur Nomenklatur der Metamorphite mit Verformungsgefügen. Eclogae geol. Helv., **78**, 273-286.

Henckel, J. and Schweitzer, J.K., 1994. Geochemical and mineralogical characteristics of a portion of the Ventersdorp Contact Reef at Elandsrand Gold Mine. S. Afr. J. Geol., **97**, 332-338.

Henning, L.T., Els, B.G. and Mayer, J.J., 1994. The Ventersdorp Contact Placer at Western Deep Levels South Gold Mine - An ancient terraced fluvial system. S. Afr. J. Geol., **97**, 308-318.

Holland, H.D., 1984. The Chemical Evolution of the Atmosphere and Oceans. Princeton, Princeton Univ. Press, 582pp.

Houseknecht, D.W., 1991. Use of cathodoluminescence petrography for understanding compaction, quartz cementation, and porosity in sandstones. *In:* Barker, C.E. and Kopp, O.C. (Eds.). Luminescence Microscopy: Quantitative and Qualitative Aspects. SEPM, 59-66.

Jaeger, J.C., 1957. The temperature in the neighborhood of a cooling intrusive sheet. Am. J. Sci., **255**, 306-318.

Kamo, S.L., Reimold, W.U., Krogh, T.E. and Colliston, W.P., 1995. Shocked zircons inVredefort pseudotachylite and the U-Pb zircon age of the Vredefort event. Abstr. Centennial Geocongress (1995), Geol. Soc. S. Afr., Johannesburg, 566-569.

Kearsley, A. and Wright, P., 1988. Geological applications of scanning cathodoluminescence imagery. Microscopy and Analysis.

Kerrich, R., Fyfe, W.S., Gorman, B.E. and Allison, I., 1977. Local modification of rock chemistry by deformation. Contrib. Mineral. Petrol., **65**, 183-190.

Killick, A.M., 1994. The geochemistry of pseudotachylyte and its host rocks from the West Rand Goldfield, Witwatersrand Basin, South Africa: implications for pseudotachylyte genesis. Lithos, 32, 193-205.

Klemd, R., Wülbers, A., Hallbauer, D.K. and Barton, J.M. Jr, 1994. Evidence for the origin of hydrothermal alteration in granitoids after Witwatersrand Basin deposition, South Africa. Austr. J. Earth Sci., **41**, 131-140.

Knipe, S.W., Foster, R.P. and Stanley, C.J., 1992. Role of sulphide surfaces in sorption of precious metals from hydrothermal fluids. Trans. Instit. Mining & Metall. (Sect. B: Appl. earth Sci.), **101**, B83-B88.

Kranidiotis, P. and MacLean, W.H., 1987. Systematics of chlorite alteration at the Phelps Dodge massive sulfide deposit, Matagami, Quebec. Econ. Geol., **82**, 1898-1911.

Krapez, B., 1985. The Ventersdorp Contact placer: a gold-pyrite placer of stream and debris-flow origins from the Archean Witwatersrand Basin of South Africa. Sedimentology, **32**, 223-234.

Krupp, R., Oberthür, T. and Hirdes, W., 1994. The early Precambrian atmosphere and hydrosphere: Thermodynamic constraints from mineral deposits. Econ. Geol., **89**, 1581-1598.

Laird, J., 1988. Chlorites: Metamorphic petrology. *In:* Bailey, S.W. (Ed.). Hydrous phyllosilicates, Reviews in Mineral., **19**, 405-454.

Landais, P., Dubessy, J., Robb, L.J. and Nouel, C., 1990. Preliminary chemical analyses and Raman spectroscopy on selected samples of Witwatersrand kerogen. E.G.R.U. Inf. Circ. No.222, Univ. Witwatersrand, Johannesburg, 8pp.

Le Roex, A.P. and Watkins, R.T., 1990. Analysis of rare earth elements in geological samples by gradient ion-chromatography: An alternative to ICP and INAA. Chem. Geol., **88**, 151-162.

Linton, P.L., McCarthy, T.S. and Brown, C.A., 1994. The sequential eruption and tectonic history of the Klipriviersberg Group as illustrated by the distribution of geochemical units. S. Afr. J. Geol., **97**, 196-204.

Marshall, D.J., 1988. Cathodoluminescence of Geological Materials. Unwin Hyman, Boston, 137pp.

MacLean, P.J. and Fleet, M.E., 1989. Detrital pyrite in the Witwatersrand gold fields of South Africa: evidence from truncated growth banding. Econ.Geol., **84**, 2008-2011.

McCarthy, T.S., Charlesworth, E.G. and Stanistreet, I.G., 1986. Post-Transvaal structural features of the northern portion of the Witwatersrand Basin. Trans. Geol. Soc. S. Afr., **89**, 311-323.

McCarthy, T.S., 1994. The tectono-sedimentary evolution of the Witwatersrand Basin with special reference to its influence on the occurrence and character of the Ventersdorp Contact Reef - A review. S. Afr. J. Geol., **97**, 247-259.

Mellor, E.T., 1916. The conglomerates of the Witwatersrand. Trans. Inst. Mingn. Metal., **25**, 226-348.

Meunier, J.D., Sellier, E. and Pagel, M., 1990. Radiation-damage rims in quartz from uranium-bearing sandstones. J. Sed. Petr., **60**, 53-58.

Meyer, F.M., Wallmach, T., Henckel, J. and Schweitzer, J.K., 1990. Chlorite compositions and fluid conditions in some Witwatersrand reefs. Abstr. Geocongress '90, Geol. Soc. S. Afr., Cape Town, 391-394.

Meyer, F.M., 1991. Chlorite thermometry in the VCR and the Carbon Leader Reef of the West Wits Line. Abstr. 7th Annual Conference, Tectonics Division, Geol. Soc. S. Afr., Univ. Witwatersrand, Johannesburg, 21-22.

Meyer, F.M., Drennan, G.R. and Robb, L.J., 1991. Conditions of Au-U mineralization in Witwatersrand reefs. *In:* Pagel, M. and Leroy, L.J. (Eds.). Source, Transport and Deposition of Metals, Balkema, Rotterdam, 681-684.

Minter, W.E.L., Goedhart, M., Knight, J. and Frimmel, H.E., 1993. Morphology of Witwatersrand gold grains from the Basal reef: Evidence for their detrital origin. Econ. Geol., **88**, 237-248.

Myers, R.E., McCarthy, T.S., Bunyard, M., Cawthorn, R.G., Falatsa, T.M., Hewitt, T., Linton, P., Myers, J.M., Palmer, K.J. and Spencer, R., 1990. Geochemical stratigraphy of the Klipriviersberg Group volcanic rocks. S. Afr. J. Geol., **93**, 224-238.

Myers, R.E., Stanistreet, I.G. and McCarthy, T.S., 1992. Two-stage basement block fault deformation in the development of the Witwatersrand Goldfields, South Africa. *In:* Bartholomew, M.J., Hyndman, D.W., Mogk and D.W., Mason, R. (Eds.).

Characterization and Comparisons of Ancient (Precambrian-Mesozoic) Continental Margins. Int. Basement Tectonics Assoc. Publ., **8**, 689-697.

Myers, R.E., Zhou, T., and Phillips, G.N., 1993. Sulphidation in the Witwatersrand goldfields: evidence from the Middelvlei Reef. Mineralog. Magaz., **57**, 395-405.

Nesbitt, H.W., and Young, G.M., 1982. Early Proterozoic climates and plate motions inferred from major element chemistry of lutites. Nature, **299**, 715-717.

Norrish, K. and Hutton, J.T., 1969. An accurate X-ray spectrographic method for the analysis of a wide range of geological samples. Geochim. et Cosmochim. Acta, **33**, 431-453.

Oberthür, T. and Saager, R., 1986. Silver and mercury in gold particles from the Proterozoic Witwatersrand placer deposits of South Africa: Metallogenic and geochemical implications. Econ. Geol., **81**, 20-31.

Owen, M.R., 1988. Radiation-damage halos in quartz. Geology, **16**, 529-532.

Phillips, G.N., 1987. Metamorphism of the Witwatersrand gold fields: conditions during peak metamorphism. J. Metam. Geol., **5**, 307-322.

Phillips, G.N., 1988. Metamorphism of the Witwatersrand gold fields: generation of chloritoid and pyrophyllite. J. Metam. Geol., **6**, 311-332.

Phillips, G.N., Klemd, R. and Robertson, N.S., 1988. Summary of some fluid inclusion data from the Witwatersrand Basin and surrounding granitoids. Mem. Geol. Soc. India, **11**, 59-65.

Phillips, G.N., Law, J.D.M. and Myers, R.E., 1990. The role of fluids in the evolution of the Witwatersrand Basin. S. Afr. J. Geol., **93**, 54-69.

Phillips, G.N. and Law, J.D.M., 1994. Metamorphism of the Witwatersrand gold fields: A review. Ore Geol. Reviews, **9**, 1-31.

Pretorius, D.A., 1976. The nature of the Witwatersrand gold-uranium deposits. *In:* Wolf, K.H. (Ed.), Handbook of Stratabound and Stratiform Ore Deposits, **7**, Elsevier, Amsterdam, 29-88.

Ramseyer, K., Baumann, J., Matter, A. and Mullis, J., 1988. Cathodoluminescence colours of - quartz. Mineralog. Mag., **52**, 669-677.

Reddy, V. and Germs, G.J.B., 1994. Stratigraphy and facies of the Venterspost Conglomerate Formation at Western Areas Gold Mine. S. Afr. J. Geol., **97**, 288-296.

Reid, A.M., Le Roex, A.P. and Minter, W.E.L., 1988. Composition of gold grains in the Vaal Placer, Klerksdorp, South Africa. Mineral. Deposita, **23**, 211-217.

Reimer, T.O. and Mossman, D.J., 1990(a). Sulfidization of Witwatersrand black sands: From enigma to myth. Geology, **18**, 426-429.

Reimer, T.O. and Mossman, D.J., 1990(b). The Witwatersrand controversy revisited. Econ. Geol., **85**, 337-343.

Remond, G., Cesbron, F., Chapoulie, R., Ohnenstetter, D., Roques-Carmes, C. and Schvoerer, M., 1992. Cathodoluminescence applied to the microcharacterization of mineral materials: A present status in experimentation and interpretation. Scanning Microscopy, **6**, 23-68.

Ritger, S.D., 1990. Evolution of the Wits Basin: Evidence from the quartzites. Ph.D. thesis (unpublished), Univ. Witwatersrand.

Robb, L.J., Davis, D.W. and Kamo, S.L., 1990. U-Pb ages on single detrital zircon grains from the Witwatersrand Basin, South Africa: Constraints on the age of sedimentation and on the evolution of granites adjacent to the basin. J. Geol., **98**, 311-328.

Robb, L.J. and Meyer, F.M., 1990. The nature of the Witwatersrand hinterland: conjectures on the source area problem. Econ. Geol., **85**, 511-536.

Robb, L.J. and Meyer, F.M., 1991. A contribution to the recent debate concerning epigenetic versus syngenetic mineralisation processes in the Witwatersrand Basin. Econ. Geol., **86**, 396-401.

Robert, F. and Kelly, W.C., 1987. Ore-forming fluids in Archean gold-bearing quartz veins at the Sigma Mine, Abitibi Greenstone Belt, Quebec, Canada. Econ. Geol., **82**, 1464-1482.

Robertson, N.S., 1985. A study of fluid inclusions from vein quartz adjacent to some Witwatersrand reefs. B.Sc. (Hons.) thesis (unpublished), Univ. Witwatersrand, 51pp.

Robinson, D., Bevins, R.E. and Rowbotham, G., 1993. The characterization of mafic phyllosilicates in low-grade metabasalts from eastern North Greenland. Am. Mineral., **78**, 377-390.

Romberger, S.B., 1991. Transport and deposition of gold in hydrothermal systems. *In:* Robert, P., Sheahan, P.A., Green, S.B. (Eds.), Greenstone gold and crustal evolution, Nuna Conference volume. Geol. Assoc. Canada, 165-182.

Saager, R., 1969. The relationship of silver and gold in the Basal Reef of the Witwatersrand System, South Africa. Mineral. Deposita, **4**, 93-113.

Santosh, M., Philip, R., Jacob, M.K. and Omana, P.K., 1992. Highly pure placer gold formation in the Nilambur Valley, Wynad Gold Field, southern India. Mineral. Deposita, **27**, 336-339.

Schidlowski, M. and Junge, C., 1973. Die Evolution der Erdatmosphäre. Phys. Blätter, **29**, 203-212.

Schiffman, P. and Fridleifsson, G.O., 1991. The smectite-chlorite transition in drillhole NJ-15, Nesjavellir geothermal field, Iceland: XRD, BSE and electron microprobe investigations. J. Metam. Geol., **9**, 679-696.

Schreyer, W. and Bisschoff, A.A., 1982. Kyanite as a metamorphic mineral in Witwatersrand sediments at Johannesburg and Krugersdorp, South Africa. Trans. Geol. Soc. S.A., **85**, 211-214.

Schweitzer, J.K., van Niekerk, A.W., Ashworth, S.G.E. and Henckel, J., 1994. Interrelationship between geomorphology, stratigraphy, and gold grade in the Ventersdorp Contact Reef, eastern portion of Elandsrand Gold Mine. S. Afr. J. Geol., **97**, 339-347.

Seward, T.M., 1984. The transport and deposition of gold in hydrothermal systems. *In:* Foster, R.P. (Ed.). 1984. Gold '82: The Geology, Geochemistry and Genesis of Gold Deposits. Balkema, Rotterdam, 165-181.

Shenberger, D.M. and Barnes, H.L., 1989. Solubility of gold in aqueous sulfide solutions from 150 to 350^{0}C. Geochim. et Cosmochim. Acta, **53**, 269-278.

Shepherd, T.J., 1977. Fluid inclusion study of the Witwatersrand gold-uranium ores. Phil. Trans. R. Soc. Lond., **286**, 549-565.

Smits, G., 1994. Note on the mineralogy of the Ventersdorp Contact Reef at Kloof Gold Mine. S. Afr. J. Geol., **97**, 357-364.

South African Committee for Stratigraphy (SACS), 1980. Part 1: Lithostratigraphy of the Republic of South Africa, South West Africa/Namibia and the Republics of Bophuthatswana, Transkei and Venda. Geol. Survey, Handbook 8, 690pp.

Sprunt, E.S., 1981. Causes of quartz cathodoluminescence colors. Scan. Electr. Micr., **4**, 525-535.

Sprunt, E.S., Dengler, L.A. and Sloan, D., 1978. Effects of metamorphism on quartz cathodoluminescence. Geology, **6**, 305-308.

Stanistreet, I.G. and McCarthy, T.S., 1991. Changing tectono-sedimentary scenarios relevant to the development to the late Archaean Witwatersrand Basin. J. Afr. Earth Sci., **13**, 65-81.

Stefan, L.D. and Martin, G.J., 1993. Hydrothermal activity and its effect on gold deportment in the VCR at North Driefontein: West Driefontein Gold Mine. Extended abstr., VCR Mini Symposium - The VCR revisited. Geol. Soc. S. Afr., 25-26 August 1993, Carletonville, 16-19.

Sterner, S.M. and Bodnar, R.J., 1984. Synthetic fluid inclusions in natural quartz I. Compositional types synthesized and applications to experimental geochemistry. Geochim. et Cosmochim. Acta, **48**, 2659-2668.

Sutton, S.J., Ritger, S.D. and Maynard, J.B., 1990. Stratigraphic control of chemistry and mineralogy in metamorphosed Witwatersrand quartzites. J. Geol., **98**, 329-341.

Tankard, A.J., Jackson, M.P.A., Eriksson, K.A., Hobday, D.K., Hunter, D.R. and Minter, W.E.L., 1982. Crustal evolution of Southern Africa. Springer, New York, 523pp.

Thomas, D.E., 1977. A sedimentological study and evaluation of the Ventersdorp Contact Reef at Vaal Reefs Exploration and Mining Company Limited, Klerksdorp, South Africa. M.Sc. thesis (unpublished), Univ. London, 96pp.

Trieloff, M., Reimold, W.U., Kunz, J., Boer, R.H. and Jessberger, E.K., 1994. ^{40}Ar-^{39}Ar thermochronology of pseudotachylite at the Ventersdorp Contact Reef, Witwatersrand basin. S. Afr. J. Geol., **97**, 365-384.

Utter, T., 1979. The morphology and silver content of gold from the Upper Witwatersrand and Ventersdorp Systems of the Klerksdorp Gold Field, South Africa. Econ. Geol., **74**, 27-44.

Voll, G., 1976. Recrystallisation of quartz, biotite, and feldspars from Erstfeld to the Leventina Nappe, Swiss Alps, and its geological significance. Schweiz. Mineral. Petrogr. Mitteil., **56**, 641-647.

Vollbrecht, A., Rüdrich, J., Weber, K. and Oberthür, T., (in press). Gefügekundliche Untersuchungen an Geröllquarzen des Witwatersrandes. Z. Angew. Geowissenschaften.

Von Gehlen, K., 1983. Silver and mercury in single gold grains from the Witwatersrand and Barberton, South Africa. Mineral. Deposita, **18**, 529-534.

Wallmach, T. and Meyer, F.M., 1990. A petrogenetic grid for metamorphosed aluminous Witwatersrand shales. S. Afr. J. Geol., **93**, 93-102.

Walraven, F. and Hattingh, E., 1993. Geochronology of the Nebo Granite, Bushveld Complex. S. Afr. J. Geol., **96**, 31-41.

White, S. and Treagus, J.E., 1975. The effects of polyphase deformation on the intracrystalline defect structures of quartz. I. The defect structures. N. Jb. Miner. Abh., **123**, 219-236.

Winter, H. de la R., 1995. Tectonic events affecting the Witwaterstand Basin with special reference to responses in the Bezuidenhout Valley. S. Afr. J. Geol., **98**, 356-370.

Zang, W. and Fyfe, W.S., 1995. Chloritization of the hydrothermally altered bedrock at the Igarapé Bahia gold deposit, Carajás, Brazil. Mineral. Deposita, **30**, 30-38.

Zhao, B., Meyer, F.M., Robb, L.J. and McWha, M., 1994. A preliminary study of alteration associated with the Ventersdorp Contact Reef at Western Deep Levels South Mine, Witwatersrand Basin, South Africa. S. Afr. J. Geol., **97**, 348-356.

Zhao, B., Robb, L.J., Meyer, M., Clauer, N. and McWha, M., 1995. The timing of metamorphism, hydrothermal alteration and mineralization in the Ventersdorp Contact Reef, Witwatersrand Basin. Extended abstr. Geol. Soc. S. Afr.: The Economic Significance of Metamorphism and Fluid Movement within the Witwatersrand Basin, 26 October 1995, Western Deep Levels, 39-42.

Zinkernagel, U., 1978. Cathodoluminescence of quartz and its application to sandstone petrology. Contrib. to Sediment., **8**, Schweizerhartsche Verlagsbuchhandlung, Stuttgart, 1-69.

APPENDIX A

Map 1 (1:5000 scale)

SCHOONSPRUIT FAULT

BUFFELSDOORN FAULT

NOOITGEDACHT FAULT

BUFFELSDOORN FAULT

NEW YEAR'S FAULT

No.10 Shaft Lease Boundary

Vaal River

No. 10 Shaft Lease Boundary

1134 N1 RSE 13(P1)

1350 N1 RSE 8 (N LEDGE)

XRF TRAVERSE

LEGEND

x 074 Sample No. (VHG__)

Fault Loss

Dyke

-1700 VCR Elevation below surface

0 50 100 150 200 250

metres

PLAN OF STUDY AREA SHOWING SAMPLE LOCALITIES AND STRUCTURE ON VCR HORIZON AT VAAL REEFS No. 10 SHAFT

MAP 1

APPENDIX B

Whole Rock XRF Analysis

Major Elements

Major element concentrations were determined on duplicate Norrish fusion glass discs using the method of Norrish and Hutton (1969). Powder samples (0.28 g) were fused with 1.5 g of lithium borate flux (Spectroflux 105) and minor $NaNO_3$ (0.02 g). Prior to the preparation of the discs, volatile constituents were estimated by first drying for 12 hours at 110^0C (determination of H_2O^-) and then ashing for the same period at 1000^0C for the Loss on Ignition (LOI) content (H_2O^+ and CO_2). The ashed samples were fused in Pt-Au crucibles and then cast in a carbon mould. All major element concentrations were determined by analysing the fusion discs with a Siemens SRS-1 XRF spectrometer, except for Na, which was determined from pressed powder briquettes. Detection limits (LLD) and the average absolute error determined by the on-line computer facility for the major elements are given in Table B1.

Method

Major element concentrations of whole rock samples were determined by X-ray fluorescence (XRF) spectroscopic technique at the Department of Geological Sciences, University of Cape Town. This technique is summarised below.

Whole rock samples with masses of 1000 - 1500 g were crushed, ground and sieved to reduce powder samples to less than 200 # grain size.

Table B1: Average absolute counting errors and detection limits for major element analyses by XRF.

OXIDE	Average Absolute Error	Lower Limit of Detection
SiO2	0.316	0.015
TiO2	0.023	0.006
Al2O3	0.193	0.012
FeO	0.101	0.009
MnO	0.010	0.006
MgO	0.095	0.013
CaO	0.053	0.004
Na2O	0.075	0.020
K2O	0.029	0.003
P2O5	0.009	0.004

Rare Earth Elements

Method

Rare earth element concentrations were obtained using a Dionex 4000i gradient ion chromatograph at the Department of Geological Sciences, University of Cape Town. The same analytical technique as described by Le Roex and Watkins (1990) was applied.

APPENDIX C

Mineral Analyses

Mineral chemistries of chlorite grain aggregates and of individual carbonate and gold particles in 2 cm x 4 cm slides were analysed with a Cameca (Camebax) 1100 electron microprobe at the Department of Geological Sciences, University of Cape Town. Nominal concentrations were corrected for by the on-line reduction facility using the ZAF correction programme.

Operating Conditions

Acceleration voltage: 15 kV (chlorite and carbonate) or 30 kV (gold)

Beam current: 15 nA (carbonate) or 40 nA (chlorite and gold)

Beam focus: 2 µm (gold) or 5 µm (chlorite and carbonate)

Counting time: 10 s

Analysing crystals: LIF (200) for elements Fe, Mn, Au, Hg
PET for elements Ca, K, Ti, Cr, Ag
TLAP: for elements Si, Al, Mg, Na

Calibration standards: The calibration standards used for the EMP analyses are shown in Table C1.

Standards used: The standards used for the different mineral analyses are given in Table C2.

Lower limits of detection: The LLD for electron microprobe analyses are shown in Table C3. The formula used for the calculation of the LLD is:

$$LLD\ (wt\%) = 6/m \times (R_b/R_t)^{1/2},$$

where m = counts/second/nominal per cent for element
R_b = counts/second on background
R_t = total counting time (peak+background).

Table C1: Table of calibration standards used in the EMP analyses.

Abbreviation	Standard	Type
CHRO	Stilwater chromite	Natural
K-P	Kakuni pyrope	Natural
K-H	Kakuni hornblende	Natural
RHOD	Rhodonite	Synthetic
RUT	Rutile	Synthetic
MN	Metal	Natural
CIN	Cinnabar	Natural

Table C2: Standards used for elements of silicate, carbonate and metal phases

Mineral	Element	Standard
Amphibole	Si, Al, Ca, Mg, Fe,	K-H
(Chlorite)	K, Na	K-H
	Ti	RUT
	Mn	RHOD
	Cr	CHRO
Carbonate	Si, Fe	K-P
	Mn	RHOD
	Ca, Mg	DIOP
Metal	Au, Ag	MN
(Gold)	Hg	CIN

Table C3: Typical lower detection limits for various mineral analyses.

	AMPH	MICA	MN
Si	0.042		
Ti	0.040		
Al	0.033		
Cr	0.045		
Fe	0.077		
Mn	0.067		
Mg	0.031		
Ca	0.028		
Na	0.034		
K	0.024		
F		0.160	
Cl		0.025	
Au			0.217
Ag			0.071
Hg			0.164

Chlorite Analyses

Sample:	VHG016															
Lithology:	VCR															
Analysis No.	Chl 1	Chl 2	Chl 3	Chl 4	Chl 5	Chl 6	Chl 7	Chl 8	Chl 9	Chl 10	Chl 11	Chl 12	Chl 13	Chl 14	Chl 15	Chl 16
Chlorite Type	II	II	II	II	II	II	II	II	II	II	II	II	II	II	II	II
SiO2	24.19	24.30	24.04	23.80	23.19	23.76	23.53	25.38	22.63	24.62	24.04	23.22	24.63	23.35	23.18	23.12
TiO2	0.00	0.00	0.00	0.00	0.00	0.00	0.00	0.00	0.00	0.00	0.00	0.00	0.00	0.00	0.00	0.00
Al2O3	24.78	23.58	23.88	25.07	23.32	24.23	23.25	24.33	23.21	24.42	24.65	24.99	24.13	24.62	23.44	24.00
Cr2O3	0.31	0.11	0.33	0.11	0.11	0.38	0.71	0.59	0.48	0.12	0.13	0.00	0.58	0.32	0.34	0.43
FeO	29.61	30.81	29.98	31.09	30.99	31.67	30.66	29.42	30.16	30.43	31.00	31.62	30.47	31.02	31.20	29.99
MnO	0.15	0.33	0.26	0.33	0.33	0.26	0.29	0.23	0.30	0.31	0.28	0.37	0.29	0.29	0.28	0.27
MgO	10.96	10.55	11.49	10.27	9.74	10.02	10.96	10.92	10.14	11.02	11.07	9.81	11.48	10.38	9.29	10.78
CaO	0.00	0.08	0.00	0.06	0.10	0.06	0.07	0.20	0.00	0.06	0.00	0.00	0.14	0.00	0.00	0.00
Na2O	0.00	0.00	0.00	0.00	0.00	0.00	0.00	0.00	0.00	0.00	0.00	0.00	0.12	0.00	0.00	0.00
K2O	0.00	0.00	0.00	0.00	0.00	0.00	0.00	0.00	0.00	0.00	0.00	0.00	0.00	0.00	0.00	0.00
F	0.00	0.00	0.00	0.00	0.00	0.00	0.00	0.00	0.00	0.00	0.00	0.00	0.00	0.00	0.00	0.00
Total	90.00	89.76	89.98	90.73	87.78	90.38	89.47	91.07	86.92	90.98	91.17	90.01	91.84	89.98	87.73	88.59
	6.29	6.36	6.32	6.29	6.55	6.35	6.41	6.20	6.60	6.24	6.26	6.37	6.20	6.36	6.55	6.44
SiIV	2.53	2.67	2.53	2.49	2.53	2.51	2.51	2.62	2.49	2.56	2.50	2.46	2.54	2.47	2.53	2.48
AlIV	1.47	1.43	1.47	1.51	1.47	1.49	1.49	1.38	1.51	1.44	1.50	1.54	1.46	1.53	1.47	1.52
T site	4.00	4.00	4.00	4.00	4.00	4.00	4.00	4.00	4.00	4.00	4.00	4.00	4.00	4.00	4.00	4.00
AlVI	1.59	1.52	1.49	1.59	1.52	1.53	1.43	1.58	1.49	1.55	1.53	1.59	1.48	1.54	1.54	1.51
Ti	0.00	0.00	0.00	0.00	0.00	0.00	0.00	0.00	0.00	0.00	0.00	0.00	0.00	0.00	0.00	0.00
Cr3+	0.03	0.01	0.03	0.01	0.01	0.03	0.06	0.05	0.04	0.01	0.01	0.00	0.05	0.03	0.03	0.04
Fe2+	2.59	2.73	2.64	2.72	2.82	2.80	2.73	2.54	2.77	2.64	2.70	2.80	2.63	2.75	2.85	2.69
Mn2+	0.01	0.03	0.02	0.03	0.03	0.02	0.03	0.02	0.03	0.03	0.02	0.03	0.03	0.03	0.03	0.02
Mg	1.71	1.66	1.80	1.60	1.58	1.58	1.74	1.68	1.66	1.71	1.72	1.55	1.77	1.64	1.51	1.72
Ca	0.00	0.01	0.00	0.01	0.01	0.01	0.01	0.02	0.00	0.01	0.00	0.00	0.02	0.00	0.00	0.00
Na	0.00	0.00	0.00	0.00	0.00	0.00	0.00	0.00	0.00	0.00	0.00	0.00	0.02	0.00	0.00	0.00
K	0.00	0.00	0.00	0.00	0.00	0.00	0.00	0.00	0.00	0.00	0.00	0.00	0.00	0.00	0.00	0.00
O site	5.93	5.96	5.98	5.96	5.98	5.97	6.00	5.89	5.99	5.94	5.98	5.98	5.98	5.98	5.95	5.99
XFe	0.60	0.62	0.59	0.63	0.64	0.64	0.61	0.60	0.63	0.61	0.61	0.64	0.60	0.63	0.65	0.61
Al/(Al+Fe+Mg)	0.42	0.40	0.40	0.42	0.40	0.41	0.40	0.41	0.40	0.41	0.41	0.42	0.40	0.41	0.41	0.41
T (°C)	305	295	307	311	303	308	309	287	313	299	311	316	304	316	301	316
XChl	0.93	0.95	0.98	0.96	0.97	0.96	1.00	0.88	0.99	0.94	0.98	0.98	0.95	0.98	0.96	0.99
i/l cat	0.00	0.01	0.00	0.01	0.01	0.01	0.01	0.02	0.00	0.01	0.00	0.00	0.04	0.00	0.00	0.00
non-i/l	9.93	9.95	9.98	9.95	9.96	9.96	9.99	9.86	9.99	9.94	9.98	9.98	9.95	9.98	9.95	9.99

Sample:	VHG021										Sample:	VHG022							
Lithology:	VCR										Lithology	VCR							
Analysis No.	Chl 1	Chl 2	Chl 3	Chl 4	Chl 5	Chl 6	Chl 7	Chl 8	Chl 9	Chl 10	Chl 1	Chl 2	Chl 3	Chl 4	Chl 5	Chl 6	Chl 7	Chl 8	Chl 9
Chlorite Type	II	II	+ C	II	+ Au	+ Au.	II	II	II	II	close to QV	II	close to QV	close to QV	II	II	II	II	II
SiO2	24.51	23.96	22.61	24.12	23.70	24.76	23.94	23.39	23.54	24.02	23.66	24.12	23.28	23.46	24.26	24.13	22.97	24.57	22.97
TiO2	0.00	0.00	0.00	0.00	0.00	0.00	0.00	0.00	0.00	0.00	0.00	0.00	0.00	0.00	0.00	0.00	0.00	0.00	0.00
Al2O3	24.38	24.04	24.26	24.22	23.95	25.22	23.53	23.29	23.42	23.43	24.40	24.89	24.83	24.98	24.29	23.57	23.85	24.87	23.71
Cr2O3	0.35	0.57	0.38	0.34	0.39	0.55	0.60	1.62	0.17	0.16	0.40	0.36	0.27	0.08	0.12	0.32	0.32	0.12	0.14
FeO	30.01	30.13	31.34	30.72	32.32	29.82	31.86	29.87	31.10	32.26	31.82	30.94	31.96	33.31	29.85	30.39	29.22	30.17	29.99
MnO	0.32	0.22	0.32	0.19	0.38	0.21	0.27	0.23	0.31	0.33	0.29	0.28	0.33	0.33	0.28	0.37	0.32	0.25	0.22
MgO	11.39	11.57	10.03	11.26	9.84	11.48	9.28	10.79	10.11	9.88	8.93	10.10	8.20	8.70	10.79	11.36	10.69	11.24	10.25
CaO	0.00	0.00	0.00	0.00	0.00	0.00	0.00	0.00	0.00	0.00	0.00	0.00	0.00	0.00	0.00	0.00	0.00	0.00	0.00
Na2O	0.11	0.00	0.00	0.00	0.00	0.00	0.07	0.00	0.08	0.00	0.00	0.00	0.00	0.00	0.00	0.00	0.00	0.00	0.00
K2O	0.00	0.00	0.00	0.00	0.00	0.00	0.00	0.00	0.00	0.00	0.00	0.00	0.00	0.00	0.00	0.00	0.00	0.00	0.00
F	0.00	0.00	0.00	0.00	0.00	0.00	0.00	0.00	0.00	0.00	0.00	0.00	0.00	0.00	0.00	0.00	0.00	0.00	0.00
Total	91.07	90.49	88.94	90.85	90.58	92.04	89.55	89.19	88.73	90.08	89.50	90.69	88.87	90.86	89.59	90.14	87.37	91.22	87.28
	6.23	6.29	6.47	6.27	6.36	6.14	6.42	6.41	6.47	6.39	6.42	6.29	6.47	6.36	6.33	6.33	6.51	6.21	6.54
SiIV	2.54	2.51	2.43	2.52	2.51	2.53	2.56	2.50	2.53	2.55	2.53	2.52	2.51	2.48	2.56	2.54	2.49	2.54	2.50
AlIV	1.46	1.49	1.57	1.48	1.49	1.47	1.44	1.50	1.47	1.45	1.47	1.48	1.49	1.52	1.44	1.46	1.51	1.46	1.50
T site	4.00	4.00	4.00	4.00	4.00	4.00	4.00	4.00	4.00	4.00	4.00	4.00	4.00	4.00	4.00	4.00	4.00	4.00	4.00
AlVI	1.52	1.48	1.51	1.50	1.50	1.57	1.52	1.43	1.50	1.49	1.60	1.59	1.66	1.60	1.57	1.47	1.54	1.57	1.54
Ti	0.00	0.00	0.00	0.00	0.00	0.00	0.00	0.00	0.00	0.00	0.00	0.00	0.00	0.00	0.00	0.00	0.00	0.00	0.00
Cr3+	0.03	0.05	0.03	0.03	0.03	0.04	0.05	0.14	0.01	0.01	0.03	0.03	0.02	0.01	0.01	0.03	0.03	0.01	0.01
Fe2+	2.60	2.64	2.82	2.68	2.86	2.55	2.85	2.67	2.80	2.87	2.84	2.71	2.88	2.95	2.63	2.68	2.65	2.61	2.73
Mn2+	0.03	0.02	0.03	0.02	0.03	0.02	0.02	0.02	0.03	0.03	0.03	0.02	0.03	0.03	0.02	0.03	0.03	0.02	0.02
Mg	1.76	1.81	1.81	1.75	1.55	1.75	1.48	1.72	1.62	1.57	1.42	1.57	1.32	1.37	1.69	1.78	1.73	1.73	1.66
Ca	0.00	0.00	0.00	0.00	0.00	0.00	0.00	0.00	0.00	0.00	0.00	0.00	0.00	0.00	0.00	0.00	0.00	0.00	0.00
Na	0.02	0.00	0.00	0.00	0.00	0.00	0.01	0.00	0.02	0.00	0.00	0.00	0.00	0.00	0.00	0.00	0.00	0.00	0.00
K	0.00	0.00	0.00	0.00	0.00	0.00	0.00	0.00	0.00	0.00	0.00	0.00	0.00	0.00	0.00	0.00	0.00	0.00	0.00
O site	5.96	5.98	6.01	5.98	5.98	5.93	5.94	5.97	5.98	5.97	5.92	5.93	5.91	5.96	5.93	5.98	5.97	5.94	5.97
XFe	0.60	0.59	0.64	0.60	0.65	0.59	0.66	0.61	0.63	0.65	0.67	0.63	0.69	0.68	0.61	0.60	0.61	0.60	0.62
Al/(Al+Fe+Mg)	0.41	0.40	0.41	0.40	0.40	0.41	0.41	0.40	0.40	0.40	0.42	0.42	0.43	0.42	0.41	0.40	0.41	0.41	0.41
T (°C)	304	311	323	308	306	307	294	312	302	296	300	304	303	308	300	304	314	304	310
XChl	0.95	0.99	1.00	0.98	0.98	0.93	0.93	0.97	0.97	0.97	0.93	0.93	0.91	0.96	0.94	0.98	0.97	0.95	0.97
i/l cat	0.02	0.00	0.00	0.00	0.00	0.00	0.01	0.00	0.02	0.00	0.00	0.00	0.00	0.00	0.00	0.00	0.00	0.00	0.00
non-i/l	9.94	9.98	10.00	9.98	9.98	9.93	9.93	9.97	9.97	9.97	9.92	9.93	9.91	9.96	9.93	9.98	9.97	9.94	9.97

Sample:	VHG024						
Lithology:	VCR						
Analysis No.	Chl 1	Chl 2	Chl 3	Chl 4	Chl 5	Chl 6	Chl 7
Chlorite Type	close to QV	close to QV	+C+Py	II	II	II	II
SiO2	23.64	24.33	23.09	24.00	23.57	24.31	24.37
TiO2	0.00	0.00	0.00	0.00	0.00	0.00	0.00
Al2O3	22.56	23.07	23.01	23.09	21.43	24.61	24.87
Cr2O3	0.11	0.09	0.09	0.08	0.00	0.95	0.95
FeO	35.19	35.72	34.98	35.56	35.13	27.75	27.71
MnO	0.14	0.00	0.00	0.00	0.14	0.17	0.19
MgO	7.97	8.20	7.97	8.20	8.19	12.43	12.24
CaO	0.08	0.09	0.00	0.13	0.00	0.00	0.00
Na2O	0.00	0.00	0.00	0.00	0.00	0.00	0.00
K2O	0.00	0.00	0.00	0.00	0.00	0.00	0.00
F	0.00	0.00	0.00	0.00	0.00	0.00	0.00
Total	89.69	91.50	89.14	91.06	88.46	90.22	90.33
	6.53	6.39	6.57	6.42	6.64	6.22	6.21
SiIV	2.57	2.59	2.52	2.57	2.60	2.52	2.52
AlIV	1.43	1.41	1.48	1.43	1.40	1.48	1.48
T site	4.00	4.00	4.00	4.00	4.00	4.00	4.00
AlVi	1.46	1.48	1.49	1.48	1.39	1.52	1.55
Ti	0.00	0.00	0.00	0.00	0.00	0.00	0.00
Cr3+	0.01	0.01	0.01	0.01	0.00	0.08	0.08
Fe2+	3.20	3.18	3.20	3.18	3.25	2.40	2.40
Mn2+	0.01	0.00	0.00	0.00	0.01	0.01	0.02
Mg	1.29	1.30	1.30	1.31	1.35	1.92	1.89
Ca	0.01	0.01	0.00	0.01	0.00	0.00	0.00
Na	0.00	0.00	0.00	0.00	0.00	0.00	0.00
K	0.00	0.00	0.00	0.00	0.00	0.00	0.00
O site	5.98	5.97	5.99	5.98	6.00	5.94	5.93
XFe	0.71	0.71	0.71	0.71	0.71	0.56	0.56
Al/(Al+Fe+Mg)	0.39	0.39	0.40	0.39	0.38	0.41	0.41
T (°C)	287	284	297	288	280	313	312
XChl	0.98	0.96	0.99	0.97	1.00	0.94	0.93
i/l cat	0.01	0.01	0.00	0.01	0.00	0.00	0.00
non-i/l	9.97	9.96	9.99	9.97	10.00	9.94	9.93

Sample:	VHG025					
Lithology	VCR					
	Chl 1	Chl 2	Chl 3	Chl 4	Chl 5	Chl 6
	close to QV	close to QV	II	II	II	II
SiO2	23.56	23.27	24.10	23.75	24.01	23.29
TiO2	0.00	0.00	0.00	0.00	0.00	0.00
Al2O3	22.47	23.66	23.09	22.99	23.50	22.76
Cr2O3	0.14	0.00	0.00	0.00	0.11	0.08
FeO	34.32	35.45	34.71	34.92	34.52	33.12
MnO	0.00	0.13	0.00	0.00	0.13	0.00
MgO	8.72	8.18	9.29	8.17	8.08	8.80
CaO	0.06	0.00	0.00	0.24	0.14	0.13
Na2O	0.06	0.00	0.00	0.00	0.00	0.12
K2O	0.00	0.00	0.00	0.00	0.00	0.00
F	0.00	0.00	0.00	0.00	0.00	0.00
Total	89.33	90.69	91.19	90.07	90.49	88.30
	6.53	6.45	6.38	6.49	6.43	6.58
SiIV	2.56	2.50	2.56	2.56	2.57	2.55
AlIV	1.44	1.50	1.44	1.44	1.43	1.45
T site	4.00	4.00	4.00	4.00	4.00	4.00
AlVi	1.44	1.50	1.45	1.49	1.53	1.48
Ti	0.00	0.00	0.00	0.00	0.00	0.00
Cr3+	0.01	0.00	0.00	0.00	0.01	0.01
Fe2+	3.12	3.18	3.08	3.15	3.09	3.03
Mn2+	0.00	0.01	0.00	0.00	0.01	0.00
Mg	1.41	1.31	1.47	1.31	1.29	1.44
Ca	0.01	0.00	0.00	0.03	0.02	0.02
Na	0.01	0.00	0.00	0.00	0.00	0.03
K	0.00	0.00	0.00	0.00	0.00	0.00
O site	6.00	6.00	6.00	5.98	5.95	6.00
XFe	0.69	0.71	0.68	0.71	0.71	0.68
Al/(Al+Fe+Mg)	0.39	0.40	0.39	0.40	0.40	0.40
T (°C)	291	302	293	289	288	295
XChl	0.98	1.00	1.00	0.96	0.94	0.96
i/l cat	0.02	0.00	0.00	0.03	0.02	0.04
non-i/l	9.98	10.00	10.00	9.96	9.93	9.96

Sample:	VHG028						
Lithology:	VCR						
	Chl 1	Chl 2	Chl 3	Chl 4	Chl 5	Chl 6	Chl 7
	II	II	II	Edge of QV	II	Close to QV	Close to QV
SiO2	23.82	23.93	23.31	23.78	23.98	23.26	23.13
TiO2	0.00	0.00	0.00	0.00	0.00	0.00	0.00
Al2O3	21.32	24.75	23.51	23.92	24.90	24.22	23.94
Cr2O3	1.29	0.00	0.00	0.24	0.00	0.44	0.27
FeO	33.23	32.12	31.69	31.66	33.34	31.78	31.82
MnO	0.24	0.20	0.20	0.27	0.22	0.17	0.23
MgO	9.66	9.63	9.66	9.39	9.15	9.23	8.83
CaO	0.00	0.00	0.00	0.00	0.00	0.08	0.08
Na2O	0.00	0.00	0.00	0.07	0.00	0.00	0.00
K2O	0.00	0.00	0.00	0.00	0.00	0.00	0.00
F	0.00	0.00	0.00	0.00	0.00	0.00	0.00
Total	89.56	90.63	88.37	89.33	91.57	89.18	88.30
	6.51	6.32	6.51	6.43	6.29	6.45	6.52
SiIV	2.58	2.52	2.52	2.54	2.51	2.50	2.51
AlIV	1.42	1.48	1.48	1.46	1.49	1.50	1.49
T site	4.00	4.00	4.00	4.00	4.00	4.00	4.00
AlVi	1.30	1.59	1.53	1.56	1.58	1.56	1.58
Ti	0.00	0.00	0.00	0.00	0.00	0.00	0.00
Cr3+	0.11	0.00	0.00	0.02	0.00	0.04	0.02
Fe2+	3.01	2.83	2.87	2.83	2.92	2.85	2.89
Mn2+	0.02	0.02	0.02	0.02	0.02	0.02	0.02
Mg	1.56	1.51	1.56	1.50	1.43	1.48	1.43
Ca	0.00	0.00	0.00	0.00	0.00	0.01	0.01
Na	0.00	0.00	0.00	0.01	0.00	0.00	0.00
K	0.00	0.00	0.00	0.00	0.00	0.00	0.00
O site	6.00	5.95	5.97	5.95	5.95	5.96	5.95
XFe	0.66	0.65	0.65	0.65	0.67	0.66	0.67
Al/(Al+Fe+Mg)	0.37	0.41	0.40	0.41	0.41	0.41	0.42
T (°C)	290	303	303	298	304	307	303
XChl	1.00	0.95	0.98	0.94	0.96	0.95	0.94
i/l cat	0.00	0.00	0.00	0.01	0.00	0.01	0.01
non-i/l	10.00	9.95	9.97	9.93	9.95	9.95	9.94

Sample:	VHG041							
Lithology:	VCR							
Analysis No.	Chl 1	Chl 2	Chl 3	Chl 5	Chl 6	Chl 7	Chl 8	Chl 9
Chlorite Type	+Py	II	II	II	+Py	II	II	II
SiO2	24.36	23.43	24.94	22.86	23.44	23.27	23.85	24.55
TiO2	0.00	0.00	0.00	0.00	0.00	0.00	0.00	0.00
Al2O3	21.64	23.51	21.11	22.37	22.37	22.47	22.58	23.02
Cr2O3	0.00	0.00	0.00	0.00	0.00	0.00	0.00	0.00
FeO	33.33	35.03	33.32	35.69	35.35	37.52	35.53	33.47
MnO	0.17	0.18	0.17	0.17	0.19	0.22	0.27	0.13
MgO	10.27	8.38	9.53	7.55	6.93	6.41	7.79	9.10
CaO	0.00	0.00	0.00	0.00	0.07	0.00	0.06	0.08
Na2O	0.00	0.00	0.09	0.00	0.00	0.00	0.00	0.00
K2O	0.00	0.00	0.00	0.00	0.00	0.00	0.00	0.00
F	0.00	0.00	0.00	0.00	0.00	0.00	0.00	0.00
Total	89.77	90.53	89.16	88.64	88.35	89.89	90.08	90.35
	6.46	6.45	6.50	6.65	6.65	6.60	6.51	6.40
SiIV	2.62	2.52	2.70	2.53	2.59	2.56	2.58	2.61
AlIV	1.38	1.48	1.30	1.47	1.41	1.44	1.42	1.39
T site	4.00	4.00	4.00	4.00	4.00	4.00	4.00	4.00
AlVI	1.36	1.49	1.39	1.45	1.51	1.47	1.47	1.50
Ti	0.00	0.00	0.00	0.00	0.00	0.00	0.00	0.00
Cr3+	0.00	0.00	0.00	0.00	0.00	0.00	0.00	0.00
Fe2+	2.99	3.15	3.01	3.30	3.27	3.45	3.22	2.98
Mn2+	0.02	0.02	0.02	0.02	0.02	0.02	0.02	0.01
Mg	1.64	1.34	1.54	1.25	1.14	1.05	1.26	1.44
Ca	0.00	0.00	0.00	0.00	0.01	0.00	0.01	0.01
Na	0.00	0.00	0.02	0.00	0.00	0.00	0.00	0.00
K	0.00	0.00	0.00	0.00	0.00	0.00	0.00	0.00
O site	6.01	6.00	5.97	6.01	5.95	5.99	5.98	5.95
XFe	0.65	0.70	0.66	0.73	0.74	0.77	0.72	0.67
Al/(Al+Fe+Mg)	0.37	0.40	0.37	0.39	0.40	0.39	0.39	0.40
T (°C)	283	299	265	294	279	285	283	281
XChl	1.00	1.00	0.95	1.00	0.95	0.99	0.97	0.94
i/I cat	0.00	0.00	0.02	0.00	0.01	0.00	0.01	0.01
non-i/I	10.00	10.00	9.95	10.00	9.94	9.99	9.97	9.94

Sample:	VHG043					
Lithology:	VCR					
	Chl 1	Chl 2	Chl 3	Chl 4	Chl 5	Chl 6
	in QV	in QV	Close to QV	II	+Cpy	II
SiO2	23.69	23.79	23.39	23.75	23.79	23.53
TiO2	0.00	0.00	0.00	0.00	0.00	0.00
Al2O3	22.70	22.01	22.82	23.05	21.23	22.02
Cr2O3	0.00	0.00	0.00	0.00	0.00	0.11
FeO	35.59	35.08	36.16	34.22	33.57	33.49
MnO	0.16	0.17	0.26	0.16	0.23	0.18
MgO	8.50	8.59	7.55	8.37	8.11	7.76
CaO	0.06	0.00	0.08	0.07	0.11	0.00
Na2O	0.00	0.00	0.00	0.00	0.00	0.00
K2O	0.00	0.00	0.00	0.00	0.00	0.00
F	0.00	0.00	0.00	0.00	0.00	0.00
Total	90.70	89.64	90.26	89.62	87.04	87.09
	6.46	6.53	6.53	6.49	6.70	6.68
SiIV	2.55	2.59	2.54	2.57	2.65	2.62
AlIV	1.45	1.41	1.46	1.43	1.35	1.38
T site	4.00	4.00	4.00	4.00	4.00	4.00
AlVI	1.43	1.41	1.46	1.50	1.44	1.51
Ti	0.00	0.00	0.00	0.00	0.00	0.00
Cr3+	0.00	0.00	0.00	0.00	0.00	0.01
Fe2+	3.20	3.19	3.28	3.09	3.13	3.12
Mn2+	0.01	0.02	0.02	0.01	0.02	0.02
Mg	1.36	1.39	1.22	1.35	1.35	1.29
Ca	0.01	0.00	0.01	0.01	0.01	0.00
Na	0.00	0.00	0.00	0.00	0.00	0.00
K	0.00	0.00	0.00	0.00	0.00	0.00
O site	6.01	6.00	6.00	5.97	5.96	5.93
XFe	0.70	0.70	0.73	0.70	0.70	0.71
Al/(Al+Fe+Mg)	0.39	0.38	0.39	0.40	0.38	0.40
T (°C)	292	285	292	289	271	277
XChl	1.00	1.00	0.99	0.96	0.95	0.94
i/I cat	0.01	0.00	0.01	0.01	0.01	0.00
non-i/I	10.00	10.00	9.99	9.96	9.94	9.93

Sample:	VHG055(A)				
Lithology:	VCR				
	Chl 1	Chl 2	Chl 3	Chl 4	Chl 5
	II	II	II	II	II
SiO2	23.46	23.78	22.94	23.71	23.83
TiO2	0.00	0.00	0.00	0.00	0.00
Al2O3	23.87	23.86	24.01	24.11	24.33
Cr2O3	0.00	0.00	0.00	0.00	0.00
FeO	33.03	30.85	32.77	31.31	31.45
MnO	0.15	0.22	0.14	0.21	0.18
MgO	9.33	10.68	9.07	10.24	10.52
CaO	0.09	0.00	0.13	0.00	0.00
Na2O	0.00	0.00	0.00	0.00	0.00
K2O	0.00	0.00	0.00	0.00	0.00
F	0.00	0.00	0.00	0.00	0.00
Total	89.93	89.39	89.06	89.58	90.31
	6.43	6.39	6.50	6.39	6.33
SiIV	2.51	2.53	2.48	2.52	2.51
AlIV	1.49	1.47	1.52	1.48	1.49
T site	4.00	4.00	4.00	4.00	4.00
AlVI	1.52	1.52	1.54	1.54	1.54
Ti	0.00	0.00	0.00	0.00	0.00
Cr3+	0.00	0.00	0.00	0.00	0.00
Fe2+	2.96	2.74	2.96	2.78	2.77
Mn2+	0.01	0.02	0.01	0.02	0.02
Mg	1.49	1.69	1.46	1.62	1.65
Ca	0.01	0.00	0.02	0.00	0.00
Na	0.00	0.00	0.00	0.00	0.00
K	0.00	0.00	0.00	0.00	0.00
O site	5.99	5.98	5.99	5.97	5.98
XFe	0.67	0.62	0.67	0.63	0.63
Al/(Al+Fe+Mg)	0.40	0.40	0.41	0.41	0.41
T (°C)	304	304	310	305	307
XChl	0.98	0.98	0.98	0.97	0.98
i/I cat	0.01	0.00	0.02	0.00	0.00
non-i/I	9.98	9.98	9.98	9.97	9.98

Sample:	VHG046												Sample:	VHG052	
Lithology:	VCR												Lithology:	VCR	
Analysis No.	Chl 1	Chl 2	Chl 3	Chl 4	Chl 5	Chl 6	Chl 7	Chl 8	Chl 9	Chl 10	Chl 11	Chl 12	Chl 1	Chl 3	Chl 6
Chlorite Type	II	II	Vein	Vein	+Py	+Py	Vein ?	+Py	II	+C	+Py	+Py	II	II	II
SiO2	22.91	23.18	22.84	22.52	22.87	23.78	23.65	23.31	23.39	23.22	23.47	22.84	22.81	24.07	23.63
TiO2	0.00	0.00	0.00	0.00	0.00	0.00	0.00	0.00	0.00	0.00	0.00	0.00	0.00	0.00	0.00
Al2O3	23.78	24.12	23.16	23.13	22.83	20.28	22.89	22.06	23.63	22.80	23.58	23.34	24.08	24.73	23.99
Cr2O3	0.20	0.22	0.10	0.13	0.24	0.16	0.15	0.19	0.13	0.57	0.21	0.26	0.98	0.49	1.14
FeO	38.63	38.43	37.68	38.02	38.43	36.46	38.86	38.01	38.32	38.78	37.71	37.87	35.25	34.08	34.66
MnO	0.00	0.14	0.14	0.14	0.00	0.18	0.00	0.14	0.15	0.26	0.17	0.18	0.32	0.30	0.28
MgO	6.12	6.16	6.06	5.80	6.31	6.94	6.13	6.32	6.00	5.94	6.45	6.46	8.07	8.41	8.40
CaO	0.15	0.00	0.08	0.00	0.00	0.09	0.13	0.00	0.00	0.00	0.00	0.00	0.00	0.00	0.00
Na2O	0.00	0.00	0.06	0.00	0.00	0.00	0.00	0.00	0.00	0.00	0.00	0.00	0.00	0.00	0.00
K2O	0.00	0.00	0.00	0.00	0.00	0.00	0.00	0.00	0.00	0.00	0.00	0.00	0.00	0.00	0.00
F	0.00	0.00	0.00	0.00	0.00	0.00	0.00	0.00	0.00	0.00	0.00	0.00	0.00	0.00	0.00
Total	91.79	92.25	90.12	89.74	90.68	87.89	91.81	90.03	91.62	91.57	91.59	90.95	91.51	92.08	92.10
	6.49	6.44	6.60	6.64	6.58	6.75	6.49	6.61	6.48	6.52	6.46	6.54	6.41	6.29	6.34
SiIV	2.47	2.48	2.51	2.49	2.50	2.67	2.55	2.57	2.52	2.52	2.52	2.48	2.44	2.52	2.49
AlIV	1.53	1.52	1.49	1.51	1.50	1.33	1.45	1.43	1.48	1.48	1.48	1.52	1.56	1.48	1.51
T site	4.00	4.00	4.00	4.00	4.00	4.00	4.00	4.00	4.00	4.00	4.00	4.00	4.00	4.00	4.00
AlVI	1.50	1.53	1.50	1.50	1.45	1.36	1.47	1.43	1.53	1.44	1.51	1.48	1.47	1.57	1.47
Ti	0.00	0.00	0.00	0.00	0.00	0.00	0.00	0.00	0.00	0.00	0.00	0.00	0.00	0.00	0.00
Cr3+	0.02	0.02	0.01	0.01	0.02	0.01	0.01	0.02	0.01	0.05	0.02	0.02	0.08	0.04	0.10
Fe2+	3.49	3.44	3.46	3.51	3.52	3.42	3.51	3.50	3.46	3.52	3.39	3.44	3.15	2.98	3.06
Mn2+	0.00	0.01	0.01	0.01	0.00	0.02	0.00	0.01	0.01	0.02	0.02	0.02	0.03	0.03	0.03
Mg	0.99	0.98	0.99	0.96	1.03	1.16	0.99	1.04	0.96	0.96	1.03	1.05	1.28	1.31	1.32
Ca	0.02	0.00	0.01	0.00	0.00	0.01	0.02	0.00	0.00	0.00	0.00	0.00	0.00	0.00	0.00
Na	0.00	0.00	0.01	0.00	0.00	0.00	0.00	0.00	0.00	0.00	0.00	0.00	0.00	0.00	0.00
K	0.00	0.00	0.00	0.00	0.00	0.00	0.00	0.00	0.00	0.00	0.00	0.00	0.00	0.00	0.00
O site	6.01	5.99	6.00	6.00	6.01	5.98	5.99	5.99	5.97	6.00	5.97	6.01	6.01	5.93	5.97
XFe	0.78	0.78	0.78	0.79	0.77	0.75	0.78	0.77	0.78	0.79	0.77	0.77	0.71	0.69	0.70
Al/(Al+Fe+Mg)	0.40	0.41	0.40	0.40	0.39	0.37	0.39	0.39	0.40	0.39	0.40	0.40	0.41	0.42	0.41
T(°C)	301	299	294	297	296	262	284	282	291	290	292	300	316	299	305
XChl	0.99	0.99	0.98	1.00	1.00	0.98	0.98	0.99	0.97	1.00	0.97	1.00	1.00	0.94	0.97
i/l cat	0.02	0.00	0.02	0.00	0.00	0.01	0.02	0.00	0.00	0.00	0.00	0.00	0.00	0.00	0.00
non-i/l	9.99	9.99	9.98	10.00	10.00	9.97	9.97	9.99	9.97	10.00	9.97	10.00	10.00	9.93	9.97

Sample:	VHG057			Sample:	VHG070						Sample:	VHG071(A)				
Lithology:	VCR			Lithology:	VCR						Lithology:	VCR				
Analysis No.	Chl 4	Chl 5	Chl 6	Chl 1	Chl 2	Chl 3	Chl 4	Chl 5	Chl 6		Chl 2	Chl 3	Chl 4	Chl 5	Chl 6	Chl 7
Chlorite Type	II	II	II	II	II	II	II	II	II		+Py	II	II	II	+Py	+Py
SiO2	24.35	23.92	24.18	23.81	24.37	24.11	23.93	24.06	23.98		22.85	23.52	23.02	22.77	23.30	24.03
TiO2	0.00	0.00	0.00	0.00	0.00	0.00	0.00	0.00	0.00		0.97	0.00	0.24	0.00	0.00	0.00
Al2O3	25.22	25.51	25.41	24.61	24.86	25.15	24.41	24.56	24.28		22.68	23.33	23.28	23.12	24.16	23.92
Cr2O3	0.00	0.00	0.00	0.00	0.00	0.00	0.09	0.13	0.00		0.14	0.16	0.31	0.00	0.38	0.23
FeO	29.35	30.35	30.39	31.30	31.10	31.32	30.94	31.18	31.03		35.05	36.37	36.22	35.78	36.68	36.11
MnO	0.18	0.20	0.19	0.15	0.17	0.14	0.00	0.19	0.16		0.25	0.22	0.22	0.16	0.18	0.21
MgO	11.83	11.27	11.86	10.62	10.93	10.49	10.63	11.16	10.45		6.91	6.89	6.82	6.69	6.59	6.79
CaO	0.00	0.00	0.00	0.00	0.00	0.00	0.07	0.00	0.08		0.10	0.00	0.00	0.00	0.00	0.00
Na2O	0.00	0.00	0.00	0.00	0.00	0.00	0.00	0.00	0.00		0.00	0.00	0.00	0.00	0.00	0.10
K2O	0.00	0.00	0.00	0.00	0.00	0.00	0.00	0.00	0.00		0.00	0.00	0.00	0.00	0.00	0.09
F	0.00	0.00	0.00	0.00	0.00	0.00	0.00	0.00	0.00		0.00	0.00	0.00	0.00	0.00	0.00
Total	90.93	91.25	92.03	90.49	91.43	91.21	90.07	91.30	89.98		88.95	90.49	90.11	88.52	91.31	91.48
	6.20	6.22	6.16	6.31	6.22	6.25	6.33	6.25	6.34		6.61	6.50	6.54	6.65	6.45	6.41
SiIV	2.51	2.48	2.48	2.50	2.52	2.51	2.52	2.50	2.53		2.51	2.55	2.51	2.52	2.50	2.56
AlIV	1.49	1.52	1.52	1.50	1.48	1.49	1.48	1.50	1.47		1.49	1.45	1.49	1.48	1.50	1.44
T site	4.00	4.00	4.00	4.00	4.00	4.00	4.00	4.00	4.00		4.00	4.00	4.00	4.00	4.00	4.00
AlVI	1.58	1.59	1.56	1.55	1.56	1.59	1.55	1.51	1.55		1.45	1.52	1.49	1.54	1.56	1.57
Ti	0.00	0.00	0.00	0.00	0.00	0.00	0.00	0.00	0.00		0.08	0.00	0.02	0.00	0.00	0.00
Cr3+	0.00	0.00	0.00	0.00	0.00	0.00	0.01	0.01	0.00		0.01	0.01	0.03	0.00	0.03	0.02
Fe2+	2.53	2.63	2.61	2.75	2.69	2.72	2.73	2.71	2.74		3.22	3.29	3.30	3.31	3.29	3.22
Mn2+	0.02	0.02	0.02	0.01	0.01	0.01	0.00	0.02	0.01		0.02	0.02	0.02	0.02	0.02	0.02
Mg	1.82	1.74	1.81	1.66	1.69	1.63	1.87	1.73	1.64		1.13	1.11	1.11	1.10	1.05	1.08
Ca	0.00	0.00	0.00	0.00	0.00	0.00	0.01	0.00	0.01		0.01	0.00	0.00	0.00	0.00	0.00
Na	0.00	0.00	0.00	0.00	0.00	0.00	0.00	0.00	0.00		0.00	0.00	0.00	0.00	0.00	0.02
K	0.00	0.00	0.00	0.00	0.00	0.00	0.00	0.00	0.00		0.00	0.00	0.00	0.00	0.00	0.01
O site	5.95	5.97	5.99	5.97	5.96	5.95	5.96	5.99	5.96		5.94	5.96	5.97	5.97	5.95	5.94
XFe	0.58	0.60	0.59	0.62	0.61	0.63	0.62	0.61	0.62		0.74	0.75	0.75	0.75	0.76	0.75
Al/(Al+Fe+Mg)	0.41	0.42	0.41	0.41	0.41	0.41	0.41	0.40	0.41		0.40	0.40	0.40	0.41	0.41	0.41
T (°C)	311	317	318	310	306	308	306	311	303		297	289	297	294	298	285
XChl	0.96	0.97	0.99	0.98	0.96	0.96	0.96	0.99	0.96		0.93	0.96	0.97	0.97	0.96	0.91
i/l cat	0.00	0.00	0.00	0.00	0.00	0.00	0.01	0.00	0.01		0.01	0.00	0.00	0.00	0.00	0.03
non-i/l	9.95	9.97	9.99	9.97	9.96	9.95	9.95	9.99	9.95		9.92	9.96	9.97	9.97	9.95	9.90

Sample	VHG062																				
Lithology:	VCR																				
Analysis No.	Chl 1	Chl 2	Chl 3	Chl 4	Chl 5	Chl 6	Chl 7	Chl 8	Chl 9	Chl 10	Chl 11	Chl 12	Chl 13	Chl 14	Chl 15	Chl 16	Chl 17	Chl 18	Chl 19	Chl 20	Chl 21	Chl 22
Chlorite Type	II	I	IV	+Au	+Au	+Au	+Au+Cpy	IV	+Py	+Py	II	IV	+Py	IV	II	+Au	+Au	+Py	IV	+Au+Py	II	II
SiO2	26.43	25.62	25.13	22.99	24.71	25.52	25.87	25.36	24.76	24.36	25.47	24.30	25.87	24.03	26.53	25.47	25.49	25.12	24.76	24.37	24.92	23.12
TiO2	0.31	0.00	0.00	0.00	0.00	0.00	0.00	0.00	0.00	0.00	0.00	0.00	0.08	0.00	0.00	0.00	0.00	0.00	0.00	0.00	0.00	0.00
Al2O3	25.66	25.35	26.97	26.82	26.62	25.22	23.19	27.00	26.14	26.04	25.81	24.77	25.31	25.65	26.54	26.79	25.51	25.09	25.65	26.24	25.87	24.90
Cr2O3	0.00	0.00	0.00	0.00	0.00	0.29	0.27	0.00	0.14	0.14	0.00	0.00	0.00	0.00	0.00	0.21	0.25	0.35	0.00	0.00	0.00	0.00
FeO	23.17	26.07	25.96	27.67	25.50	22.20	22.50	22.27	25.83	25.11	24.66	26.10	23.91	25.13	24.12	23.89	23.26	23.86	23.28	23.25	23.92	24.65
MnO	0.16	0.24	0.18	0.26	0.22	0.25	0.30	0.23	0.00	0.20	0.13	0.21	0.23	0.18	0.26	0.22	0.23	0.24	0.21	0.23	0.26	0.23
MgO	14.34	13.71	13.57	11.00	14.08	16.03	15.15	14.68	12.54	14.30	13.95	12.96	14.18	13.60	14.28	13.90	15.68	15.44	15.51	14.66	14.59	13.39
CaO	0.05	0.07	0.00	0.07	0.00	0.00	0.11	0.00	0.00	0.00	0.14	0.11	0.00	0.12	0.07	0.06	0.00	0.00	0.00	0.00	0.07	0.11
Na2O	0.06	0.00	0.00	0.06	0.06	0.00	0.06	0.05	0.00	0.00	0.08	0.10	0.00	0.07	0.00	0.00	0.00	0.00	0.00	0.00	0.06	0.00
K2O	0.00	0.00	0.00	0.00	0.00	0.00	0.06	0.00	0.00	0.00	0.00	0.00	0.00	0.00	0.00	0.00	0.00	0.00	0.00	0.00	0.00	0.00
F	0.00	0.00	0.00	0.00	0.00	0.00	0.00	0.00	0.00	0.00	0.00	0.00	0.00	0.00	0.00	0.00	0.00	0.00	0.00	0.00	0.00	0.00
Total	90.18	91.06	91.81	88.87	91.19	89.51	87.51	89.59	89.41	90.15	90.24	88.55	89.58	88.78	91.80	90.54	90.42	90.10	89.41	88.75	89.69	86.40
	6.02	6.07	6.01	6.31	6.05	6.07	6.24	6.04	6.18	6.12	6.08	6.28	6.10	6.23	5.94	6.03	6.03	6.09	6.11	6.16	6.11	6.42
SiIV	2.65	2.59	2.51	2.42	2.49	2.58	2.68	2.55	2.55	2.48	2.58	2.54	2.63	2.49	2.62	2.56	2.56	2.54	2.52	2.50	2.53	2.47
AlIV	1.35	1.41	1.49	1.58	1.51	1.42	1.32	1.45	1.45	1.52	1.42	1.46	1.37	1.51	1.38	1.44	1.44	1.46	1.48	1.50	1.47	1.53
T site	4.00	4.00	4.00	4.00	4.00	4.00	4.00	4.00	4.00	4.00	4.00	4.00	4.00	4.00	4.00	4.00	4.00	4.00	4.00	4.00	4.00	4.00
AlVI	1.68	1.61	1.69	1.74	1.65	1.58	1.52	1.75	1.71	1.61	1.66	1.59	1.65	1.63	1.71	1.73	1.58	1.54	1.59	1.67	1.64	1.60
Ti	0.02	0.00	0.00	0.00	0.00	0.00	0.00	0.00	0.00	0.00	0.00	0.00	0.01	0.00	0.00	0.00	0.00	0.00	0.00	0.00	0.00	0.00
Cr3+	0.00	0.00	0.00	0.00	0.00	0.02	0.02	0.00	0.01	0.01	0.00	0.00	0.00	0.00	0.00	0.00	0.02	0.02	0.03	0.00	0.00	0.00	0.00
Fe2+	1.94	2.20	2.17	2.43	2.15	1.87	1.95	1.87	2.22	2.14	2.09	2.28	2.03	2.18	1.99	2.01	1.95	2.02	1.98	1.99	2.03	2.20
Mn2+	0.01	0.02	0.02	0.02	0.02	0.02	0.03	0.02	0.00	0.02	0.01	0.02	0.02	0.02	0.02	0.02	0.02	0.02	0.02	0.02	0.02	0.02
Mg	2.14	2.06	2.02	1.72	2.11	2.41	2.34	2.20	1.92	2.17	2.10	2.02	2.14	2.10	2.10	2.08	2.35	2.33	2.35	2.24	2.21	2.13
Ca	0.01	0.01	0.00	0.01	0.00	0.00	0.01	0.00	0.00	0.00	0.02	0.01	0.00	0.01	0.01	0.01	0.00	0.00	0.00	0.00	0.01	0.01
Na	0.01	0.00	0.00	0.01	0.01	0.00	0.01	0.01	0.00	0.00	0.02	0.02	0.00	0.01	0.00	0.00	0.00	0.00	0.00	0.00	0.01	0.00
K	0.00	0.00	0.00	0.00	0.00	0.00	0.01	0.00	0.00	0.00	0.00	0.00	0.00	0.00	0.00	0.00	0.00	0.00	0.00	0.00	0.00	0.00
O site	5.82	5.90	5.90	5.93	5.94	5.91	5.90	5.85	5.87	5.95	5.89	5.95	5.85	5.95	5.84	5.85	5.92	5.94	5.94	5.92	5.92	5.97
XFe	0.48	0.52	0.52	0.59	0.50	0.44	0.45	0.46	0.54	0.50	0.50	0.53	0.49	0.51	0.49	0.49	0.45	0.46	0.46	0.47	0.48	0.51
Al/(Al+Fe+Mg)	0.43	0.41	0.43	0.44	0.43	0.41	0.40	0.44	0.43	0.42	0.42	0.42	0.42	0.42	0.43	0.44	0.41	0.41	0.42	0.43	0.42	0.42
T (°C)	292	301	317	332	324	311	287	315	309	326	305	310	296	323	297	311	313	315	322	325	316	328
XChl	0.82	0.91	0.91	0.92	0.93	0.92	0.88	0.86	0.88	0.95	0.88	0.92	0.87	0.93	0.84	0.86	0.93	0.95	0.95	0.92	0.91	0.96
i/l cat	0.02	0.01	0.00	0.02	0.01	0.00	0.03	0.01	0.00	0.00	0.03	0.03	0.00	0.03	0.01	0.01	0.00	0.00	0.00	0.00	0.02	0.01
non-i/l	9.80	9.90	9.90	9.91	9.93	9.91	9.87	9.84	9.87	9.95	9.86	9.91	9.85	9.93	9.83	9.85	9.92	9.94	9.94	9.92	9.90	9.96

Sample	VHG063(A)																								
Lithology	VCR																								
Analysis No	Chl 1	Chl 2	Chl 3	Chl 4	Chl 5	Chl 6	Chl 7	Chl 8	Chl 9	Chl 10	Chl 11	Chl 12	Chl 13	Chl 14	Chl 15 R	Chl 16 R	Chl 17	Chl 18	Chl 19	Chl 20	Chl 21	Chl 22	Chl 23	Chl 24	Chl 25	Chl 26	Chl 27
Chlorite Type	II	II	II	IV	IV	IV	+Au	+Au	+Au	+Au	+Au	+Py	+Py	IV	IV	IV	+Au+Py	+Au+Py	II	II	+Au	II	IV	IV	+Py	+Au	II
SiO2	24.17	24.22	24.87	23.94	24.16	24.91	24.73	24.10	24.00	24.01	24.05	24.93	25.06	24.98	24.83	25.12	24.02	24.61	24.12	25.17	24.48	25.72	24.48	23.72	25.11	23.29	24.04
TiO2	0.00	0.00	0.00	0.00	0.00	0.00	0.00	0.00	0.00	0.00	0.00	0.00	0.00	0.00	0.00	0.00	0.00	0.00	0.00	0.00	0.00	0.00	0.00	0.00	0.00	0.00	0.00
Al2O3	25.63	25.69	26.00	25.25	26.01	26.63	26.50	26.48	26.98	27.12	27.69	26.04	26.14	25.83	26.93	25.09	25.96	25.78	25.40	26.19	25.95	25.92	25.86	25.74	26.45	26.51	23.73
Cr2O3	0.09	0.00	0.09	0.00	0.00	0.00	0.00	0.00	0.00	0.00	0.00	0.00	0.10	0.22	0.17	0.00	0.12	0.13	0.00	0.00	0.00	0.00	0.12	0.11	0.09	0.00	0.00
FeO	25.30	24.13	22.80	24.53	24.21	23.48	24.43	23.90	25.31	24.75	26.30	23.77	24.05	21.76	23.50	23.41	23.77	22.17	23.33	24.34	24.68	23.23	23.57	24.47	24.02	28.35	24.79
MnO	0.22	0.28	0.23	0.20	0.21	0.25	0.25	0.30	0.29	0.28	0.29	0.15	0.21	0.29	0.27	0.23	0.28	0.26	0.25	0.22	0.30	0.17	0.27	0.24	0.22	0.32	0.23
MgO	13.94	14.37	15.17	13.82	13.71	14.84	14.16	14.31	13.57	13.90	12.81	15.44	14.75	16.27	15.44	14.71	15.31	15.85	14.06	13.90	13.81	14.66	15.06	14.27	15.00	11.60	14.28
CaO	0.00	0.00	0.06	0.11	0.13	0.00	0.00	0.00	0.00	0.00	0.00	0.00	0.00	0.00	0.00	0.12	0.00	0.00	0.00	0.00	0.00	0.00	0.00	0.00	0.00	0.00	0.00
Na2O	0.00	0.00	0.00	0.00	0.00	0.00	0.00	0.00	0.00	0.00	0.00	0.00	0.00	0.00	0.00	0.08	0.00	0.00	0.00	0.00	0.00	0.00	0.00	0.00	0.00	0.00	0.00
K2O	0.00	0.00	0.00	0.00	0.00	0.00	0.00	0.00	0.00	0.00	0.00	0.00	0.00	0.00	0.00	0.06	0.00	0.00	0.00	0.00	0.00	0.00	0.00	0.00	0.00	0.00	0.00
F	0.00	0.00	0.00	0.00	0.00	0.00	0.00	0.00	0.00	0.00	0.00	0.00	0.00	0.00	0.00	0.00	0.00	0.00	0.00	0.00	0.00	0.00	0.00	0.00	0.00	0.00	0.00
Total	89.35	88.69	89.32	87.85	88.43	90.11	90.07	89.09	90.15	90.06	91.14	90.33	90.31	89.35	91.14	88.80	89.46	88.80	87.16	89.82	89.22	89.70	89.36	88.55	90.89	90.07	87.07
	6.19	6.20	6.10	6.28	6.22	6.06	6.09	6.16	6.13	6.11	6.08	6.06	6.06	6.07	5.99	6.16	6.14	6.13	6.29	6.10	6.17	6.07	6.13	6.23	6.02	6.24	6.36
SiIV	2.49	2.50	2.53	2.50	2.50	2.51	2.51	2.47	2.45	2.44	2.43	2.51	2.53	2.52	2.48	2.58	2.45	2.51	2.52	2.56	2.51	2.60	2.50	2.46	2.52	2.42	2.54
AlIV	1.51	1.50	1.47	1.50	1.50	1.49	1.49	1.53	1.55	1.56	1.57	1.49	1.47	1.48	1.52	1.42	1.55	1.49	1.48	1.44	1.49	1.40	1.50	1.54	1.48	1.58	1.46
T site	4.00	4.00	4.00	4.00	4.00	4.00	4.00	4.00	4.00	4.00	4.00	4.00	4.00	4.00	4.00	4.00	4.00	4.00	4.00	4.00	4.00	4.00	4.00	4.00	4.00	4.00	4.00
AlVI	1.60	1.62	1.65	1.62	1.67	1.68	1.68	1.67	1.69	1.69	1.74	1.61	1.64	1.60	1.64	1.61	1.58	1.61	1.66	1.69	1.66	1.68	1.61	1.61	1.64	1.67	1.51
Ti	0.00	0.00	0.00	0.00	0.00	0.00	0.00	0.00	0.00	0.00	0.00	0.00	0.00	0.00	0.00	0.00	0.00	0.00	0.00	0.00	0.00	0.00	0.00	0.00	0.00	0.00	0.00
Cr3+	0.01	0.00	0.01	0.00	0.00	0.00	0.00	0.00	0.00	0.00	0.00	0.00	0.01	0.02	0.01	0.00	0.01	0.01	0.00	0.00	0.00	0.00	0.01	0.01	0.01	0.00	0.00
Fe2+	2.18	2.08	1.94	2.15	2.10	1.98	2.07	2.05	2.16	2.11	2.22	2.00	2.03	1.84	1.96	2.01	2.03	1.89	2.04	2.07	2.12	1.96	2.01	2.12	2.01	2.46	2.19
Mn2+	0.02	0.02	0.02	0.02	0.02	0.02	0.02	0.03	0.03	0.02	0.02	0.01	0.02	0.02	0.02	0.02	0.02	0.02	0.02	0.02	0.03	0.01	0.02	0.02	0.02	0.03	0.02
Mg	2.14	2.21	2.29	2.15	2.11	2.23	2.14	2.19	2.06	2.11	1.93	2.32	2.22	2.45	2.29	2.25	2.33	2.41	2.19	2.10	2.11	2.21	2.29	2.21	2.24	1.80	2.25
Ca	0.00	0.00	0.01	0.01	0.01	0.00	0.00	0.00	0.00	0.00	0.00	0.00	0.00	0.00	0.00	0.01	0.00	0.00	0.00	0.00	0.00	0.00	0.00	0.00	0.00	0.00	0.00
Na	0.00	0.00	0.00	0.00	0.00	0.00	0.00	0.00	0.00	0.00	0.00	0.00	0.00	0.00	0.00	0.01	0.00	0.00	0.00	0.00	0.00	0.00	0.00	0.00	0.00	0.00	0.00
K	0.00	0.00	0.00	0.00	0.00	0.00	0.00	0.00	0.00	0.00	0.00	0.00	0.00	0.00	0.00	0.01	0.00	0.00	0.00	0.00	0.00	0.00	0.00	0.00	0.00	0.00	0.00
O site	5.95	5.94	5.91	5.95	5.92	5.91	5.91	5.93	5.93	5.93	5.92	5.94	5.91	5.93	5.93	5.92	5.98	5.94	5.91	5.88	5.92	5.86	5.94	5.96	5.92	5.96	5.97
XFe	0.50	0.49	0.46	0.50	0.50	0.47	0.49	0.48	0.51	0.50	0.54	0.46	0.48	0.43	0.46	0.47	0.47	0.44	0.48	0.50	0.50	0.47	0.47	0.49	0.47	0.58	0.49
Al/(Al+Fe+Mg)	0.42	0.42	0.42	0.42	0.43	0.43	0.43	0.43	0.43	0.44	0.44	0.42	0.42	0.42	0.43	0.42	0.42	0.42	0.43	0.43	0.43	0.43	0.42	0.42	0.42	0.43	0.40
T (°C)	323	323	318	321	322	322	321	330	332	334	333	322	318	323	330	308	335	325	318	310	319	304	325	331	321	331	313
XChl	0.95	0.94	0.91	0.94	0.91	0.91	0.92	0.94	0.94	0.94	0.92	0.95	0.92	0.94	0.94	0.90	0.98	0.94	0.92	0.89	0.92	0.87	0.95	0.97	0.93	0.96	0.98
i/l cat	0.00	0.00	0.01	0.01	0.01	0.00	0.00	0.00	0.00	0.00	0.00	0.00	0.00	0.00	0.00	0.03	0.00	0.00	0.00	0.00	0.00	0.00	0.00	0.00	0.00	0.00	0.00
non-i/l	9.95	9.94	9.90	9.93	9.90	9.91	9.91	9.93	9.93	9.93	9.92	9.94	9.91	9.93	9.93	9.89	9.98	9.94	9.91	9.88	9.92	9.86	9.94	9.96	9.92	9.96	9.97

Sample:	VHG074																
Lithology:	VCR																
Analysis No.	Chl 1	Chl 2	Chl 3	Chl 4	Chl 5	Chl 6	Chl 7	Chl 8 +Au	Chl 9 +Au	Chl 17	Chl 18 +Au	Chl 10 +Au	Chl 11 +Au	Chl 12 +Au	Chl 13 +Au	Chl 19 +Au	Chl 20 +Au
Chlorite Type	II	II	II	II	IV	II	IV			II							
SiO2	23.11	24.47	23.96	24.21	24.75	23.51	23.76	22.99	23.71	23.58	22.93	24.32	24.46	23.58	23.71	24.22	24.49
TiO2	0.00	0.00	0.00	0.00	0.00	0.00	0.00	0.00	0.00	0.00	0.00	0.00	0.00	0.00	0.00	0.00	0.00
Al2O3	23.48	24.67	23.51	24.58	24.16	24.71	25.57	24.92	26.04	25.55	25.39	25.03	25.54	25.68	25.78	24.82	24.09
Cr2O3	0.00	0.58	0.55	0.00	0.09	0.00	0.00	0.14	0.00	0.00	0.00	0.00	0.00	0.00	0.00	0.00	0.24
FeO	31.81	26.04	26.62	26.03	25.56	30.15	26.36	28.81	30.38	28.57	31.51	24.95	27.04	30.12	27.90	25.52	25.05
MnO	0.19	0.22	0.22	0.19	0.28	0.16	0.16	0.20	0.14	0.16	0.12	0.20	0.18	0.18	0.16	0.24	0.23
MgO	10.07	13.44	12.94	13.52	12.61	10.30	12.18	11.46	10.27	11.66	9.63	13.82	12.01	10.53	11.70	13.22	14.23
CaO	0.00	0.00	0.00	0.00	0.12	0.00	0.00	0.00	0.00	0.00	0.00	0.00	0.00	0.00	0.00	0.00	0.00
Na2O	0.00	0.00	0.00	0.00	0.00	0.00	0.00	0.00	0.00	0.00	0.00	0.00	0.00	0.00	0.00	0.00	0.00
K2O	0.00	0.00	0.00	0.00	0.05	0.00	0.00	0.00	0.00	0.00	0.00	0.00	0.00	0.00	0.00	0.00	0.00
F	0.00	0.00	0.00	0.00	0.00	0.00	0.00	0.00	0.00	0.00	0.00	0.00	0.00	0.00	0.00	0.00	0.00
Total	88.66	89.42	87.80	88.53	87.62	88.83	88.03	88.52	90.54	89.52	89.58	88.32	89.23	90.09	89.25	88.02	88.33
	6.50	6.22	6.38	6.28	6.33	6.40	6.32	6.39	6.26	6.29	6.39	6.25	6.24	6.30	6.28	6.30	6.27
SiIV	2.50	2.53	2.54	2.53	2.61	2.50	2.50	2.45	2.47	2.47	2.44	2.53	2.54	2.47	2.48	2.54	2.55
AlIV	1.50	1.47	1.46	1.47	1.39	1.50	1.50	1.55	1.53	1.53	1.56	1.47	1.46	1.53	1.52	1.46	1.45
T site	4.00	4.00	4.00	4.00	4.00	4.00	4.00	4.00	4.00	4.00	4.00	4.00	4.00	4.00	4.00	4.00	4.00
AlVI	1.49	1.54	1.49	1.56	1.61	1.61	1.67	1.57	1.67	1.62	1.63	1.60	1.67	1.64	1.66	1.61	1.52
Ti	0.00	0.00	0.00	0.00	0.00	0.00	0.00	0.00	0.00	0.00	0.00	0.00	0.00	0.00	0.00	0.00	0.00
Cr3+	0.00	0.05	0.05	0.00	0.01	0.00	0.00	0.01	0.00	0.00	0.00	0.00	0.00	0.00	0.00	0.00	0.02
Fe2+	2.88	2.25	2.36	2.27	2.25	2.69	2.32	2.56	2.65	2.50	2.80	2.17	2.35	2.64	2.44	2.24	2.19
Mn2+	0.02	0.02	0.02	0.02	0.02	0.01	0.01	0.02	0.01	0.01	0.01	0.02	0.02	0.02	0.01	0.02	0.02
Mg	1.62	2.07	2.05	2.11	1.98	1.64	1.91	1.82	1.60	1.82	1.53	2.14	1.86	1.64	1.82	2.06	2.21
Ca	0.00	0.00	0.00	0.00	0.01	0.00	0.00	0.00	0.00	0.00	0.00	0.00	0.00	0.00	0.00	0.00	0.00
Na	0.00	0.00	0.00	0.00	0.00	0.00	0.00	0.00	0.00	0.00	0.00	0.00	0.00	0.00	0.00	0.00	0.00
K	0.00	0.00	0.00	0.00	0.01	0.00	0.00	0.00	0.00	0.00	0.00	0.00	0.00	0.00	0.00	0.00	0.00
O site	6.01	5.94	5.96	5.96	5.89	5.94	5.91	5.98	5.93	5.96	5.97	5.93	5.89	5.94	5.93	5.93	5.95
XFe	0.64	0.62	0.64	0.62	0.63	0.62	0.65	0.69	0.62	0.58	0.65	0.50	0.56	0.62	0.57	0.52	0.50
Al/(Al+Fe+Mg)	0.40	0.41	0.40	0.41	0.41	0.42	0.43	0.42	0.43	0.42	0.42	0.42	0.43	0.43	0.43	0.42	0.40
T (°C)	309	313	309	313	296	309	317	325	316	321	321	315	307	317	319	312	310
XChl	1.00	0.94	0.97	0.96	0.88	0.95	0.92	0.99	0.93	0.96	0.97	0.94	0.90	0.95	0.94	0.93	0.96
i/l cat	0.00	0.00	0.00	0.00	0.02	0.00	0.00	0.00	0.00	0.00	0.00	0.00	0.00	0.00	0.00	0.00	0.00
non-i/l	10.00	9.94	9.96	9.96	9.87	9.94	9.91	9.98	9.93	9.96	9.97	9.93	9.89	9.94	9.93	9.93	9.95

Sample:	VHG066						Sample:	VHG085						
Lithology:	VCR						Lithology	VCR						
Analysis No.	Chl 1	Chl 2	Chl 3	Chl 4	Chl 5	Chl 6	Chl 1	Chl 2	Chl 3	Chl 4	Chl 5	Chl 6	Chl 7	Chl 8
Chlorite Type	II	+Py	+Py	II	II	II	II	II	II	II	II	II	II	II
SiO2	23.88	23.05	24.01	24.12	24.43	23.36	23.66	23.32	23.37	22.12	23.58	26.90	24.92	23.37
TiO2	0.00	0.08	0.00	0.00	0.00	0.00	0.00	0.00	0.00	0.00	0.00	0.00	0.00	0.00
Al2O3	21.96	21.53	22.30	22.49	22.00	22.02	21.73	22.09	22.60	23.28	22.51	20.15	20.00	22.08
Cr2O3	0.00	0.00	0.00	0.00	0.00	0.00	0.00	0.00	0.00	0.00	0.00	0.47	0.00	0.14
FeO	36.81	36.33	37.09	36.84	36.97	37.32	32.29	34.85	32.40	35.53	33.75	30.29	31.62	35.52
MnO	0.17	0.12	0.15	0.16	0.00	0.17	0.39	0.17	0.55	0.39	0.31	0.35	0.37	0.19
MgO	7.66	6.75	7.36	7.21	7.18	7.01	9.72	8.37	9.52	6.27	8.20	10.40	10.92	7.76
CaO	0.05	0.08	0.00	0.00	0.07	0.00	0.00	0.00	0.00	0.18	0.00	0.00	0.00	0.00
Na2O	0.00	0.00	0.00	0.00	0.00	0.00	0.00	0.00	0.00	0.00	0.00	0.00	0.00	0.00
K2O	0.00	0.00	0.00	0.00	0.00	0.00	0.00	0.00	0.00	0.00	0.00	0.00	0.00	0.00
F	0.00	0.00	0.00	0.00	0.00	0.00	0.00	0.00	0.00	0.00	0.00	0.00	0.00	0.00
Total	90.53	87.94	90.91	90.82	90.65	89.88	87.79	88.80	88.44	87.77	88.35	88.56	87.83	89.06
	6.52	6.74	6.49	6.49	6.50	6.60	6.59	6.60	6.55	6.73	6.59	6.42	6.56	6.60
SiIV	2.59	2.58	2.59	2.60	2.64	2.57	2.60	2.56	2.55	2.48	2.59	2.87	2.72	2.57
AlIV	1.41	1.42	1.41	1.40	1.36	1.43	1.40	1.44	1.45	1.52	1.41	1.13	1.28	1.43
T site	4.00	4.00	4.00	4.00	4.00	4.00	4.00	4.00	4.00	4.00	4.00	4.00	4.00	4.00
AlVI	1.40	1.43	1.43	1.47	1.45	1.42	1.41	1.42	1.45	1.56	1.50	1.41	1.29	1.43
Ti	0.00	0.01	0.00	0.00	0.00	0.00	0.00	0.00	0.00	0.00	0.00	0.00	0.00	0.00
Cr3+	0.00	0.00	0.00	0.00	0.00	0.00	0.00	0.00	0.00	0.00	0.00	0.04	0.00	0.01
Fe2+	3.34	3.41	3.35	3.33	3.34	3.43	2.96	3.20	2.95	3.33	3.10	2.70	2.89	3.26
Mn2+	0.02	0.01	0.01	0.01	0.00	0.02	0.04	0.02	0.05	0.04	0.03	0.03	0.03	0.02
Mg	1.24	1.13	1.19	1.16	1.16	1.15	1.59	1.37	1.55	1.05	1.34	1.65	1.78	1.27
Ca	0.01	0.01	0.00	0.00	0.01	0.00	0.00	0.00	0.00	0.02	0.00	0.00	0.00	0.00
Na	0.00	0.00	0.00	0.00	0.00	0.00	0.00	0.00	0.00	0.00	0.00	0.00	0.00	0.00
K	0.00	0.00	0.00	0.00	0.00	0.00	0.00	0.00	0.00	0.00	0.00	0.00	0.00	0.00
O site	6.00	5.99	5.99	5.97	5.96	6.01	6.00	6.01	6.00	5.99	5.96	5.84	5.99	6.00
XFe	0.73	0.75	0.74	0.74	0.74	0.75	0.65	0.70	0.66	0.76	0.70	0.62	0.62	0.72
Al/(Al+Fe+Mg)	0.38	0.39	0.39	0.39	0.38	0.38	0.38	0.38	0.39	0.41	0.40	0.37	0.36	0.39
T (°C)	281	260	279	277	269	284	287	290	297	302	285	231	264	287
XChl	1.00	0.98	0.99	0.97	0.95	1.00	1.00	1.00	1.00	0.97	0.96	0.85	0.99	1.00
i/l cat	0.01	0.01	0.00	0.00	0.01	0.00	0.00	0.00	0.00	0.02	0.00	0.00	0.00	0.00
non-i/l	10.00	9.98	9.99	9.97	9.95	10.00	10.00	10.00	10.00	9.97	9.96	9.84	9.99	10.00

Sample:	VHG087						
Lithology:	VCR						
Analysis No.	Chl 1	Chl 2	Chl 3	Chl 4	Chl 5	Chl 6	Chl 7
Chlorite Type	II	II	II	II	II	II	II
SiO2	25.32	24.78	25.27	24.67	24.28	24.66	23.50
TiO2	0.00	0.00	0.00	0.00	0.00	0.00	0.00
Al2O3	24.99	25.19	25.19	24.98	24.62	24.19	23.79
Cr2O3	0.00	0.00	0.00	0.00	0.00	0.00	0.00
FeO	26.08	26.67	26.35	26.09	26.44	28.04	27.43
MnO	0.21	0.22	0.25	0.19	0.17	0.23	0.24
MgO	12.96	12.79	12.85	12.86	12.98	11.23	11.56
CaO	0.00	0.00	0.00	0.00	0.00	0.00	0.00
Na2O	0.00	0.00	0.06	0.00	0.00	0.09	0.00
K2O	0.00	0.00	0.06	0.00	0.00	0.09	0.00
F	0.00	0.00	0.00	0.00	0.00	0.00	0.00
Total	89.56	89.65	90.03	88.79	88.49	88.53	86.52
	6.18	6.20	6.16	6.25	6.29	6.34	6.50
SiIV	2.60	2.56	2.59	2.56	2.54	2.60	2.54
AlIV	1.40	1.44	1.41	1.44	1.46	1.40	1.46
T site	4.00	4.00	4.00	4.00	4.00	4.00	4.00
AlVI	1.63	1.62	1.63	1.63	1.58	1.61	1.58
Ti	0.00	0.00	0.00	0.00	0.00	0.00	0.00
Cr3+	0.00	0.00	0.00	0.00	0.00	0.00	0.00
Fe2+	2.24	2.30	2.26	2.27	2.32	2.47	2.48
Mn2+	0.02	0.02	0.02	0.02	0.02	0.02	0.02
Mg	1.99	1.97	1.96	1.99	2.03	1.77	1.86
Ca	0.00	0.00	0.00	0.00	0.00	0.00	0.00
Na	0.00	0.00	0.01	0.00	0.00	0.02	0.00
K	0.00	0.00	0.01	0.00	0.00	0.01	0.00
O site	5.88	5.91	5.90	5.90	5.94	5.90	5.94
XFe	0.53	0.54	0.54	0.53	0.53	0.58	0.57
Al/(Al+Fe+Mg)	0.42	0.42	0.42	0.42	0.41	0.42	0.41
T (°C)	297	306	299	305	310	292	306
XChl	0.89	0.92	0.89	0.91	0.94	0.88	0.95
i/l cat	0.00	0.00	0.02	0.00	0.00	0.03	0.00
non-i/l	9.88	9.91	9.88	9.90	9.94	9.87	9.94

Sample:	VHG088															
Lithology:	VCR															
	Chl 1 close to Au	Chl 2 close to Au	Chl 3	Chl 4	Chl 5	Chl 6	Chl 7 +Py	Chl 8	Chl 9 +Au	Chl 10 Vein	Chl 11 Vein	Chl 12 +Py
			II	IV	I	II		II				
SiO2	23.78	23.77	23.59	24.20	23.45	23.43	24.19	24.93	24.07	24.14	24.24	23.95
TiO2	0.00	0.00	0.00	0.53	0.00	0.00	0.00	0.00	0.00	0.00	0.00	0.00
Al2O3	24.73	24.58	24.54	23.86	24.14	23.20	24.34	24.42	24.36	24.40	24.15	23.78
Cr2O3	0.10	0.14	0.08	0.12	0.29	0.00	0.00	0.00	0.00	0.00	0.00	0.00
FeO	33.70	34.54	34.35	35.19	32.85	35.13	29.13	29.32	31.01	29.61	28.66	31.17
MnO	0.20	0.20	0.18	0.19	0.14	0.19	0.14	0.00	0.14	0.16	0.13	0.15
MgO	7.76	8.20	8.25	8.28	8.36	8.10	11.46	12.27	10.92	11.78	12.07	10.49
CaO	0.00	0.00	0.00	0.14	0.00	0.00	0.00	0.00	0.14	0.00	0.00	0.00
Na2O	0.00	0.00	0.00	0.00	0.00	0.00	0.00	0.00	0.00	0.00	0.00	0.00
K2O	0.00	0.00	0.00	0.00	0.00	0.00	0.00	0.00	0.00	0.00	0.00	0.00
F	0.00	0.00	0.00	0.00	0.00	0.00	0.00	0.00	0.00	0.00	0.00	0.00
Total	90.27	91.43	90.99	92.51	89.23	90.05	89.26	90.94	90.64	90.09	89.25	89.54
	6.41	6.35	6.38	6.30	6.47	6.50	6.33	6.19	6.30	6.28	6.31	6.38
SiIV	2.53	2.51	2.50	2.54	2.53	2.53	2.55	2.57	2.52	2.52	2.55	2.54
AlIV	1.47	1.49	1.50	1.46	1.47	1.47	1.45	1.43	1.48	1.48	1.45	1.46
T site	4.00	4.00	4.00	4.00	4.00	4.00	4.00	4.00	4.00	4.00	4.00	4.00
AlVI	1.64	1.58	1.58	1.49	1.59	1.49	1.57	1.54	1.53	1.53	1.54	1.52
Ti	0.00	0.00	0.00	0.04	0.00	0.00	0.00	0.00	0.00	0.00	0.00	0.00
Cr3+	0.01	0.01	0.01	0.01	0.02	0.00	0.00	0.00	0.00	0.00	0.00	0.00
Fe2+	3.00	3.05	3.05	3.09	2.96	3.16	2.56	2.53	2.72	2.59	2.52	2.77
Mn2+	0.02	0.02	0.02	0.02	0.01	0.02	0.01	0.00	0.01	0.01	0.01	0.01
Mg	1.23	1.29	1.31	1.29	1.34	1.31	1.80	1.88	1.70	1.84	1.89	1.66
Ca	0.00	0.00	0.00	0.02	0.00	0.00	0.00	0.00	0.02	0.00	0.00	0.00
Na	0.00	0.00	0.00	0.00	0.00	0.00	0.00	0.00	0.00	0.00	0.00	0.00
K	0.00	0.00	0.00	0.00	0.00	0.00	0.00	0.00	0.00	0.00	0.00	0.00
O site	5.91	5.95	5.96	5.95	5.93	5.99	5.94	5.95	5.98	5.97	5.96	5.97
XFe	0.71	0.70	0.70	0.70	0.69	0.71	0.59	0.57	0.61	0.59	0.57	0.63
Al/(Al+Fe+Mg)	0.42	0.41	0.41	0.40	0.42	0.40	0.41	0.40	0.40	0.40	0.40	0.40
T (°C)	295	300	302	295	299	295	304	300	306	309	305	301
XChl	0.91	0.95	0.96	0.94	0.94	0.99	0.95	0.95	0.97	0.97	0.96	0.97
i/l cat	0.00	0.00	0.00	0.02	0.00	0.00	0.00	0.00	0.02	0.00	0.00	0.00
non-i/l	9.91	9.95	9.96	9.93	9.93	9.99	9.94	9.95	9.96	9.97	9.96	9.97

Sample:	VHG091(B)										
Lithology:	VCR										
Analysis No.	Chl 6	Chl 7	Chl 9	Chl 10	Chl 11	Chl 12	Chl 13	Chl 14	Chl 15	Chl 16	Chl 17
Chlorite Type	+Au	+Au	+Au	II	+Py	+Au	+Au	II	II	IV	II
SiO2	23.24	23.10	29.36	24.42	24.32	23.98	23.75	25.04	24.26	24.50	23.62
TiO2	0.00	1.15	0.00	0.00	0.00	0.00	0.00	0.00	0.00	0.00	0.00
Al2O3	26.94	23.79	24.10	25.04	25.41	25.32	25.62	25.20	25.13	25.51	24.78
Cr2O3	0.00	0.23	0.00	0.00	0.13	0.00	0.00	0.00	0.00	0.00	0.00
FeO	26.66	23.33	24.04	25.64	26.00	27.30	25.66	25.12	25.31	25.15	25.01
MnO	0.14	0.66	0.20	0.25	0.20	0.21	0.27	0.28	0.19	0.26	0.22
MgO	9.31	12.69	12.40	12.73	13.07	11.33	12.74	13.53	13.35	13.75	12.46
CaO	0.00	0.14	0.00	0.00	0.00	0.00	0.00	0.00	0.00	0.00	0.00
Na2O	0.00	0.08	0.00	0.00	0.00	0.00	0.00	0.00	0.00	0.00	0.00
K2O	0.00	0.00	0.00	0.00	0.00	0.00	0.00	0.00	0.00	0.00	0.00
F	0.00	0.00	0.00	0.00	0.00	0.00	0.00	0.00	0.00	0.00	0.00
Total	88.51	85.17	90.10	88.08	89.13	88.14	88.04	89.17	68.24	89.17	86.09
	6.36	6.50	6.01	6.29	6.23	6.34	6.30	6.18	6.27	6.19	6.43
SiIV	2.46	2.50	2.93	2.56	2.52	2.53	2.49	2.58	2.53	2.52	2.53
AlIV	1.54	1.50	1.07	1.44	1.48	1.47	1.51	1.42	1.47	1.48	1.47
T site	4.00	4.00	4.00	4.00	4.00	4.00	4.00	4.00	4.00	4.00	4.00
AlVI	1.62	1.53	1.77	1.65	1.62	1.68	1.66	1.63	1.62	1.62	1.66
Ti	0.00	0.09	0.00	0.00	0.00	0.00	0.00	0.00	0.00	0.00	0.00
Cr3+	0.00	0.02	0.00	0.00	0.01	0.00	0.00	0.00	0.00	0.00	0.00
Fe2+	2.56	2.11	2.01	2.24	2.25	2.41	2.25	2.16	2.21	2.17	2.24
Mn2+	0.01	0.06	0.02	0.02	0.02	0.02	0.02	0.02	0.02	0.02	0.02
Mg	1.47	2.05	1.85	1.99	2.02	1.78	1.99	2.07	2.08	2.11	1.99
Ca	0.00	0.02	0.00	0.00	0.00	0.00	0.00	0.00	0.00	0.00	0.00
Na	0.00	0.02	0.00	0.00	0.00	0.00	0.00	0.00	0.00	0.00	0.00
K	0.00	0.00	0.00	0.00	0.00	0.00	0.00	0.00	0.00	0.00	0.00
O site	5.86	5.90	5.85	5.90	5.92	5.89	5.93	5.89	5.92	5.93	5.91
XFe	0.64	0.51	0.52	0.53	0.53	0.57	0.53	0.51	0.52	0.51	0.53
Al/(Al+Fe+Mg)	0.46	0.42	0.42	0.42	0.42	0.43	0.43	0.42	0.42	0.42	0.43
T (°C)	318	321	227	307	315	308	321	304	314	316	313
XChl	0.87	0.87	0.68	0.91	0.93	0.90	0.93	0.90	0.93	0.93	0.91
I/I cat	0.00	0.03	0.00	0.00	0.00	0.00	0.00	0.00	0.00	0.00	0.00
non-I/I	9.86	9.86	9.85	9.90	9.92	9.89	9.93	9.89	9.92	9.93	9.91

Sample:	VHG092				
Lithology:	VCR				
	Chl 1	Chl 3	Chl 4	Chl 6	Chl 7
	II	II	II	II	II
	23.03	23.80	22.80	23.50	23.85
	0.00	0.00	0.00	0.00	0.00
	24.23	24.17	22.19	25.52	25.68
	0.11	0.00	0.14	0.00	0.00
	32.33	31.61	31.55	32.01	29.84
	0.26	0.26	0.26	0.22	0.30
	9.16	9.62	8.68	9.78	11.08
	0.00	0.00	0.11	0.00	0.00
	0.00	0.00	0.00	0.00	0.00
	0.00	0.00	0.00	0.00	0.00
	0.00	0.00	0.00	0.00	0.00
	89.12	89.46	85.73	91.03	90.75
	6.47	6.41	6.75	6.29	6.24
	2.48	2.54	2.56	2.46	2.48
	1.52	1.46	1.44	1.54	1.52
	4.00	4.00	4.00	4.00	4.00
	1.56	1.57	1.50	1.61	1.62
	0.00	0.00	0.00	0.00	0.00
	0.01	0.00	0.01	0.00	0.00
	2.91	2.82	2.96	2.80	2.59
	0.02	0.02	0.02	0.02	0.03
	1.47	1.53	1.45	1.53	1.71
	0.00	0.00	0.01	0.00	0.00
	0.00	0.00	0.00	0.00	0.00
	0.00	0.00	0.00	0.00	0.00
	5.98	5.94	5.97	5.96	5.95
	0.66	0.65	0.67	0.65	0.60
	0.41	0.41	0.40	0.42	0.42
	310	300	293	316	317
	0.98	0.95	0.96	0.97	0.96
	0.00	0.00	0.01	0.00	0.00
	9.98	9.94	9.96	9.96	9.95

Sample:	VHG093(A)																
Lithology:	VCR																
Analysis No.	Chl 1	Chl 2	Chl 3	Chl 4	Chl 6	Chl 7	Chl 8	Chl 9	Chl 10	Chl 11	Chl 12	Chl 13	Chl 14	Chl 15	Chl 16	Chl 17	Chl 18
Chlorite Type	II	IV	+Au	+Au	+Au	IV	IV	IV	+Au	IV	+Au	IV	II	in Apatite	II	II	II
SiO2	24.81	24.70	25.09	24.70	24.76	24.96	25.27	25.19	24.98	25.12	24.45	24.74	24.86	24.50	24.27	25.02	24.91
TiO2	0.00	0.00	0.00	0.00	0.00	0.00	0.00	0.00	0.00	0.00	0.00	0.00	0.00	0.00	0.00	0.00	0.00
Al2O3	27.15	27.05	26.85	26.11	27.03	27.29	27.23	27.55	27.19	26.61	27.88	26.67	27.85	25.85	26.40	26.32	25.79
Cr2O3	0.48	0.58	0.57	0.00	0.43	0.25	0.23	0.22	0.36	0.28	0.22	0.29	0.13	0.17	0.00	0.00	0.09
FeO	22.56	21.89	22.68	26.00	22.73	23.46	23.93	23.95	23.08	21.45	21.67	23.10	22.94	24.16	21.31	24.41	24.30
MnO	0.28	0.27	0.22	0.28	0.30	0.21	0.29	0.21	0.22	0.21	0.32	0.24	0.29	0.30	0.19	0.20	0.34
MgO	15.25	15.88	15.35	13.36	15.25	14.82	14.49	14.28	15.52	15.82	15.96	15.89	15.45	14.65	16.35	14.82	15.26
CaO	0.00	0.00	0.00	0.00	0.00	0.00	0.00	0.00	0.00	0.00	0.00	0.00	0.00	0.00	0.00	0.00	0.00
Na2O	0.00	0.00	0.00	0.00	0.00	0.00	0.00	0.00	0.00	0.08	0.00	0.00	0.00	0.00	0.00	0.00	0.00
K2O	0.00	0.00	0.00	0.00	0.00	0.00	0.00	0.00	0.00	0.00	0.00	0.00	0.00	0.00	0.00	0.00	0.00
F	0.00	0.00	0.00	0.00	0.00	0.00	0.00	0.00	0.00	0.00	0.00	0.00	0.00	0.00	0.00	0.00	0.00
Total	90.53	90.37	90.76	90.45	90.50	90.99	91.44	91.40	91.35	89.57	90.70	90.93	91.52	89.63	88.52	90.77	90.69
	6.01	6.00	5.99	6.12	6.02	5.99	5.97	5.97	5.96	6.03	5.97	6.00	5.94	6.13	6.11	6.04	6.06
SiIV	2.48	2.47	2.50	2.52	2.48	2.49	2.51	2.50	2.48	2.52	2.43	2.47	2.46	2.50	2.47	2.52	2.51
AlIV	1.52	1.53	1.50	1.48	1.52	1.51	1.49	1.50	1.52	1.48	1.57	1.53	1.54	1.50	1.53	1.48	1.49
T site	4.00	4.00	4.00	4.00	4.00	4.00	4.00	4.00	4.00	4.00	4.00	4.00	4.00	4.00	4.00	4.00	4.00
AlVI	1.66	1.65	1.66	1.65	1.67	1.70	1.70	1.73	1.66	1.67	1.70	1.61	1.70	1.61	1.64	1.63	1.58
Ti	0.00	0.00	0.00	0.00	0.00	0.00	0.00	0.00	0.00	0.00	0.00	0.00	0.00	0.00	0.00	0.00	0.00
Cr3+	0.04	0.05	0.04	0.00	0.03	0.02	0.02	0.02	0.03	0.02	0.02	0.02	0.01	0.01	0.00	0.00	0.01
Fe2+	1.89	1.83	1.89	2.21	1.90	1.96	1.99	1.99	1.92	1.80	1.82	1.93	1.90	2.06	1.81	2.05	2.05
Mn2+	0.02	0.02	0.02	0.02	0.03	0.02	0.02	0.02	0.02	0.02	0.03	0.02	0.02	0.03	0.02	0.02	0.03
Mg	2.27	2.36	2.28	2.03	2.28	2.20	2.15	2.12	2.30	2.37	2.36	2.36	2.28	2.23	2.48	2.22	2.29
Ca	0.00	0.00	0.00	0.00	0.00	0.00	0.00	0.00	0.00	0.00	0.00	0.00	0.00	0.00	0.00	0.00	0.00
Na	0.00	0.00	0.00	0.00	0.00	0.00	0.00	0.00	0.00	0.02	0.00	0.00	0.00	0.00	0.00	0.00	0.00
K	0.00	0.00	0.00	0.00	0.00	0.00	0.00	0.00	0.00	0.00	0.00	0.00	0.00	0.00	0.00	0.00	0.00
O site	5.90	5.92	5.90	5.92	5.91	5.90	5.88	5.87	5.92	5.90	5.93	5.95	5.91	5.94	5.95	5.92	5.95
XFe	0.45	0.44	0.45	0.52	0.46	0.47	0.48	0.48	0.45	0.43	0.43	0.45	0.45	0.48	0.42	0.48	0.47
Al/(Al+Fe+Mg)	0.43	0.43	0.43	0.42	0.43	0.44	0.44	0.44	0.43	0.43	0.44	0.42	0.44	0.42	0.42	0.42	0.41
T (°C)	330	334	325	316	330	327	321	322	330	323	342	333	335	323	335	320	322
XChl	0.91	0.92	0.91	0.92	0.92	0.90	0.89	0.88	0.92	0.89	0.93	0.95	0.92	0.94	0.95	0.93	0.96
i/l cat	0.00	0.00	0.00	0.00	0.00	0.00	0.00	0.00	0.00	0.02	0.00	0.00	0.00	0.00	0.00	0.00	0.00
non-i/l	9.90	9.92	9.90	9.92	9.91	9.90	9.88	9.87	9.92	9.88	9.93	9.95	9.91	9.94	9.95	9.92	9.95

Sample:	VHG093(B)													Sample:	VHG095									
Lithology:	VCR													Lithology:	VCR									
Analysis No.	Chl 1	Chl 2	Chl 3	Chl 4	Chl 5	Chl 6	Chl 7	Chl 8	Chl 9	Chl 10	Chl 11	Chl 12	Chl 13		Chl 1	Chl 2	Chl 3	Chl 4	Chl 5	Chl 6	Chl 7	Chl 8	Chl 9	Chl 10	Chl 11
Chlorite Type	II	+Au	+Au	+Au	+Au+Py	II	+Au	+Au+Py	+Au	+Au	+Au	+Au	II		+Py	+Py	II	II	II	II	II	II	II	II	II
SiO2	24.56	24.80	24.33	24.92	24.29	25.43	24.24	24.45	24.52	24.92	24.91	25.14	23.80		23.68	23.84	23.35	23.25	23.74	23.09	23.81	23.24	23.87	23.63	24.35
TiO2	0.00	0.00	0.00	0.00	0.00	0.00	0.00	0.00	0.00	0.00	0.00	0.00	0.43		0.00	0.00	0.00	0.00	0.00	0.00	0.00	0.00	0.00	0.00	0.00
Al2O3	25.47	26.12	25.30	25.54	27.03	26.24	26.81	27.03	27.60	26.59	26.34	26.30	25.32		24.01	24.89	23.99	24.36	24.39	24.29	23.54	23.73	23.63	24.34	22.33
Cr2O3	0.00	0.00	0.17	0.21	0.20	0.00	0.12	0.00	0.00	0.17	0.16	0.17	0.00		0.17	0.13	0.00	0.09	0.12	0.09	0.17	0.35	0.25	0.30	0.76
FeO	26.29	23.11	21.76	21.80	22.23	20.88	23.27	22.16	23.75	20.86	20.81	21.06	22.78		33.24	32.09	32.44	33.70	32.18	34.75	33.61	33.57	33.28	32.09	32.84
MnO	0.28	0.14	0.18	0.15	0.24	0.21	0.28	0.27	0.25	0.28	0.23	0.33	0.50		0.17	0.24	0.22	0.21	0.18	0.18	0.23	0.24	0.20	0.18	0.16
MgO	12.40	14.53	15.49	15.65	15.06	16.00	14.25	15.00	14.00	16.29	16.23	15.15	13.69		8.91	9.62	9.19	8.22	9.25	7.35	8.90	9.19	9.07	9.43	9.17
CaO	0.00	0.00	0.00	0.00	0.00	0.00	0.00	0.00	0.00	0.00	0.00	0.00	0.27		0.00	0.00	0.00	0.00	0.00	0.00	0.00	0.00	0.00	0.00	0.00
Na2O	0.00	0.00	0.00	0.00	0.00	0.00	0.00	0.00	0.00	0.00	0.00	0.00	0.00		0.00	0.00	0.00	0.00	0.00	0.00	0.00	0.00	0.00	0.00	0.00
K2O	0.00	0.00	0.00	0.00	0.00	0.00	0.00	0.00	0.00	0.00	0.00	0.00	0.00		0.00	0.00	0.00	0.00	0.00	0.00	0.00	0.00	0.00	0.00	0.00
F	0.00	0.00	0.00	0.00	0.00	0.00	0.00	0.00	0.00	0.00	0.00	0.00	0.00		0.00	0.00	0.00	0.00	0.00	0.00	0.00	0.00	0.00	0.00	0.00
Total	88.00	88.70	87.23	88.27	89.05	88.76	88.97	88.91	90.12	89.11	88.68	88.15	86.79		90.16	90.81	89.19	89.83	89.86	89.75	90.26	90.32	90.30	89.97	89.61
	6.24	6.15	6.23	6.14	6.10	6.06	6.14	6.10	6.06	6.05	6.06	6.12	6.32		6.41	6.31	6.48	6.46	6.39	6.50	6.42	6.43	6.41	6.39	6.45
BIIV	2.55	2.54	2.62	2.56	2.47	2.57	2.46	2.48	2.47	2.51	2.52	2.56	2.50		2.53	2.51	2.51	2.50	2.53	2.50	2.54	2.49	2.54	2.51	2.62
AlIV	1.45	1.46	1.48	1.45	1.53	1.43	1.52	1.52	1.53	1.49	1.48	1.44	1.50		1.47	1.49	1.49	1.50	1.47	1.50	1.46	1.51	1.46	1.49	1.38
T site	4.00	4.00	4.00	4.00	4.00	4.00	4.00	4.00	4.00	4.00	4.00	4.00	4.00		4.00	4.00	4.00	4.00	4.00	4.00	4.00	4.00	4.00	4.00	4.00
AlVI	1.67	1.69	1.61	1.63	1.70	1.69	1.71	1.72	1.76	1.67	1.68	1.72	1.64		1.55	1.59	1.55	1.58	1.56	1.60	1.51	1.48	1.51	1.56	1.44
Ti	0.00	0.00	0.00	0.00	0.00	0.00	0.00	0.00	0.00	0.00	0.00	0.00	0.03		0.00	0.00	0.00	0.00	0.00	0.00	0.00	0.00	0.00	0.00	0.00
Cr3+	0.00	0.00	0.01	0.02	0.02	0.00	0.01	0.00	0.00	0.01	0.01	0.01	0.00		0.01	0.01	0.00	0.01	0.01	0.01	0.01	0.03	0.02	0.03	0.06
Fe2+	2.28	1.96	1.89	1.86	1.89	1.76	1.99	1.88	2.00	1.76	1.76	1.79	2.00		2.97	2.82	2.92	3.03	2.86	3.14	3.00	3.00	2.97	2.85	2.95
Mn2+	0.02	0.01	0.02	0.01	0.02	0.02	0.02	0.02	0.02	0.02	0.02	0.03	0.04		0.02	0.02	0.02	0.02	0.02	0.02	0.02	0.02	0.02	0.02	0.01
Mg	1.92	2.21	2.39	2.38	2.28	2.41	2.17	2.27	2.10	2.44	2.45	2.30	2.15		1.42	1.51	1.47	1.32	1.47	1.19	1.42	1.47	1.44	1.49	1.47
Ca	0.00	0.00	0.00	0.00	0.00	0.00	0.00	0.00	0.00	0.00	0.00	0.00	0.03		0.00	0.00	0.00	0.00	0.00	0.00	0.00	0.00	0.00	0.00	0.00
Na	0.00	0.00	0.00	0.00	0.00	0.00	0.00	0.00	0.00	0.00	0.00	0.00	0.00		0.00	0.00	0.00	0.00	0.00	0.00	0.00	0.00	0.00	0.00	0.00
K	0.00	0.00	0.00	0.00	0.00	0.00	0.00	0.00	0.00	0.00	0.00	0.00	0.00		0.00	0.00	0.00	0.00	0.00	0.00	0.00	0.00	0.00	0.00	0.00
O site	5.89	5.89	5.92	5.90	5.91	5.87	5.90	5.90	5.89	5.91	5.90	5.85	5.90		5.96	5.95	5.97	5.96	5.94	5.95	5.97	6.00	5.96	5.95	5.94
XFe	0.54	0.47	0.44	0.44	0.45	0.42	0.48	0.45	0.49	0.42	0.42	0.44	0.48		0.68	0.65	0.66	0.70	0.66	0.73	0.68	0.67	0.67	0.66	0.67
Al/(Al+Fe+Mg	0.43	0.43	0.42	0.42	0.44	0.43	0.44	0.44	0.44	0.43	0.43	0.44	0.43		0.41	0.42	0.41	0.42	0.41	0.42	0.40	0.40	0.40	0.41	0.39
T (°C)	307	317	322	317	333	316	326	329	326	327	325	316	322		300	306	304	304	301	301	295	308	296	305	282
XChl	0.90	0.90	0.93	0.91	0.91	0.88	0.91	0.91	0.89	0.91	0.91	0.87	0.88		0.96	0.95	0.97	0.96	0.95	0.95	0.97	1.00	0.96	0.95	0.94
i/l cat	0.00	0.00	0.00	0.00	0.00	0.00	0.00	0.00	0.00	0.00	0.00	0.00	0.03		0.00	0.00	0.00	0.00	0.00	0.00	0.00	0.00	0.00	0.00	0.00
non-i/l	9.89	9.89	9.92	9.90	9.91	9.87	9.90	9.90	9.89	9.91	9.90	9.85	9.87		9.96	9.95	9.97	9.96	9.94	9.95	9.97	10.00	9.96	9.95	9.94

Sample:	VHG103														
Lithology:	VCR														
Analysis No.	Chl 1	Chl 2	Chl 3	Chl 4	Chl 5	Chl 6	Chl 7	Chl 10	Chl 11	Chl 12	Chl 13	Chl 14	Chl 15	Chl 16	Chl 17
Chlorite Type	II	II	IV	II	IV	IV	IV	II	+Au	+Au	+Au	II	+Au	+Au	IV
SiO2	24.81	23.93	24.08	24.35	25.02	23.74	24.55	24.11	25.05	22.67	24.50	24.05	24.90	24.20	24.59
TiO2	0.00	0.00	0.00	0.00	0.00	0.00	0.00	0.00	0.00	0.00	0.00	0.00	0.00	0.00	0.00
Al2O3	25.96	25.73	25.60	26.28	26.79	24.37	25.79	25.35	27.13	25.42	25.00	26.39	26.87	25.80	26.36
Cr2O3	0.00	0.00	0.00	0.00	0.00	0.00	0.00	0.00	0.00	0.00	0.00	0.00	0.00	0.09	0.00
FeO	24.53	24.78	25.49	24.37	25.33	23.16	24.94	24.29	24.02	25.22	23.40	24.79	23.40	23.94	25.31
MnO	0.24	0.17	0.24	0.21	0.19	0.18	0.16	0.29	0.25	0.29	0.23	0.24	0.22	0.25	0.25
MgO	13.38	13.96	13.59	14.25	14.17	13.92	13.98	13.42	14.45	13.16	14.32	14.12	13.92	13.92	13.77
CaO	0.00	0.00	0.00	0.00	0.00	0.00	0.00	0.06	0.07	0.00	0.00	0.05	0.00	0.00	0.00
Na2O	0.00	0.00	0.00	0.00	0.00	0.00	0.00	0.00	0.00	0.00	0.08	0.00	0.00	0.00	0.00
K2O	0.00	0.00	0.00	0.00	0.00	0.00	0.00	0.07	0.04	0.00	0.00	0.00	0.00	0.00	0.04
F	0.00	0.00	0.00	0.00	0.00	0.00	0.00	0.00	0.00	0.00	0.00	0.00	0.00	0.00	0.00
Total	88.92	88.57	89.00	89.46	91.50	85.37	89.42	87.59	91.01	86.76	87.53	89.64	89.31	88.20	90.32
	6.18	6.23	6.22	6.14	6.01	6.43	6.16	6.29	6.01	6.41	6.26	6.15	6.10	6.23	6.11
SiIV	2.55	2.48	2.49	2.49	2.50	2.54	2.52	2.52	2.51	2.42	2.55	2.46	2.53	2.51	2.50
AlIV	1.45	1.52	1.51	1.51	1.50	1.46	1.48	1.48	1.49	1.58	1.45	1.54	1.47	1.49	1.50
T site	4.00	4.00	4.00	4.00	4.00	4.00	4.00	4.00	4.00	4.00	4.00	4.00	4.00	4.00	4.00
AlVI	1.70	1.63	1.62	1.66	1.67	1.61	1.63	1.65	1.70	1.62	1.62	1.65	1.75	1.66	1.66
Ti	0.00	0.00	0.00	0.00	0.00	0.00	0.00	0.00	0.00	0.00	0.00	0.00	0.00	0.00	0.00
Cr3+	0.00	0.00	0.00	0.00	0.00	0.00	0.00	0.00	0.00	0.00	0.00	0.00	0.00	0.01	0.00
Fe2+	2.11	2.15	2.21	2.08	2.12	2.07	2.14	2.13	2.01	2.25	2.04	2.12	1.99	2.07	2.15
Mn2+	0.02	0.01	0.02	0.02	0.02	0.02	0.01	0.03	0.02	0.03	0.02	0.02	0.02	0.02	0.02
Mg	2.05	2.16	2.10	2.17	2.11	2.22	2.14	2.09	2.15	2.09	2.22	2.15	2.11	2.15	2.09
Ca	0.00	0.00	0.00	0.00	0.00	0.00	0.00	0.01	0.01	0.00	0.00	0.01	0.00	0.00	0.00
Na	0.00	0.00	0.00	0.00	0.00	0.00	0.00	0.00	0.00	0.00	0.02	0.00	0.00	0.00	0.00
K	0.00	0.00	0.00	0.00	0.00	0.00	0.00	0.01	0.01	0.00	0.00	0.00	0.00	0.00	0.01
O site	5.88	5.95	5.94	5.93	5.92	5.92	5.92	5.92	5.90	5.98	5.92	5.95	5.86	5.91	5.92
XFe	0.51	0.50	0.51	0.49	0.50	0.48	0.50	0.50	0.48	0.52	0.48	0.50	0.49	0.49	0.51
Al/(Al+Fe+Mg)	0.43	0.42	0.42	0.43	0.43	0.42	0.42	0.43	0.43	0.42	0.42	0.43	0.44	0.43	0.43
T (°C)	310	326	322	325	321	315	318	316	322	337	313	330	317	321	321
XChl	0.89	0.95	0.95	0.93	0.92	0.93	0.93	0.91	0.90	0.98	0.91	0.95	0.87	0.92	0.92
I/I cat	0.00	0.00	0.00	0.00	0.00	0.00	0.00	0.02	0.01	0.00	0.02	0.01	0.00	0.00	0.01
non-I/I	9.88	9.95	9.94	9.93	9.92	9.92	9.92	9.90	9.89	9.98	9.90	9.94	9.86	9.91	9.92

Sample:	VHQ105														Sample:	VHQ107					
Lithology:	VCR														Lithology:	VCR					
Analysis No.	Chl 1	Chl 2	Chl 4	Chl 5	Chl 6	Chl 7	Chl 8	Chl 9	Chl 10	Chl 11	Chl 12	Chl 13	Chl 14	Chl 15		Chl 1	Chl 2	Chl 3	Chl 5	Chl 6	Chl 7
Chlorite Type	+Sph	II	II	II	+Sph	I	I	II	I	+Au	II	+Py	I ?	+Py		II	II	II	II	II	I
SiO2	23.86	24.82	24.89	25.50	24.52	25.81	24.77	25.14	23.76	25.01	24.72	25.36	25.05	24.63		23.38	22.99	23.11	22.96	25.61	24.93
TiO2	0.00	0.00	0.00	0.00	0.00	0.00	0.00	0.00	0.00	0.00	0.00	0.00	0.00	0.00		0.00	0.00	0.00	0.00	0.00	0.00
Al2O3	26.32	25.71	25.88	26.57	26.26	24.13	25.65	25.87	26.83	25.91	25.60	25.86	24.95	24.96		25.08	25.13	25.23	24.97	24.06	25.25
Cr2O3	0.00	0.00	0.00	0.00	0.00	0.00	0.00	0.00	0.00	0.00	0.00	0.00	0.55	0.13		0.00	0.00	0.00	0.00	0.21	0.00
FeO	27.07	27.38	26.82	26.37	26.81	26.26	27.66	26.28	26.71	27.00	26.33	27.30	27.36	27.59		33.04	33.22	33.61	33.40	30.49	32.08
MnO	0.21	0.00	0.16	0.16	0.15	0.18	0.16	0.15	0.17	0.00	0.14	0.24	0.35	0.15		0.15	0.00	0.15	0.20	0.15	0.15
MgO	12.30	12.29	12.61	11.65	12.98	13.65	11.69	13.02	12.65	12.61	12.72	11.47	10.90	12.18		9.33	9.37	8.99	8.72	8.62	9.11
CaO	0.00	0.00	0.00	0.06	0.00	0.00	0.00	0.00	0.00	0.00	0.00	0.12	0.09	0.00		0.00	0.00	0.00	0.00	0.11	0.00
Na2O	0.00	0.00	0.00	0.00	0.00	0.00	0.00	0.00	0.00	0.00	0.00	0.00	0.00	0.00		0.00	0.00	0.00	0.00	0.00	0.00
K2O	0.00	0.00	0.00	0.00	0.00	0.00	0.00	0.00	0.00	0.00	0.00	0.00	0.00	0.00		0.00	0.00	0.00	0.00	0.05	0.08
F	0.00	0.00	0.00	0.00	0.00	0.00	0.00	0.00	0.00	0.00	0.00	0.00	0.00	0.00		0.00	0.00	0.00	0.00	0.00	0.00
Total	89.76	90.20	90.16	90.31	90.72	90.03	89.93	90.46	90.12	90.53	89.51	90.35	89.25	89.64		90.98	90.71	91.09	90.25	89.30	91.60
	6.21	6.17	6.16	6.11	6.12	6.15	6.20	6.12	6.17	6.13	6.19	8.16	6.26	6.24		6.34	6.37	6.35	6.41	6.34	6.23
SiIV	2.47	2.55	2.55	2.59	2.50	2.64	2.56	2.56	2.44	2.55	2.55	2.60	2.61	2.56		2.47	2.44	2.44	2.45	2.70	2.58
AlIV	1.53	1.45	1.45	1.41	1.50	1.36	1.44	1.44	1.56	1.45	1.45	1.40	1.39	1.44		1.53	1.56	1.56	1.55	1.30	1.42
T site	4.00	4.00	4.00	4.00	4.00	4.00	4.00	4.00	4.00	4.00	4.00	4.00	4.00	4.00		4.00	4.00	4.00	4.00	4.00	4.00
AlVI	1.67	1.66	1.66	1.78	1.65	1.55	1.68	1.66	1.69	1.67	1.66	1.72	1.68	1.61		1.58	1.57	1.59	1.59	1.70	1.67
Ti	0.00	0.00	0.00	0.00	0.00	0.00	0.00	0.00	0.00	0.00	0.00	0.00	0.00	0.00		0.00	0.00	0.00	0.00	0.00	0.00
Cr3+	0.00	0.00	0.00	0.00	0.00	0.00	0.00	0.00	0.00	0.00	0.00	0.00	0.05	0.01		0.00	0.00	0.00	0.00	0.02	0.00
Fe2+	2.34	2.35	2.30	2.24	2.29	2.25	2.39	2.24	2.29	2.30	2.27	2.34	2.38	2.39		2.91	2.94	2.97	2.98	2.69	2.78
Mn2+	0.02	0.00	0.01	0.01	0.01	0.02	0.01	0.01	0.01	0.00	0.01	0.02	0.03	0.01		0.01	0.00	0.01	0.02	0.01	0.01
Mg	1.90	1.88	1.93	1.77	1.97	2.08	1.80	1.98	1.94	1.92	1.95	1.75	1.69	1.88		1.47	1.48	1.42	1.39	1.36	1.41
Ca	0.00	0.00	0.00	0.01	0.00	0.00	0.00	0.00	0.00	0.00	0.00	0.01	0.01	0.00		0.00	0.00	0.00	0.00	0.01	0.00
Na	0.00	0.00	0.00	0.00	0.00	0.00	0.00	0.00	0.00	0.00	0.00	0.00	0.00	0.00		0.00	0.00	0.00	0.00	0.00	0.00
K	0.00	0.00	0.00	0.00	0.00	0.00	0.00	0.00	0.00	0.00	0.00	0.00	0.00	0.00		0.00	0.00	0.00	0.00	0.01	0.01
O site	5.93	5.89	5.90	5.81	5.92	5.90	5.88	5.89	5.94	5.89	5.90	5.85	5.84	5.91		5.98	6.00	5.99	5.98	5.80	5.88
XFe	0.55	0.56	0.54	0.56	0.54	0.52	0.57	0.53	0.54	0.55	0.54	0.57	0.58	0.56		0.67	0.67	0.68	0.68	0.66	0.66
Al/(Al+Fe+Mg	0.43	0.42	0.42	0.44	0.43	0.40	0.43	0.42	0.43	0.42	0.42	0.43	0.43	0.42		0.42	0.42	0.42	0.42	0.43	0.42
T (°C)	324	306	307	296	316	290	303	306	330	306	308	294	290	304		314	320	317	315	263	289
XChl	0.93	0.90	0.90	0.82	0.93	0.91	0.89	0.90	0.94	0.90	0.90	0.85	0.84	0.92		0.98	1.00	0.99	0.98	0.80	0.88
i/l cat	0.00	0.00	0.00	0.01	0.00	0.00	0.00	0.00	0.00	0.00	0.00	0.01	0.01	0.00		0.00	0.00	0.00	0.00	0.02	0.01
non-i/l	9.93	9.89	9.90	9.81	9.92	9.90	9.88	9.89	9.94	9.89	9.90	9.83	9.83	9.91		9.98	10.00	9.99	9.98	9.78	9.87

Sample:	VHG120					Sample:	VHG125											
Lithology:	VCR					Lithology:	VCR											
Analysis No.	Chl 2	Chl 6	Chl 7	Chl 10	Chl 11		Chl 1	Chl 3	Chl 4	Chl 5	Chl 6	Chl 7	Chl 8	Chl 9	Chl 10	Chl 11	Chl 12	Chl 13	Chl 14
Chlorite Type	II	I	II	II	II		III	I	+Gn	+Au	+Gn	IV	+Au	+Gn	+Au	II	IV	III	IV
SiO2	24.94	23.72	23.00	23.30	24.74		22.87	22.68	24.22	24.92	24.26	24.46	24.63	23.82	24.44	24.41	24.10	24.42	24.40
TiO2	0.00	0.00	0.00	0.00	0.00		0.00	0.00	0.00	0.00	0.00	0.00	0.00	0.00	0.00	0.00	0.00	0.00	0.00
Al2O3	24.47	23.84	24.11	23.59	23.19		25.94	26.25	25.99	24.52	25.31	25.92	25.87	24.37	25.90	25.12	24.81	25.72	25.70
Cr2O3	0.17	0.58	0.10	0.00	0.08		0.00	0.00	0.00	0.00	0.00	0.00	0.00	0.00	0.11	0.00	0.00	0.00	0.00
FeO	32.38	32.13	36.42	35.38	32.96		31.73	32.80	26.69	26.07	26.84	27.83	26.94	26.45	26.06	26.59	25.69	25.41	26.95
MnO	0.30	0.42	0.23	0.22	0.29		0.25	0.19	0.21	0.22	0.21	0.27	0.24	0.16	0.20	0.22	0.23	0.19	0.19
MgO	9.40	9.22	7.35	7.61	9.66		9.28	8.85	13.33	14.24	13.15	12.65	14.09	12.75	13.02	13.03	13.19	14.76	13.08
CaO	0.10	0.06	0.00	0.00	0.00		0.09	0.00	0.00	0.00	0.00	0.00	0.00	0.00	0.00	0.13	0.00	0.00	0.00
Na2O	0.00	0.00	0.00	0.00	0.00		0.00	0.00	0.00	0.00	0.00	0.00	0.00	0.00	0.00	0.00	0.00	0.00	0.00
K2O	0.00	0.00	0.00	0.00	0.00		0.00	0.00	0.00	0.00	0.00	0.00	0.00	0.00	0.00	0.00	0.00	0.00	0.00
F	0.00	0.00	0.00	0.00	0.00		0.00	0.00	0.00	0.00	0.00	0.00	0.00	0.00	0.00	0.00	0.00	0.00	0.00
Total	91.76	89.97	91.21	90.10	90.92		90.16	90.97	90.44	89.97	89.77	91.13	91.77	87.55	89.73	89.50	88.02	90.50	90.32
	6.24	6.41	6.45	6.50	6.34		6.36	6.33	6.15	6.17	6.21	6.14	6.06	6.37	6.18	6.22	6.31	6.11	6.17
SiIV	2.59	2.53	2.47	2.52	2.61		2.42	2.41	2.48	2.56	2.51	2.50	2.49	2.53	2.51	2.53	2.53	2.48	2.50
AlIV	1.41	1.47	1.53	1.48	1.39		1.58	1.59	1.52	1.44	1.49	1.50	1.51	1.47	1.49	1.47	1.47	1.52	1.50
T site	4.00	4.00	4.00	4.00	4.00		4.00	4.00	4.00	4.00	4.00	4.00	4.00	4.00	4.00	4.00	4.00	4.00	4.00
AlVI	1.59	1.53	1.52	1.53	1.49		1.66	1.67	1.62	1.52	1.59	1.62	1.56	1.57	1.65	1.60	1.60	1.56	1.61
Ti	0.00	0.00	0.00	0.00	0.00		0.00	0.00	0.00	0.00	0.00	0.00	0.00	0.00	0.00	0.00	0.00	0.00	0.00
Cr3+	0.01	0.05	0.01	0.00	0.01		0.00	0.00	0.00	0.00	0.00	0.00	0.00	0.00	0.01	0.00	0.00	0.00	0.00
Fe2+	2.81	2.87	3.27	3.20	2.91		2.81	2.89	2.28	2.24	2.32	2.38	2.27	2.35	2.24	2.30	2.25	2.16	2.31
Mn2+	0.03	0.04	0.02	0.02	0.03		0.02	0.02	0.02	0.02	0.02	0.02	0.02	0.01	0.02	0.02	0.02	0.02	0.02
Mg	1.48	1.47	1.18	1.23	1.52		1.46	1.39	2.03	2.18	2.02	1.92	2.12	2.02	1.99	2.01	2.06	2.24	2.00
Ca	0.01	0.01	0.00	0.00	0.00		0.01	0.00	0.00	0.00	0.00	0.00	0.00	0.00	0.00	0.01	0.00	0.00	0.00
Na	0.00	0.00	0.00	0.00	0.00		0.00	0.00	0.00	0.00	0.00	0.00	0.00	0.00	0.00	0.00	0.00	0.00	0.00
K	0.00	0.00	0.00	0.00	0.00		0.00	0.00	0.00	0.00	0.00	0.00	0.00	0.00	0.00	0.00	0.00	0.00	0.00
O site	5.91	5.95	6.00	5.98	5.95		5.96	5.96	5.95	5.96	5.95	5.94	5.98	5.95	5.91	5.94	5.94	5.98	5.94
XFe	0.66	0.66	0.74	0.72	0.66		0.66	0.68	0.53	0.51	0.53	0.55	0.52	0.54	0.53	0.53	0.52	0.49	0.54
Al/(Al+Fe+Mg)	0.41	0.41	0.41	0.40	0.39		0.43	0.43	0.42	0.40	0.42	0.42	0.41	0.41	0.43	0.42	0.42	0.41	0.42
T (°C)	287	300	306	297	284		324	325	323	309	317	317	323	312	316	312	313	326	317
XChl	0.91	0.95	1.00	0.98	0.95		0.96	0.96	0.96	0.96	0.96	0.95	0.98	0.95	0.92	0.94	0.94	0.98	0.95
i/I cat	0.01	0.01	0.00	0.00	0.00		0.01	0.00	0.00	0.00	0.00	0.00	0.00	0.00	0.00	0.01	0.00	0.00	0.00
non-i/I	9.90	9.94	10.00	9.98	9.95		9.95	9.96	9.95	9.96	9.95	9.94	9.98	9.95	9.91	9.93	9.94	9.98	9.94

Sample:	VHG130			Sample:	VHG131					Sample:	VHG135							Sample:	VHG136				
Lithology:	VCR			Lithology:	VCR					Lithology:	VCR							Lithology:	VCR				
Analysis No.	Chl 2	Chl 3	Chl 4	Chl 1	Chl 2	Chl 3	Chl 4	Chl 5	Chl 6	Chl 1	Chl 2	Chl 3	Chl 4	Chl 5	Chl 6	Chl 7		Chl 2	Chl 3	Chl 4	Chl 5	Chl 10	
Chlorite Type	II	II	II	II	Vein	II	+Py	II	+Au	II	II	Stylol.	II	II	II	I		I	I	I	II	I	
SiO2	23.30	22.91	23.34	23.39	22.85	23.13	23.47	23.36	23.60	23.69	23.55	23.41	23.50	23.46	22.82	23.94		23.37	24.00	23.23	23.11	23.23	
TiO2	0.00	0.00	0.00	0.00	0.00	0.00	0.00	0.00	0.00	0.00	0.00	0.00	0.00	0.00	0.00	0.00		0.00	0.00	0.00	0.00	0.00	
Al2O3	24.33	24.10	23.70	24.62	23.90	24.97	24.54	24.94	24.85	24.60	25.12	25.17	24.54	24.33	25.26	25.07		23.45	23.97	23.84	23.52	24.36	
Cr2O3	0.25	0.41	0.19	0.09	0.00	0.00	0.14	0.00	0.00	0.00	0.00	0.20	0.00	0.00	0.00	0.18		0.00	0.00	0.00	0.00	0.00	
FeO	36.15	37.53	36.28	32.13	32.56	34.41	34.06	33.77	33.63	33.91	34.35	33.56	33.70	34.24	35.95	33.34		35.51	34.97	34.57	35.09	35.30	
MnO	0.00	0.00	0.00	0.29	0.25	0.20	0.18	0.22	0.15	0.21	0.15	0.21	0.16	0.17	0.00	0.19		0.16	0.16	0.16	0.00	0.00	
MgO	7.70	6.76	7.28	10.26	9.29	8.56	8.74	8.89	8.64	8.77	8.61	9.17	8.65	8.90	7.45	8.77		8.01	8.68	8.52	7.97	8.21	
CaO	0.00	0.06	0.00	0.10	0.16	0.06	0.07	0.00	0.00	0.00	0.00	0.00	0.00	0.00	0.00	0.00		0.07	0.08	0.13	0.09	0.00	
Na2O	0.00	0.00	0.00	0.00	0.00	0.00	0.00	0.00	0.07	0.00	0.00	0.00	0.00	0.00	0.00	0.00		0.00	0.00	0.00	0.00	0.00	
K2O	0.00	0.00	0.00	0.00	0.00	0.00	0.00	0.00	0.00	0.00	0.00	0.00	0.00	0.00	0.00	0.00		0.00	0.00	0.00	0.00	0.00	
F	0.00	0.00	0.00	0.00	0.00	0.00	0.00	0.00	0.00	0.00	0.00	0.00	0.00	0.00	0.00	0.00		0.00	0.00	0.00	0.00	0.00	
Total	91.73	91.77	90.79	90.88	89.01	91.33	91.20	91.18	90.94	91.18	91.78	91.72	90.55	91.10	91.48	91.49		90.57	91.86	90.45	89.76	91.10	
	6.39	6.45	6.47	6.33	6.50	6.37	6.36	6.35	6.36	6.35	6.32	6.30	6.39	6.37	6.40	6.30		6.47	6.34	6.45	6.52	6.41	
SiIV	2.48	2.46	2.51	2.46	2.47	2.45	2.49	2.47	2.50	2.50	2.48	2.46	2.50	2.49	2.43	2.51		2.52	2.53	2.49	2.51	2.48	
AlIV	1.52	1.54	1.49	1.54	1.53	1.55	1.51	1.53	1.50	1.50	1.52	1.54	1.50	1.51	1.57	1.49		1.48	1.47	1.51	1.49	1.52	
T site	4.00	4.00	4.00	4.00	4.00	4.00	4.00	4.00	4.00	4.00	4.00	4.00	4.00	4.00	4.00	4.00		4.00	4.00	4.00	4.00	4.00	
AlVI	1.53	1.51	1.52	1.52	1.52	1.57	1.55	1.57	1.60	1.57	1.59	1.57	1.58	1.53	1.60	1.61		1.49	1.51	1.51	1.51	1.54	
Ti	0.00	0.00	0.00	0.00	0.00	0.00	0.00	0.00	0.00	0.00	0.00	0.00	0.00	0.00	0.00	0.00		0.00	0.00	0.00	0.00	0.00	
Cr3+	0.02	0.03	0.02	0.01	0.00	0.00	0.01	0.00	0.00	0.00	0.00	0.02	0.00	0.00	0.00	0.01		0.00	0.00	0.00	0.00	0.00	
Fe2+	3.22	3.37	3.27	2.83	2.95	3.05	3.02	2.98	2.98	3.00	3.02	2.94	3.00	3.04	3.20	2.92		3.20	3.08	3.10	3.18	3.15	
Mn2+	0.00	0.00	0.00	0.03	0.02	0.02	0.02	0.02	0.01	0.02	0.01	0.02	0.01	0.02	0.00	0.02		0.01	0.01	0.01	0.00	0.00	
Mg	1.22	1.08	1.17	1.61	1.50	1.35	1.38	1.40	1.36	1.38	1.35	1.43	1.37	1.41	1.18	1.37		1.29	1.36	1.36	1.29	1.30	
Ca	0.00	0.01	0.00	0.01	0.02	0.01	0.01	0.00	0.00	0.00	0.00	0.00	0.00	0.00	0.00	0.00		0.01	0.01	0.01	0.01	0.00	
Na	0.00	0.00	0.00	0.00	0.00	0.00	0.00	0.00	0.01	0.00	0.00	0.00	0.00	0.00	0.00	0.00		0.00	0.00	0.00	0.00	0.00	
K	0.00	0.00	0.00	0.00	0.00	0.00	0.00	0.00	0.00	0.00	0.00	0.00	0.00	0.00	0.00	0.00		0.00	0.00	0.00	0.00	0.00	
O site	5.99	6.00	5.97	6.01	6.01	5.99	5.98	5.98	5.96	5.96	5.97	5.98	5.96	5.99	5.98	5.93		6.00	5.98	6.00	5.99	5.99	
XFe	0.72	0.76	0.74	0.64	0.66	0.69	0.69	0.68	0.69	0.68	0.69	0.67	0.69	0.68	0.73	0.68		0.71	0.69	0.69	0.71	0.71	
Al/(Al+Fe+Mg)	0.41	0.41	0.40	0.41	0.41	0.41	0.41	0.41	0.42	0.41	0.42	0.42	0.41	0.41	0.42	0.42		0.40	0.40	0.40	0.40	0.41	
T (°C)	305	306	297	316	312	314	307	312	305	304	309	315	304	307	315	303		298	297	305	301	307	
XChl	0.99	0.99	0.98	1.00	0.99	0.99	0.97	0.98	0.95	0.97	0.97	0.98	0.96	0.99	0.99	0.94		0.99	0.98	0.99	0.99	0.99	
i/l cat	0.00	0.01	0.00	0.01	0.02	0.01	0.01	0.00	0.01	0.00	0.00	0.00	0.00	0.00	0.00	0.00		0.01	0.01	0.01	0.01	0.00	
non-i/l	9.99	9.99	9.97	10.00	9.99	9.99	9.97	9.98	9.95	9.96	9.97	9.98	9.96	9.99	9.98	9.93		9.99	9.97	9.99	9.98	9.99	

Sample:	VHG147(A)									Sample:	VHG148(B)								
Lithology:	VCR (10cm below top contact)									Lithology:	VCR (1m below top contact)								
Analysis No.	Chl 1	Chl 2	Chl 3	Chl 4	Chl 5	Chl 6	Chl 7	Chl 8	Chl 9		Chl 1	Chl 2	Chl 3	Chl 4	Chl 5	Chl 6	Chl 7	Chl 8	Chl 9
Chlorite Type	II	II	II	II	II	II	II	II	II		II	II	II	II	II	II	+Po	II	II
SiO2	23.45	23.53	23.81	23.46	23.48	23.84	23.25	24.02	24.23		23.23	22.83	23.13	23.29	23.38	23.31	22.33	23.25	22.98
TiO2	0.00	0.00	0.00	0.00	0.00	0.00	0.00	0.00	0.00		0.00	0.00	0.00	0.00	0.00	0.00	0.00	0.00	0.00
Al2O3	24.51	24.71	24.37	24.24	23.91	23.59	23.16	22.84	24.47		24.79	24.46	24.65	25.15	24.85	25.16	24.75	24.42	25.56
Cr2O3	0.00	0.00	0.00	0.11	0.00	0.11	0.44	1.07	0.31		0.16	0.54	0.42	0.70	0.50	0.32	0.24	0.26	0.30
FeO	31.78	33.21	31.71	32.57	32.42	31.85	30.69	30.75	30.97		33.73	32.46	32.48	33.62	33.53	32.73	33.36	32.88	34.57
MnO	0.18	0.17	0.22	0.19	0.22	0.20	0.20	0.16	0.19		0.14	0.17	0.16	0.16	0.19	0.17	0.19	0.17	0.00
MgO	9.86	8.87	10.51	9.13	9.39	9.99	10.57	11.27	11.24		7.33	8.98	9.35	7.65	7.94	8.97	7.54	8.53	6.97
CaO	0.00	0.00	0.13	0.00	0.05	0.00	0.00	0.00	0.00		0.00	0.00	0.00	0.00	0.00	0.00	0.00	0.00	0.00
Na2O	0.00	0.00	0.00	0.00	0.00	0.00	0.00	0.00	0.00		0.00	0.00	0.00	0.00	0.00	0.00	0.00	0.00	0.00
K2O	0.00	0.00	0.00	0.00	0.00	0.00	0.00	0.00	0.00		0.00	0.00	0.00	0.00	0.00	0.00	0.00	0.00	0.00
F	0.00	0.00	0.00	0.00	0.00	0.00	0.00	0.00	0.00		0.00	0.00	0.00	0.00	0.00	0.00	0.00	0.00	0.00
Total	89.78	90.49	90.75	89.70	89.47	89.58	88.31	90.11	91.41		89.38	89.44	90.17	90.57	90.39	90.66	88.41	89.51	90.38
	6.39	6.38	6.32	6.43	6.44	6.41	6.49	6.36	6.24		6.48	6.46	6.39	6.40	6.41	6.36	6.57	6.45	6.43
SiIV	2.49	2.50	2.50	2.51	2.52	2.54	2.51	2.54	2.51		2.51	2.45	2.46	2.48	2.49	2.47	2.44	2.50	2.46
AlIV	1.51	1.50	1.50	1.49	1.48	1.46	1.49	1.46	1.49		1.49	1.55	1.54	1.52	1.51	1.53	1.56	1.50	1.54
T site	4.00	4.00	4.00	4.00	4.00	4.00	4.00	4.00	4.00		4.00	4.00	4.00	4.00	4.00	4.00	4.00	4.00	4.00
AlVI	1.57	1.59	1.52	1.56	1.54	1.51	1.46	1.39	1.51		1.66	1.55	1.55	1.63	1.62	1.60	1.63	1.59	1.68
Ti	0.00	0.00	0.00	0.00	0.00	0.00	0.00	0.00	0.00		0.00	0.00	0.00	0.00	0.00	0.00	0.00	0.00	0.00
Cr3+	0.00	0.00	0.00	0.01	0.00	0.01	0.04	0.09	0.03		0.01	0.05	0.04	0.06	0.04	0.03	0.02	0.02	0.03
Fe2+	2.83	2.95	2.79	2.91	2.91	2.84	2.77	2.72	2.69		3.04	2.92	2.89	2.99	2.99	2.89	3.05	2.95	3.09
Mn2+	0.02	0.02	0.02	0.02	0.02	0.02	0.02	0.01	0.02		0.01	0.02	0.01	0.01	0.02	0.02	0.02	0.02	0.00
Mg	1.56	1.40	1.65	1.46	1.50	1.59	1.70	1.78	1.74		1.18	1.44	1.48	1.21	1.26	1.41	1.23	1.37	1.11
Ca	0.00	0.00	0.01	0.00	0.01	0.00	0.00	0.00	0.00		0.00	0.00	0.00	0.00	0.00	0.00	0.00	0.00	0.00
Na	0.00	0.00	0.00	0.00	0.00	0.00	0.00	0.00	0.00		0.00	0.00	0.00	0.00	0.00	0.00	0.00	0.00	0.00
K	0.00	0.00	0.00	0.00	0.00	0.00	0.00	0.00	0.00		0.00	0.00	0.00	0.00	0.00	0.00	0.00	0.00	0.00
O site	5.97	5.96	5.99	5.96	5.97	5.97	5.99	5.99	5.98		5.91	5.97	5.97	5.91	5.93	5.95	5.95	5.95	5.92
XFe	0.64	0.68	0.63	0.67	0.66	0.64	0.62	0.60	0.61		0.72	0.67	0.66	0.71	0.70	0.67	0.71	0.68	0.74
Al/(Al+Fe+Mg)	0.41	0.42	0.41	0.41	0.41	0.40	0.40	0.39	0.40		0.43	0.42	0.41	0.43	0.42	0.42	0.43	0.42	0.43
T (°C)	310	306	309	304	303	299	308	303	309		300	315	315	306	304	313	314	305	308
XChl	0.97	0.96	0.98	0.96	0.97	0.97	0.99	0.99	0.98		0.92	0.98	0.98	0.92	0.93	0.96	0.96	0.95	0.92
i/l cat	0.00	0.00	0.01	0.00	0.01	0.00	0.00	0.00	0.00		0.00	0.00	0.00	0.00	0.00	0.00	0.00	0.00	0.00
non-i/l	9.97	9.96	9.98	9.96	9.97	9.97	9.99	9.99	9.98		9.91	9.97	9.97	9.91	9.93	9.95	9.95	9.95	9.92

Sample:	VHG152(A)																
Lithology:	VCR (10cm below top contact)																
Analysis No.	Chl 1	Chl 2	Chl 3	Chl 4	Chl 5	Chl 6	Chl 7	Chl 8	Chl 9	Chl 10	Chl 12	Chl 13	Chl 14	Chl 15	Chl 16	Chl 17	Chl 18
Chlorite Type	+Cc	Vn 4	II	II	II	Vn 4	II	VN 1	VN 1	II	Vn 1	Vn 1	II	Vn 2	+Au	+Au	Vn 3
SiO2	23.25	24.52	23.94	23.61	23.86	23.98	24.63	24.20	24.40	24.24	25.08	24.89	24.28	25.05	23.90	24.32	24.04
TiO2	0.00	0.00	0.00	0.00	0.00	0.00	0.07	0.00	0.00	0.00	0.00	0.00	0.00	0.00	0.00	0.00	0.00
Al2O3	24.26	21.96	22.59	23.33	22.74	23.63	21.20	23.01	21.90	22.26	22.08	21.16	23.47	21.93	22.65	20.63	22.10
Cr2O3	0.07	0.00	0.00	0.08	0.00	0.00	0.48	0.00	0.00	0.00	0.00	0.00	0.00	0.00	0.27	0.00	0.00
FeO	34.19	34.21	33.53	33.41	33.45	33.45	32.58	33.06	32.47	33.43	31.46	32.22	32.24	32.32	32.85	32.59	32.93
MnO	0.20	0.16	0.26	0.17	0.21	0.21	0.21	0.19	0.15	0.18	0.14	0.20	0.00	0.00	0.23	0.20	0.19
MgO	8.00	9.50	9.07	8.81	8.97	8.73	10.30	9.16	10.44	9.58	11.28	10.63	9.87	10.64	9.36	10.03	9.75
CaO	0.00	0.00	0.00	0.00	0.00	0.00	0.10	0.00	0.00	0.00	0.00	0.00	0.00	0.00	0.00	0.00	0.00
Na2O	0.00	0.00	0.00	0.00	0.00	0.00	0.00	0.00	0.00	0.00	0.00	0.00	0.00	0.00	0.00	0.00	0.00
K2O	0.00	0.00	0.00	0.00	0.00	0.00	0.00	0.00	0.00	0.00	0.00	0.00	0.00	0.00	0.00	0.00	0.00
F	0.00	0.00	0.00	0.00	0.00	0.00	0.00	0.00	0.00	0.00	0.00	0.00	0.00	0.00	0.00	0.00	0.00
Total	89.97	90.35	89.39	89.61	89.23	89.98	89.57	89.62	89.36	89.69	90.04	89.10	89.86	89.94	89.26	87.77	89.01
	6.46	6.43	6.49	6.46	6.50	6.43	6.46	6.44	6.45	6.46	6.35	6.46	6.39	6.38	6.48	6.60	6.50
SiIV	2.50	2.62	2.59	2.56	2.58	2.56	2.65	2.60	2.62	2.81	2.65	2.68	2.58	2.66	2.58	2.67	2.60
AlIV	1.50	1.38	1.41	1.44	1.42	1.44	1.35	1.40	1.38	1.39	1.35	1.32	1.42	1.34	1.42	1.33	1.40
T site	4.00	4.00	4.00	4.00	4.00	4.00	4.00	4.00	4.00	4.00	4.00	4.00	4.00	4.00	4.00	4.00	4.00
AlVI	1.58	1.40	1.46	1.52	1.48	1.54	1.33	1.50	1.39	1.43	1.40	1.36	1.52	1.41	1.46	1.34	1.42
Ti	0.00	0.00	0.00	0.00	0.00	0.00	0.01	0.00	0.00	0.00	0.00	0.00	0.00	0.00	0.00	0.00	0.00
Cr3+	0.01	0.00	0.00	0.01	0.00	0.00	0.04	0.00	0.00	0.00	0.00	0.00	0.00	0.00	0.02	0.00	0.00
Fe2+	3.08	3.06	3.03	3.00	3.03	2.99	2.93	2.96	2.92	3.01	2.78	2.90	2.87	2.87	2.96	2.99	2.98
Mn2+	0.02	0.01	0.02	0.02	0.02	0.02	0.02	0.02	0.01	0.02	0.01	0.02	0.00	0.00	0.02	0.02	0.02
Mg	1.28	1.52	1.46	1.41	1.45	1.39	1.65	1.46	1.67	1.53	1.78	1.70	1.56	1.68	1.50	1.64	1.57
Ca	0.00	0.00	0.00	0.00	0.00	0.00	0.01	0.00	0.00	0.00	0.00	0.00	0.00	0.00	0.00	0.00	0.00
Na	0.00	0.00	0.00	0.00	0.00	0.00	0.00	0.00	0.00	0.00	0.00	0.00	0.00	0.00	0.00	0.00	0.00
K	0.00	0.00	0.00	0.00	0.00	0.00	0.00	0.00	0.00	0.00	0.00	0.00	0.00	0.00	0.00	0.00	0.00
O site	5.96	5.99	5.98	5.96	5.97	5.95	5.99	5.95	5.99	5.98	5.97	5.98	5.95	5.97	5.97	5.99	5.99
XFe	0.71	0.67	0.67	0.68	0.68	0.68	0.64	0.67	0.64	0.66	0.61	0.63	0.65	0.63	0.66	0.65	0.65
Al/(Al+Fe+Mg)	0.41	0.38	0.39	0.40	0.39	0.40	0.37	0.40	0.38	0.38	0.38	0.37	0.40	0.38	0.39	0.37	0.38
T(C)	302	279	287	292	288	291	277	286	283	284	279	272	291	275	290	272	286
XChl	0.96	0.99	0.98	0.96	0.97	0.95	0.98	0.95	0.99	0.98	0.98	0.98	0.95	0.97	0.97	0.99	0.99
i/l cat	0.00	0.00	0.00	0.00	0.00	0.00	0.01	0.00	0.00	0.00	0.00	0.00	0.00	0.00	0.00	0.00	0.00
non-i/l	9.96	9.99	9.98	9.96	9.97	9.95	9.98	9.95	9.99	9.98	9.97	9.98	9.95	9.97	9.97	9.99	9.99

Sample:	VHG150(B)						Sample:	VHG153(A)							Sample:	VHG156								
Lithology:	VCR (50cm up from bottom contact)						Lithology:	VCR with siderite							Lithology:	VCR (10cm up from bottom contact)								
Analysis No.	Chl 1	Chl 2	Chl 3	Chl 4	Chl 5	Chl 6		Chl 1	Chl 2	Chl 3	Chl 4	Chl 5	Chl 6	Chl 7		Chl 1	Chl 2	Chl 3	Chl 4	Chl 5	Chl 6	Chl 7	Chl 8	Chl 9	Chl 10
Chlorite Type	II	II	II	+Py Vn	+Py	+Py		II	II	II	II	II	II	II		II	II	II	+Py Vn	+Py	+Py	in brecc.z	+Py	+Py	+Py Vn
SiO2	22.90	23.87	23.07	23.52	23.46	23.23		23.11	22.74	23.26	23.38	22.71	22.89	22.20		24.18	24.01	24.05	24.26	24.88	24.40	24.51	24.07	24.83	25.26
TiO2	0.00	0.00	0.00	0.00	0.00	0.00		0.00	0.00	0.00	0.00	0.00	0.00	0.00		0.00	0.00	0.00	0.00	0.00	0.00	0.00	0.00	0.00	0.00
Al2O3	26.18	24.73	24.04	25.54	24.33	24.28		24.11	23.85	23.84	24.19	24.07	24.04	23.62		26.30	26.46	25.29	26.67	26.16	25.85	25.89	25.56	26.48	25.46
Cr2O3	0.16	0.15	0.27	0.13	0.48	0.33		0.00	0.00	0.00	0.00	0.00	0.00	1.51		0.09	0.00	0.00	0.00	0.00	0.00	0.09	0.07	0.00	0.00
FeO	33.21	33.75	32.48	33.98	32.78	33.24		37.51	39.15	37.46	37.72	38.62	38.27	38.57		27.58	27.74	27.39	27.66	27.21	27.05	27.37	27.89	26.30	27.16
MnO	0.17	0.13	0.16	0.18	0.16	0.00		0.00	0.00	0.00	0.16	0.00	0.12	0.00		0.19	0.25	0.21	0.16	0.24	0.19	0.20	0.21	0.13	0.17
MgO	7.41	7.26	8.45	7.06	8.07	8.35		6.13	5.57	6.33	6.28	5.86	5.79	5.24		10.47	11.02	11.05	10.98	10.54	11.12	11.25	10.78	11.11	11.52
CaO	0.00	0.00	0.00	0.00	0.00	0.00		0.00	0.00	0.00	0.00	0.00	0.00	0.00		0.06	0.00	0.00	0.00	0.00	0.00	0.00	0.00	0.00	0.00
Na2O	0.00	0.00	0.00	0.00	0.00	0.00		0.00	0.00	0.00	0.00	0.00	0.00	0.00		0.00	0.00	0.00	0.00	0.00	0.00	0.00	0.00	0.00	0.00
K2O	0.00	0.00	0.00	0.00	0.00	0.00		0.00	0.00	0.00	0.00	0.00	0.00	0.00		0.00	0.00	0.00	0.00	0.00	0.00	0.00	0.00	0.00	0.00
F	0.00	0.00	0.00	0.00	0.00	0.00		0.00	0.00	0.00	0.00	0.00	0.00	0.00		0.00	0.00	0.00	0.00	0.00	0.00	0.00	0.00	0.00	0.00
Total	89.03	89.89	88.47	90.43	89.27	89.41		90.86	91.31	90.91	91.75	91.05	91.11	91.14		88.87	89.48	87.99	89.73	89.03	88.61	89.11	88.58	88.85	89.59
	6.50	6.43	6.53	6.40	6.47	6.47		6.50	6.54	6.50	6.44	6.54	6.52	6.57		6.29	6.25	6.36	6.22	6.25	6.28	6.26	6.33	6.22	6.20
BIIV	2.48	2.55	2.51	2.50	2.52	2.50		2.50	2.47	2.52	2.51	2.47	2.48	2.43		2.53	2.50	2.54	2.51	2.59	2.55	2.55	2.53	2.57	2.61
AlIV	1.52	1.45	1.49	1.50	1.48	1.50		1.50	1.53	1.48	1.49	1.53	1.52	1.57		1.47	1.50	1.46	1.49	1.41	1.45	1.45	1.47	1.43	1.39
T site	4.00	4.00	4.00	4.00	4.00	4.00		4.00	4.00	4.00	4.00	4.00	4.00	4.00		4.00	4.00	4.00	4.00	4.00	4.00	4.00	4.00	4.00	4.00
AlVI	1.69	1.68	1.59	1.71	1.81	1.56		1.56	1.53	1.56	1.56	1.56	1.56	1.47		1.77	1.74	1.70	1.76	1.79	1.74	1.71	1.71	1.81	1.71
Ti	0.00	0.00	0.00	0.00	0.00	0.00		0.00	0.00	0.00	0.00	0.00	0.00	0.00		0.00	0.00	0.00	0.00	0.00	0.00	0.00	0.00	0.00	0.00
Cr3+	0.01	0.01	0.02	0.01	0.04	0.03		0.00	0.00	0.00	0.00	0.00	0.00	0.13		0.01	0.00	0.00	0.00	0.00	0.00	0.01	0.01	0.00	0.00
Fe2+	3.00	3.02	2.95	3.03	2.95	2.99		3.40	3.56	3.39	3.38	3.51	3.47	3.53		2.41	2.41	2.42	2.39	2.37	2.37	2.38	2.46	2.26	2.35
Mn2+	0.02	0.01	0.01	0.02	0.01	0.00		0.00	0.00	0.00	0.02	0.00	0.01	0.00		0.02	0.02	0.02	0.01	0.02	0.02	0.02	0.02	0.01	0.01
Mg	1.19	1.16	1.37	1.12	1.29	1.34		0.99	0.90	1.02	1.00	0.92	0.94	0.85		1.63	1.71	1.74	1.69	1.63	1.73	1.75	1.69	1.72	1.77
Ca	0.00	0.00	0.00	0.00	0.00	0.00		0.00	0.00	0.00	0.00	0.00	0.00	0.00		0.01	0.00	0.00	0.00	0.00	0.00	0.00	0.00	0.00	0.00
Na	0.00	0.00	0.00	0.00	0.00	0.00		0.00	0.00	0.00	0.00	0.00	0.00	0.00		0.00	0.00	0.00	0.00	0.00	0.00	0.00	0.00	0.00	0.00
K	0.00	0.00	0.00	0.00	0.00	0.00		0.00	0.00	0.00	0.00	0.00	0.00	0.00		0.00	0.00	0.00	0.00	0.00	0.00	0.00	0.00	0.00	0.00
O site	5.91	5.88	5.94	5.89	5.91	5.94		5.98	6.00	5.98	5.97	5.99	5.98	5.98		5.65	5.88	5.88	5.86	5.81	5.85	5.87	5.88	5.81	5.84
XFe	0.72	0.72	0.68	0.73	0.70	0.69		0.77	0.80	0.77	0.77	0.79	0.79	0.80		0.60	0.59	0.58	0.59	0.59	0.58	0.58	0.59	0.57	0.57
Al/(Al+Fe+Mg)	0.43	0.43	0.42	0.44	0.42	0.42		0.41	0.41	0.41	0.41	0.41	0.41	0.41		0.45	0.44	0.43	0.44	0.44	0.44	0.43	0.43	0.45	0.43
T (°C)	307	289	303	299	298	303		296	299	293	295	301	298	309		308	314	305	312	295	303	303	306	300	292
XChl	0.92	0.89	0.95	0.90	0.92	0.95		0.96	1.00	0.97	0.97	0.99	0.98	0.99		0.85	0.89	0.89	0.87	0.83	0.87	0.88	0.89	0.83	0.86
i/l cat	0.00	0.00	0.00	0.00	0.00	0.00		0.00	0.00	0.00	0.00	0.00	0.00	0.00		0.01	0.00	0.00	0.00	0.00	0.00	0.00	0.00	0.00	0.00
non-i/l	9.91	9.88	9.94	9.89	9.91	9.94		9.96	10.00	9.96	9.97	9.99	9.98	9.98		9.84	9.88	9.88	9.86	9.81	9.85	9.87	9.88	9.81	9.84

Sample:	VHG158(B)										Sample:	VHG162												
Lithology:	VCR with siderite										Lithology:	VCR												
Analysis No.	Chl 1	Chl 2	Chl 3	Chl 4	Chl 5	Chl 6	Chl 7	Chl 9	Chl 9	Chl 10	Chl 1	Chl 2	Chl 3	Chl 4	Chl 5	Chl 6	Chl 7 (Lar	Chl 8	Chl 9	Chl 10	Chl 11	Chl 12	Chl 13	Chl 14
Chlorite Type	II	II	II	II	II	II	II	II	+Py	+Py Vn	II	II	II	II	II	II	I	Vn 1	Vn 1	Vn 1	II	Vn 2	Vn 2	II
SiO2	22.48	22.56	22.40	22.87	22.85	22.74	23.07	22.46	24.83	25.26	23.17	23.32	23.42	23.13	23.14	23.07	22.95	23.64	23.21	23.93	22.75	23.17	23.66	23.81
TiO2	0.00	0.00	0.00	0.00	0.00	0.00	0.00	0.00	0.00	0.00	0.00	0.00	0.00	0.00	0.00	0.00	0.00	0.00	0.00	0.00	0.00	0.00	0.00	0.00
Al2O3	23.64	23.83	22.80	23.10	23.84	23.26	23.95	23.80	26.48	25.46	24.11	24.80	24.53	24.54	24.13	24.01	24.57	25.04	24.90	23.85	23.58	24.80	24.45	23.81
Cr2O3	0.00	0.00	0.00	0.00	0.00	0.00	0.00	0.00	0.00	0.00	0.00	0.00	0.00	0.00	0.00	0.00	0.00	0.00	0.00	0.00	0.00	0.00	0.00	0.00
FeO	36.19	36.98	36.56	36.37	36.02	37.90	36.01	36.92	26.30	27.16	36.77	35.88	35.45	35.65	35.74	35.92	35.39	35.39	35.44	35.22	35.19	35.92	35.72	36.05
MnO	0.00	0.16	0.00	0.00	0.00	0.13	0.00	0.00	0.13	0.17	0.14	0.23	0.15	0.20	0.14	0.15	0.12	0.21	0.19	0.15	0.15	0.00	0.13	0.00
MgO	5.69	6.01	5.55	5.81	6.00	5.69	6.12	6.11	11.11	11.52	7.43	7.01	7.40	7.41	7.21	7.22	7.02	7.47	7.26	7.87	7.07	7.33	7.41	7.55
CaO	0.07	0.00	0.00	0.00	0.00	0.00	0.00	0.00	0.00	0.00	0.00	0.00	0.00	0.00	0.00	0.00	0.00	0.05	0.00	0.00	0.00	0.00	0.00	0.00
Na2O	0.00	0.00	0.00	0.00	0.00	0.00	0.00	0.00	0.00	0.00	0.00	0.00	0.00	0.00	0.00	0.00	0.00	0.00	0.00	0.00	0.00	0.00	0.00	0.00
K2O	0.00	0.00	0.00	0.00	0.00	0.00	0.00	0.00	0.00	0.00	0.00	0.00	0.00	0.00	0.00	0.00	0.00	0.00	0.00	0.00	0.00	0.00	0.00	0.00
F	0.00	0.00	0.00	0.00	0.00	0.00	0.00	0.00	0.00	0.00	0.00	0.00	0.00	0.00	0.00	0.00	0.00	0.00	0.00	0.00	0.00	0.00	0.00	0.00
Total	90.07	89.54	89.11	90.15	90.51	89.92	91.15	89.29	88.85	89.59	91.62	91.32	90.95	90.93	90.36	90.37	90.05	91.80	91.02	91.02	88.72	91.32	91.37	91.02
	6.61	6.61	6.71	6.61	6.56	6.61	6.50	6.62	6.22	6.20	6.43	6.41	6.42	6.44	6.49	6.49	6.50	6.35	6.42	6.40	6.61	6.41	6.39	6.44
SiIV	2.47	2.48	2.50	2.51	2.47	2.50	2.50	2.48	2.57	2.61	2.48	2.49	2.50	2.48	2.50	2.49	2.48	2.50	2.48	2.55	2.50	2.47	2.52	2.53
AlIV	1.53	1.52	1.50	1.49	1.53	1.50	1.50	1.52	1.43	1.39	1.52	1.51	1.50	1.52	1.50	1.51	1.52	1.50	1.52	1.45	1.50	1.53	1.48	1.47
T site	4.00	4.00	4.00	4.00	4.00	4.00	4.00	4.00	4.00	4.00	4.00	4.00	4.00	4.00	4.00	4.00	4.00	4.00	4.00	4.00	4.00	4.00	4.00	4.00
AlVI	1.54	1.57	1.48	1.51	1.54	1.52	1.55	1.57	1.81	1.71	1.52	1.62	1.59	1.58	1.57	1.55	1.61	1.62	1.61	1.55	1.58	1.60	1.58	1.53
Ti	0.00	0.00	0.00	0.00	0.00	0.00	0.00	0.00	0.00	0.00	0.00	0.00	0.00	0.00	0.00	0.00	0.00	0.00	0.00	0.00	0.00	0.00	0.00	0.00
Cr3+	0.00	0.00	0.00	0.00	0.00	0.00	0.00	0.00	0.00	0.00	0.00	0.00	0.00	0.00	0.00	0.00	0.00	0.00	0.00	0.00	0.00	0.00	0.00	0.00
Fe2+	3.51	3.40	3.60	3.53	3.47	3.49	3.44	3.40	2.28	2.35	3.29	3.20	3.17	3.19	3.23	3.25	3.20	3.13	3.17	3.14	3.24	3.20	3.18	3.23
Mn2+	0.00	0.01	0.00	0.00	0.00	0.01	0.00	0.00	0.01	0.01	0.01	0.02	0.01	0.02	0.01	0.01	0.01	0.02	0.02	0.01	0.01	0.00	0.01	0.00
Mg	0.83	0.99	0.92	0.95	0.98	0.97	0.99	1.00	1.72	1.77	1.18	1.11	1.18	1.16	1.16	1.16	1.13	1.18	1.16	1.25	1.16	1.16	1.17	1.21
Ca	0.01	0.00	0.00	0.00	0.00	0.00	0.00	0.00	0.00	0.00	0.00	0.00	0.00	0.00	0.00	0.00	0.00	0.01	0.00	0.00	0.00	0.00	0.00	0.00
Na	0.00	0.00	0.00	0.00	0.00	0.00	0.00	0.00	0.00	0.00	0.00	0.00	0.00	0.00	0.00	0.00	0.00	0.00	0.00	0.00	0.00	0.00	0.00	0.00
K	0.00	0.00	0.00	0.00	0.00	0.00	0.00	0.00	0.00	0.00	0.00	0.00	0.00	0.00	0.00	0.00	0.00	0.00	0.00	0.00	0.00	0.00	0.00	0.00
O site	6.00	5.97	6.01	5.99	5.99	5.99	5.98	5.98	5.81	5.84	6.00	5.95	5.95	5.97	5.97	5.96	5.95	5.94	5.95	5.95	5.97	5.97	5.95	5.97
XFe	0.79	0.78	0.80	0.79	0.78	0.78	0.79	0.77	0.57	0.57	0.74	0.74	0.73	0.73	0.74	0.74	0.74	0.73	0.73	0.72	0.74	0.73	0.73	0.73
Al/(Al+Fe+Mg)	0.41	0.41	0.40	0.40	0.41	0.40	0.41	0.41	0.45	0.43	0.40	0.42	0.42	0.41	0.41	0.41	0.42	0.42	0.42	0.41	0.41	0.42	0.41	0.40
T (°C)	300	300	293	292	301	295	297	301	300	292	304	302	300	306	300	301	303	301	305	291	299	306	296	294
XChl	0.99	0.98	1.00	0.99	0.99	0.99	0.98	0.98	0.83	0.86	1.00	0.95	0.96	0.97	0.97	0.98	0.96	0.94	0.96	0.95	0.97	0.97	0.95	0.97
I/I cat	0.01	0.00	0.00	0.00	0.00	0.00	0.00	0.00	0.00	0.00	0.00	0.00	0.00	0.00	0.00	0.00	0.00	0.01	0.00	0.00	0.00	0.00	0.00	0.00
non-I/I	9.99	9.97	10.00	9.99	9.99	9.99	9.98	9.98	9.81	9.84	10.00	9.95	9.95	9.97	9.97	9.98	9.95	9.94	9.95	9.95	9.97	9.97	9.95	9.97

Sample:	VHG164									Sample:	VHG170					Sample:	VHG173(B)					
Lithology:	VCR									Lithology:	VCR					Lithology:	VCR					
Analysis No.	Chl 1	Chl 2	Chl 3	Chl 4	Chl 5	Chl 6	Chl 7	Chl 8	Chl 9	Chl 1	Chl 2	Chl 3	Chl 4	Chl 5		Chl 1	Chl 2	Chl 3	Chl 4	Chl 5	Chl 6
Chlorite Type	II	+Au	II	II	I	II	+Po	II	II	II	II	II	+Py	II		II	+Gn+Sp	+Gn	II	II	+Sph
SiO2	23.51	22.89	23.38	22.87	22.70	22.79	22.42	22.83	22.98	24.12	23.97	22.90	23.96	23.46		23.61	23.49	23.35	22.60	24.38	23.47
TiO2	0.00	0.00	0.00	0.00	0.00	0.00	0.00	0.00	0.00	0.00	0.00	0.00	0.00	0.00		0.00	0.00	0.00	0.00	0.00	0.00
Al2O3	22.68	22.12	21.54	23.91	23.60	23.71	24.25	23.73	23.78	26.09	25.57	25.48	25.99	26.07		25.60	24.50	24.90	26.13	24.47	24.92
Cr2O3	0.00	0.16	0.14	0.00	0.31	0.15	0.09	0.00	0.00	0.00	0.00	0.00	0.00	0.00		0.08	0.00	0.00	0.00	0.00	0.00
FeO	38.88	38.89	39.25	38.95	37.08	38.40	37.19	37.14	38.03	29.26	30.20	30.41	29.05	30.26		28.96	33.13	29.00	32.47	28.42	28.75
MnO	0.00	0.00	0.00	0.15	0.00	0.00	0.00	0.13	0.00	0.19	0.00	0.13	0.00	0.00		0.16	0.17	0.26	0.17	0.15	0.20
MgO	6.13	4.85	5.08	6.00	5.90	5.90	5.86	6.07	5.82	11.02	9.85	9.59	10.79	9.99		10.88	7.77	10.78	6.98	10.16	10.55
CaO	0.00	0.00	0.00	0.00	0.00	0.00	0.00	0.00	0.00	0.00	0.00	0.00	0.00	0.00		0.00	0.00	0.00	0.00	0.00	0.00
Na2O	0.00	0.00	0.00	0.00	0.00	0.00	0.00	0.00	0.00	0.00	0.00	0.00	0.00	0.00		0.00	0.00	0.00	0.00	0.00	0.00
K2O	0.00	0.00	0.00	0.00	0.00	0.00	0.00	0.00	0.00	0.00	0.00	0.00	0.00	0.00		0.00	0.00	0.00	0.00	0.00	0.00
F	0.00	0.00	0.00	0.00	0.00	0.00	0.00	0.00	0.00	0.00	0.00	0.00	0.00	0.00		0.00	0.00	0.00	0.00	0.00	0.00
Total	91.20	88.91	89.39	89.88	89.59	88.95	89.81	89.90	90.61	90.68	89.59	88.51	89.79	89.78		89.29	89.06	88.29	88.35	87.58	87.89
	6.53	6.74	6.71	6.57	6.61	6.63	6.59	6.58	6.55	6.21	6.32	6.44	6.27	6.31		6.32	6.48	6.41	6.52	6.42	6.42
SiIV	2.56	2.57	2.61	2.50	2.50	2.51	2.46	2.50	2.50	2.49	2.52	2.45	2.50	2.47		2.48	2.53	2.49	2.45	2.60	2.51
AlIV	1.44	1.43	1.39	1.50	1.50	1.49	1.54	1.50	1.50	1.51	1.48	1.55	1.50	1.53		1.52	1.47	1.51	1.55	1.40	1.49
T site	4.00	4.00	4.00	4.00	4.00	4.00	4.00	4.00	4.00	4.00	4.00	4.00	4.00	4.00		4.00	4.00	4.00	4.00	4.00	4.00
AlVI	1.46	1.49	1.44	1.58	1.56	1.60	1.59	1.56	1.56	1.67	1.69	1.67	1.69	1.70		1.66	1.65	1.62	1.79	1.69	1.65
Ti	0.00	0.00	0.00	0.00	0.00	0.00	0.00	0.00	0.00	0.00	0.00	0.00	0.00	0.00		0.00	0.00	0.00	0.00	0.00	0.00
Cr3+	0.00	0.01	0.01	0.00	0.03	0.01	0.01	0.00	0.00	0.00	0.00	0.00	0.00	0.00		0.01	0.00	0.00	0.00	0.00	0.00
Fe2+	3.53	3.65	3.66	3.38	3.41	3.36	3.41	3.40	3.47	2.53	2.66	2.72	2.53	2.66		2.55	2.99	2.59	2.94	2.54	2.57
Mn2+	0.00	0.00	0.00	0.01	0.00	0.00	0.00	0.01	0.00	0.02	0.00	0.01	0.00	0.00		0.01	0.02	0.02	0.02	0.01	0.02
Mg	0.99	0.81	0.85	0.98	0.97	0.97	0.96	0.99	0.95	1.70	1.54	1.53	1.68	1.56		1.70	1.25	1.71	1.13	1.62	1.68
Ca	0.00	0.00	0.00	0.00	0.00	0.00	0.00	0.00	0.00	0.00	0.00	0.00	0.00	0.00		0.00	0.00	0.00	0.00	0.00	0.00
Na	0.00	0.00	0.00	0.00	0.00	0.00	0.00	0.00	0.00	0.00	0.00	0.00	0.00	0.00		0.00	0.00	0.00	0.00	0.00	0.00
K	0.00	0.00	0.00	0.00	0.00	0.00	0.00	0.00	0.00	0.00	0.00	0.00	0.00	0.00		0.00	0.00	0.00	0.00	0.00	0.00
O site	5.99	5.96	5.97	5.96	5.96	5.94	5.97	5.97	5.97	5.92	5.89	5.94	5.90	5.92		5.93	5.91	5.94	5.88	5.86	5.92
XFe	0.78	0.82	0.80	0.78	0.78	0.78	0.78	0.77	0.79	0.60	0.63	0.80	0.60	0.63		0.60	0.71	0.80	0.72	0.61	0.60
Al/(Al+Fe+Mg)	0.39	0.40	0.39	0.41	0.41	0.42	0.42	0.41	0.41	0.43	0.43	0.43	0.43	0.43		0.43	0.42	0.42	0.45	0.43	0.42
T (°C)	284	278	270	296	296	293	304	296	294	314	305	304	312	317		316	295	296	311	289	310
XChl	0.99	0.97	0.97	0.96	0.96	0.94	0.97	0.97	0.97	0.92	0.90	0.94	0.91	0.93		0.93	0.91	0.95	0.89	0.87	0.93
i/l cat	0.00	0.00	0.00	0.00	0.00	0.00	0.00	0.00	0.00	0.00	0.00	0.00	0.00	0.00		0.00	0.00	0.00	0.00	0.00	0.00
non-i/l	9.99	9.96	9.97	9.96	9.96	9.94	9.97	9.97	9.97	9.92	9.89	9.94	9.90	9.92		9.93	9.91	9.94	9.88	9.86	9.92

Sample:	VHG017															
Lithology:	FW: Contact Z.															
Analysis No.	Chl 1	Chl 2	Chl 3	Chl 4	Chl 5	Chl 6	Chl 7	Chl 8	Chl 9	Chl 10	Chl 11	Chl 12	Chl 13	Chl 14	Chl 15	Chl 16
Chlorite Type	II	II	II	II	II	II	II	II	II	II	II	II	II	II	II	II
SiO2	24.72	24.22	23.35	24.24	23.19	23.64	24.78	23.21	24.62	24.31	23.87	25.11	24.14	25.13	24.24	23.27
TiO2	1.58	0.00	0.00	0.00	0.00	0.00	0.00	0.00	0.00	0.00	0.00	0.00	0.00	0.00	0.00	0.00
Al2O3	25.53	26.59	24.91	26.57	24.92	25.01	25.91	24.82	25.96	26.46	25.56	26.69	25.83	26.44	26.00	23.92
Cr2O3	0.08	0.00	0.00	0.00	0.00	0.00	0.00	0.00	0.00	0.00	0.00	0.00	0.00	0.00	0.00	0.00
FeO	28.14	28.25	28.97	29.11	30.17	29.47	26.55	29.57	29.41	29.33	29.53	29.26	30.09	28.45	30.15	29.52
MnO	0.21	0.16	0.22	0.25	0.19	0.19	0.17	0.16	0.15	0.22	0.19	0.18	0.26	0.17	0.14	0.15
MgO	10.58	11.10	10.25	10.03	10.18	10.65	11.64	10.13	10.25	10.76	10.01	10.99	10.17	10.33	10.21	9.98
CaO	0.00	0.00	0.12	0.00	0.00	0.08	0.00	0.07	0.06	0.00	0.00	0.09	0.00	0.00	0.00	0.08
Na2O	0.00	0.00	0.00	0.00	0.00	0.00	0.00	0.00	0.00	0.00	0.00	0.06	0.00	0.00	0.00	0.00
K2O	0.00	0.00	0.06	0.18	0.00	0.00	0.18	0.00	0.00	0.00	0.00	0.00	0.00	0.31	0.00	0.00
F	0.00	0.00	0.00	0.00	0.00	0.00	0.00	0.00	0.00	0.00	0.00	0.00	0.00	0.00	0.00	0.00
Total	90.84	90.32	87.88	90.38	88.65	89.04	89.13	87.96	90.45	91.08	89.16	92.38	90.49	90.83	90.74	86.92
	6.16	6.20	6.44	6.22	6.42	6.36	6.23	6.46	6.22	6.18	6.34	6.07	6.25	6.15	6.23	6.54
SiIV	2.53	2.50	2.50	2.51	2.48	2.50	2.57	2.49	2.55	2.50	2.52	2.54	2.51	2.57	2.51	2.53
AlIV	1.47	1.50	1.50	1.49	1.52	1.50	1.43	1.51	1.45	1.50	1.48	1.46	1.49	1.43	1.49	1.47
T site	4.00	4.00	4.00	4.00	4.00	4.00	4.00	4.00	4.00	4.00	4.00	4.00	4.00	4.00	4.00	4.00
AlVI	1.62	1.73	1.65	1.76	1.62	1.62	1.73	1.64	1.72	1.71	1.70	1.72	1.68	1.77	1.69	1.60
Ti	0.12	0.00	0.00	0.00	0.00	0.00	0.00	0.00	0.00	0.00	0.00	0.00	0.00	0.00	0.00	0.00
Cr3+	0.01	0.00	0.00	0.00	0.00	0.00	0.00	0.00	0.00	0.00	0.00	0.00	0.00	0.00	0.00	0.00
Fe2+	2.41	2.44	2.60	2.52	2.70	2.61	2.30	2.66	2.55	2.52	2.61	2.47	2.62	2.44	2.61	2.69
Mn2+	0.02	0.01	0.02	0.02	0.02	0.02	0.01	0.01	0.01	0.02	0.02	0.02	0.02	0.01	0.01	0.01
Mg	1.62	1.71	1.64	1.55	1.62	1.68	1.78	1.62	1.58	1.65	1.57	1.66	1.58	1.58	1.58	1.62
Ca	0.00	0.00	0.01	0.00	0.00	0.01	0.00	0.01	0.01	0.00	0.00	0.01	0.00	0.00	0.00	0.01
Na	0.00	0.00	0.00	0.00	0.00	0.00	0.00	0.00	0.00	0.00	0.00	0.01	0.00	0.00	0.00	0.00
K	0.00	0.00	0.01	0.02	0.00	0.00	0.02	0.00	0.00	0.00	0.00	0.00	0.00	0.04	0.00	0.00
O site	5.80	5.89	5.93	5.87	5.95	5.94	5.85	5.94	5.87	5.90	5.89	5.88	5.90	5.84	5.90	5.93
XFe	0.60	0.59	0.61	0.62	0.62	0.61	0.56	0.62	0.62	0.60	0.62	0.60	0.62	0.61	0.62	0.62
Al/(Al+Fe+Mg)	0.43	0.44	0.43	0.44	0.42	0.42	0.44	0.42	0.43	0.43	0.43	0.44	0.43	0.44	0.43	0.42
T (℃)	305	314	310	308	315	311	301	312	300	312	306	304	307	296	307	303
XChl	0.81	0.90	0.91	0.86	0.96	0.94	0.84	0.94	0.87	0.91	0.90	0.87	0.91	0.81	0.91	0.93
i/l cat	0.00	0.00	0.02	0.02	0.00	0.01	0.02	0.01	0.01	0.00	0.00	0.02	0.00	0.04	0.00	0.01
non-i/l	9.80	9.89	9.91	9.85	9.95	9.93	9.83	9.93	9.86	9.90	9.89	9.86	9.90	9.80	9.90	9.93

Sample:	VHG058						Sample:	VHG063(B)					Sample:	VHG074				Sample:	VHG096						
Lithology:	FW: Contact Z.						Lithology	FW: Contact Z.					Lithology:	FW: Contact Z.				Lithology:	FW: Contact Z.						
Analysis No.	Chl 1	Chl 2	Chl 3	Chl 4	Chl 5	Chl 6	Chl 2	Chl 3	Chl 5	Chl 6	Chl 7		Chl 16	Chl 19	Chl 20	Chl 21		Chl 1	Chl 2	Chl 3	Chl 4	Chl 5	Chl 6	Chl 7
Chlorite Type	I	II	II	II	II	II	II	II	I	II	II		II	II	II	II								
SiO2	24.87	25.34	25.19	24.11	24.62	25.00	25.08	26.54	25.52	25.62	25.08		23.98	24.22	24.49	25.16		23.31	23.01	23.25	24.51	24.32	24.19	23.82
TiO2	0.00	0.00	0.00	0.00	0.00	0.00	0.00	0.00	0.00	0.00	0.00		0.00	0.00	0.00	0.00		0.00	0.00	0.00	0.00	0.00	0.00	0.00
Al2O3	26.80	26.77	26.96	25.58	26.62	26.75	27.25	26.36	27.63	27.09	26.82		24.39	24.82	24.09	24.59		25.53	26.00	25.85	26.66	25.87	25.77	26.05
Cr2O3	0.10	0.00	0.00	0.15	0.00	0.00	0.15	0.09	0.00	0.07	0.13		0.00	0.00	0.24	0.00		0.08	0.00	0.00	0.00	0.00	0.08	0.00
FeO	24.25	24.41	24.89	24.01	24.78	23.62	23.91	22.61	22.20	21.88	23.27		25.76	25.52	25.05	25.11		26.80	30.19	26.12	26.65	25.24	25.49	25.32
MnO	0.27	0.32	0.23	0.27	0.26	0.23	0.19	0.19	0.20	0.21	0.22		0.25	0.24	0.23	0.25		0.16	0.20	0.21	0.18	0.14	0.15	0.13
MgO	14.24	13.91	13.81	14.21	14.37	14.60	14.37	14.03	14.46	14.36	14.24		13.85	13.22	14.23	14.78		11.22	10.48	11.11	10.86	11.19	11.92	11.13
CaO	0.00	0.06	0.06	0.06	0.06	0.00	0.08	0.11	0.08	0.00	0.06		0.00	0.00	0.00	0.00		0.05	0.00	0.00	0.00	0.06	0.00	0.00
Na2O	0.00	0.00	0.06	0.00	0.00	0.00	0.10	0.07	0.00	0.00	0.08		0.00	0.00	0.00	0.00		0.00	0.00	0.00	0.00	0.00	0.00	0.00
K2O	0.00	0.00	0.00	0.08	0.00	0.00	0.00	0.06	0.23	0.20	0.00		0.00	0.00	0.00	0.00		0.05	0.00	0.05	0.00	0.04	0.00	0.00
F	0.00	0.00	0.00	0.00	0.00	0.00	0.00	0.00	0.00	0.00	0.00		0.00	0.00	0.00	0.00		0.00	0.00	0.00	0.00	0.00	0.00	0.00
Total	90.53	90.81	91.20	88.47	90.71	90.20	91.13	90.06	90.34	89.43	89.90		88.23	88.02	88.33	89.89		87.20	89.88	88.59	88.86	86.86	87.60	86.45
	6.05	6.03	6.02	6.22	6.06	6.05	6.00	6.01	5.99	6.04	6.06		6.30	6.30	6.27	6.14		6.41	6.32	6.43	6.24	6.36	6.31	6.39
SiIV	2.51	2.54	2.52	2.50	2.48	2.52	2.50	2.65	2.54	2.57	2.53		2.51	2.54	2.55	2.57		2.49	2.42	2.49	2.55	2.57	2.54	2.53
AlIV	1.49	1.46	1.48	1.50	1.52	1.48	1.50	1.35	1.46	1.43	1.47		1.49	1.46	1.45	1.43		1.51	1.58	1.51	1.45	1.43	1.46	1.47
T site	4.00	4.00	4.00	4.00	4.00	4.00	4.00	4.00	4.00	4.00	4.00		4.00	4.00	4.00	4.00		4.00	4.00	4.00	4.00	4.00	4.00	4.00
AlVI	1.69	1.71	1.71	1.62	1.65	1.69	1.71	1.76	1.79	1.78	1.72		1.53	1.61	1.52	1.53		1.70	1.65	1.75	1.81	1.80	1.73	1.80
Ti	0.00	0.00	0.00	0.00	0.00	0.00	0.00	0.00	0.00	0.00	0.00		0.00	0.00	0.00	0.00		0.00	0.00	0.00	0.00	0.00	0.00	0.00
Cr3+	0.01	0.00	0.00	0.01	0.00	0.00	0.01	0.01	0.00	0.01	0.01		0.00	0.00	0.02	0.00		0.01	0.00	0.00	0.00	0.00	0.01	0.00
Fe2+	2.04	2.05	2.09	2.08	2.09	1.99	2.00	1.89	1.85	1.84	1.96		2.26	2.24	2.19	2.15		2.39	2.66	2.34	2.31	2.23	2.24	2.25
Mn2+	0.02	0.03	0.02	0.02	0.02	0.02	0.02	0.02	0.02	0.02	0.02		0.02	0.02	0.02	0.02		0.01	0.02	0.02	0.02	0.01	0.01	0.01
Mg	2.14	2.08	2.06	2.19	2.16	2.19	2.14	2.09	2.15	2.15	2.14		2.16	2.06	2.21	2.25		1.78	1.64	1.77	1.68	1.76	1.87	1.76
Ca	0.00	0.01	0.01	0.01	0.01	0.00	0.01	0.01	0.01	0.00	0.01		0.00	0.00	0.00	0.00		0.01	0.00	0.00	0.00	0.01	0.00	0.00
Na	0.00	0.00	0.01	0.00	0.00	0.00	0.02	0.01	0.00	0.00	0.02		0.00	0.00	0.00	0.00		0.00	0.00	0.00	0.00	0.00	0.00	0.00
K	0.00	0.00	0.00	0.01	0.00	0.00	0.00	0.01	0.03	0.03	0.00		0.00	0.00	0.00	0.00		0.01	0.00	0.01	0.00	0.01	0.00	0.00
O site	5.90	5.88	5.89	5.94	5.93	5.89	5.90	5.80	5.84	5.82	5.88		5.98	5.93	5.95	5.95		5.91	5.97	5.88	5.82	5.82	5.86	5.83
XFe	0.49	0.50	0.50	0.49	0.49	0.48	0.48	0.47	0.46	0.46	0.48		0.51	0.52	0.50	0.49		0.57	0.62	0.57	0.58	0.56	0.55	0.56
Al/(Al+Fe+Mg	0.43	0.43	0.43	0.42	0.43	0.43	0.44	0.44	0.45	0.45	0.44		0.41	0.42	0.40	0.40		0.43	0.43	0.44	0.45	0.45	0.44	0.45
T (°C)	322	313	316	324	326	320	322	291	316	309	317		317	312	310	308		318	327	318	305	301	309	309
XChl	0.91	0.88	0.88	0.93	0.93	0.90	0.88	0.79	0.82	0.81	0.87		0.98	0.93	0.96	0.95		0.90	0.97	0.89	0.84	0.82	0.87	0.85
i/I cat	0.00	0.01	0.02	0.02	0.01	0.00	0.03	0.03	0.04	0.03	0.02		0.00	0.00	0.00	0.00		0.01	0.00	0.01	0.00	0.01	0.00	0.00
non-i/I	9.90	9.87	9.87	9.92	9.93	9.89	9.87	9.77	9.80	9.80	9.86		9.98	9.93	9.95	9.95		9.89	9.97	9.88	9.82	9.81	9.86	9.83

Sample:	VHG091(B)						Sample:	VHG125				Sample:	VHG170			
Lithology:	FW: Contact Z.						Lithology:	FW:Contact Z.				Lithology	FW: Contact Z.			
Analysis No.	Chl 1	Chl 2	Chl 3	Chl 4	Chl 5	Chl 8	Chl 15	Chl 16	Chl 17	Chl 18	Chl 19	Chl 6	Chl 7	Chl 8 +Gn	Chl 9	Chl 10
Chlorite Type	I	II	II	II	II	II	II	II	II	II	II	II	II		II	II
SiO2	24.45	24.40	24.27	24.74	24.78	24.42	24.18	24.59	25.24	24.26	24.40	23.54	23.46	23.73	23.45	23.66
TiO2	0.00	0.00	0.00	0.00	0.11	0.00	0.00	0.00	0.00	0.00	0.00	0.00	0.00	0.00	0.00	0.00
Al2O3	25.39	25.29	25.68	26.06	25.48	25.78	25.95	26.24	26.11	26.20	25.83	25.81	26.17	25.20	25.96	26.03
Cr2O3	0.09	0.09	0.14	0.24	0.09	0.08	0.00	0.09	0.00	0.00	0.09	0.00	0.00	0.00	0.00	0.00
FeO	24.31	25.14	24.74	24.66	24.52	24.64	26.69	26.26	26.75	26.20	26.95	31.81	32.99	31.07	30.73	29.71
MnO	0.17	0.17	0.22	0.26	0.25	0.26	0.23	0.25	0.24	0.24	0.18	0.16	0.14	0.00	0.18	0.18
MgO	14.37	13.45	12.71	12.87	13.35	13.52	13.46	14.13	12.66	13.45	13.13	9.42	7.18	8.22	9.40	9.84
CaO	0.00	0.00	0.00	0.00	0.00	0.00	0.00	0.00	0.00	0.00	0.00	0.00	0.06	0.00	0.00	0.00
Na2O	0.00	0.00	0.00	0.00	0.00	0.00	0.00	0.00	0.00	0.00	0.00	0.00	0.00	0.00	0.00	0.00
K2O	0.00	0.06	0.13	0.18	0.00	0.00	0.00	0.00	0.17	0.00	0.00	0.00	0.05	0.00	0.10	0.00
F	0.00	0.00	0.00	0.00	0.00	0.00	0.00	0.00	0.00	0.00	0.00	0.00	0.00	0.00	0.00	0.00
Total	88.78	88.60	87.89	89.01	88.58	88.70	90.51	91.56	91.17	90.35	90.58	90.74	90.05	88.22	89.82	89.42
	6.19	6.24	6.27	6.18	6.21	6.21	6.15	6.06	6.08	6.14	6.15	6.30	6.39	6.46	6.34	6.32
SiIV	2.52	2.53	2.53	2.55	2.56	2.52	2.47	2.48	2.56	2.48	2.50	2.47	2.49	2.55	2.47	2.49
AlIV	1.48	1.47	1.47	1.45	1.44	1.48	1.53	1.52	1.44	1.52	1.50	1.53	1.51	1.45	1.53	1.51
T site	4.00	4.00	4.00	4.00	4.00	4.00	4.00	4.00	4.00	4.00	4.00	4.00	4.00	4.00	4.00	4.00
AlVI	1.61	1.63	1.70	1.71	1.66	1.66	1.60	1.60	1.67	1.64	1.61	1.66	1.77	1.74	1.70	1.72
Ti	0.00	0.00	0.00	0.00	0.01	0.00	0.00	0.00	0.00	0.00	0.00	0.00	0.00	0.00	0.00	0.00
Cr3+	0.01	0.01	0.01	0.02	0.01	0.01	0.00	0.01	0.00	0.00	0.01	0.00	0.00	0.00	0.00	0.00
Fe2+	2.10	2.18	2.16	2.12	2.12	2.13	2.28	2.21	2.27	2.24	2.31	2.79	2.93	2.79	2.71	2.82
Mn2+	0.01	0.01	0.02	0.02	0.02	0.02	0.02	0.02	0.02	0.02	0.02	0.01	0.01	0.00	0.02	0.02
Mg	2.21	2.08	1.98	1.97	2.06	2.08	2.05	2.12	1.91	2.05	2.00	1.47	1.14	1.32	1.48	1.54
Ca	0.00	0.00	0.00	0.00	0.00	0.00	0.00	0.00	0.00	0.00	0.00	0.00	0.01	0.00	0.00	0.00
Na	0.00	0.00	0.00	0.00	0.00	0.00	0.00	0.00	0.00	0.00	0.00	0.00	0.00	0.00	0.00	0.00
K	0.00	0.01	0.02	0.02	0.00	0.00	0.00	0.00	0.02	0.00	0.00	0.00	0.01	0.00	0.01	0.00
O site	5.93	5.92	5.88	5.87	5.88	5.90	5.96	5.96	5.89	5.94	5.94	5.94	5.87	5.85	5.92	5.89
XFe	0.49	0.51	0.52	0.52	0.51	0.51	0.53	0.51	0.54	0.52	0.54	0.65	0.72	0.68	0.65	0.63
Al/(Al+Fe+Mg)	0.42	0.42	0.43	0.44	0.43	0.43	0.42	0.42	0.43	0.42	0.42	0.43	0.45	0.44	0.44	0.44
T(°C)	318	314	312	310	308	316	325	325	306	324	319	314	302	294	314	312
XChl	0.94	0.92	0.88	0.86	0.89	0.91	0.96	0.96	0.88	0.95	0.95	0.94	0.87	0.87	0.91	0.90
i/l cat	0.00	0.01	0.02	0.02	0.00	0.00	0.00	0.00	0.02	0.00	0.00	0.00	0.01	0.00	0.01	0.00
non-i/l	9.93	9.91	9.86	9.84	9.88	9.90	9.96	9.96	9.87	9.94	9.94	9.94	9.86	9.85	9.90	9.89

Sample:	VHG026							Sample: VHG045							
Lithology:	HW: Contact Z.							Lithology: HW: Contact Z.							
Analysis No.	Chl 1	Chl 2	Chl 3	Chl 4	Chl 5	Chl 6	Chl 7	Chl 1	Chl 2	Chl 3	Chl 4	Chl 5	Chl 6	Chl 7	Chl 8
Chlorite Type															
SiO2	24.53	23.97	24.29	24.57	24.90	24.81	24.04	24.80	25.36	24.32	25.48	23.93	23.69	24.06	25.52
TiO2	0.00	0.00	0.00	0.00	0.00	0.00	0.00	0.00	0.07	0.00	0.08	0.00	0.00	0.00	0.00
Al2O3	25.08	24.16	24.38	24.75	24.70	24.52	24.94	23.87	21.49	24.87	22.53	23.30	24.47	24.18	24.25
Cr2O3	0.00	0.08	0.00	0.00	0.09	0.00	0.10	0.11	0.00	0.13	0.00	0.10	0.10	0.09	0.11
FeO	29.08	29.33	29.39	29.56	29.35	29.78	29.87	30.01	26.26	28.46	28.79	28.65	27.57	28.80	28.65
MnO	0.15	0.00	0.00	0.17	0.13	0.18	0.14	0.25	0.16	0.14	0.26	0.14	0.00	0.19	0.13
MgO	11.66	11.88	11.81	12.05	11.82	11.75	11.78	11.95	14.22	12.16	13.86	12.43	12.36	12.83	13.42
CaO	0.00	0.00	0.00	0.00	0.00	0.00	0.00	0.13	0.06	0.00	0.00	0.00	0.00	0.00	0.00
Na2O	0.00	0.00	0.00	0.00	0.00	0.00	0.00	0.00	0.00	0.00	0.00	0.00	0.00	0.00	0.00
K2O	0.00	0.00	0.00	0.00	0.00	0.00	0.00	0.00	0.00	0.00	0.00	0.00	0.00	0.00	0.00
F	0.00	0.00	0.00	0.00	0.00	0.00	0.00	0.00	0.00	0.00	0.00	0.00	0.00	0.00	0.00
Total	90.50	89.42	89.87	91.10	90.99	91.04	90.87	91.12	87.62	90.08	91.00	88.55	88.19	90.15	92.08
	6.22	6.33	6.28	6.20	6.19	6.21	6.23	6.22	6.37	6.24	6.19	6.38	6.36	6.26	6.09
SiIV	2.54	2.52	2.54	2.53	2.57	2.56	2.49	2.57	2.69	2.53	2.63	2.54	2.51	2.51	2.59
AlIV	1.46	1.48	1.46	1.47	1.43	1.44	1.51	1.43	1.31	1.47	1.37	1.46	1.49	1.49	1.41
T site	4.00	4.00	4.00	4.00	4.00	4.00	4.00	4.00	4.00	4.00	4.00	4.00	4.00	4.00	4.00
AlVI	1.60	1.52	1.55	1.54	1.57	1.55	1.54	1.48	1.37	1.57	1.36	1.46	1.56	1.48	1.48
Ti	0.00	0.00	0.00	0.00	0.00	0.00	0.00	0.00	0.01	0.00	0.01	0.00	0.00	0.00	0.00
Cr3+	0.00	0.01	0.00	0.00	0.01	0.00	0.01	0.01	0.00	0.01	0.00	0.01	0.01	0.01	0.01
Fe2+	2.52	2.58	2.57	2.55	2.53	2.57	2.59	2.60	2.33	2.47	2.48	2.55	2.44	2.51	2.43
Mn2+	0.01	0.00	0.00	0.01	0.01	0.02	0.01	0.02	0.01	0.01	0.02	0.01	0.00	0.02	0.01
Mg	1.80	1.86	1.84	1.85	1.82	1.81	1.82	1.84	2.25	1.88	2.13	1.97	1.95	1.99	2.03
Ca	0.00	0.00	0.00	0.00	0.00	0.00	0.00	0.01	0.01	0.00	0.00	0.00	0.00	0.00	0.00
Na	0.00	0.00	0.00	0.00	0.00	0.00	0.00	0.00	0.00	0.00	0.00	0.00	0.00	0.00	0.00
K	0.00	0.00	0.00	0.00	0.00	0.00	0.00	0.00	0.00	0.00	0.00	0.00	0.00	0.00	0.00
O site	5.93	5.97	5.96	5.96	5.93	5.94	5.98	5.97	5.97	5.95	6.00	5.99	5.96	6.00	5.96
XFe	0.58	0.58	0.58	0.58	0.58	0.59	0.59	0.58	0.51	0.57	0.54	0.56	0.56	0.56	0.55
Al/(Al+Fe+Mg)	0.41	0.40	0.41	0.41	0.41	0.41	0.41	0.40	0.37	0.41	0.37	0.39	0.41	0.40	0.39
T (°C)	305	309	305	307	300	300	315	299	281	310	291	307	315	315	299
XChl	0.94	0.98	0.96	0.96	0.94	0.95	0.98	0.96	0.97	0.95	1.00	1.00	0.96	1.00	0.96
i/l cat	0.00	0.00	0.00	0.00	0.00	0.00	0.00	0.01	0.01	0.00	0.00	0.00	0.00	0.00	0.00
non-i/l	9.93	9.97	9.96	9.96	9.93	9.94	9.98	9.96	9.96	9.95	10.00	9.99	9.96	10.00	9.96

Sample:	VHG055(A)				Sample:	VHG171				
Lithology:	HW: Contact Z.				Lithology:	HW: Contact Z.				
Analysis No.	Chl 6	Chl 7	Chl 9	Chl 10	Chl 1	Chl 2	Chl 3	Chl 4	Chl 5	Chl 6
Chlorite Type					Amyg	Amyg	Vn	Amyg	Amyg	Amyg
SiO2	23.73	23.88	23.64	24.57	24.00	23.49	23.09	24.01	23.93	24.41
TiO2	0.00	0.00	0.28	0.00	0.00	0.00	0.00	0.00	0.00	0.00
Al2O3	24.06	24.42	24.63	24.65	25.65	25.55	25.57	25.43	24.80	24.77
Cr2O3	0.15	0.15	0.00	0.09	0.00	0.08	0.00	0.00	0.00	0.09
FeO	31.24	31.45	30.52	32.55	28.53	29.10	29.79	28.34	28.85	28.71
MnO	0.13	0.00	0.00	0.00	0.24	0.17	0.22	0.24	0.23	0.22
MgO	10.64	10.27	10.61	9.65	10.85	10.73	9.95	11.33	11.25	11.47
CaO	0.00	0.00	0.00	0.00	0.00	0.00	0.00	0.00	0.00	0.06
Na2O	0.00	0.00	0.00	0.00	0.00	0.00	0.00	0.00	0.00	0.00
K2O	0.00	0.00	0.00	0.00	0.09	0.00	0.00	0.07	0.00	0.00
F	0.00	0.00	0.00	0.00	0.00	0.00	0.00	0.00	0.00	0.00
Total	89.95	90.17	89.68	91.51	89.36	89.12	88.62	89.42	89.06	89.73
	6.36	6.34	6.34	6.26	6.29	6.34	6.41	6.28	6.33	6.28
SiIV	2.51	2.52	2.50	2.56	2.51	2.48	2.46	2.51	2.52	2.55
AlIV	1.49	1.48	1.50	1.44	1.49	1.52	1.54	1.49	1.48	1.45
T site	4.00	4.00	4.00	4.00	4.00	4.00	4.00	4.00	4.00	4.00
AlVI	1.51	1.56	1.56	1.58	1.68	1.65	1.68	1.65	1.60	1.60
Ti	0.00	0.00	0.02	0.00	0.00	0.00	0.00	0.00	0.00	0.00
Cr3+	0.01	0.01	0.00	0.01	0.00	0.01	0.00	0.00	0.00	0.01
Fe2+	2.77	2.77	2.70	2.83	2.50	2.57	2.66	2.48	2.54	2.51
Mn2+	0.01	0.00	0.00	0.00	0.02	0.02	0.02	0.02	0.02	0.02
Mg	1.68	1.61	1.67	1.50	1.69	1.69	1.58	1.77	1.77	1.79
Ca	0.00	0.00	0.00	0.00	0.00	0.00	0.00	0.00	0.00	0.01
Na	0.00	0.00	0.00	0.00	0.00	0.00	0.00	0.00	0.00	0.00
K	0.00	0.00	0.00	0.00	0.01	0.00	0.00	0.01	0.00	0.00
O site	5.98	5.96	5.95	5.92	5.91	5.93	5.93	5.92	5.94	5.93
XFe	0.62	0.63	0.62	0.65	0.60	0.60	0.60	0.58	0.59	0.58
Al/(Al+Fe+Mg)	0.40	0.41	0.41	0.41	0.43	0.43	0.43	0.42	0.42	0.42
T (°C)	308	305	312	295	310	317	302	311	308	303
XChl	0.98	0.96	0.95	0.93	0.90	0.94	0.94	0.92	0.94	0.93
i/l cat	0.00	0.00	0.00	0.00	0.01	0.00	0.00	0.01	0.00	0.01
non-i/l	9.98	9.96	9.95	9.92	9.89	9.93	9.93	9.91	9.94	9.92

Sample:	VHG047																
Lithology:	HW: Dark Pheno Zone																
Analysis No.	Chl 1	Chl 2	Chl 3	Chl 4	Chl 5 around Cc	Chl 6	Chl 7	Chl 8	Chl 9	Chl 10	Chl 11	Chl 1a	Chl 2a	Chl 3a	Chl 4a	Chl 5a	Chl 6a
Chlorite Type																	
SiO2	25.21	25.76	25.88	25.58	25.25	25.83	25.68	26.15	26.56	25.15	30.28	25.25	25.83	25.68	26.15	26.56	25.15
TiO2	0.30	0.00	0.00	1.81	0.55	0.00	0.17	0.00	0.13	0.27	0.00	0.55	0.00	0.17	0.00	0.13	0.27
Al2O3	22.78	22.49	24.20	21.73	23.45	23.22	23.36	23.17	22.57	23.73	22.15	23.45	23.22	23.36	23.17	22.57	23.73
Cr2O3	1.47	0.25	0.00	0.11	0.37	0.38	0.35	0.66	0.63	0.75	0.00	0.37	0.38	0.35	0.66	0.63	0.75
FeO	26.78	25.76	26.05	25.78	26.90	26.15	26.21	26.44	26.29	26.79	25.48	26.90	26.15	26.21	26.44	26.29	26.79
MnO	0.00	0.13	0.12	0.00	0.14	0.00	0.00	0.14	0.00	0.00	0.00	0.14	0.00	0.00	0.14	0.00	0.00
MgO	14.23	14.55	14.44	15.03	14.18	13.52	14.38	14.33	14.15	14.36	13.63	14.18	13.52	14.38	14.33	14.15	14.36
CaO	0.00	0.00	0.12	0.18	0.00	0.08	0.00	0.00	0.00	0.11	0.42	0.00	0.08	0.00	0.00	0.00	0.11
Na2O	0.00	0.00	0.00	0.00	0.00	0.00	0.00	0.00	0.00	0.00	0.00	0.00	0.00	0.00	0.00	0.00	0.00
K2O	0.00	0.00	0.00	0.00	0.06	0.00	0.00	0.13	0.12	0.00	0.00	0.06	0.00	0.00	0.13	0.12	0.00
F	0.00	0.00	0.00	0.00	0.00	0.00	0.00	0.00	0.00	0.00	0.00	0.00	0.00	0.00	0.00	0.00	0.00
Total	90.77	88.94	90.81	90.22	90.90	89.18	90.15	91.02	90.45	91.16	91.96	90.90	89.18	90.15	91.02	90.45	91.16
	6.16	6.23	6.09	6.16	6.14	6.22	6.15	6.11	6.13	6.12	5.94	6.14	6.22	6.15	6.11	6.13	6.12
SiIV	2.59	2.67	2.62	2.62	2.58	2.67	2.63	2.66	2.71	2.56	2.99	2.58	2.67	2.63	2.66	2.71	2.56
AlIV	1.41	1.33	1.38	1.38	1.42	1.33	1.37	1.34	1.29	1.44	1.01	1.42	1.33	1.37	1.34	1.29	1.44
T site	4.00	4.00	4.00	4.00	4.00	4.00	4.00	4.00	4.00	4.00	4.00	4.00	4.00	4.00	4.00	4.00	4.00
AlVI	1.34	1.42	1.52	1.25	1.40	1.51	1.45	1.43	1.43	1.41	1.57	1.40	1.51	1.45	1.43	1.43	1.41
Ti	0.02	0.00	0.00	0.14	0.04	0.00	0.01	0.00	0.01	0.02	0.00	0.04	0.00	0.01	0.00	0.01	0.02
Cr3+	0.12	0.02	0.00	0.01	0.03	0.03	0.03	0.05	0.05	0.06	0.00	0.03	0.03	0.03	0.05	0.05	0.06
Fe2+	2.30	2.24	2.21	2.21	2.30	2.26	2.25	2.25	2.24	2.28	2.11	2.30	2.26	2.25	2.25	2.24	2.28
Mn2+	0.00	0.01	0.01	0.00	0.01	0.00	0.00	0.01	0.00	0.00	0.00	0.01	0.00	0.00	0.01	0.00	0.00
Mg	2.18	2.25	2.18	2.30	2.16	2.09	2.19	2.17	2.15	2.18	2.01	2.16	2.09	2.19	2.17	2.15	2.18
Ca	0.00	0.00	0.01	0.02	0.00	0.01	0.00	0.00	0.00	0.01	0.04	0.00	0.01	0.00	0.00	0.00	0.01
Na	0.00	0.00	0.00	0.00	0.00	0.00	0.00	0.00	0.00	0.00	0.00	0.00	0.00	0.00	0.00	0.00	0.00
K	0.00	0.00	0.00	0.00	0.01	0.00	0.00	0.02	0.02	0.00	0.00	0.01	0.00	0.00	0.02	0.02	0.00
O site	5.95	5.94	5.93	5.93	5.95	5.90	5.93	5.93	5.90	5.97	5.73	5.95	5.90	5.93	5.93	5.90	5.97
XFe	0.51	0.50	0.50	0.49	0.52	0.52	0.51	0.51	0.51	0.51	0.51	0.52	0.52	0.51	0.51	0.51	0.51
Al/(Al+Fe+Mg)	0.38	0.38	0.40	0.37	0.39	0.39	0.39	0.39	0.38	0.39	0.39	0.39	0.39	0.39	0.39	0.38	0.39
T (°C)	302	285	295	296	303	283	293	287	276	307	216	303	283	293	287	276	307
XChl	0.96	0.95	0.93	0.91	0.95	0.90	0.94	0.92	0.89	0.96	0.72	0.95	0.90	0.94	0.92	0.89	0.96
i/l cat	0.00	0.00	0.01	0.02	0.01	0.01	0.00	0.02	0.02	0.01	0.04	0.01	0.01	0.00	0.02	0.02	0.01
non-i/l	9.95	9.94	9.92	9.91	9.94	9.89	9.93	9.91	9.88	9.96	9.69	9.94	9.89	9.93	9.91	9.88	9.96

Sample:	VHG082						VHG083						VHG084							VHG084(A)						
Lithology:	HW: Black Phenocryst Z.						HW: Black Phenocryst Z.						HW: Contact Z.							HW: Contact Z.						
Analysis No.	Chl 1	Chl 2	Chl 3	Chl 4	Chl 5	Chl 6	Chl 2	Chl 3	Chl 4	Chl 5	Chl 6	Chl 7	Chl 1	Chl 2	Chl 3	Chl 4	Chl 5	Chl 6	Chl 7	Chl 1	Chl 2	Chl 3	Chl 4	Chl 5	Chl 6	Chl 7
Chlorite Type																										
SiO2	30.39	24.68	25.19	24.37	24.81	24.53	24.43	24.43	24.10	23.88	24.06	24.34	23.93	23.88	24.43	24.03	24.44	24.61	24.17	24.41	23.80	24.24	24.47	24.29	24.76	24.58
TiO2	0.00	0.00	0.25	0.00	0.17	0.00	0.10	0.00	0.00	0.00	0.00	0.00	0.00	0.00	0.00	0.00	0.00	0.00	0.00	0.00	0.00	0.00	0.00	0.00	0.00	0.00
Al2O3	22.05	24.56	23.29	24.77	24.25	24.21	23.09	23.07	25.32	24.59	24.30	23.85	25.18	25.43	24.43	25.63	25.49	25.24	24.81	24.92	24.85	24.76	25.53	24.38	26.21	24.87
Cr2O3	0.00	0.00	0.00	0.00	0.00	0.00	1.54	0.59	0.08	0.48	0.08	0.40	0.00	0.11	0.00	0.00	0.00	0.10	0.00	0.00	0.00	0.00	0.00	0.09	0.22	0.13
FeO	23.21	24.82	25.01	25.09	24.97	24.93	25.33	26.87	25.23	26.46	26.00	26.44	28.14	28.26	28.10	27.68	27.54	27.80	28.45	28.70	28.22	29.63	27.39	27.88	28.96	27.58
MnO	0.17	0.00	0.00	0.00	0.23	0.12	0.16	0.22	0.18	0.19	0.17	0.21	0.16	0.17	0.24	0.14	0.15	0.24	0.24	0.22	0.21	0.16	0.29	0.26	0.25	0.22
MgO	13.88	14.18	14.68	14.10	14.64	14.35	13.44	14.27	12.88	13.14	13.81	13.56	11.81	11.72	12.56	11.52	11.72	12.17	12.47	11.81	11.82	11.56	12.18	12.81	11.52	12.14
CaO	0.30	0.12	0.12	0.07	0.17	0.44	0.00	0.00	0.00	0.00	0.19	0.00	0.00	0.00	0.00	0.00	0.00	0.05	0.00	0.00	0.00	0.00	0.00	0.00	0.00	0.00
Na2O	0.00	0.00	0.00	0.00	0.00	0.00	0.00	0.00	0.00	0.00	0.00	0.00	0.00	0.00	0.00	0.00	0.00	0.00	0.00	0.00	0.00	0.00	0.00	0.00	0.00	0.00
K2O	0.06	0.00	0.00	0.00	0.00	0.00	0.00	0.00	0.05	0.00	0.00	0.00	0.00	0.00	0.00	0.00	0.00	0.00	0.00	0.00	0.00	0.00	0.00	0.00	0.00	0.00
F	0.00	0.00	0.00	0.00	0.00	0.00	0.00	0.00	0.00	0.00	0.00	0.00	0.00	0.00	0.00	0.00	0.00	0.00	0.00	0.00	0.00	0.00	0.00	0.00	0.22	0.00
Total	90.06	88.36	88.74	88.40	89.24	88.56	88.09	88.45	87.84	88.74	88.61	88.80	89.04	89.57	89.76	88.98	89.34	90.21	90.14	90.06	88.90	90.37	89.84	89.71	90.18	89.52
	6.00	6.24	6.23	6.25	6.20	6.26	5.32	5.30	5.30	5.29	5.29	5.29	5.31	5.27	5.26	5.29	5.25	5.20	5.24	5.26	5.33	5.26	5.21	5.26	5.17	5.25
SiIV	3.03	2.56	2.61	2.54	2.56	2.55	2.57	2.56	2.53	2.50	2.52	2.55	2.51	2.49	2.54	2.51	2.54	2.54	2.51	2.54	2.51	2.52	2.53	2.53	2.54	2.56
AlIV	0.97	1.44	1.39	1.46	1.44	1.45	1.43	1.44	1.47	1.50	1.48	1.45	1.49	1.51	1.46	1.49	1.46	1.46	1.49	1.46	1.49	1.48	1.47	1.47	1.46	1.44
T site	4.00	4.00	4.00	4.00	4.00	4.00	4.00	4.00	4.00	4.00	4.00	4.00	4.00	4.00	4.00	4.00	4.00	4.00	4.00	4.00	4.00	4.00	4.00	4.00	4.00	4.00
AlVI	1.83	1.57	1.46	1.57	1.51	1.52	1.44	1.42	1.65	1.54	1.52	1.49	1.63	1.62	1.54	1.66	1.67	1.61	1.55	1.59	1.59	1.56	1.64	1.52	1.72	1.60
Ti	0.00	0.00	0.02	0.00	0.01	0.00	0.01	0.00	0.00	0.00	0.00	0.00	0.00	0.00	0.00	0.00	0.00	0.00	0.00	0.00	0.00	0.00	0.00	0.00	0.00	0.00
Cr3+	0.00	0.00	0.00	0.00	0.00	0.00	0.13	0.05	0.01	0.04	0.01	0.03	0.00	0.01	0.00	0.00	0.00	0.01	0.00	0.00	0.00	0.00	0.00	0.01	0.02	0.01
Fe2+	1.94	2.18	2.17	2.18	2.15	2.17	2.23	2.27	2.21	2.32	2.28	2.31	2.47	2.47	2.45	2.42	2.40	2.40	2.47	2.50	2.49	2.58	2.37	2.43	2.32	2.40
Mn2+	0.01	0.00	0.00	0.00	0.02	0.01	0.01	0.02	0.02	0.02	0.02	0.02	0.02	0.02	0.02	0.01	0.01	0.02	0.02	0.02	0.02	0.01	0.03	0.02	0.02	0.02
Mg	2.08	2.20	2.30	2.19	2.25	2.23	2.11	2.23	2.01	2.05	2.15	2.11	1.82	1.82	1.95	1.80	1.82	1.87	1.83	1.83	1.86	1.80	1.87	1.99	1.76	1.88
Ca	0.03	0.01	0.01	0.01	0.02	0.05	0.00	0.00	0.00	0.00	0.02	0.00	0.00	0.00	0.00	0.00	0.00	0.01	0.00	0.00	0.00	0.00	0.00	0.00	0.00	0.00
Na	0.00	0.00	0.00	0.00	0.00	0.00	0.00	0.00	0.00	0.00	0.00	0.00	0.00	0.00	0.00	0.00	0.00	0.00	0.00	0.00	0.00	0.00	0.00	0.00	0.00	0.00
K	0.01	0.00	0.00	0.00	0.00	0.00	0.00	0.00	0.01	0.00	0.00	0.00	0.00	0.00	0.00	0.00	0.00	0.00	0.00	0.00	0.00	0.00	0.00	0.00	0.03	0.00
O site	5.88	5.94	5.95	5.95	5.96	5.98	5.92	5.99	5.91	5.98	5.99	5.97	5.93	5.94	5.96	5.90	5.89	5.92	5.97	5.94	5.95	5.96	5.91	5.97	5.86	5.91
XFe	0.48	0.50	0.49	0.50	0.49	0.49	0.51	0.50	0.52	0.53	0.51	0.52	0.58	0.58	0.56	0.57	0.57	0.56	0.58	0.58	0.57	0.59	0.56	0.55	0.57	0.56
Al/(Al+Fe+Mg	0.39	0.41	0.39	0.41	0.40	0.40	0.40	0.39	0.43	0.41	0.40	0.40	0.42	0.42	0.41	0.43	0.43	0.42	0.41	0.41	0.42	0.41	0.42	0.40	0.44	0.42
T (°C)	210	308	300	314	310	311	305	308	314	319	317	310	312	316	307	312	306	307	314	307	314	308	310	311	306	304
XChl	0.67	0.93	0.94	0.95	0.95	0.94	0.93	0.99	0.91	0.96	0.97	0.97	0.94	0.94	0.96	0.91	0.90	0.92	0.97	0.94	0.96	0.96	0.92	0.97	0.85	0.92
i/l cat	0.04	0.01	0.01	0.01	0.02	0.05	0.00	0.00	0.01	0.00	0.02	0.00	0.00	0.00	0.00	0.00	0.00	0.01	0.00	0.00	0.00	0.00	0.00	0.00	0.03	0.00
non-i/l	9.64	9.92	9.94	9.94	9.94	9.93	9.92	9.99	9.90	9.96	9.97	9.97	9.93	9.94	9.96	9.90	9.89	9.92	9.97	9.94	9.95	9.96	9.91	9.97	9.84	9.91

Sample:	VHG126				Sample:	VHG183				
Lithology:	HW 150m above VCR				Lithology:	HW > 200m above VCR				
Analysis No.	Chl 1	Chl 2	Chl 3	Chl 4		Chl 1	Chl 2	Chl 4	Chl 6	Chl 7
Chlorite Type	Amyg	Amyg	Amyg							
SiO2	25.71	25.85	25.61	25.47		25.22	25.86	25.96	26.32	26.57
TiO2	0.00	0.00	0.00	0.00		0.00	0.00	0.00	0.00	0.00
Al2O3	20.57	20.56	21.05	21.14		21.33	20.59	20.23	20.23	20.33
Cr2O3	0.00	0.00	0.00	0.00		0.00	0.00	0.00	0.00	0.00
FeO	32.45	33.06	33.19	32.64		27.97	28.85	28.90	28.40	28.46
MnO	0.29	0.32	0.30	0.33		0.31	0.29	0.27	0.28	0.27
MgO	11.51	11.70	11.44	11.19		14.14	13.78	13.94	14.17	14.03
CaO	0.08	0.07	0.08	0.14		0.00	0.00	0.00	0.05	0.00
Na2O	0.00	0.00	0.00	0.00		0.00	0.00	0.00	0.00	0.00
K2O	0.00	0.00	0.00	0.00		0.00	0.00	0.00	0.00	0.00
F	0.00	0.00	0.00	0.00		0.00	0.00	0.00	0.00	0.00
Total	90.61	91.56	91.67	90.91		88.97	89.37	89.30	89.45	89.66
	6.35	6.30	6.30	6.34		6.33	6.32	6.33	6.30	6.28
SiIV	2.72	2.71	2.68	2.69		2.66	2.72	2.74	2.76	2.78
AlIV	1.28	1.29	1.32	1.31		1.34	1.28	1.26	1.24	1.22
T site	4.00	4.00	4.00	4.00		4.00	4.00	4.00	4.00	4.00
AlVI	1.28	1.25	1.29	1.32		1.31	1.28	1.25	1.26	1.28
Ti	0.00	0.00	0.00	0.00		0.00	0.00	0.00	0.00	0.00
Cr3+	0.00	0.00	0.00	0.00		0.00	0.00	0.00	0.00	0.00
Fe2+	2.87	2.90	2.91	2.88		2.46	2.54	2.55	2.49	2.49
Mn2+	0.03	0.03	0.03	0.03		0.03	0.03	0.02	0.02	0.02
Mg	1.81	1.83	1.79	1.76		2.22	2.16	2.19	2.21	2.18
Ca	0.01	0.01	0.01	0.02		0.00	0.00	0.00	0.01	0.00
Na	0.00	0.00	0.00	0.00		0.00	0.00	0.00	0.00	0.00
K	0.00	0.00	0.00	0.00		0.00	0.00	0.00	0.00	0.00
O site	6.00	6.02	6.02	6.00		6.02	6.00	6.01	5.99	5.97
XFe	0.61	0.61	0.62	0.62		0.53	0.54	0.54	0.53	0.53
Al/(Al+Fe+Mg)	0.35	0.35	0.36	0.36		0.36	0.35	0.35	0.35	0.35
T(oC)	265	266	271	270		286	271	268	264	260
XChl	0.99	1.00	1.00	0.99		1.00	1.00	1.00	0.99	0.98
i/l cat	0.01	0.01	0.01	0.02		0.00	0.00	0.00	0.01	0.00
non-i/l	9.99	10.00	10.00	9.99		10.00	10.00	10.00	9.99	9.97

Sample:	VHG038			Sample:	VHG137							Sample:	VHG165						Sample:	VHG168					
Lithology:	Bedding parallel QV			Lithology:	Qtz/Cc/Cpy Vein in FW							Lithology:	Bed|| QV + PT in VCR						Lithology	PT/Cc Vein at VCR-HW contact					
Analysis No.	Chl 1	Chl 2	Chl 3		Chl 1	Chl 2	Chl 3	Chl 4	Chl 5	Chl 6	Chl 7		Chl 1	Chl 2	Chl 3	Chl 4	Chl 5	Chl 6		Chl 1	Chl 2	Chl 3	Chl 4	Chl 5	Chl 6
Chlorite Type					+Cc	+Cc	+Cpy	+Cpy																	
SiO2	22.86	23.00	22.85		24.03	24.69	24.20	24.18	23.79	24.03	23.97		24.37	24.06	24.51	24.31	24.50	24.83		24.40	24.08	24.33	23.28	23.96	24.28
TiO2	0.08	0.19	0.00		0.00	0.00	0.00	0.00	0.00	0.00	0.00		0.00	0.00	0.00	0.00	0.00	0.00		0.00	0.00	0.40	0.00	0.00	0.00
Al2O3	22.12	22.15	22.69		24.23	24.07	23.85	23.91	23.37	23.28	23.50		25.35	24.27	25.33	26.19	25.03	25.26		25.39	24.77	25.22	24.36	24.87	24.93
Cr2O3	0.00	0.15	0.09		0.00	0.00	0.00	0.00	0.00	0.00	0.00		0.26	0.65	0.00	0.00	0.00	0.32		0.00	0.00	0.00	0.08	0.11	0.00
FeO	28.68	29.88	30.00		29.53	29.53	30.73	30.99	32.52	31.22	33.42		28.91	29.00	29.23	27.54	28.15	28.77		30.21	30.33	30.46	29.91	31.04	30.29
MnO	0.16	0.12	0.17		0.20	0.16	0.15	0.13	0.14	0.22	0.15		0.34	0.34	0.30	0.24	0.21	0.29		0.18	0.25	0.19	0.16	0.23	0.19
MgO	10.52	9.97	10.17		11.76	12.13	10.97	10.83	9.59	10.34	9.34		11.06	11.26	11.61	12.34	12.63	12.01		10.54	10.63	10.65	10.27	10.32	10.08
CaO	0.13	0.10	0.08		0.07	0.06	0.07	0.07	0.00	0.00	0.04		0.08	0.07	0.00	0.00	0.00	0.00		0.07	0.19	0.11	0.05	0.00	0.00
Na2O	0.00	0.05	0.03		0.00	0.00	0.00	0.00	0.00	0.00	0.00		0.00	0.00	0.00	0.00	0.00	0.00		0.00	0.00	0.00	0.00	0.00	0.00
K2O	0.00	0.00	0.03		0.00	0.00	0.00	0.00	0.00	0.00	0.00		0.00	0.00	0.00	0.00	0.00	0.00		0.00	0.00	0.00	0.00	0.00	0.00
F	0.00	0.00	0.00		0.00	0.00	0.00	0.00	0.00	0.00	0.00		0.00	0.00	0.00	0.00	0.00	0.00		0.00	0.00	0.00	0.00	0.00	0.00
Total	84.55	85.61	86.11		89.82	90.64	89.97	90.11	89.41	89.09	90.42		90.37	89.65	90.98	90.62	90.58	91.54		90.79	90.25	91.36	88.11	90.53	69.77
	6.74	6.69	6.65		6.31	6.24	6.33	6.33	6.45	6.43	6.40		6.24	6.32	6.19	6.16	6.19	6.14		6.24	6.30	6.21	6.46	6.30	6.32
SiIV	2.56	2.56	2.53		2.52	2.56	2.55	2.55	2.55	2.57	2.55		2.53	2.53	2.53	2.49	2.52	2.54		2.53	2.53	2.51	2.50	2.51	2.55
AlIV	1.44	1.44	1.47		1.48	1.44	1.45	1.45	1.45	1.43	1.45		1.47	1.47	1.47	1.51	1.48	1.46		1.47	1.47	1.49	1.50	1.49	1.45
T site	4.00	4.00	4.00		4.00	4.00	4.00	4.00	4.00	4.00	4.00		4.00	4.00	4.00	4.00	4.00	4.00		4.00	4.00	4.00	4.00	4.00	4.00
AlVI	1.49	1.47	1.49		1.52	1.51	1.52	1.52	1.51	1.50	1.50		1.63	1.54	1.60	1.66	1.57	1.58		1.64	1.59	1.59	1.59	1.58	1.64
Ti	0.01	0.02	0.00		0.00	0.00	0.00	0.00	0.00	0.00	0.00		0.00	0.00	0.00	0.00	0.00	0.00		0.00	0.00	0.03	0.00	0.00	0.00
Cr3+	0.00	0.01	0.01		0.00	0.00	0.00	0.00	0.00	0.00	0.00		0.02	0.05	0.00	0.00	0.00	0.03		0.00	0.00	0.00	0.01	0.01	0.00
Fe2+	2.69	2.78	2.78		2.59	2.56	2.71	2.73	2.92	2.79	2.98		2.51	2.55	2.52	2.36	2.43	2.46		2.62	2.66	2.63	2.69	2.72	2.66
Mn2+	0.02	0.01	0.02		0.02	0.01	0.01	0.01	0.01	0.02	0.01		0.03	0.03	0.03	0.02	0.02	0.03		0.02	0.02	0.02	0.01	0.02	0.02
Mg	1.76	1.65	1.68		1.84	1.88	1.72	1.70	1.53	1.65	1.48		1.71	1.76	1.78	1.89	1.94	1.83		1.63	1.66	1.64	1.65	1.61	1.58
Ca	0.02	0.01	0.01		0.01	0.01	0.01	0.01	0.00	0.00	0.00		0.01	0.01	0.00	0.00	0.01	0.01		0.01	0.02	0.01	0.01	0.00	0.00
Na	0.00	0.01	0.01		0.00	0.00	0.00	0.00	0.00	0.00	0.00		0.00	0.00	0.00	0.00	0.00	0.00		0.00	0.00	0.00	0.00	0.00	0.00
K	0.00	0.00	0.00		0.00	0.00	0.00	0.00	0.00	0.00	0.00		0.00	0.00	0.00	0.00	0.00	0.00		0.00	0.00	0.00	0.00	0.00	0.00
O site	5.97	5.97	5.99		5.98	5.97	5.97	5.97	5.97	5.96	5.98		5.91	5.94	5.93	5.93	5.96	5.93		5.92	5.95	5.92	5.95	5.95	5.90
XFe	0.60	0.63	0.62		0.58	0.58	0.61	0.62	0.66	0.63	0.67		0.59	0.59	0.80	0.56	0.56	0.57		0.62	0.62	0.80	0.62	0.63	0.63
Al/(Al+Fe+Mg	0.40	0.40	0.40		0.40	0.40	0.40	0.40	0.40	0.40	0.40		0.42	0.41	0.42	0.43	0.41	0.42		0.42	0.41	0.42	0.42	0.41	0.42
T (°C)	298	297	304		309	301	300	301	296	295	295		307	307	288	318	311	307		304	306	290	310	307	299
XChl	0.96	0.95	0.97		0.98	0.96	0.97	0.97	0.97	0.97	0.97		0.91	0.94	0.94	0.93	0.95	0.93		0.92	0.94	0.92	0.95	0.95	0.91
i/l cat	0.02	0.02	0.02		0.01	0.01	0.01	0.01	0.00	0.00	0.00		0.01	0.01	0.00	0.00	0.01	0.01		0.01	0.02	0.01	0.01	0.00	0.00
non-i/l	9.96	9.95	9.97		9.97	9.96	9.96	9.96	9.97	9.96	9.97		9.90	9.94	9.93	9.93	9.95	9.92		9.91	9.93	9.91	9.95	9.95	9.90

Sample:	VHG169															Sample:	VHG172					
Lithology:	In QV part of PT/QV															Lithology	Qtz/Cc vein at VCR-FW contact					
Analysis No.	Chl 1	Chl 2	Chl 3	Chl 4	Chl 5	Chl 6	Chl 7	Chl 8	Chl 9	Chl 10	Chl 11	Chl 15	Chl 16	Chl 17	Chl 18		Chl 1	Chl 2	Chl 3	Chl 4	Chl 5	Chl 6
Chlorite Type	'Blue Chl	'Blue Chl	'Blue Chl	'Blue Chl	'Blue Chl	'Blue Chl	'Blue Chl	'Brwn' C	'Brwn' C	'Brwn' C	'Brwn' C	'Brwn' Vn	'Brwn' Vn	'Brwn' Vn	'Brwn' C							
SiO2	24.05	23.82	24.05	23.21	24.29	23.77	24.65	26.83	25.85	26.46	24.61	25.97	25.67	24.79	25.36		23.86	23.55	24.21	23.26	23.54	24.10
TiO2	0.00	0.00	0.00	0.00	0.00	0.00	0.00	0.00	0.00	0.00	0.00	0.00	0.00	0.00	0.00		0.00	0.00	0.00	0.00	0.00	0.00
Al2O3	25.84	26.18	25.98	26.05	26.13	26.07	25.61	26.14	25.60	25.81	25.60	25.14	24.01	22.57	25.93		25.53	25.98	25.67	26.06	25.44	25.23
Cr2O3	0.00	0.00	0.00	0.00	0.00	0.00	0.00	0.00	0.00	0.00	0.00	0.00	0.00	0.00	0.00		0.19	0.16	0.09	0.13	0.10	0.11
FeO	31.33	31.23	29.76	30.92	31.59	29.95	31.81	30.41	31.68	29.81	33.46	32.67	32.10	33.54	31.04		26.37	27.53	27.01	28.21	27.03	27.25
MnO	0.17	0.00	0.16	0.17	0.21	0.14	0.13	0.14	0.19	0.14	0.19	0.14	0.14	0.13	0.20		0.00	0.22	0.20	0.21	0.00	0.18
MgO	8.06	8.35	8.85	8.85	8.45	9.22	7.72	6.75	6.58	6.67	6.32	8.04	8.73	8.47	6.38		12.00	11.17	11.77	11.14	12.19	12.32
CaO	0.00	0.00	0.00	0.00	0.00	0.00	0.06	0.18	0.15	0.13	0.13	0.00	0.00	0.00	0.15		0.00	0.00	0.00	0.00	0.00	0.00
Na2O	0.00	0.00	0.00	0.00	0.00	0.00	0.00	0.00	0.00	0.00	0.00	0.00	0.00	0.00	0.00		0.00	0.00	0.00	0.00	0.00	0.00
K2O	0.00	0.00	0.00	0.00	0.00	0.00	0.00	0.26	0.21	0.05	0.00	0.00	0.00	0.00	0.08		0.00	0.00	0.05	0.00	0.00	0.00
F	0.00	0.00	0.00	0.00	0.00	0.00	0.00	0.00	0.00	0.00	0.00	0.00	0.00	0.00	0.00		0.00	0.00	0.00	0.00	0.00	0.00
Total	89.45	89.58	88.80	89.20	90.87	89.15	89.98	90.71	90.46	89.07	90.31	91.96	90.65	89.50	89.14		87.95	88.61	89.00	89.01	88.30	89.19
	6.37	6.35	6.36	6.39	6.28	6.35	6.33	6.19	6.27	6.29	6.37	6.19	6.29	6.46	6.35		6.32	6.32	6.27	6.32	6.33	6.27
SiIV	2.55	2.52	2.55	2.47	2.54	2.51	2.60	2.76	2.70	2.77	2.61	2.68	2.69	2.66	2.68		2.51	2.48	2.52	2.45	2.48	2.51
AlIV	1.45	1.48	1.45	1.53	1.46	1.49	1.40	1.24	1.30	1.23	1.39	1.32	1.31	1.34	1.32		1.49	1.52	1.48	1.55	1.52	1.49
T site	4.00	4.00	4.00	4.00	4.00	4.00	4.00	4.00	4.00	4.00	4.00	4.00	4.00	4.00	4.00		4.00	4.00	4.00	4.00	4.00	4.00
AlVI	1.78	1.78	1.79	1.73	1.76	1.76	1.78	1.94	1.87	1.96	1.81	1.73	1.65	1.52	1.91		1.68	1.70	1.68	1.68	1.64	1.62
Ti	0.00	0.00	0.00	0.00	0.00	0.00	0.00	0.00	0.00	0.00	0.00	0.00	0.00	0.00	0.00		0.00	0.00	0.00	0.00	0.00	0.00
Cr3+	0.00	0.00	0.00	0.00	0.00	0.00	0.00	0.00	0.00	0.00	0.00	0.00	0.00	0.00	0.00		0.02	0.01	0.01	0.01	0.01	0.01
Fe2+	2.78	2.76	2.63	2.75	2.76	2.65	2.80	2.62	2.77	2.61	2.96	2.82	2.81	3.01	2.75		2.32	2.42	2.36	2.48	2.38	2.38
Mn2+	0.02	0.00	0.01	0.02	0.02	0.01	0.01	0.01	0.02	0.01	0.02	0.01	0.01	0.01	0.02		0.00	0.02	0.02	0.02	0.00	0.02
Mg	1.27	1.31	1.40	1.40	1.32	1.45	1.21	1.04	1.02	1.04	1.00	1.24	1.36	1.36	1.01		1.88	1.75	1.83	1.75	1.91	1.91
Ca	0.00	0.00	0.00	0.00	0.00	0.00	0.01	0.02	0.02	0.01	0.01	0.00	0.00	0.00	0.02		0.00	0.00	0.00	0.00	0.00	0.00
Na	0.00	0.00	0.00	0.00	0.00	0.00	0.00	0.00	0.00	0.00	0.00	0.00	0.00	0.00	0.00		0.00	0.00	0.00	0.00	0.00	0.00
K	0.00	0.00	0.00	0.00	0.00	0.00	0.00	0.03	0.03	0.01	0.00	0.00	0.00	0.00	0.01		0.00	0.00	0.01	0.00	0.00	0.00
O site	5.84	5.85	5.83	5.90	5.85	5.87	5.81	5.86	5.73	5.64	5.80	5.80	5.83	5.91	5.71		5.90	5.91	5.90	5.93	5.94	5.93
XFe	0.69	0.68	0.80	0.66	0.68	0.65	0.70	0.72	0.73	0.71	0.75	0.70	0.67	0.69	0.73		0.55	0.58	0.80	0.59	0.55	0.55
Al/(Al+Fe+Mg)	0.44	0.44	0.45	0.44	0.44	0.44	0.44	0.46	0.46	0.47	0.45	0.43	0.42	0.40	0.46		0.43	0.44	0.43	0.43	0.42	0.42
T (°C)	294	301	284	313	297	306	282	245	258	244	276	266	266	269	261		314	319	288	325	321	314
XChl	0.85	0.86	0.85	0.91	0.86	0.88	0.82	0.64	0.71	0.65	0.80	0.81	0.85	0.91	0.71		0.91	0.91	0.90	0.94	0.94	0.94
i/l cat	0.00	0.00	0.00	0.00	0.00	0.00	0.01	0.05	0.04	0.02	0.01	0.00	0.00	0.00	0.03		0.00	0.00	0.01	0.00	0.00	0.00
non-i/l	9.84	9.85	9.83	9.90	9.85	9.87	9.81	9.61	9.68	9.62	9.78	9.80	9.83	9.91	9.68		9.90	9.91	9.89	9.93	9.94	9.93

Sample:	VHG163(A)										Sample:	VHG163(B)								
Lithology:	Auriferous QV with Gn, Sph										Lithology:	Auriferous QV with Gn, Sph, Au								
Analysis No.	Chl 1	Chl 2	Chl 3	Chl 4	Chl 5	Chl 6	Chl 7	Chl 8	Chl 9	Chl 10	Chl 1 +Py ?	Chl 2	Chl 3	Chl 4	Chl 5	Chl 6	Chl 7	Chl 8 +Au	Chl 9	Chl 10
Chlorite Type																				
SiO2	23.54	24.19	24.27	24.06	24.42	23.63	23.95	23.84	23.69	23.99	23.37	23.98	24.12	24.47	24.16	23.97	24.29	24.22	24.46	23.99
TiO2	0.00	0.00	0.00	0.00	0.00	0.00	0.00	0.00	0.00	0.00	0.00	0.00	0.00	0.00	0.00	0.00	0.00	0.00	0.00	0.00
Al2O3	26.51	26.14	26.05	26.41	26.41	26.34	26.15	26.18	26.11	26.46	25.35	25.47	26.02	25.52	26.83	26.81	25.42	25.20	24.35	26.48
Cr2O3	0.00	0.00	0.00	0.00	0.00	0.00	0.00	0.00	0.00	0.00	0.27	0.00	0.00	0.00	0.00	0.00	0.00	0.00	0.00	0.00
FeO	26.43	26.67	27.66	27.57	26.10	28.30	28.43	27.48	27.39	27.22	31.06	27.47	26.46	25.63	25.43	26.45	30.80	28.60	29.69	27.22
MnO	0.27	0.17	0.16	0.18	0.20	0.19	0.18	0.23	0.20	0.17	0.23	0.13	0.20	0.31	0.27	0.24	0.17	0.16	0.18	0.17
MgO	12.71	12.56	11.82	11.95	13.04	11.69	11.72	11.93	11.99	12.22	9.73	12.20	12.83	13.40	12.96	12.62	10.49	11.19	10.86	12.22
CaO	0.00	0.00	0.00	0.00	0.00	0.00	0.00	0.00	0.00	0.00	0.00	0.00	0.00	0.00	0.00	0.00	0.00	0.00	0.00	0.00
Na2O	0.00	0.00	0.00	0.00	0.00	0.00	0.00	0.00	0.00	0.00	0.00	0.00	0.00	0.00	0.00	0.05	0.00	0.00	0.00	0.00
K2O	0.00	0.00	0.00	0.00	0.00	0.00	0.00	0.00	0.00	0.00	0.00	0.00	0.00	0.00	0.00	0.00	0.00	0.00	0.00	0.00
F	0.00	0.00	0.00	0.00	0.00	0.00	0.00	0.00	0.00	0.00	0.00	0.00	0.00	0.00	0.00	0.00	0.00	0.00	0.00	0.00
Total	89.46	89.73	89.96	90.17	90.17	90.15	90.43	89.66	89.38	90.08	90.01	89.25	89.63	89.33	89.65	90.14	91.17	89.37	89.54	90.08
	6.22	6.20	6.21	6.19	6.14	6.23	6.21	6.23	6.25	6.19	6.35	6.27	6.20	6.20	6.16	6.16	6.23	6.29	6.32	6.19
SiIV	2.44	2.49	2.51	2.48	2.50	2.45	2.47	2.47	2.47	2.47	2.47	2.50	2.49	2.52	2.48	2.46	2.52	2.54	2.57	2.47
AlIV	1.56	1.51	1.49	1.52	1.50	1.55	1.53	1.53	1.53	1.53	1.53	1.50	1.51	1.48	1.52	1.54	1.48	1.46	1.43	1.53
T site	4.00	4.00	4.00	4.00	4.00	4.00	4.00	4.00	4.00	4.00	4.00	4.00	4.00	4.00	4.00	4.00	4.00	4.00	4.00	4.00
AlVI	1.67	1.67	1.68	1.69	1.68	1.67	1.66	1.68	1.67	1.69	1.62	1.63	1.65	1.63	1.72	1.70	1.62	1.65	1.59	1.69
Ti	0.00	0.00	0.00	0.00	0.00	0.00	0.00	0.00	0.00	0.00	0.00	0.00	0.00	0.00	0.00	0.00	0.00	0.00	0.00	0.00
Cr3+	0.00	0.00	0.00	0.00	0.00	0.00	0.00	0.00	0.00	0.00	0.02	0.00	0.00	0.00	0.00	0.00	0.00	0.00	0.00	0.00
Fe2+	2.29	2.30	2.39	2.38	2.23	2.45	2.46	2.38	2.38	2.34	2.74	2.40	2.28	2.21	2.18	2.27	2.67	2.50	2.61	2.34
Mn2+	0.02	0.01	0.01	0.02	0.02	0.02	0.02	0.02	0.02	0.01	0.02	0.01	0.02	0.03	0.02	0.02	0.01	0.01	0.02	0.01
Mg	1.96	1.93	1.82	1.84	1.99	1.81	1.80	1.84	1.86	1.88	1.53	1.90	1.97	2.06	1.98	1.93	1.62	1.75	1.70	1.88
Ca	0.00	0.00	0.00	0.00	0.00	0.00	0.00	0.00	0.00	0.00	0.00	0.00	0.00	0.00	0.00	0.00	0.00	0.00	0.00	0.00
Na	0.00	0.00	0.00	0.00	0.00	0.00	0.00	0.00	0.00	0.00	0.00	0.00	0.00	0.00	0.00	0.01	0.00	0.00	0.00	0.00
K	0.00	0.00	0.00	0.00	0.00	0.00	0.00	0.00	0.00	0.00	0.00	0.00	0.00	0.00	0.00	0.00	0.00	0.00	0.00	0.00
O site	5.95	5.92	5.91	5.92	5.91	5.94	5.93	5.93	5.93	5.92	5.94	5.93	5.93	5.92	5.90	5.93	5.93	5.91	5.92	5.92
XFe	0.54	0.54	0.57	0.56	0.53	0.58	0.58	0.56	0.56	0.56	0.64	0.56	0.54	0.52	0.52	0.54	0.62	0.59	0.61	0.56
Al/(Al+Fe+Mg)	0.43	0.43	0.43	0.43	0.43	0.43	0.43	0.43	0.43	0.43	0.42	0.42	0.43	0.42	0.44	0.44	0.42	0.42	0.41	0.43
T (°C)	331	319	314	320	320	325	320	321	323	323	315	316	321	315	324	327	306	306	297	323
XChl	0.95	0.92	0.91	0.92	0.92	0.95	0.94	0.93	0.94	0.93	0.95	0.94	0.93	0.93	0.91	0.92	0.94	0.92	0.93	0.93
i/l cat	0.00	0.00	0.00	0.00	0.00	0.00	0.00	0.00	0.00	0.00	0.00	0.00	0.00	0.00	0.00	0.01	0.00	0.00	0.00	0.00
non-i/l	9.95	9.92	9.91	9.92	9.91	9.94	9.93	9.93	9.93	9.92	9.94	9.93	9.93	9.92	9.90	9.92	9.93	9.91	9.92	9.92

Sample:	VHG177						Sample:	VHG182					
Lithology:	QV: Buffelsdoorn Fault						Lithology:	QV: New Year's Fault					
Analysis No.	Chl 1	Chl 2	Chl 3	Chl 4	Chl 5	Chl 6		Chl 1	Chl 2	Chl 3	Chl 4	Chl 5	Chl 6
Chlorite Type													
SiO2	25.16	25.41	24.86	25.09	25.39	24.39		25.26	24.11	24.18	24.61	24.02	24.35
TiO2	0.00	0.00	0.00	0.00	0.00	0.00		0.00	0.00	0.00	0.00	0.00	0.00
Al2O3	23.59	23.65	23.43	23.63	23.42	24.11		24.07	24.50	24.56	24.72	24.97	24.73
Cr2O3	0.00	0.00	0.00	0.00	0.00	0.00		0.00	0.00	0.00	0.00	0.00	0.00
FeO	27.04	27.13	26.46	27.26	26.72	26.43		28.45	29.73	29.78	28.69	29.94	29.27
MnO	0.20	0.18	0.20	0.18	0.16	0.26		0.15	0.17	0.21	0.00	0.17	0.22
MgO	12.92	13.43	14.17	13.30	13.69	13.41		12.71	11.22	10.74	11.84	11.06	11.46
CaO	0.08	0.06	0.06	0.11	0.00	0.12		0.00	0.00	0.06	0.00	0.00	0.05
Na2O	0.00	0.00	0.00	0.00	0.00	0.00		0.13	0.00	0.00	0.00	0.00	0.00
K2O	0.00	0.00	0.00	0.00	0.00	0.00		0.09	0.00	0.00	0.07	0.00	0.00
F	0.00	0.00	0.00	0.00	0.00	0.00		0.00	0.00	0.00	0.00	0.00	0.00
Total	88.99	89.86	89.18	89.57	89.38	88.72		90.86	89.73	89.53	89.93	90.16	90.08
	6.27	6.21	6.25	6.24	6.23	6.29		6.18	6.31	6.33	6.25	6.28	6.27
SiIV	2.63	2.62	2.59	2.61	2.63	2.55		2.60	2.53	2.55	2.56	2.51	2.54
AlIV	1.37	1.38	1.41	1.39	1.37	1.45		1.40	1.47	1.45	1.44	1.49	1.46
T site	4.00	4.00	4.00	4.00	4.00	4.00		4.00	4.00	4.00	4.00	4.00	4.00
AlVI	1.53	1.50	1.46	1.50	1.49	1.53		1.51	1.57	1.60	1.59	1.59	1.58
Ti	0.00	0.00	0.00	0.00	0.00	0.00		0.00	0.00	0.00	0.00	0.00	0.00
Cr3+	0.00	0.00	0.00	0.00	0.00	0.00		0.00	0.00	0.00	0.00	0.00	0.00
Fe2+	2.36	2.34	2.30	2.37	2.32	2.31		2.45	2.61	2.62	2.49	2.62	2.55
Mn2+	0.02	0.02	0.02	0.02	0.01	0.02		0.01	0.02	0.02	0.00	0.02	0.02
Mg	2.01	2.07	2.20	2.06	2.11	2.09		1.95	1.76	1.69	1.83	1.72	1.78
Ca	0.01	0.01	0.01	0.01	0.00	0.01		0.00	0.00	0.01	0.00	0.00	0.01
Na	0.00	0.00	0.00	0.00	0.00	0.00		0.03	0.00	0.00	0.00	0.00	0.00
K	0.00	0.00	0.00	0.00	0.00	0.00		0.01	0.00	0.00	0.01	0.00	0.00
O site	5.93	5.94	5.98	5.95	5.94	5.97		5.96	5.95	5.93	5.93	5.95	5.94
XFe	0.54	0.53	0.80	0.53	0.52	0.53		0.56	0.60	0.80	0.58	0.60	0.59
Al/(Al+Fe+Mg)	0.40	0.40	0.39	0.40	0.39	0.40		0.40	0.41	0.41	0.41	0.41	0.41
T (°C)	291	292	275	296	292	308		296	306	284	302	309	305
XChl	0.92	0.94	0.98	0.95	0.94	0.96		0.93	0.95	0.93	0.93	0.95	0.94
i/l cat	0.01	0.01	0.01	0.01	0.00	0.01		0.04	0.00	0.01	0.01	0.00	0.01
non-i/l	9.92	9.93	9.97	9.94	9.94	9.95		9.92	9.95	9.92	9.92	9.95	9.94

Sample:	VHG018		Sample:	VHG122				Sample:	VHG128					Sample:	VHG129						Sample:	VHG027							
Lithology:	FW Pseudotachylit		Lithology:	FW Pseudotachylite				Lithology:	Pseudotachylite (top contact)					Lithology:	Pseudotachylite (bottom contact)						Lithology	Ultramylonite (top contact)							
Analysis No.:	Chl 1	Chl 2	Chl 6	Chl 7	Chl 8	Chl 9		Chl 1	Chl 2 +Py	Chl 3	Chl 4	Chl 5		Chl 2	Chl 3	Chl 4	Chl 5	Chl 6	Chl 7		Chl 1	Chl 2	Chl 3 yellow	Chl 4	Chl 5	Chl 6	Chl 7	Chl 8
Chlorite Type	II	II	PT	PT	PT	PT																						
SiO2	26.72	24.18	23.07	24.21	26.56	23.80		24.30	24.35	24.13	24.68	26.59		24.15	24.00	23.67	23.65	23.78	26.61		24.21	24.19	24.59	24.04	24.29	24.40	23.87	24.00
TiO2	0.24	0.00	0.00	0.00	0.10	0.00		2.41	0.00	0.00	0.00	0.00		0.00	0.00	0.00	0.00	1.05	0.00		0.00	0.00	0.00	0.00	0.09	0.00	0.00	0.00
Al2O3	27.24	24.90	26.19	24.26	23.98	24.50		23.99	24.34	24.83	25.17	24.35		25.13	26.02	25.79	25.72	25.80	23.61		24.27	24.30	23.99	24.11	24.09	24.48	24.26	24.72
Cr2O3	0.00	0.17	0.00	0.00	0.00	0.00		0.11	0.00	0.00	0.00	0.15		0.00	0.12	0.00	0.00	0.15	0.00		0.14	0.00	0.00	0.00	0.15	0.00	0.11	0.00
FeO	23.66	26.56	33.50	34.17	30.26	34.26		26.41	30.64	30.16	30.16	26.01		31.44	32.66	31.06	30.88	32.63	26.75		29.03	29.66	26.94	29.97	29.02	29.51	26.29	29.66
MnO	0.15	0.14	0.26	0.22	0.20	0.21		0.12	0.12	0.17	0.16	0.13		0.17	0.19	0.20	0.15	0.00	0.19		0.00	0.14	0.14	0.14	0.00	0.00	0.14	0.20
MgO	10.54	9.23	7.12	7.81	8.25	7.47		10.36	10.67	10.80	9.88	9.49		9.60	8.60	9.26	9.48	8.64	9.55		11.53	11.79	12.06	11.68	11.75	11.79	11.92	11.43
CaO	0.07	0.09	0.12	0.00	0.00	0.00		0.09	0.00	0.00	0.00	0.00		0.00	0.12	0.00	0.00	0.11	0.00		0.00	0.00	0.00	0.00	0.00	0.00	0.00	0.00
Na2O	0.00	0.00	0.05	0.00	0.00	0.00		0.00	0.00	0.00	0.00	0.00		0.00	0.00	0.00	0.00	0.08	0.00		0.00	0.00	0.00	0.00	0.00	0.00	0.00	0.00
K2O	0.11	0.00	0.00	0.00	0.14	0.00		0.13	0.00	0.00	0.00	0.39		0.00	0.16	0.00	0.00	0.05	0.00		0.07	0.00	0.00	0.00	0.00	0.00	0.00	0.00
F	0.00	0.00	0.00	0.00	0.00	0.00		0.00	0.00	0.00	0.00	0.00		0.00	0.00	0.00	0.00	0.00	0.00		0.00	0.00	0.00	0.00	0.00	0.00	0.00	0.00
Total	88.75	85.27	90.30	90.67	91.51	90.26		89.92	90.12	90.09	90.05	91.11		90.49	90.17	90.00	89.88	90.27	90.71		89.25	90.08	89.72	89.94	89.39	90.18	88.69	90.01
	6.11	6.53	6.40	6.39	6.11	6.43		6.27	6.31	6.30	6.28	6.07		6.30	6.37	6.33	6.33	6.36	6.12		6.32	6.29	6.28	6.31	6.31	6.26	6.35	6.29
SiIV	2.72	2.63	2.46	2.57	2.91	2.55		2.53	2.56	2.53	2.58	2.69		2.53	2.55	2.49	2.49	2.52	2.91		2.55	2.53	2.57	2.52	2.55	2.54	2.53	2.51
AlIV	1.28	1.37	1.54	1.43	1.09	1.45		1.47	1.44	1.47	1.42	1.11		1.47	1.45	1.51	1.51	1.48	1.09		1.45	1.47	1.43	1.48	1.45	1.46	1.47	1.49
T site	4.00	4.00	4.00	4.00	4.00	4.00		4.00	4.00	4.00	4.00	4.00		4.00	4.00	4.00	4.00	4.00	4.00		4.00	4.00	4.00	4.00	4.00	4.00	4.00	4.00
AlVI	1.98	1.82	1.75	1.81	1.76	1.63		1.48	1.57	1.59	1.88	1.79		1.84	1.80	1.70	1.69	1.73	1.75		1.56	1.53	1.53	1.51	1.53	1.55	1.55	1.56
Ti	0.02	0.00	0.00	0.00	0.01	0.00		0.19	0.00	0.00	0.00	0.00		0.00	0.00	0.00	0.00	0.08	0.00		0.00	0.00	0.00	0.00	0.01	0.00	0.00	0.00
Cr3+	0.00	0.01	0.00	0.00	0.00	0.00		0.01	0.00	0.00	0.00	0.01		0.00	0.01	0.00	0.00	0.01	0.00		0.01	0.00	0.00	0.00	0.01	0.00	0.01	0.00
Fe2+	2.01	2.42	2.98	3.04	2.58	3.07		2.48	2.69	2.64	2.64	2.37		2.78	2.92	2.74	2.72	2.89	2.45		2.55	2.59	2.53	2.63	2.55	2.57	2.50	2.60
Mn2+	0.01	0.01	0.02	0.02	0.02	0.02		0.01	0.01	0.02	0.01	0.01		0.02	0.02	0.02	0.01	0.00	0.02		0.00	0.01	0.01	0.01	0.00	0.00	0.01	0.02
Mg	1.60	1.50	1.13	1.24	1.25	1.19		1.61	1.67	1.69	1.54	1.43		1.50	1.04	1.46	1.48	1.05	1.45		1.81	1.84	1.88	1.83	1.84	1.83	1.88	1.78
Ca	0.01	0.01	0.01	0.00	0.00	0.00		0.01	0.00	0.00	0.00	0.00		0.00	0.01	0.00	0.00	0.01	0.00		0.00	0.00	0.00	0.00	0.00	0.00	0.00	0.00
Na	0.00	0.00	0.01	0.00	0.00	0.00		0.00	0.00	0.00	0.00	0.00		0.00	0.00	0.00	0.00	0.01	0.00		0.00	0.00	0.00	0.00	0.00	0.00	0.00	0.00
K	0.01	0.00	0.00	0.00	0.02	0.00		0.02	0.00	0.00	0.00	0.05		0.00	0.02	0.00	0.00	0.01	0.00		0.01	0.00	0.00	0.00	0.00	0.00	0.00	0.00
O site	5.64	5.77	5.91	5.91	5.85	5.91		5.81	5.94	5.94	5.87	5.86		5.91	5.83	5.91	5.91	5.80	5.87		5.94	5.97	5.95	5.98	5.94	5.95	5.95	5.96
XFe	0.56	0.62	0.73	0.71	0.67	0.72		0.61	0.62	0.61	0.63	0.62		0.65	0.74	0.65	0.65	0.73	0.63		0.59	0.59	0.57	0.59	0.58	0.58	0.57	0.59
Al/(Al+Fe+Mg)	0.47	0.45	0.44	0.42	0.43	0.42		0.42	0.41	0.41	0.43	0.43		0.42	0.45	0.43	0.43	0.45	0.42		0.41	0.40	0.40	0.40	0.40	0.41	0.41	0.41
T (°C)	271	283	310	286	219	291		305	299	305	293	227		301	290	309	310	298	222		304	307	300	308	303	305	308	310
XChl	0.65	0.78	0.89	0.91	0.66	0.92		0.80	0.94	0.94	0.88	0.64		0.92	0.81	0.91	0.92	0.78	0.69		0.94	0.97	0.95	0.98	0.95	0.96	0.96	0.96
I/I cat	0.02	0.01	0.02	0.00	0.02	0.00		0.03	0.00	0.00	0.00	0.05		0.00	0.04	0.00	0.00	0.03	0.00		0.01	0.00	0.00	0.00	0.00	0.00	0.00	0.00
non-I/I	9.82	9.78	9.88	9.91	9.83	9.91		9.78	9.94	9.94	9.87	9.81		9.91	9.80	9.91	9.91	9.77	9.87		9.93	9.97	9.95	9.98	9.94	9.95	9.95	9.96

Sample	VHG023							Sample:	VHG133			Sample:	VHG134				Sample:	VHG138			Sample:	VHG142			
Lithology	Dyke							Lithology:	Dyke (8m wide)			Lithology:	Dyke (20cm wide)				Lithology:	Dyke (60cm wide)			Lithology:	Dyke (1.2m wide)			
Analysis No	Chl 1	Chl 2	Chl 3	Chl 4	Chl 5	Chl 6	Chl 7	Chl 1	Chl 2	Chl 3	Chl 4	Chl 1	Chl 2	Chl 3	Chl 4	Chl 5	Chl 1	Chl 2	Chl 3	Chl 4	Chl 1	Chl 2	Chl 3	Chl 4	Chl 5
Chlorite Type	Vein	Vein																							
SiO2	24.25	24.84	23.94	24.19	23.43	24.31	24.37	28.13	26.85	25.93	26.22	29.04	29.53	29.62	29.28	29.33	24.95	25.21	25.07	24.92	23.77	23.43	24.14	25.11	23.67
TiO2	0.00	0.00	0.00	0.00	0.00	0.00	0.00	0.00	0.00	0.00	0.00	0.00	0.00	0.00	0.00	0.00	0.00	0.00	0.00	0.00	0.00	0.00	0.00	0.00	0.00
Al2O3	24.46	23.96	24.13	24.49	23.69	24.61	24.87	21.17	20.61	21.36	20.90	16.25	16.70	16.50	16.98	16.71	25.92	26.73	26.51	26.43	27.29	26.60	27.86	25.95	26.50
Cr2O3	0.47	0.43	0.85	1.00	0.88	0.95	0.95	0.13	0.10	0.00	0.09	0.37	0.35	0.43	0.26	0.35	0.00	0.00	0.00	0.00	0.00	0.00	0.00	0.00	0.00
FeO	26.60	26.25	26.85	27.39	27.22	27.75	27.71	30.19	29.91	29.59	29.28	23.81	24.96	24.53	24.54	24.55	24.42	24.22	24.95	24.63	27.58	27.56	25.87	26.84	27.56
MnO	0.21	0.16	0.17	0.18	0.15	0.17	0.19	0.21	0.27	0.28	0.25	0.00	0.00	0.00	0.00	0.00	0.49	0.34	0.39	0.37	0.38	0.32	0.28	0.27	0.34
MgO	12.87	12.89	12.69	12.31	11.93	12.43	12.24	13.13	13.86	13.73	13.87	19.69	19.15	19.69	19.02	19.56	13.68	13.43	13.81	13.00	11.21	11.70	11.39	11.42	11.32
CaO	0.00	0.05	0.00	0.00	0.00	0.00	0.00	0.05	0.00	0.00	0.00	0.00	0.09	0.06	0.00	0.00	0.00	0.00	0.00	0.00	0.00	0.00	0.00	0.08	0.00
Na2O	0.00	0.00	0.00	0.00	0.00	0.00	0.00	0.00	0.00	0.00	0.00	0.00	0.00	0.00	0.00	0.00	0.00	0.00	0.00	0.00	0.00	0.00	0.00	0.00	0.00
K2O	0.00	0.00	0.00	0.00	0.00	0.00	0.00	0.00	0.00	0.00	0.00	0.00	0.00	0.00	0.00	0.00	0.06	0.00	0.00	0.22	0.00	0.00	0.40	0.00	0.00
F	0.00	0.00	0.00	0.00	0.00	0.00	0.00	0.00	0.00	0.00	0.00	0.00	0.00	0.00	0.00	0.00	0.00	0.00	0.00	0.00	0.00	0.00	0.00	0.00	0.00
Total	88.86	88.60	88.83	89.56	87.30	90.22	90.33	91.01	91.40	90.91	90.81	89.16	90.78	90.83	90.08	90.50	89.52	89.93	90.73	89.57	90.23	89.61	89.94	89.87	89.39
	6.28	6.28	6.31	6.27	6.45	6.22	6.21	6.24	6.20	6.23	6.24	6.16	6.07	6.06	6.11	6.08	6.14	6.09	6.06	6.14	6.19	6.25	6.15	6.19	6.26
SiIV	2.54	2.60	2.51	2.52	2.51	2.52	2.52	2.71	2.75	2.69	2.72	2.98	2.99	2.99	2.98	2.97	2.55	2.55	2.53	2.54	2.45	2.44	2.47	2.59	2.47
AlIV	1.46	1.40	1.49	1.48	1.49	1.48	1.48	1.29	1.25	1.31	1.28	1.02	1.01	1.01	1.02	1.03	1.45	1.45	1.47	1.46	1.55	1.56	1.53	1.41	1.53
T elte	4.00	4.00	4.00	4.00	4.00	4.00	4.00	4.00	4.00	4.00	4.00	4.00	4.00	4.00	4.00	4.00	4.00	4.00	4.00	4.00	4.00	4.00	4.00	4.00	4.00
AlVI	1.55	1.55	1.50	1.53	1.51	1.52	1.55	1.30	1.25	1.30	1.28	0.94	0.98	0.95	1.01	0.98	1.87	1.74	1.68	1.73	1.76	1.70	1.83	1.74	1.72
Ti	0.00	0.00	0.00	0.00	0.00	0.00	0.00	0.00	0.00	0.00	0.00	0.00	0.00	0.00	0.00	0.00	0.00	0.00	0.00	0.00	0.00	0.00	0.00	0.00	0.00
Cr3+	0.04	0.04	0.07	0.08	0.07	0.08	0.08	0.01	0.01	0.00	0.01	0.03	0.03	0.03	0.02	0.03	0.00	0.00	0.00	0.00	0.00	0.00	0.00	0.00	0.00
Fe2+	2.33	2.30	2.36	2.39	2.44	2.40	2.40	2.62	2.58	2.58	2.54	2.04	2.11	2.07	2.09	2.08	2.09	2.05	2.10	2.10	2.38	2.40	2.21	2.31	2.40
Mn2+	0.02	0.02	0.02	0.02	0.01	0.01	0.02	0.02	0.02	0.02	0.02	0.00	0.00	0.00	0.00	0.00	0.04	0.03	0.03	0.03	0.03	0.03	0.02	0.02	0.03
Mg	2.01	2.01	2.02	1.91	1.91	1.92	1.88	2.03	2.13	2.12	2.15	3.01	2.89	2.96	2.88	2.95	2.08	2.03	2.08	1.98	1.72	1.81	1.74	1.75	1.76
Ca	0.00	0.01	0.00	0.00	0.00	0.00	0.00	0.01	0.00	0.00	0.00	0.00	0.01	0.01	0.00	0.00	0.00	0.00	0.00	0.00	0.00	0.00	0.00	0.01	0.00
Na	0.00	0.00	0.00	0.00	0.00	0.00	0.00	0.00	0.00	0.00	0.00	0.00	0.00	0.00	0.00	0.00	0.00	0.00	0.00	0.00	0.00	0.00	0.00	0.00	0.00
K	0.00	0.00	0.00	0.00	0.00	0.00	0.00	0.00	0.00	0.00	0.00	0.00	0.00	0.00	0.00	0.00	0.01	0.00	0.00	0.03	0.00	0.00	0.05	0.00	0.00
O site	5.84	5.91	5.86	5.93	5.85	5.84	5.83	5.99	5.99	6.01	6.00	6.02	6.01	6.02	6.00	6.02	5.89	5.85	5.90	5.87	5.89	5.93	5.86	5.84	5.91
XFe	0.54	0.53	0.54	0.56	0.56	0.56	0.56	0.56	0.55	0.55	0.54	0.40	0.42	0.41	0.42	0.41	0.50	0.50	0.50	0.52	0.58	0.57	0.56	0.57	0.58
Al/(Al+Fe+Mg)	0.41	0.41	0.41	0.41	0.41	0.41	0.41	0.38	0.35	0.36	0.35	0.28	0.28	0.28	0.29	0.28	0.43	0.44	0.43	0.44	0.45	0.44	0.46	0.44	0.44
T (°C)	311	298	315	312	313	313	312	271	264	278	271	229	228	228	228	230	311	310	315	311	325	329	322	297	322
XChl	0.84	0.91	0.86	0.84	0.85	0.84	0.83	0.89	1.00	1.00	1.00	1.00	1.00	1.00	1.00	1.00	0.89	0.86	0.90	0.85	0.90	0.94	0.82	0.84	0.92
I/I cat	0.00	0.01	0.00	0.00	0.00	0.00	0.00	0.01	0.00	0.00	0.00	0.00	0.01	0.01	0.00	0.00	0.01	0.00	0.00	0.03	0.00	0.00	0.05	0.01	0.00
non-I/I	8.84	8.91	8.86	8.83	8.85	8.84	8.83	8.98	8.99	10.00	10.00	10.00	10.00	10.00	10.00	10.00	8.88	8.85	8.90	8.84	8.89	8.93	8.81	8.83	8.91

Carbonate Analyses

SAMPLE	Ca	Fe	Mg	Mn	Total	Comments
VHG045 (HW: Contact Z.)						
Cc1	95.55	2.37	0.96	0.52	99.42	in amygdale
Cc2	96.46	2.20	0.80	1.19	100.65	in amygdale
Cc3	95.29	2.71	1.12	1.46	100.58	with qtz in amygdale
Cc4	89.12	4.13	3.35	1.57	98.17	
Cc5	93.97	2.22	1.16	1.77	99.12	
Cc6	96.09	2.67	1.16	1.84	101.76	
Cc7	92.60	2.84	1.42	1.87	98.73	
VHG055(A) (HW: Contact Z.)						
Cc1	92.82	3.99	0.91	1.34	99.06	vein
Cc2	92.63	3.96	0.68	1.42	98.69	vein
Cc3	91.53	4.34	1.04	1.79	98.70	vein
VHG128 (Pseudotachylite)						
Cc1	95.53	1.66	0.78	1.26	99.23	rim around qtz clast
Cc2	96.46	1.47	0.56	0.47	98.98	
Cc4	92.63	2.64	1.08	1.33	97.68	around py
Cc5	92.01	3.01	1.33	1.35	97.70	in qtz clast
VHG137 (Qtz/Calcite Vein)						
Cc1	96.98	0.97	0.53	0.63	99.11	
Cc2	97.03	1.14	0.56	0.64	99.37	
Cc3	96.36	1.20	0.60	0.46	98.62	
Cc4	95.18	2.14	1.32	1.13	99.77	
Cc5	96.19	1.13	0.60	0.50	98.42	
Cc6	98.59	0.95	0.57	0.68	100.79	
VHG168 (PT/Calcite Vein)						
Cc1	95.81	1.36	0.61	2.95	100.73	
Cc2	95.72	1.33	0.49	1.35	98.89	around hex qtz
Cc3	97.47	0.90	0.45	2.06	100.88	around cc vn
Cc4	97.12	1.26	0.75	1.43	100.56	cc vein
Cc5	95.32	1.90	0.95	1.90	100.07	cc vein
Cc6	95.74	1.02	0.59	2.67	100.02	
Cc7	97.05	1.01	0.51	2.41	100.98	
VHG172 (Qtz/Calcite Vein)						
Cc1	96.31	1.13	0.36	1.67	99.47	
Cc2	95.78	1.32	0.45	1.10	98.65	
Cc3	94.7	1.89	0.59	1.41	98.59	
Cc4	96.86	1.11	0.00	1.88	99.85	
VHG177 (Buffelsdoorn Flt Zone)						
Cc1	95.70	2.27	0.35	0.00	98.32	
Cc2	96.44	0.94	0.00	1.66	99.04	clear
Cc4	97.55	1.04	0.00	1.49	100.08	opaque
Cc5	96.24	2.12	0.27	1.35	99.98	
Cc6	97.39	0.64	0.00	1.16	99.19	clear
Cc7	94.98	2.46	0.36	1.63	99.43	
VHG178(B) (Nooitgedacht Flt Zone)						
Cc1	96.76	0.87	0.68	1.27	99.58	
Cc2	98.92	0.00	0.00	0.83	99.75	vein
Cc3	98.93	0.00	0.00	0.98	99.91	vein
Cc4	98.63	0.00	0.00	0.89	99.52	vein
Cc5	98.70	0.00	0.00	1.21	99.91	around vn
Cc6	97.86	0.55	0.00	1.38	99.79	
Cc7	96.57	0.69	0.62	1.11	98.99	
Cc8	97.07	1.02	0.65	1.16	99.90	

SAMPLE	Ca	Fe	Mg	Mn	Total	Comments
VHG153(A) (Fe-metasomatised VCR)						
Sid 1	0.48	94.58	1.23	0.82	97.11	
Sid 3	0.43	95.77	0.55	1.22	97.97	
Sid 4	0.37	98.44	0.51	0.84	100.16	nxt chl
Sid 5	0.58	97.55	0.84	1.55	100.52	in qtz
Sid 6	0.46	97.79	0.53	1.12	99.90	core —\
Sid 7	0.60	97.09	0.65	1.41	99.75	middle >
Sid 8	0.32	96.05	1.38	0.68	100.43	rim —/
Sid 9	0.34	98.02	1.14	0.48	99.98	
Sid 10	0.73	97.07	0.69	1.53	100.02	
Sid 11	0.96	96.25	3.50	0.94	101.65	
Sid 12	1.20	93.62	4.05	1.23	100.10	—\
Sid 13	0.36	98.68	0.78	0.70	100.52	same as sid 11
Sid 12A	0.33	97.29	0.58	0.71	98.91	—/
Sid 14	0.30	98.80	0.39	1.08	100.57	
Sid 15	0.46	96.90	2.77	0.96	101.09	
Sid 16	0.51	97.16	2.12	0.86	100.65	
Sid 17	0.32	97.89	1.07	0.63	99.91	core –\
Sid 17A	1.00	94.55	3.71	1.22	100.48	rim –/
Sid 18	0.65	98.14	0.81	1.49	101.09	core —\
Sid 18A	0.49	97.56	0.40	0.83	99.28	middle \
Sid 18B	0.86	95.65	3.82	1.18	101.51	rim /
Sid 18C	0.32	98.78	0.86	0.60	100.56	rim —/
VHG158(B) (Fe-metasomatised VCR)						
Sid1	0.29	98.91	0.62	0.73	100.55	
Sid2	0.27	98.76	0.34	0.83	100.20	
Sid3	0.75	96.74	0.55	1.52	99.56	around chl
Sid4	0.32	99.37	0.42	0.91	101.02	
Sid5	0.28	96.94	0.41	0.86	98.49	
Sid6	0.36	96.88	0.42	1.04	98.70	small xtls around sid5
VHG164 (Fe-metasomatised VCR)						
Ank 1	50.05	32.77	16.13	2.58	101.53	
Ank 2	50.10	32.73	16.23	2.37	101.43	
Sid 3	0.65	96.21	2.86	0.62	100.34	
Sid 4	1.07	95.41	3.92	1.25	101.65	
Ank 5	49.20	29.80	15.63	4.21	98.84	
Sid 6	0.36	98.36	0.38	0.59	99.69	close to sid 5
Sid 7	0.33	80.75	9.84	7.15	98.07	tiny laths @ edge sid 6
Sid 8	0.19	99.08	0.52	0.83	100.62	
Sid 9	1.51	87.25	11.01	0.00	99.77	rim —\
Sid 10	0.55	97.12	0.85	1.68	100.20	core —/
Sid 11	0.34	98.71	0.53	0.84	100.42	
Sid 12	0.29	96.93	0.36	0.99	98.57	
Sid 13	0.39	95.02	2.25	0.63	98.29	around chl
Sid 14	0.39	96.91	0.34	1.04	98.68	around chl
Sid 15	0.27	97.54	0.39	0.71	98.91	around Au
Ank 16	49.65	32.23	16.22	1.98	100.08	
Sid 17	0.46	97.59	2.38	0.93	101.36	
Sid 18	0.33	97.73	0.58	0.78	99.42	
Cc 19	96.99	0.66	0.99	2.45	101.09	cc 'vein'
Cc 20	96.65	0.69	0.99	2.16	100.49	cc 'vein'
Cc 21	93.04	2.67	0.99	4.04	100.74	cc 'vein'
Sid 22	1.13	95.83	1.08	2.09	100.13	nxt C

Gold Particle Analyses

SAMPLE VHG021

Gold Analysis No. & Comments	Au	Ag	Hg	TOTAL	Fineness	Corresp. Chl Anal.
Gold 1 (in Chl)	87.67	8.7	3.98	100.35	910	Chl 5
Gold 2/4 (in Chl)	88.29	8.27	3.88	100.44	914	Chl 6

SAMPLE VHG046

Gold Analysis No. & Comments	Au	Ag	Hg	TOTAL	Fineness	Corresp. Chl Anal.
Gold 1 (Chl)	88.61	8.34	3.87	100.82	914	Chl 5&6
Gold 2 (crack in Py)	88.3	8.27	3.99	100.56	914	Chl 5&6
Gold 4 (on Carbon)	92.52	6.66	2.24	101.42	933	Chl 10

SAMPLE: VHG062

Gold Analysis No. & Comments	Au	Ag	Hg	TOTAL	Fineness	Corresp. Chl Anal.
Gold 1 + Cpy (Rim around Py)	88.62	7.07	4.76	100.45	926	Chl 8
Gold 2 (Qtz)	88.19	6.27	4.71	99.17	934	
Gold 3 (Chl/Qtz)	89.98	6.68	4.4	101.06	931	
Gold 4 (edge of cubic Py)	88.79	6.7	4.92	100.41	930	Chl 7
Gold 5 (Chl/Qtz)	89.82	6.7	4.74	101.26	931	Chl 7
Gold 6 (Chl)	88.97	6.78	4.74	100.49	929	Chl 7
Gold 7 (porous Py)	89.58	6.61	4.53	100.72	931	
Gold 8 (Chl)	89.26	6.53	4.62	100.41	932	Chl 18 ??
Gold 9 (edge of Py)	89.52	6.94	4.52	100.98	928	
Gold 10 (Qtz)	88.71	6.68	4.83	100.22	930	
Gold 11 (Qtz)	89.4	6.53	4.82	100.75	932	
Gold 13 (in Chl next to Carbon)	89.1	6.54	3.48	99.12	932	
Gold 14 (porous Py)	89.78	6.9	4.24	100.92	929	Chl 9
Gold 15 (Qtz next to Chl)	90.2	8.81	1.06	100.07	911	Chl 3
Gold 16 (Chl vein)	87.27	7.6	4.76	99.63	920	Chl 3
Gold 1 (Qtz)	90.13	6.43	4.77	101.33	933	
Gold 2 (Qtz w Chl)	89.59	6.59	4.59	100.77	931	
Gold 3 (Qtz w Chl)	88.66	6.52	4.64	99.82	931	
Gold 4 (Qtz)	89.89	6.34	4.69	100.92	934	
Gold 5 (porous Py)	89.39	7.18	4.8	101.37	926	Chl 20 ?
Gold 6 (Porous Py)	89.32	7.05	4.76	101.13	927	Chl 20 ?
Gold 7 Chl)	89.74	6.63	4.65	101.02	931	Chl 19
Gold 8 (Qtz)	89.45	6.9	4.7	101.05	928	Chl 19

SAMPLE VHG063(A)

Gold Analysis & Comments	Au	Ag	Hg	TOTAL	Fineness	Corresp. Chl Anal.
Gold 1 (vein in Py)	87.66	7.31	4.78	99.75	923	
Gold 2 (Chl)	88.75	7.31	4.86	100.92	924	Chl7, 8, 9
Gold 3 (Chl)	89.5	7.32	4.58	101.4	924	10, 11
Gold 4 (Chl)	88.77	7.24	4.79	100.8	925	"
Gold 5 (attached to Py)	88	7.25	4.59	99.84	924	Chl 17&18
Gold 6 (crack in Py)	87.86	7.55	4.75	100.16	921	Chl 17&18
Gold 7 (Py)	88.44	7.5	4.67	100.61	922	Chl 17&18
Gold 8 (Chl)	88.84	7.21	4.76	100.81	925	Chl 17&18
Gold 9 (Chl)	88.18	7.39	4.65	100.22	923	Chl 17&18
Gold 10 (Chl)	87.87	7.24	4.83	99.94	924	
Gold 11 (Py)	88.53	7.31	4.8	100.64	924	
Gold 12 (next to Py + ?)	88.38	7.32	4.77	100.47	924	
Gold 13 (Chl)	87.81	7.5	4.79	100.1	921	
Gold 14 (Chl)	89.14	8.5	2.69	100.33	913	Chl 23
Gold 15 (next to Py)	87.75	7.54	4.93	100.22	921	Chl 23
Gold 16 (next to Py)	89.56	6.69	4.59	100.84	930	Chl 23
Gold 17 (next to Py)	88.68	7.16	4.53	100.37	925	Chl 22
Gold 18 (in Chl)	88.81	7.86	4.77	101.44	919	Chl 22
Gold 19 (Py)	88.29	7.56	4.62	100.47	921	Chl 22
Gold 20 (Chl)	88.36	7.47	4.9	100.73	922	Chl 22
Gold 21 (crack in Py)	88.8	7.31	4.78	100.89	924	Chl 22
Gold 22 (Chl)	88.88	7.19	4.38	100.45	925	Chl 22
Gold 1 (Qtz)	91.44	7.37	1.97	100.78	925	Chl 7-11
Gold 2 (Qtz)	88.89	7.39	2.24	98.52	923	Chl 7-11
Gold 4 (Chl)	88.61	7.32	4.63	100.56	924	Chl 7-11
Gold 5 (Chl)	89.38	7.38	4.59	101.35	924	Chl 7-11
Gold 6 (Chl)	89.01	7.36	4.73	101.1	924	Chl 7-11
Gold 7 (Qtz)	88.9	7.4	4.76	101.06	923	Chl 7-11
Gold 8 (Py)	88.55	7.18	4.78	100.51	925	?
Gold 10 (Qtz)	88.6	7	4.88	100.48	927	?

SAMPLE VHG074

Gold Analysis No. & Comments	Au	Ag	Hg	TOTAL	Fineness	Corresp. Chl Anal.
Gold 1 (next to Chl+-Py) R	83.03	11.11	5.36	99.5	882	Chl 8&9
Gold 2 (next to Chl+-Py) R	82.51	11.03	5.46	99	882	Chl 8&9
Gold 3 (next to Chl+-Py) R	82.59	11.16	5.53	99.28	881	Chl 8&9
Gold 4 (next to Chl+-Py) R	84.62	10.92	5.77	101.31	886	Chl 8&9
Gold 5&10 (Chl) Y	87.38	7.76	5.47	100.61	918	Chl 8&9
Gold 6 (Py)	89.45	8.38	2.09	99.92	914	
Gold 7 (Py) R	89.77	8.22	2.12	100.11	916	Chl 8&9
Gold 8 (Py)	91.16	6.87	0.83	98.86	930	Chl 8&9
Gold 9 (Py)	92.88	6.03	1.02	99.93	939	Chl 8&9
Gold 11 (Qtz next to Chl) R	87.06	7.02	5.18	99.26	925	Chl 8&9
Gold 13 (Chl)	86.46	7.75	5.06	99.27	918	Chl 8&9
Gold 14/15 (Chl nxt Py) Y + R	85.53	9.65	5.37	100.55	899	Chl 17
Gold 16 (Qtz next to Chl)	88.29	6.55	5.59	100.43	931	Chl 18
Gold 17 (Qtz)	91.64	6.49	1.66	99.79	934	Chl 18
Gold 18 (Chl)	87.29	7.7	5.19	100.18	919	Chl 13
Gold 19/20 (Qtz) Y + R	88.37	6.85	5.48	100.7	928	Chl 20
Gold 22 (Chl/Qtz) Y + R	88.31	7.41	5.47	101.19	923	Chl 20
Gold 23 (Chl/Qtz) Y + R	88.1	7.01	5.52	100.63	926	Chl 20
Gold 25 (Chl/Qtz) Y + R	87.23	7.88	5.13	100.24	917	Chl 20
Gold 26 (Chl/Qtz)	87.3	7.59	5.18	100.07	920	
Gold 28 (Chl/Qtz))	87.93	7.14	5.26	100.33	925	Chl 12
Gold 31 (Chl/Qtz) Y	88.25	7.29	5.58	101.12	924	Chl 10&11
Gold 32 (next to Gn?) Y	88.54	7.26	5.31	101.11	924	Chl 10&11
Gold 33 (Chl/Qtz) R	89.83	6.51	4.28	100.62	932	Chl 19

Y - yellow tinge
R - distinct reddish tinge

SAMPLE VHG088

Gold Analysis No. & Comment	Au	Ag	Hg	TOTAL	Fineness	Corresp. Chl Anal.
Gold 1 (next to Py)	88.47	8.25	3.95	100.67	915	Chl 1&2
Gold 2 (Chl next to Cc vein)	89.58	6.92	3.69	100.19	928	Chl 9
Gold 3 (Chl)	86.15	9.33	4.06	99.54	902	Chl 1&2

SAMPLE VHG091(B)

Gold Analysis No. & Comment	Au	Ag	Hg	TOTAL	Fineness	Corresp. Chl Anal.
Gold 2 (Chl/Qtz)	85.11	10.44	4.59	100.14	891	Chl 6
Gold 3	86.71	8.82	3.65	99.18	908	Chl 6
Gold 5 (Chl/Qtz)	85.62	9.86	4.13	99.61	897	Chl 6
Gold 6 (Chl/Qtz)	87.67	8	4.85	100.52	916	Chl 12
Gold 7 (Pyr next to Py)	85.93	8.73	4.53	99.19	908	Chl 11
Gold 11 (Chl/Qtz)	86.12	7.89	4.65	98.66	916	Chl 9&13

SAMPLE VHG093(A)

Gold Analysis No.& Comment	Au	Ag	Hg	TOTAL	Fineness	Corresp. Chl Anal.
Gold 1 (Chl/Qtz)	90.65	6.78	3.63	101.06	930	
Gold 2 (Qtz)	91.23	6.22	1.63	99.08	936	
Gold 3 (Qtz)	90.82	8.59	1.23	100.64	914	
Gold 4 (Chl)	88.63	6.94	4.38	99.95	927	
Gold 5 (next to Chl)	89.63	7.05	4.48	101.16	927	
Gold 6 (Chl +Py)	87.94	7.12	4.41	99.47	925	
Gold 7 (Qtz)	88.03	6.9	4.27	99.2	927	
Gold 8 (Chl +Py)	89.33	6.97	4.37	100.67	928	
Gold 9 (Chl +Py)	88.23	7.33	4.33	99.89	923	
Gold 10 (Chl +Py)	89.3	7.32	4.45	101.07	924	
Gold 11 (Chl +Py)	89.94	7.1	4.21	101.25	927	
Gold 14 (Chl +Py)	89.75	7.1	4.31	101.16	927	
Gold 15 (Qtz)	91.08	7.95	2.09	101.12	920	
Gold 16 (Qtz)	91.99	6.94	2.12	101.05	930	
Gold 17 (Qtz)	92.1	6.82	1.7	100.62	931	
Gold 18 (with Py+Pyr)	87.94	7.27	4.72	99.93	924	
Gold 20 (next to Py)	88.97	7.08	4.48	100.53	926	
Gold 22 (Chl next to Py)	88.37	6.76	4.42	99.55	929	
Gold 23 (next to Py)	89.71	7.17	4.45	101.33	926	
Gold 25 (next to Py)	90	7.07	4.32	101.39	927	
Gold 26 (Chl/Qtz)	89.53	7.07	4.44	101.04	927	
Gold 27/28 (Chl/Qz next to Py	89.8	6.93	4.69	101.42	928	
Gold 30 (next to Py)	89.82	6.77	4.36	100.95	930	
Gold 32 (Qtz)	89.49	6.82	4.32	100.63	929	
Gold 33 (Chl/Qtz)	87.79	6.5	4.62	98.91	931	
Gold 34 (Chl/Qtz)	89.01	6.93	2.99	98.93	928	
Gold 35 (Chl)	87.17	7.25	4.19	98.61	923	
Gold 36 (Qtz)	88.81	7.47	4.37	100.65	922	
Gold 37/43 (Pyr vein)	90.66	6.94	2.41	100.01	929	

SAMPLE VHG093(B)

Gold Analysis No.& Comments	Au	Ag	Hg	TOTAL	Fineness	Corresp. Chl Anal.
Gold 1 (Chl + Py)	87.81	8.37	4.94	101.12	913	Chl 2
Gold 2 (Chl)	86.39	7.95	4.81	99.15	916	Chl 2
Gold 4 (Qtz)	87.55	9.32	2.79	99.66	904	
Gold 5 (Qtz)	86.16	7.85	5.82	99.83	916	
Gold 6 (Qtz next to Py)	86.98	7.97	4.8	99.75	916	
Gold 7 (Qtz)	90.25	8.56	1.03	99.84	913	Chl 3&4
Gold 8 (Qtz)	90.46	9.35	0.97	100.78	906	Chl 3&4
Gold 9 (Py)	87.41	7.6	5.13	100.14	920	Chl 3&4
Gold 10 (Py)	87.18	7.52	4.88	99.58	921	Chl 3&4
Gold 11 (Py)	87.13	7.7	4.94	99.77	919	Chl 3&4
Gold 12 (Qtz)	85.98	8.5	5.19	99.67	910	Chl 3&4
Gold 13 (Qtz)	87.43	8.47	4.74	100.64	912	Chl 3&4
Gold 14 (Qtz)	87.3	7.59	4.85	99.74	920	Chl 3&4
Gold 15 (Qtz)	87.23	8.3	4.86	100.39	913	Chl 3&4
Gold 16 (Qtz)	88.07	7.62	4.8	100.49	920	Chl 3&4
Gold 18 (Qtz)	86.72	7.76	5.05	99.53	918	
Gold 19 (Qtz)	86.63	8.76	4.17	99.56	908	
Gold 20 (Qtz)	88.41	7.69	3.18	99.28	920	
Gold 21 (Qtz)	89.49	7.8	2.76	100.05	920	
Gold 22 (Qtz)	87.21	7.26	4.55	99.02	923	
Gold 23 (Chl next to Py)	88.34	7.5	4.38	100.22	922	Chl 5
Gold 24 (next to Py)	87.48	7.68	4.35	99.51	919	Chl 5
Gold 25 (Chl next to Py)	87.54	7.5	4.45	99.49	921	Chl 5
Gold 26 (Chl/Qtz)	87.69	7.55	4.4	99.64	921	Chl 7
Gold 27 (Qtz)	91.33	7.01	0.84	99.18	929	Chl 7
Gold 28 (Chl/Qtz)	90.79	9.13	1.02	100.94	909	Chl 7
Gold 29 (Qtz)	90.46	8.45	0.87	99.78	915	Chl 8
Gold 30 (Qtz)	92.6	6.73	0.85	100.18	932	Chl 8
Gold 31 (Qtz)	88.34	7.3	4.78	100.42	924	Chl 8
Gold 32 (Chl/Qtz rim around Py)	87.67	7.65	4.37	99.69	920	Chl 8
Gold 33 (Chl/Qtz)	90.38	7.45	1	98.83	924	Chl 10
Gold 34 (Chl/Qtz)	90.59	6.59	1.88	99.06	932	Chl 10
Gold 35 (next to Py)	87.63	7.74	4.44	99.81	919	Chl 12
Gold 36 (Chl/Qtz)	89.73	7.4	2.36	99.49	924	
Gold 37 (Chl/Qtz next to Py)	88.34	7.73	4.52	100.59	920	
Gold 38 (Chl/Qtz)	87.83	7.04	3.8	98.67	926	
Gold 39 (Qtz)	90.62	7.1	2.03	99.75	927	
Gold 40 (Qtz)	87.84	7.23	4.71	99.78	924	
Gold 41 (Chl/Qtz)	86.86	8.08	4.13	99.07	915	
Gold 42 (Chl/Qtz)	88.96	7.41	4.37	100.74	923	
Gold 44 (Chl/Qtz)	87.17	8.11	4.77	100.05	915	Chl 11
Gold 45 (Chl/Qtz)	87.37	7.71	4.3	99.38	919	Chl 11
Gold 46 (Chl/Qtz)	87.55	7.97	4.46	99.98	917	
Gold 47 (Chl/Qtz)	91.76	7.19	0.93	99.88	927	
Gold 48 (Chl)	87.55	8.07	4.65	100.27	916	
Gold 49 (Chl next to Py)	87.98	8.23	4.4	100.61	914	
Gold 50 (Qtz)	90.68	6.92	2.67	100.27	929	
Gold 51 (Chl next to Py)	87.29	7.59	4.5	99.38	920	
Gold 52 (with Pyr ? in vein ?)	87.2	7.43	4.95	99.58	921	
Gold 53 (Chl/Qtz)	87.52	7.74	4.55	99.81	919	
Gold 54 (Qtz)	88.75	7.56	4.88	101.19	922	Chl 9
Gold 55 (Chl/Qtz)	90.04	7.99	2.15	100.18	918	Chl 9
Gold 56 (Chl next to Py)	87.28	8.08	4.51	99.87	915	Chl 9
Gold 57 (porous Py)	86.07	8.1	4.5	98.67	914	
Gold 58 (Cpy+Py)	87.04	7.26	4.46	98.76	923	
Gold 59 (next to Py)	86.73	7.45	4.34	98.52	921	
Gold 60 (next to Py)	88.06	7.77	4.43	100.26	919	
Gold 61 (Qtz)	91.09	8.2	0.64	99.93	917	
Gold 62 (Py)	86.58	8.55	4.49	99.62	910	

SAMPLE VHG095

Gold Analysis No.& Comment	Au	Ag	Hg	TOTAL	Fineness	Corresp. Chl Anal.
Gold 1 (next to Py)	87.39	9.17	4.2	100.76	905	
Gold 2 (next to Py)	86.27	8.18	4.11	98.56	913	
Gold 3 (next to Py)	88.2	8.65	4.16	101.01	911	
Gold 4/5 (next to Ru+Pyr)	87.28	8.37	4.33	99.98	912	

SAMPLE VHG103

Gold Analysis No.& Comment	Au	Ag	Hg	TOTAL	Fineness	Corresp. Chl Anal.
Gold 3 (Qtz +-Chl)	88.41	7.26	4.99	100.66	924	Chl 11
Gold 5 (Qtz)	92.63	7.2	0.93	100.76	928	Chl 11
Gold 6 (Qtz)	88.11	8.11	5.02	101.24	916	Chl 11
Gold 7 (Qtz)	87.82	8.07	5.04	100.93	916	Chl 11
Gold 9 (Chl)	88.48	8.09	4.49	101.06	916	Chl 13& 16
Gold 10 (Chl)	88.55	8.2	4.59	101.34	915	Chl 13& 16
Gold 11 (Chl)	88.49	8.21	4.79	101.49	915	Chl 13& 16
Gold 12 (Chl)	88.83	8.03	4.4	101.26	917	Chl 13& 16
Gold 14 (Chl)	87.71	8.1	5.06	100.87	915	Chl 13& 16
Gold 15 (Chl)	88.06	8.31	4.7	101.07	914	Chl 13& 16
Gold 16 (Qtz)	88.17	7.51	4.61	100.29	922	Chl 13& 16
Gold 17 (Qtz)	87.32	8.02	4.52	99.86	916	Chl 13& 16
Gold 18 (Chl)	86.87	7.87	5.32	100.06	917	Chl 13& 16
Gold 19 (attached Py)	87.06	8.02	4.58	99.66	916	Chl 13& 16
Gold 20 (in Py)	87.23	8.38	4.66	100.27	912	Chl 13& 16
Gold 21 (Qtz)	87.85	8.12	5.41	101.38	915	Chl 13& 16
Gold 22 (attached Py)	88.23	8.19	4.69	101.11	915	
Gold 23 (Chl)	88.47	7.97	5.04	101.48	917	
Gold 25/27 (in Gers)	88.08	8.13	4.88	101.09	915	
Gold 28 (in Py ??)	86.8	8.24	4.71	99.75	913	
Gold 29 (Chl)	87.57	8.29	4.83	100.69	914	Chl 14& 15
Gold 30 (Qtz)	86.57	8.42	4.98	99.97	911	
Gold 31 (Qtz)	87.59	8.39	4.66	100.64	913	
Gold 32/34 (Qtz)	88.79	7.69	4.25	100.73	920	

SAMPLE VHG105

Gold Analysis No. & Comment	Au	Ag	Hg	TOTAL	Fineness	Chl Anal.
Gold 1 (Chl nxt Py)	86.49	8.56	4.47	99.52	910	
Gold 3 (C nodule)	86.18	8.16	4.24	98.58	914	
Gold 4/5 (Chl @ edge of 2nd	87.92	6.71	4.40	99.03	929	
Gold 6 (Chl nxt Py)	88.41	7.10	4.43	99.94	926	
Gold 7 (Chl in Qtz)	88.41	7.51	4.42	100.34	922	
Gold 8 (Py nxt C nodule)	87.51	7.54	4.39	99.44	921	
Gold 9/12 (in Qtz w Chl)	88.01	7.19	4.67	99.87	924	
Gold 13 (Chl nxt Qtz)	88.91	7.21	4.57	100.69	925	Chl 12
Gold 14/16 (Chl)	87.63	7.25	4.74	99.62	924	Chl 12
Gold 17 (Chl nxt Py)	87.39	7.37	4.56	99.32	922	Chl 12

SAMPLE VHG107

Gold Analysis & Comments	Au	Ag	Hg	TOTAL	Fineness	Corresp. Chl Anal.
Gold 1 (Qtz)	88.98	8.77	2.81	100.56	910	
Gold 2 (Qtz)	88.61	8.64	4.05	101.3	911	
Gold 3 (Qtz)	87.87	8.63	3.06	99.56	911	
Gold 4/6 (Chl)	87.9	8.46	3.94	100.3	912	
Gold 7/8 (@ Qtz margn)	88.52	8.59	3.96	101.07	912	
Gold10 (@ Qtz margn)	87.52	8.6	4.8	100.92	911	
Gold 11 (Qtz)	89.33	8.34	3.79	101.46	915	
Gold 12 (attached Py)	88.11	8.36	4.41	100.88	913	
Gold 13 (Py)	87.04	8.77	3.91	99.72	908	
Gold 14 (Qtz)	88.14	8.98	4.12	101.24	908	
Gold 15 (attached Py)	87.3	8.5	4.02	99.82	911	
Gold 16 (Qtz)	88.02	8.35	4.14	100.51	913	
Gold18 (@ Qtz margn)	88.53	8.38	4.25	101.16	914	
Gold 19/24 (@Qtz margn)	88.45	8.68	3.97	101.1	911	
Gold26 (Qtz margn wChl)	88.3	8.7	4.35	101.35	910	
Gold27 (Qtz margn wChl)	87.63	8.6	4.22	100.45	911	
Gold28 (in Qtz closeto C)	87.9	8.51	4.18	100.59	912	
Gold29 (@ Qtz margn)	88.01	8.11	4.08	100.2	916	
Gold30 (in Chl nxt C)	88.17	8.03	3.79	99.99	917	Chl 5
Gold31 (in Chl nxt C)	89.33	7.73	4	101.06	920	Chl 5
Gold 32 (Qtz)	88.06	8.76	4.02	100.84	910	
Gold 33 (Qtz)	90.45	9.03	1.82	101.3	909	
Gold 34 (Chl)	86.92	8.8	4.11	99.83	908	
Gold 35 (Qtz)	88.35	7.9	3.98	100.23	918	
Gold 36/41 (@Qtz margn)	88.57	8.43	3.9	100.9	913	
Gold 43 (Py)	86.62	9.39	4.2	100.21	902	

SAMPLE VHG120

Gold Analysis No. & Comments	Au	Ag	Hg	TOTAL	Fineness	Corresp. Chl Anal.
Gold 2 (Py)	89.24	8.09	4.01	101.34	917	
Gold 4 (nxt Py)	89.24	7.57	3.86	100.67	922	
Gold 5 (nxt Py)	88.66	8.02	3.83	100.51	917	
Gold 6 (Py)	89.47	8.01	3.91	101.39	918	
Gold 7/11 (between Py)	89.21	7.96	4.01	101.18	918	
Gold 14/15 (in Py)	89.28	7.98	3.92	101.18	918	
Gold 17 (in Py)	89.53	7.87	3.89	101.29	919	
Gold 19/26 (nxt Py +- Qtz)	89.27	7.75	4.01	101.03	920	

SAMPLE VHG125

Gold Analysis No. & Comments	Au	Ag	Hg	TOTAL	Fineness	Chl Anal.
Gold 5 (Chl)	91.71	6.83	1.35	99.89	931	Chl 1
Gold 6 (Chl)	88.88	7.62	4.85	101.35	921	Chl 1
Gold 7 (Chl nxt Qtz)	88.55	6.71	4.7	99.96	930	Chl 2
Gold 8 (in Py)	88.2	7.67	4.63	100.5	920	Chl 4& 5
Gold9 (on Chltwirl in Qtz)	91.91	6.85	1.77	100.53	931	Chl 4& 5
Gold10 (w Chl in Qtz)	90.33	6.19	4.34	100.86	936	Chl 4& 5
Gold 11 (Chl)	87.53	7.64	4.8	99.97	920	Chl 6-9
Gold 12 (w Py in Chl)	88.21	7.48	4.81	100.5	922	Chl 6-9
Gold13 (wPyr?? in Qtz)	88.04	7.58	4.62	100.24	921	Chl 6-9
Gold 14 (Py)	88.49	7.38	4.79	100.66	923	Chl 6-9
Gold 15 (Chl)	89.42	6.71	4.43	100.56	930	
Gold 16 (Py)	87.01	7.13	4.56	98.7	924	
Gold17 (in Qtz w Chl)	89.46	7.07	4.91	101.44	927	
Gold 19 (Chl)	89.41	7.37	4.62	101.4	924	
Gold 20 (Chl)	88.35	7	4.73	100.08	927	
Gold 21 (Chl)	88.12	7.21	4.7	100.03	924	
Gold 22 (Chl)	89.16	6.75	4.72	100.63	930	

SAMPLE VHG130

Gold Analysis No. & Comment	Au	Ag	Hg	TOTAL	Fineness	Corresp. Chl Anal.
Gold 2 (in Chl ??)	89.59	8.03	3.23	100.85	918	
Gold3/4(inChl?? nxt Pyr?)	89.82	7.81	3.45	101.08	920	
Gold 5 (in Pyr ??)	88.92	7.57	3.3	99.79	922	
Gold 6 (in Chl ??)	88.85	8	3.46	100.31	917	
Gold 7 (Py)	88.58	8.02	3.54	100.14	917	
Gold 8 (Qtz)	89.93	8.76	2.3	100.99	911	
Gold 9 (Qtz)	89.48	9.04	1.85	100.37	908	
Gold 10/16 (Qtz nxt Chl)	89.5	7.9	3.39	100.79	919	
Gold 17 (Py)	88.59	8.16	3.65	100.4	916	

SAMPLE VHG131

Gold Analysis No. & Comment	Au	Ag	Hg	TOTAL	Fineness	Corrsp. Chl Anal.
Gold 2/3 (in round Py)	88.14	9.01	3.99	101.14	907	
Gold 5 (Py)	88.15	9.24	4.08	101.47	905	
Gold 7 (w Gn in Py)	86.19	8.69	5.62	100.5	908	
Gold 8 (Chl)	87.49	8.66	4.77	100.92	910	
Gold 9/10 (w Cpy in Py)	86.54	8.81	5.67	101.02	908	
Gold 11 (Qtz)	89.19	8.68	1.99	99.86	911	Chl 6
Gold 12 (Chl wQtz)	86.65	9.42	4.82	100.89	902	Chl 6
Gold 13 (Chl)	86.69	9.26	4.67	100.62	903	Chl 6
Gold 14 (Chl/Qtz)	87.27	9.09	4.36	100.72	906	Chl 6
Gold 15 (Qtz w Chl)	87.79	9.85	3.67	101.31	899	Chl 6
Gold17 (Qtz margn wChl)	88.84	9.31	2.88	101.03	905	Chl 6
Gold 18 (Qtz)	89.06	9.46	1.72	100.24	904	Chl 8
Gold20 (wChl attchd Py)	86.91	8.53	4.86	100.3	911	Chl 8
Gold 22 (w Chl attchd Py)	85.31	8.3	4.99	98.6	911	Chl 8

SAMPLE VHG150(B)

Gold Analysis No. & Comment	Au	Ag	Hg	TOTAL	Fineness	Corresp. Chl Anal.
Gold 1 (Qtz)	88.13	7.7	3.61	99.44	920	
Gold 2/8 (in Qtz +- w Py)	88.22	7.73	3.88	99.83	919	
Gold 9 (Chl nxt Qtz)	87.6	7.86	3.66	99.12	918	
Gold 10/12 (Qtz)	88.12	7.48	3.69	99.29	922	

SAMPLE VHG164

Gold Analysis No. & Comment	Au	Ag	Hg	TOTAL	Fineness	Corresp. Chl Anal.
Gold 1/3 (in Sid)	86.43	8.77	4.99	100.19	908	
Gold 4 (in Sid)	85.83	8.78	4.67	99.28	907	
Gold 5/6 (Chl w ??)	86.08	9.18	4.55	99.81	904	
Gold 7/8 (nxt sheared Sid/Chl	86.23	8.66	4.96	99.85	909	
Gold 9 (C nodule @ edge qtz)	85.85	9.05	4.24	99.14	905	
Gold 10 (C nodule @ edge qt	86.49	8.46	3.95	98.90	911	
Gold 11 (C nodule @ edge qt	86.87	8.94	3.44	99.25	907	
Gold 12 (Qtz)	88.70	8.67	3.08	100.45	911	
Gold 13 (Sid)	85.08	8.80	4.91	98.79	906	
Gold 14 (Sid)	86.95	8.85	4.50	100.30	908	
Gold 15/16 (Sid @ edge C no	86.77	8.81	4.61	100.19	908	
Gold 17/18 (in Sid)	86.22	8.71	4.68	99.61	908	
Gold 19 (C nodule)	86.23	8.71	3.67	98.61	908	
Gold 20 (C nodule w Gn)	87.36	8.74	3.91	100.01	909	
Gold 22/23 (Edge C nodule w	86.84	8.66	4.07	99.57	909	
Gold 24 (Edge C nodule w Sid	87.90	8.43	3.30	99.63	912	
Gold 25 (Edge C+Sid, w Gn)	87.39	8.78	3.65	99.82	909	
Gold 26 (Sid)	87.00	8.69	4.78	100.47	909	
Gold 27 (Edge C nodule w Sid	86.93	7.23	4.55	98.71	923	
Gold 28 (in Sid w Gn)	86.91	8.44	4.56	99.91	911	
Gold 29 (Sid)	86.65	8.67	4.76	100.08	909	
Gold 30 (Sid @ edge C nodul	87.43	9.21	4.71	101.35	905	
Gold 31 (Chl ? amongst Sid)	86.40	8.93	4.71	100.04	906	
Gold 32/34 (in Sid w Chl arou	87.11	8.69	4.85	100.65	909	

SAMPLE VHG163(B)

Gold Analysis No. & Comment	Au	Ag	Hg	TOTAL	Fineness	Corresp. Chl Anal.
QV Gold 1/3 (w Sph nxt Chl)	86.60	9.50	4.03	100.13	901	Chl 8
QV Gold 4/6 (w Gn nxt Chl?)	85.66	9.50	4.24	99.40	900	
QV Gold 7 (w Sph nxt Qtz)	86.44	9.64	4.28	100.36	900	

SAMPLE VHG163(C)

Gold Analysis No. & Comment	Au	Ag	Hg	TOTAL	Fineness	Corresp. Chl Anal.
QV Gold 1 (f gr Qtz)	88.02	7.28	4.18	99.48	924	
QV Gold 2 (f gr Qtz)	88.02	7.56	4.09	99.67	921	
QV Gold 3/4 (Qtz w Gn)	88.18	7.34	4.17	99.69	923	
QV Gold 5 (Qtz w Gn)	89.24	7.52	4.03	100.79	922	
QV Gold 6 (f gr Qtz)	88.79	7.76	4.24	100.79	920	
QV Gold 7 (Qtz)	87.95	7.37	4.05	99.37	923	
QV Gold 8 (Qtz)	88.88	7.27	3.91	100.06	924	
QV Gold 9/11 (nxt Gn, Large	88.97	7.13	4.07	100.17	926	
QV Gold 12	89.84	7.03	3.87	100.74	927	
QV Gold 13/14 (close to Qtz)	89.17	6.90	4.11	100.18	928	
QV Gold 15 (w Gn close to Qt	87.95	7.02	4.06	99.03	926	
QV Gold 16 (Qtz)	88.52	7.01	3.97	99.50	927	
QV Gold 17/18 (Qtz)	88.84	7.21	4.12	100.17	925	
QV Gold 19/23 (away from Gn	89.05	6.79	3.90	99.74	929	
QV Gold 24/25 (nxt Brav?)	88.92	6.63	4.19	99.74	931	
QV Gold 26 (in Gn + Brav?)	88.07	7.01	4.10	99.18	926	
QV Gold 27 (Qtz)	88.07	6.91	4.11	99.09	927	
QV Gold 28 (edge Gn w Qtz)	89.30	6.96	4.02	100.28	928	
QV Gold 29 (Qzt)	88.26	7.09	4.09	99.44	926	
QV Gold 30 (Qtz)	88.09	7.50	4.09	99.68	922	
QV Gold 31 (nxt Gn)	89.25	6.58	4.22	100.05	931	
QV Gold 32 (nxt Brav?)	88.64	6.99	4.29	99.92	927	
QV Gold 33/34 (Qtz)	88.49	7.05	3.95	99.49	926	
QV Gold 35 (Gn)	88.52	7.13	3.80	99.45	925	
QV Gold 36/37 (w Gn in Qtz)	88.51	6.93	4.18	99.62	927	
QV Gold 38 (Qtz)	88.27	6.84	3.94	99.05	928	
QV Gold 39 (Qtz)	88.99	6.90	4.04	99.93	928	

APPENDIX D

Fluid Inclusion Microthermometric Technique

Method

The sample material was in the form of thin (<100 μm) polished wafers. Temperatures of phase changes were obtained with a FLUID INC.-adapted U.S.G.S. gas-flow heating-freezing system which operates by passing cooled N_2 gas or heated air directly above and beneath the sample. The system was calibrated using synthetic fluid inclusions in quartz provided by SYNFLINC (Sterner and Bodnar, 1984), at -56.6°C (triple point of CO_2), 0.0°C (triple point of pure H_2O), and 374.1°C (critical point of pure H_2O). Reproducibility of measurements during calibration was always within 0.2°C of the -56.6°C standard, within 0.1°C of the 0.0°C standard, and within 1°C of the 374.1°C standard. Accuracy of the system is estimated to be better than ± 0.2°C below 0°C, and better than ± 1°C on heating the sample, as long as the thermocouple tip is not farther than 2.5 mm from the fluid inclusion studied.

Bedding parallel QV

Sample No.	Size (um)	V/L (%)	Te	Tm	Th	Salinity	Type	Comments
VHG 038	6	10		1.8	117	3.06	II	
	5	8		3.4	119	5.56	II	
	2	8		3	128	4.96	II	–\
	2	8		3.1	127	5.11	II	\ Along microfract
	2	8		2.9	132	4.80	II	/
	2	8		3.2	137	5.26	II	–/
	4	8		3.7	148	6.01	II	
	5	8		1.3	125	2.24	II	
	4	8		3.3	136	5.41	II	
	4	8		2.8	139	4.65	II	
	6	8		2.9	137	4.80	II	
	2	8		2.6	104	4.34	II	–\
	4	8		3		4.96	II	\ Along microfract
	2	8			111		II	/
	2	10			101		II	–/
	4	5		3.2	155	5.26	II	
	4	8			142		II	
	3	5			90		II	–\
	3	5			93		II	> Along microfract
	2	5			97		II	–/
	8	8		3	121	4.96	II	
	8	5		3	115	4.96	II	
	2	10			113		II	–\
	3	10			115		II	\
	2	10			107		II	> Along microfract
	4	10			111		II	/
	3	10		2.5	118	4.18	II	–/
	6	8		2.4	101	4.03	II	
	5	10			118		II	
VHG 055(B)	3	10		0.9		1.57	III	
(Qz/Cc vein)	7	15	<-31.1		130		II	
	6	10	<-29.7	3.7	113	6.01	III	
	6	25		3.2	213	5.26	III	
	4	10			165		II	
	4	15		2.6		4.34	III	fibrous xstal

Bedding parallel QV

Sample No.	Size (um)	V/L (%)	Te	Tm	Th	Salinity	Type	Comments
VHG 087	3	10		1.7	132	2.90	II	
	3	15		1.8	140	3.06	II	–\ Along inc trail
	4	10		1.9	137	3.23	II	–/
	4	8		3	210	4.96	II	–\
	3	10		3.7	205	6.01	II	\
	5	10	-31	4.8		7.59	II	\
	3	10		4		6.45	II	> Along inc trail
	3	10		4.3		6.88	II	/ (60 to QV margin)
	3	10		4.8		7.59	II	/
	3	10		4.5		7.17	II	–/
	4	10		1.5	134	2.57	II	–\
	4	12		1.7	124	2.90	II	\
	3	12		1.5	134	2.57	II	> Same inc trail
	4	15		1.7	135	2.90	II	/ (bed ||)
	3	10		1.8	134	3.06	II	–/
	3	10		1.2	137	2.07	II	–\
	3	10		1.2	147	2.07	II	\ Same inc trail
	2	10		1.1	145	1.91	II	/ (bed ||)
	2	12		1.3	140	2.24	II	–/
	3	10		2	139	3.39	II	–\
	3	10		2.2	143	3.71	II	\
	5	10		2.1	136	3.55	II	\
	3	10		2	149	3.39	II	> Same inc trail
	3	10		2	141	3.39	II	/ (bed ||)
	3	10		2.1	153	3.55	II	/
	3	10		2	144	3.39	II	–/
	4	10			135		II	–\
	5	10		1.6	154	2.74	II	\
	4	15		1.6	143	2.74	II	> Same inc trail
	3	10		1.5	146	2.57	II	/ (bed ||)
	4	12			135		II	–/
	4	10		1.8	135	3.06	II	–\
	2	10		1.6	144	2.74	II	\ Same inc trail
	5	8		1.4	138	2.41	II	/ (bed ||)
	3	10		1.6	145	2.74	II	–/

Bedding parallel QV

Sample No.	Size (um)	V/L (%)	Te	Tm	Th	Salinity	Type	Comments
VHG 137	5	15		2.2	148	3.71	III	fibrous xstal
(Qz/Cc vein)	6	15			125		II	
	5	10		2	146	3.39	II	
	5	10		2	142	3.39	II	
	5	10		2.5	135	4.18	II	-\
	4	12		2.4	142	4.03	II	> Along microfract
	5	12		2.4	148	4.03	II	-/
	5			2.4	145	4.03	II	
	10	10		2.4	133	4.03	III	
	6	10		2.3	143	3.87	III	-\
	6	15		2.2	136	3.71	III	-/
	5	10	<-34.2	2.5	132	4.18	III	-\
	4	15			129		II	\ Along microfract
	5	12		2.9	131	4.80	II	/
	3	15			121		II	-/
	7	15		1.9	167	3.23	III	
	5	15		2.3	155	3.87	II	
	7	12		2.6	136	4.34	II	
	7	15		2.5	147	4.18	III	-\
	7	15		2.5	167	4.18	II	> One gp
	6	15		2.6	168	4.34	II	-/
	12	20			148		III	
	7	15		2.3	154	3.87	II	
	9	15		2.2	169	3.71	II	
	4	15		2.3	166	3.87	II	

Bedding parallel QV

Sample No.	Size (um)	V/L (%)	Te	Tm	Th	Salinity	Type	Comments
VHG 166	9	8		4.2	182	6.74	II	
	5	8		4	170	6.45	II	
	13	10		3	183	4.96	II	
	5	15		2.6	164	4.34	II	
	5	15		3.4	162	5.56	II	–\
	4	15		3.2	153	5.26	II	\ Along microfract
	2	10		2.9		4.80	II	/
	3	10		2.8		4.65	II	–/
	8	8	<-29.8	2.8	129	4.65	II	–\
	5	8		2.7		4.49	II	\ Along microfract
	4	8	<-33.1	2.6	121	4.34	II	/
	6	8	<-30	2.6	119	4.34	II	–/
	15	8		2.7	209	4.49	II	–\
	8	8	<-29.1	2.5	173	4.18	II	–/
	5	15		2	155	3.39	II	
	15	15		2		3.39	II	
	6	10		2		3.39	II	
	6	8		2.5		4.18	II	
	6	5	<-32.4		120		II	
	6	8			128		II	
	8	10	<-35.7	4	133	6.45	III	
	9	8	<-33	3.8	97	6.16	II	
	4	10	<-30.7	4	114	6.45	II	–\
	5	15	<-30.7	3.8	125	6.16	II	> Along 'shallow'
	7	8		3.7	129	6.01	II	–/ microfract plane
	5	8	<-29.7	3.8	104	6.16	II	
	5	8		2.2	134	3.71	II	
	5	8		2.8	141	4.65	II	–\
	5	10		3	133	4.96	II	> Along 'shallow'
	4	10		3	143	4.96	II	–/ perp. QV margin ??
	5	8		2.6	134	4.34	II	
	5	12		2.8	148	4.65	II	
	6	8		2.7	102	4.49	II	
	9	10		2.4	132	4.03	II	–\
	5	10		2.3	127	3.87	II	\ In loose gp
	4	10	<-30.4	2.5	126	4.18	II	/
	5	10		2.3	130	3.87	II	–/
VHG 172	4	15		1.3	189	2.24	III	Aniso xstal attached to inc
	5	15	<-31.2	3.3	178	5.41	II	–\
	4	18		2.9	176	4.80	II	> Same microfracture
	3	15		3.1	175	5.11	II	–/ (45 to QV margin)
	2	15		3.1	146	5.11	II	–\
	3	15		3.2	157	5.26	II	\ Close gp along microfract
	2	15		3.0	142	4.96	II	/ (perp to QV margin)
	3	12		3.3	152	5.41	II	–/
	3	15		2.2	142	3.71	II	
	4	18		1.8	160	3.06	II	–\
	4	15		1.7	137	2.90	II	\
	4	15		2.2	160	3.71	II	\ In one loose gp in qtz gr
	4	12		2.8	161	4.65	II	/
	4	15		2.7	158	4.49	II	/
	5	12	<-31.6	2.7	162	4.49	II	–/
	4	15		2.4	170	4.03	II	–\
	4	12	<-28.4	2.9	155	4.80	II	\
	5	12	<-29.9	2.4	166	4.03	II	\ All in one gp (possibly along
	5	15		2.9	156	4.80	II	/ microfract || QV margin)
	5	15		2.7	165	4.49	II	–/
	5	15		2.3	149	3.87	II	
	6	12			132		II	–\
	4	12			131		II	\
	4	12		1.8	129	3.06	II	> All along microfract
	3	18		1.7	142	2.90	II	/ (perp to QV margin)
	3	15		1.6	139	2.74	II	–/

Bedding perpendicular QV

Sample No.	Size (um)	V/L %	Te	Tm	Th	Salinity	Type	Xstal ?	Comments
VHG 016	3	10		4.5	136	7.17	III	xstal	–\ Same trail
	3	10	-10.2	4.4	130	7.02	II		–/
	4	10	<-28	9.7	109	13.62	II		–\ Same trail
	2	10	<-24	9.6	98	13.72	II		–/
	4	10		4.2	122	6.74	II		
	3	10		4.8	120	7.59	II		
	4	10		4.9	98	7.73	III	xstal	
	4	10		5.3	108	8.28	II		
	3	10		5.3	105	8.28	III	xstal	
	4	10		4.4	97	7.02	III	xstal	
	4	10	-22.6	4.9	106	7.73	III	xstal	
	2	10	<-20	5.9	131	9.08	III	xstal	–\
	5	10	<-23	6.3	132	9.60	III	xstal	> Same trail
	4	10		7	129	10.49	III	xstal	–/
	3	10		4.6	124	7.31	II		
	5	10	<-21.6	3.7	128	6.01	III	xstal	
	4	10		4	97	6.45	III	xstal	
	6	5	<-25	4.4	97	7.02	III	xstal	
	5	5		9.7	106	13.62	III	xstal	
	5	6	<-31.8	4.4	96	7.02	III	xstal	
	5	10	<-29	4.4	131	7.02	III	xstal	
	3	10		4.8		7.59	III	xstal	
	5	8		4.7	132	7.45	III	xstal	
VHG 039	6	8	<-21.9		138		II		
	8	10		2.6	147	4.34	II		
	7	8	-24.9	2.9	128	4.80	II		
	8	10		2.6	155	4.34	II		
	5	7		2.3	114	3.87	II		
	4	8	-22	4.1	107	6.59	II		–\
	4	8	<-22.1	4.5	107	7.17	II		> Along microfract
	4	10	<-21.8	4.3	106	6.88	II		–/
	5	10		2.4	149	4.03	II		
	5	8	<-22.8	2.5	115	4.18	II		
	6	8		2.6		4.34	II		
	4	10		2.9	149	4.80	II		
	5	10		3.2	149	5.26	II		
	2	15		3	164	4.96	II		–\
	2	10		3	165	4.96	II		\ Along microfract
	3	15		3.1	164	5.11	II		/
	4	15		3.2	167	5.26	II		–/
	5	15		3.9	164	6.30	II		
	4	15		3.1	163	5.11	II		–\
	3	15		3.1	165	5.11	II		–/
	3	10		3.1	164	5.11	II		
	6	8	<-25.4		116		II		
	4	8		4.2	141	6.74	II		
	6	15		2.5	148	4.18	II		
	5	15		2.6	148	4.34	II		
	6	8		2.9	143	4.80	II		
	5	8		2.8	160	4.65	II		
	4	10		2.7	137	4.49	II		
	4	10		2.8	180	4.65	II		
	5	10		2.9	174	4.80	II		

Bedding perpendicular QV

Sample No.	Size (um)	V/L %	Te	Tm	Th	Salinity	Type	Xstal ?	Comments
VHG 093(A)	3	12		2.6	131	4.34	III	iso xstal	
	4	10		2.6	127	4.34	II		-ve Xstal shape
	6	10		2.9	154	4.80	II		
	5	8		3.1	141	5.11	II		
	5	8		3	107	4.96	II		
	4	10		2.6	107	4.34	II		
	4	8		2.6	117	4.34	II		
	4	8		2.8	112	4.65	II		
VHG 174	9	8	-28.1	2.5	129	4.18	II		-\
	11	8	<-30.2	2.4	157	4.03	II		\
	6	8	<-29.7	2.2	110	3.71	II		> Elongate incs ||
	6	10	<-30.1	2.4	135	4.03	II		/ to QV margin
	9	8	<-30	2.8	143	4.65	II		-/
	20	10		2.2	159	3.71	II		-\ Elongate incs ||
	6	10		2.4	138	4.03	II		-/ to QV margin
	6	7	<-30	2.9	142	4.80	II		-\
	8	8		3.3	131	5.41	II		> Elongate incs ||
	9	8		2.5	123	4.18	II		-/ to QV margin
	4	10		3.3		5.41	II		
	6	10	<-28.1	3.7	127	6.01	II		-\
	4	8	<-31.8	3.5	96	5.71	II		> Along same microfract
	4	7	<-35.2	3.8	90	6.16	II		-/ || QV margin
	4	7		3.9		6.30	II		
	5	10		3.3	149	5.41	II		
	4	12		3.1	144	5.11	II		-\
	5	15	<-30.5	2.5	142	4.18	II		> Along same microfract
	5	12	<-28.9	3	151	4.96	II		-/ || QV margin
	6	12	<-30.5	3.1	125	5.11	II		
	4	8	<29.5	3.9	84	6.30	II		-\
	3	10		2.3	127	3.87	II		\
	3	12		2.6	146	4.34	II		> All in same QV
	4	10		3	138	4.96	II		/ Qtz grain
	3	10		2.8	123	4.65	II		-/
	12	10		4.8	134	7.59	II		
	6	8	<-34	3.1	107	5.11	II		
	5	8	<-31.1	3.3	133	5.41	II		
	12	8	<-33.7	3.6	129	5.86	II		
	10	12	<-34.5	3.4	111	5.56	II		-\
	5	15		3	126	4.96	II		\ Towards centre
	4	15		3	135	4.96	II		/ of QV grain
	4	15	<-36.5	3	116	4.96	II		-/

Bedding perpendicular QV

Sample No.	Size (um)	V/L %	Te	Tm	Th	Salinity	Type	Xstal ?	Comments
VHG 180	2	10		2.3	134	3.87	II		--\
	2	10		2.3	139	3.87	II		--/
	4	15	-36.6	2.6	159	4.34	II		--\
	4	12		2.8	161	4.65	II		\
	3	15		2.5	148	4.18	II		> 2 Gps of gen
	2	15		2.8	147	4.65	II		/ angular incs
	2	10		2	145	3.39	II		--/
	4	8			114		III	Aniso	--\ together
	4	10		2.9	127	4.80	III	gr aniso	--/
	4	15	-32.5	2.3	186	3.87	II		--\
	3	15	-31.1	2.8	150	4.65	II		\ together
	3	12		2.7	134	4.49	II		/
	3	10	-31.7	2.2	114	3.71	II		--/
	5	12	-30	2.1	153		II		--\
	3	10		3	157		II		> together
	5	18		3.2	178		II		--/
	2	15		2.6			II		--\
	4	12		2.2	128		II		> together
	3	10	<-26.6	2.5	158		II		--/
	7	15	-30.4	2.4	136		II		--\
	3	15		2.6	127		II		\ together
	3	15		2.2	149		II		/
	3	18		2.7	167		II		--/
	5	8	-62.6				IV		--\ CO2-rich inclusions
	10	8			29		IV		--/

Auriferous QV

Sample No.	Size (um)	V/L %	Te	Tm	Th	Salinity	Type	Comments
VHG 163(A)	9	10		3.4	138	5.56	III	
Marginal Zone	5	20		2.9		4.80	II	
	8	18		3.5	136	5.71	III	
	9	8		4.4	130	7.02	III	
	10	8		4.5	123	7.17	III	
	7	8		3.1		5.11	II	
	4	20		2.9		4.80	II	
	6	10	<-36	4.2	131	6.74	II	
	6	15		3.8	137	6.16	II	
	7	18		2.8		4.65	II	
	8	8	<-42	4	126	6.45	III	
	7	10	<-39.2	3.9	122	6.30	III	
	4	12	<-38.9	3.8	129	6.16	II	-\
	3	15	<-36	3.8	135	6.16	II	> Along microfract
	3	12		3.8	133	6.16	II	-/
	10	15	<-37	4.6	143	7.31	II	
	4	12		3.8	141	6.16	II	
	5	12		3.8	133	6.16	II	
	7	8	<-36.9	2.7	104	4.49	II	
							II	
	6	15		3.0	233	4.96	II	
	5	15		3.6	222	5.86	II	
	6	22			191		III	
	5	25		3.3	191	5.41	II	
	4	22		4.3	210	6.88	II	
	3	25		3.9	212	6.30	II	
	4	22		3.2	220	5.26	II	
	4	18		5.1	227	8.00	II	
	6	18			214		II	
	6	18			190		II	
	6	20		2.9	201	4.80	II	
	4	20			198		II	
	5	20		4.9	211	7.73	II	
	5	25		3.4	213	5.56	III	
	9	25		3	224	4.96	II	
	13	28		1.9	244	3.23	III	
	7	25		4.2	208	6.74	III	
	10	25		4.1	189	6.59	III	
	7	30	<-39.8	3.6	198	5.86	III	
	5	28		3.9		6.30	III	
	5	20		2.9	173	4.80	III	
	5	25		3.4		5.56	III	
	6	23	<-36.5	1.4	212	2.41	III	
	4	23	<-40.1		220		II	
	6	15	<-39.8	4.3	169	6.88	III	

Auriferous QV

Sample No.	Size (um)	V/L %	Te	Tm	Th	Salinity	Type	Comments
VHG 163(A)	7	10	-44.5	6.1	136	9.34	III	
Central Zone	6	8	<-38	5	129	7.86	III	
	5	8	<-37.6	3	116	4.96	III	
	4	8	<-36.6	3	111	4.96	III	
	4	8			117		II	
	4	10		3.4	135	5.56	II	
	10	8	<-39.2	5.8	80	8.95	III	
	5	8	<-38.9	3.3	116	5.41	II	
	7	8		2.9		4.80	III	
	5	5	<-40	2.8		4.65	II	
	9	5	<-36.2	4.8		7.59	II	
	5	10	<-40	3.6	125	5.86	II	
	5	8	<-40	3.6	120	5.86	II	
	7	10	<-39.3	3.8	120	6.16	III	
	4	15		3.6	144	5.86	III	
	5	10		3.1	133	5.11	III	
	10	12		4.2	134	6.74	II	
	7	12		3.3	135	5.41	III	
	7	15	<-36.2	6.2	86	9.47	II	
	6	18	<-41.4	4.7	138	7.45	III	
	16	10		3.5	118	5.71	III	
	6	12	<-40.2	3.4	144	5.56	III	
	5	15		3.7	151	6.01	III	
	5	10	<-39	4	112	6.45	III	
	4	12		3.6	143	5.86	II	
	5	12		3.3	139	5.41	III	
	6	10		6.4		9.73	III	
	4	10	<-39.1	3	117	4.96	II	
	8	10	<-41.6	3.5		5.71	III	
	7	15		3.4	108	5.56	II	

Nooitgedacht Fault QV

Sample No.	Size (um)	V/L (%)	Te	Tm	Th	Salinity	Type	Comments
VHG 178(B)	5	10		3.4	171	5.56	II	–\
	5	15		2.7	150	4.49	II	\
	5	15		3.8		6.16	II	> In loose gp
	6	10	<-33.5	3.9	109	6.30	II	/
	10	12	<-36.9	3.3		5.41	II	–/
	4	10		3.8	171	6.16	II	–\
	3	15		4.6	213	7.31	II	\
	3	12		4	179	6.45	II	> in microfract at 45
	3	15		3.3	187	5.41	II	/ to QV margin
	4	15		4.7	201	7.45	II	–/
	7	20		3.5	152	5.71	III	
	9	8		3.5	158	5.71	II	
	4	10			145		II	
	4	15		3.8	180	6.16	II	
	4	12		3.2	126	5.26	II	
	4	15		3.2	171	5.26	II	
	5	15			189		III	
	6	85	-59.4		11		IV	–\
	5	85	-56.5		11		IV	\
	6	60	-56.5		13		IV	> CO_2-rich inclusions
	5	75			17		IV	/
	6	80	-56.6	>=3.1	20		IV	–/

VCR Quartzite Fluid Inclusions

Sample No.	Size (um)	V/L (%)	Te	Tm	Th	Salinity	Type	Comments
VHG 055(B)	4	12		2.4		4.03	II	-\
	3	15	<-28.7	2.8	169	4.65	II	\ Along microfract
	3	15			168		II	/
	6	10	<-21.4	2.6		4.34	II	-/
	4	10	<-27.1	3.8	131	6.16	II	
	3	10		1.5		2.57	II	
	13	18		2.8	157	4.65	III	-\
	5	15		2.9	154	4.80	II	\ Along microfract
	4	10		2.8	164	4.65	II	/
	6	10	<-28.2	2.9	150	4.80	II	-/
	5	12	<-21.8	2.6	148	4.34	II	
	6	10		2.7	170	4.49	II	-\
	5	18		2.8	192	4.65	II	\
	5	8	-27.7	2.8	153	4.65	II	/
	9	25		2.4	177	4.03	II	-/
	13	15		2.8	197	4.65	III	w Cc attached to incs
	5	15		2.8	140	4.65	II	-\ w Cc attached to incs
	10	15			196		II	-/
	6	8		2.5		4.18	III	
	5	8		3.7		6.01	II	
	12	15		2.7	153	4.49	III	-\
	5	10		3.1	137	5.11	II	\ Along microfract
	8	8		2.6	141	4.34	III	/
	5	8		3	152	4.96	II	-/
	8	10	<-21.4	2.5		4.18	III	-\
	3	10		2.5		4.18	III	> In same grain as previous
	5	12		3.2	163	5.26	III	-/
	8	8		2.4		4.03	II	
	4	15		3.6		5.86	II	-\
	11	20	<-23.7	3.2	204	5.26	II	
	3	8		3		4.96	II	\
	3	8	<-25.2	2.3	147	3.87	II	
	4	8		2.8	168	4.65	II	\ all together along
	3	8	<-29.5	3.1		5.11	II	/ same fracture plane
	4	8		3.2	216	5.26	II	in qtz grain
	10	20		3.8	252	6.16	II	/
	3	15		3.9	217	6.30	II	
	4	25			256		II	-/
	5	18			24		IV	-\
	3	15			20		IV	> CO2-rich inclusions
	3	15			24		IV	-/
VHG 063(A)	3	15		3.3		5.41	III	
	3	10		3.5		5.71	II	-\
	6	10		2.9		4.80	III	\ Along same microfract
	6	8	<-28	3.3	123	5.41	III	/
	6	10	<-28	3.3	127	5.41	II	-/
	5	15		2.4		4.03	II	
	5	10	<-28	2.6	123	4.34	III	
	3	10			128		III	
	3	10		2.4	121	4.03	III	
	4	10	<-29	3.6	98	5.86	II	
	4	8		1.4	129	2.41	III	

VCR Quartzite Fluid Inclusions

Sample No.	Size (um)	V/L (%)	Te	Tm	Th	Salinity	Type	Comments
VHG 074	7	8		3.2	125	5.26	III	
	4	10			153		III	--\ along same microfract
	2	15		2.8	159	4.65	III	--/
	5	10		3.5	132	5.71	III	
VHG 093(A)	5			3		4.96	III	
	3	18		3	148	4.96	III	
	5	15	<-31.3	2.8	136	4.65	III	
	3	15	<-23	3.2	128	5.26	II	
	5	12	<-31.3	3.1		5.11	II	
	7	15	<-30.7	2.5	163	4.18	II	
	6	20	<-25	2.8		4.65	III	
	4	10		3.1	152	5.11	II	
	6	8			80		III	
	7	15		3.6	192	5.86	II	--\ In qtz gr containing Au
	6	15		4	162	6.45	II	--/
	5	10		4.1	194	6.59	II	In qtz gr containing Au
VHG 093(B)	6	12		4.2		6.74	III	
	5	12			144		III	
	5	10		1.8	120	3.06	III	
	5	10		1.8	159	3.06	III	
	5	8		5.2	96	8.14	III	
	4	8			86		III	
	8	8		2.9	126	4.80	III	
	5	10		3	161	4.96	III	--\
	4	10		3.2	153	5.26	III	> together
	6	10		2.5	161	4.18	III	--/
	7	6	<-29	2		3.39	III	
	5	6	<-31	4.2	99	6.74	III	
	3	8		3.8	98	6.16	III	
	7	10		3	126	4.96	II	
		8	<-29.5	3.2	140	5.26	III	--\
	5	8	<-29.5	3.2		5.26	II	\ Along microfract
	5	8		3.4	145	5.56	III	/
	5	10		2.8	143	4.65	III	--/
	6	8		2.9	118	4.80	III	
	4	8	<-29.5	3.4	133	5.56	III	--\
	4	10			137		III	\ Along microfract
	4	8	<-29.5	3.3		5.41	III	/
	3	10	<-29.5	3.2	131	5.26	III	--/
VHG 130	3	18			144		II	
	5	10			128		II	--\ together
	4	8			154		II	--/

VCR Quartzite Fluid Inclusions

Sample No.	Size (um)	V/L (%)	Te	Tm	Th	Salinity	Type	Comments
VHG 131	6	10		2.8		4.65	III	
	6	10		2	142	3.39	III	
	7	10			152		III	
	5	12	<-22.8	1.4	154	2.41	II	
	5	15		2.6		4.34	III	
	5	15	<-25	2.4	148	4.03	III	
	5	10			141		II	
	5	10		1.7	138	2.90	II	
	7	10		1.5	152	2.57	III	
	3	8			124		III	
	5	10	<-28	2	125	3.39	III	
	3	10		1.6	124	2.74	III	
	4	10		2.3	139	3.87	III	
VHG 158(B)	5	15		1.8	151	3.06	III	–\ together
	3	15		1.8		3.06	II	–/
	5	12			153		III	–\
	4	15			152		II	\
	5	15		1.2	168	2.07	III	> together in group
	4	12	<<-27.7	1.6	156	2.74	II	/
	4	12		1.3	132	2.24	II	–/
	6	8	<-26	1.6	138	2.74	III	
	4	10		1.5	145	2.57	II	
	3	18		2.4	147	4.03	II	–\
	3	15		2	144	3.39	III	\ In qtz gr along
	4	15		0.8	164	1.40	III	/ microfract
	6	15		1.6	153	2.74	III	–/
	10	10		0.7	143	1.22	II	
	5	10		1.6	152	2.74	II	–\ together
	3	12		2.1	157	3.55	II	–/
	6	20		2.6		4.34	III	–\
	4	15		2.5	178	4.18	II	> Along microfract
	9	15		2.3	185	3.87	III	–/
	6	18		2	189	3.39	II	–\
	4	18		2.3	174	3.87	III	\ In zone with sc laths
	4	15		2.9	161	4.80	II	/ in qtz gr
	4	18		2.2	153	3.71	II	–/
	7	10		0.6	136	1.05	III	with sid xstal
	7	20		0.7	143	1.22	III	
	5	15		2.1	168	3.55	III	–\ In qtz gr nxt to type II chl
	6	18		1.6	157	2.74	III	–/

APPENDIX E

SEM-Cathodoluminescence Study

The instrument which was used for the SEM-CL investigation is a Cambridge Stereoscan S440 scanning electron microscope housed at the Electron Microscope Unit, University of Cape Town.

Method

Carbon-coated chips of polished sections were inserted into the specimen chamber and bombarded with electrons using a tungsten filament. The beam current and acceleration voltage for the acquisition of CL spectra varied from 35 - 840 nA and 10 - 15 kV, respectively. The grating of the Oxford monochromator (used for the acquisition of CL spectra) was 1200/mm, with the slits variable from 10 μm to 5 mm. The resolution of the monochromator is 0.5 mm and the dispersion is estimated at 1.8 nm/mm.

Step-scanning was done in 3 nm intervals in the wavelength range of 400 - 700 nm. The resultant photon intensities were corrected for the response function of the photomultiplier tube by dividing the measured intensity by a factor at given wavelength (see Table E1).

Table E1: Wavelength correction curve applied to correct for photomultiplier tube sensitivity.

Wavelength nm	Factor	Wavelength nm	Factor
400	**3966**	553	22745
403	4290	556	22744
406	4614	559	22744
409	4938	562	22720
412	5262	565	22684
415	5586	568	22648
418	5910	571	22612
421	6296	574	22576
424	6804	577	22540
427	7312	**580**	**22501**
430	7820	583	22377
433	8328	586	22253
436	8836	589	22129
439	9344	592	22005
442	9857	595	21881
445	10370	598	21757
448	10883	601	21634
451	11396	604	21515
454	11909	607	21396
457	12422	610	21277
460	**12935**	613	21158
463	13416	616	21039
466	13896	619	20920
469	14376	622	20727
472	14856	625	20492
475	15336	628	20257
478	15816	631	20022
481	16273	634	19787
484	16692	637	19552
487	17111	**640**	**19317**
490	17530	643	19012
493	17949	646	18707
496	18368	649	18402
499	18787	652	18097
502	19159	655	17792
505	19510	658	17487
508	19861	661	17198
511	20212	664	16931
514	20563	667	16664
517	20914	670	16397
520	**21265**	673	16130
523	21487	676	15863
526	21709	679	15596
529	21931	682	15322
532	22153	685	15046
535	22375	688	14770
538	22597	691	14494
541	22747	694	14218
544	22747	697	13942
547	22746	**700**	**13666**
550	22746		

Spectra corrected for photomultiplier tube sensitivity (Fig.9.1(a))

Sample No.	VHG063(A)	VHG158(B)	VHG158(B)	Sample No.	VHG063(A)	VHG158(B)	VHG158(B)
Curve No.	(Q2S1)	(LB13)	(L5S2)	Curve No.	(Q2S1)	(LB13)	(L5S2)
400	21506	17487	17601	550	4976	2206	4061
403	20524	16725	17234	553	5086	2266	4188
406	18831	15878	16561	556	5150	2295	4332
409	17798	15244	15691	559	5195	2370	4470
412	16895	14416	15056	562	5205	2400	4652
415	15988	13661	14268	565	5334	2459	4738
418	14830	12949	13633	568	5396	2510	4902
421	13674	12103	12590	571	5437	2572	4962
424	12566	11355	11828	574	5425	2638	5160
427	11696	10583	10918	577	5386	2675	5158
430	10950	9817	10115	580	5468	2740	5352
433	10308	9139	9340	583	5575	2779	5368
436	9619	8547	8840	586	5590	2828	5562
439	8908	7917	8117	589	5604	2868	5591
442	8173	7419	7747	592	5543	2918	5723
445	7773	6932	7170	595	5560	2982	5774
448	7511	6482	6847	598	5625	3001	5860
451	7102	6107	6348	601	5742	3025	5935
454	6748	5710	6089	604	5757	3056	5941
457	6337	5403	5681	607	5766	3062	6059
460	6025	5107	5418	610	5728	3106	6056
463	5814	4846	5155	613	5864	3104	6200
466	5608	4549	4899	616	6060	3103	6179
469	5384	4292	4634	619	6116	3099	6373
472	5162	4036	4447	622	6226	3096	6306
475	4971	3840	4249	625	6274	3121	6516
476	4803	3625	4072	628	6375	3116	6513
481	4714	3445	3895	631	6514	3112	6621
484	4588	3274	3704	634	6598	3115	6598
487	4516	3074	3596	637	6570	3103	6716
490	4387	2936	3445	640	6520	3080	6724
493	4284	2823	3371	643	6420	3090	6718
496	4248	2672	3264	646	6370	3047	6689
499	4230	2570	3208	649	6330	3017	6527
502	4174	2446	3109	652	6220	2985	6559
505	4187	2354	3095	655	6022	2941	6361
508	4135	2284	3063	658	5822	2893	6358
511	4150	2216	3025	661	5722	2839	6069
514	4134	2154	3001	664	5598	2783	5991
517	4179	2101	3082	667	5393	2733	5761
520	4252	2093	3090	670	5192	2649	5619
523	4312	2062	3152	673	4971	2603	5378
526	4354	2036	3208	676	4786	2525	5239
529	4420	2052	3292	679	4698	2473	5012
532	4499	2060	3364	682	4502	2412	4845
535	4583	2064	3487	685	4356	2340	4663
538	4630	2071	3568	688	4094	2320	4444
541	4699	2096	3650	691	3925	2249	4349
544	4770	2114	3790	694	3877	2202	4137
547	4847	2148	3908	697	3763	2173	4063

Spectra corrected for photomultiplier tube sensitivity (Fig.9.1(b))

Sample No	VHG173(B)	VHG173(B)	VHG063(A)	Sample No	VHG173(B)	VHG173(B)	VHG063(A)
Curve No.	(T3S2)	(T4S2)	(Q4S3)	Curve No.	(T3S2)	(T4S2)	(Q4S3)
400	4863	4988	4758	550	2102	2515	2866
403	4624	4764	4668	553	2144	2631	2890
406	4308	4436	4504	556	2213	2783	2937
409	4077	4024	4311	559	2243	2687	2931
412	3781	3756	4194	562	2301	3069	2990
415	3486	3468	3998	565	2340	3185	2952
418	3266	3187	3750	568	2386	3320	2961
421	3040	2906	3583	571	2409	3460	2972
424	2834	2723	3345	574	2437	3588	2984
427	2696	2489	3220	577	2493	3696	2977
430	2550	2347	3070	580	2491	3856	3032
433	2356	2225	2942	583	2516	3992	2980
436	2287	2108	2897	586	2571	4120	2967
439	2161	2006	2793	589	2598	4237	2948
442	2097	1899	2703	592	2615	4335	2946
445	2020	1805	2648	595	2629	4414	2953
448	1941	1744	2621	598	2671	4484	2928
451	1874	1657	2568	601	2680	4555	2947
454	1828	1628	2511	604	2678	4624	2972
457	1773	1572	2500	607	2745	4668	3006
460	1735	1489	2455	610	2786	4718	3056
463	1678	1454	2444	613	2822	4752	3151
466	1653	1419	2404	616	2858	4762	3227
469	1630	1400	2418	619	2907	4790	3335
472	1605	1368	2371	622	2953	4790	3465
475	1578	1327	2380	625	3016	4807	3597
478	1566	1298	2355	628	3038	4809	3727
481	1553	1286	2379	631	3098	4817	3821
484	1538	1279	2365	634	3104	4807	3871
487	1529	1259	2356	637	3145	4791	3920
490	1504	1238	2384	640	3152	4778	3963
493	1505	1237	2380	643	3103	4733	3941
496	1532	1249	2391	646	3080	4720	3856
499	1516	1259	2394	649	3061	4685	3852
502	1525	1264	2402	652	2994	4641	3782
505	1524	1297	2398	655	2935	4597	3661
508	1539	1338	2420	658	2856	4551	3583
511	1562	1378	2441	661	2796	4461	3477
514	1598	1411	2479	664	2726	4358	3381
517	1610	1468	2505	667	2684	4267	3225
520	1650	1527	2549	670	2576	4186	3100
523	1695	1592	2587	673	2522	4038	2973
526	1708	1690	2617	676	2435	3967	2840
529	1785	1783	2652	679	2392	3832	2713
532	1814	1851	2704	682	2322	3752	2596
535	1848	1935	2703	685	2228	3667	2494
538	1886	2017	2743	688	2216	3533	2389
541	1939	2140	2762	691	2111	3416	2269
544	1993	2246	2818	694	2070	3328	2202
547	2062	2391	2865	697	2017	3222	2156

Spectra corrected for photomultiplier tube sensitivity (Fig.9.1(c))

Sample No. / Curve No.	VHG181 (S1S1)	VHG181 (S2S2)	VHG172 (R1S4)	VHG163(A) (JI9)	Sample No. / Curve No.	VHG181 (S1S1)	VHG181 (S2S2)	VHG172 (R1S4)	VHG163(A) (JI9)
400	4131	7048	3322	7326	550	2027	1676	2265	2407
403	3931	6668	3208	7504	553	2134	1695	2388	2499
406	3796	6200	3105	7311	556	2194	1760	2489	2521
409	3632	5864	2896	6865	559	2316	1807	2638	2630
412	3401	5358	2744	6334	562	2432	1850	2683	2617
415	3177	5036	2590	5861	565	2496	1863	2823	2774
418	3012	4687	2430	5308	568	2619	1899	2880	2718
421	2743	4250	2248	4832	571	2723	1952	3030	2860
424	2604	3917	2109	4386	574	2802	2012	3067	2799
427	2420	3607	1954	3978	577	2865	2031	3232	2844
430	2283	3359	1804	3702	580	3014	2056	3274	2846
433	2139	3138	1757	3464	583	3091	2035	3431	2894
436	2037	2909	1664	3221	586	3162	2103	3486	2909
439	1926	2740	1659	3070	589	3252	2163	3629	2939
442	1848	2586	1531	2872	592	3336	2197	3638	2957
445	1761	2448	1472	2741	595	3430	2220	3767	2933
448	1683	2302	1418	2618	598	3519	2187	3771	3005
451	1633	2167	1380	2537	601	3575	2213	3873	2958
454	1585	2079	1346	2364	604	3627	2287	3947	3032
457	1513	1985	1281	2321	607	3679	2328	4001	2945
460	1467	1899	1263	2243	610	3680	2361	4053	3080
463	1425	1862	1237	2152	613	3731	2399	4050	3047
466	1397	1771	1229	2095	616	3781	2436	4073	3198
469	1337	1699	1199	2006	619	3733	2490	4059	3152
472	1306	1641	1190	1959	622	3776	2589	4142	3358
475	1265	1608	1144	1934	625	3807	2647	4081	3293
478	1236	1571	1148	1850	628	3802	2680	4163	3510
481	1231	1532	1143	1824	631	3761	2689	4084	3454
484	1223	1501	1148	1779	634	3822	2734	4151	3562
487	1195	1467	1151	1767	637	3763	2810	4010	3557
490	1183	1424	1147	1745	640	3719	2837	4099	3556
493	1182	1404	1171	1702	643	3748	2809	3987	3516
496	1179	1388	1168	1719	646	3741	2778	3998	3492
499	1160	1365	1185	1695	649	3640	2721	3921	3462
502	1166	1381	1196	1734	652	3634	2679	3885	3360
505	1176	1345	1231	1714	655	3619	2679	3785	3341
508	1191	1347	1255	1753	658	3509	2633	3725	3225
511	1206	1352	1298	1739	661	3449	2600	3553	3189
514	1240	1357	1316	1783	664	3439	2512	3498	3033
517	1275	1362	1395	1810	667	3303	2407	3355	2990
520	1319	1382	1425	1871	670	3230	2389	3305	2795
523	1361	1397	1506	1905	673	3183	2327	3112	2802
526	1428	1427	1580	1946	676	3116	2271	3067	2620
529	1472	1459	1642	2027	679	2991	2227	2931	2614
532	1533	1479	1723	2064	682	2976	2101	2821	2443
535	1609	1493	1811	2123	685	2884	2060	2707	2431
538	1661	1523	1909	2153	688	2802	2017	2581	2291
541	1749	1575	2005	2241	691	2717	1999	2501	2244
544	1841	1607	2076	2286	694	2725	1967	2368	2147
547	1906	1661	2178	2363	697	2606	1902	2291	2126

Spectra corrected for photomultiplier tube sensitivity (Fig.9.2(a))

Sample No. / Curve No.	VHG093(A) (P5S1)	VHG093(A) (P5S2)	Sample No. / Curve No.	VHG093(A) (P5S1)	VHG093(A) (P5S2)
400	4656	2496	550	727	508
403	4496	2340	553	750	530
406	4322	2227	556	767	544
409	4131	2148	559	775	544
412	3877	1988	562	802	557
415	3713	1861	565	817	562
418	3445	1760	568	827	589
421	3278	1670	571	830	586
424	3055	1594	574	859	587
427	2846	1421	577	870	603
430	2643	1344	580	879	619
433	2420	1236	583	897	627
436	2268	1169	586	913	636
439	2088	1067	589	929	646
442	1960	1002	592	940	661
445	1856	970	595	973	663
448	1712	915	598	1004	663
451	1616	856	601	994	674
454	1514	805	604	991	684
457	1433	780	607	988	697
460	1349	750	610	1022	701
463	1290	706	613	1056	697
466	1215	678	616	1028	703
469	1153	664	619	1057	708
472	1098	629	622	1071	724
475	1051	602	625	1066	736
478	993	581	628	1105	728
481	948	567	631	1103	733
484	904	552	634	1102	729
487	903	536	637	1119	728
490	834	508	640	1141	753
493	804	507	643	1116	746
496	775	491	646	1105	735
499	753	475	649	1065	737
502	740	470	652	1082	715
505	722	467	655	1054	696
508	692	463	658	1043	716
511	682	458	661	1004	697
514	670	445	664	984	683
517	657	450	667	977	684
520	668	450	670	927	666
523	654	456	673	931	642
526	661	461	676	910	639
529	664	461	679	868	635
532	679	462	682	858	617
535	689	474	685	853	600
538	685	475	688	822	595
541	695	485	691	787	590
544	721	498	694	768	582
547	714	517	697	756	571

Spectra corrected for photomultiplier tube sensitivity (Fig.9.2(b))

Sample No / Curve No.	VHG093(A) (P5S3)	VHG093(A) (P5S4)	VHG093(A) (P6S3)	Sample No / Curve No.	VHG093(A) (P5S3)	VHG093(A) (P5S4)	VHG093(A) (P6S3)
400	2408	1789	3396	550	868	525	887
403	2318	1732	3204	553	884	535	892
406	2189	1667	3011	556	913	549	918
409	2034	1562	2819	559	943	572	933
412	1840	1469	2690	562	965	591	947
415	1740	1394	2560	565	1002	592	981
418	1633	1296	2391	568	1019	611	985
421	1530	1194	2225	571	1040	627	985
424	1429	1104	2041	574	1064	632	1026
427	1332	1028	1886	577	1094	645	1027
430	1256	958	1796	580	1112	657	1051
433	1194	878	1666	583	1126	665	1061
436	1112	858	1596	586	1154	676	1088
439	1056	795	1492	589	1173	690	1102
442	999	754	1411	592	1191	693	1108
445	952	726	1348	595	1222	711	1125
448	891	682	1280	598	1223	708	1163
451	873	664	1223	601	1235	745	1163
454	836	630	1161	604	1250	737	1190
457	790	589	1120	607	1275	738	1166
460	779	569	1086	610	1309	748	1183
463	752	558	1043	613	1325	768	1206
466	723	539	1011	616	1302	782	1216
469	712	535	979	619	1326	781	1222
472	690	523	954	622	1356	787	1257
475	672	504	927	625	1370	812	1258
478	643	495	916	628	1366	822	1272
481	636	468	866	631	1408	830	1286
484	628	463	862	634	1390	821	1289
487	609	454	843	637	1376	841	1301
490	599	445	824	640	1387	842	1296
493	588	442	793	643	1389	835	1290
496	588	434	784	646	1363	837	1291
499	589	431	774	649	1339	833	1287
502	583	430	761	652	1310	823	1292
505	584	420	772	655	1286	817	1263
508	585	416	748	658	1263	790	1263
511	595	415	749	661	1232	782	1227
514	606	422	738	664	1201	779	1233
517	615	408	736	667	1166	773	1208
520	641	432	754	670	1131	745	1168
523	656	434	761	673	1093	716	1167
526	679	448	769	676	1062	716	1172
529	693	465	772	679	1037	691	1145
532	708	457	794	682	1001	677	1106
535	775	465	789	685	979	671	1123
538	751	479	806	688	956	661	1085
541	785	485	821	691	923	644	1092
544	809	502	834	694	871	651	1075
547	828	503	859	697	868	630	1073

Spectra corrected for photomultiplier tube sensitivity (Fig.9.3)

Sample No. / Curve No.	VHG063(A) (Q2S3)	VHG063(A) (Q2S4)	VHG063(A) (Q3S1)	Sample No. / Curve No.	VHG063(A) (Q2S3)	VHG063(A) (Q2S4)	VHG063(A) (Q3S1)
400	17544	9050	9355	550	4620	4526	4251
403	16687	8537	8915	553	4756	4859	4380
406	15512	7855	8233	556	4836	4808	4497
409	14274	7404	7764	559	4875	4911	4628
412	13452	6812	7167	562	4905	4963	4671
415	12727	6395	6558	565	4972	4971	4693
418	12002	5951	6144	568	5101	5056	4775
421	11108	5504	5536	571	5174	5192	4878
424	10191	5136	5168	574	5205	5282	4983
427	9388	4863	4827	577	5164	5280	4961
430	8810	4692	4574	580	5166	5278	4957
433	8278	4457	4335	583	5272	5265	5014
436	7810	4265	4072	586	5397	5392	5149
439	7253	4042	3905	589	5449	5525	5255
442	6740	3846	3759	592	5414	5545	5189
445	6353	3752	3661	595	5367	5536	5195
448	6081	3650	3502	598	5451	5450	5200
451	5838	3529	3415	601	5557	5536	5352
454	5538	3425	3315	604	5650	5709	5447
457	5250	3336	3223	607	5657	5788	5409
460	5022	3264	3150	610	5644	5829	5397
463	4790	3228	3082	613	5641	5797	5502
466	4659	3133	3017	616	5812	5901	5667
469	4494	3116	2980	619	6026	6077	5792
472	4358	3044	2906	622	6111	6270	5800
475	4215	3068	2919	625	6185	6383	5848
478	4094	3006	2883	628	6158	6445	5987
481	3957	2980	2869	631	6296	6409	6107
484	3921	2985	2854	634	6441	6565	6176
487	3855	2994	2835	637	6498	6675	6127
490	3771	2995	2891	640	6410	6844	6042
493	3703	3013	2888	643	6316	6519	6020
496	3653	3044	2890	646	6188	6361	6046
499	3608	3064	2934	649	6189	6252	5968
502	3621	3102	2955	652	6122	6267	5768
505	3622	3147	3001	655	5980	6160	5651
508	3612	3203	3036	658	5768	6008	5509
511	3634	3263	3083	661	5562	5749	5432
514	3641	3306	3142	664	5445	5548	5329
517	3691	3390	3241	667	5351	5472	5088
520	3778	3508	3305	670	5162	5379	4916
523	3863	3642	3378	673	4985	5153	4754
526	3908	3720	3490	676	4689	4923	4674
529	3964	3813	3577	679	4551	4671	4519
532	4076	3904	3668	682	4436	4560	4275
535	4156	4012	3767	685	4309	4470	4130
538	4246	4133	3843	688	4124	4336	3976
541	4319	4224	3945	691	3925	4102	3885
544	4402	4357	4108	694	3772	3947	3799
547	4499	4420	4183	697	3674	3791	3591

Spectra corrected for photomultiplier tube sensitivity (Fig.9.4)

Sample No. / Curve No.	VHG173(B) (T4S1)	VHG173(B) (T4S2)	VHG173(B) (T4S3)	VHG173(B) (T4S4)	Sample No. / Curve No.	VHG173(B) (T4S1)	VHG173(B) (T4S2)	VHG173(B) (T4S3)	VHG173(B) (T4S4)
400	18263	4988	4399	7996	550	3040	2515	2273	3774
403	17763	4764	4380	7893	553	3144	2631	2382	3983
406	17166	4436	4221	7574	556	3216	2763	2477	4189
409	16405	4024	3997	7362	559	3345	2887	2598	4405
412	15796	3756	3823	7220	562	3440	3069	2680	4616
415	14952	3468	3599	6884	565	3589	3185	2757	4831
418	14229	3187	3426	6645	568	3670	3320	2867	5050
421	13408	2906	3141	6143	571	3789	3460	2954	5257
424	12578	2723	2894	5668	574	3898	3588	3045	5389
427	11703	2489	2646	5181	577	4014	3696	3135	5667
430	10848	2347	2417	4682	580	4144	3856	3226	5867
433	10221	2225	2295	4333	583	4230	3992	3327	6017
436	9517	2108	2206	4094	586	4347	4120	3409	6203
439	8931	2006	2057	3903	589	4426	4237	3492	6438
442	8252	1899	1997	3655	592	4544	4335	3590	6568
445	7789	1805	1882	3462	595	4558	4414	3677	6735
448	7265	1744	1807	3317	598	4663	4484	3790	6888
451	6838	1657	1754	3149	601	4783	4555	3838	7017
454	6444	1628	1673	3018	604	4793	4624	3934	7064
457	6057	1572	1604	2848	607	4817	4668	4001	7206
460	5734	1489	1565	2740	610	4836	4718	4057	7168
463	5413	1454	1498	2627	613	4849	4752	4084	7230
466	5114	1419	1463	2553	616	4895	4762	4131	7314
469	4785	1400	1438	2449	619	4829	4790	4158	7398
472	4564	1368	1402	2390	622	4910	4790	4202	7468
475	4340	1327	1356	2316	625	4915	4807	4249	7475
478	4127	1298	1355	2242	628	4925	4809	4263	7456
481	3914	1286	1304	2157	631	4956	4817	4244	7643
484	3721	1279	1302	2122	634	4920	4807	4257	7672
487	3567	1259	1270	2060	637	4956	4791	4208	7712
490	3423	1238	1255	2027	640	4913	4778	4192	7673
493	3260	1237	1233	1997	643	4907	4733	4163	7640
496	3109	1249	1247	1977	646	4902	4720	4112	7616
499	2982	1259	1256	1984	649	4840	4685	4047	7584
502	2900	1264	1260	1962	652	4810	4641	4011	7490
505	2807	1297	1276	1983	655	4728	4597	3961	7426
508	2742	1338	1283	1992	656	4627	4551	3914	7332
511	2673	1378	1296	2054	661	4547	4461	3811	7193
514	2617	1411	1351	2105	664	4457	4358	3703	7111
517	2588	1468	1391	2182	667	4315	4267	3636	6940
520	2589	1527	1441	2270	670	4202	4186	3604	6846
523	2605	1592	1489	2351	673	4099	4038	3461	6667
526	2594	1690	1568	2472	676	4030	3967	3429	6458
529	2599	1783	1645	2602	679	3904	3832	3366	6360
532	2634	1851	1701	2748	682	3782	3752	3308	6161
535	2685	1935	1782	2904	685	3664	3687	3239	6004
538	2724	2017	1870	3005	688	3613	3533	3128	5868
541	2808	2140	1960	3189	691	3497	3416	3095	5620
544	2866	2246	2072	3379	694	3412	3328	3004	5488
547	2941	2391	2172	3569	697	3343	3222	2955	5332

Spectra corrected for photomultiplier tube sensitivity (Fig.9.5)

Sample No	VHG163(A)	VHG163(A)	VHG163(A)	VHG163(A)	Sample No	VHG163(A)	VHG163(A)	VHG163(A)	VHG163(A)
Curve No.	(JA1)	(JA2)	(JA7)	(JA8)	Curve No.	(JA1)	(JA2)	(JA7)	(JA8)
400	6945	6270	6680	5432	550	1859	2221	1473	1565
403	6766	6347	6290	5505	553	1911	2213	1428	1609
406	6314	5966	5833	5204	556	1949	2310	1482	1675
409	5903	5503	5468	4925	559	1978	2381	1469	1687
412	5529	5144	5175	4518	562	2043	2356	1449	1734
415	5216	4890	4965	4284	565	2055	2460	1474	1787
418	5100	4672	4624	4016	568	2096	2444	1493	1792
421	4807	4403	4346	3874	571	2066	2485	1485	1834
424	4353	4029	4091	3466	574	1871	2209	1490	1866
427	4184	4003	3774	3182	577	1885	2290	1508	1910
430	3682	3517	3650	2990	580	1937	2372	1511	1951
433	3050	3431	3432	2856	583	2196	2453	1507	1968
436	2778	3267	3230	2755	586	2224	2531	1507	2025
439	2720	3014	3054	2541	589	2266	2557	1505	2031
442	2579	2885	2977	2464	592	2296	2630	1541	2072
445	2392	2754	2908	2325	595	2357	2664	1565	2081
448	2293	2688	2601	2221	598	2385	2697	1558	2135
451	2164	2693	2300	2130	601	2387	2677	1540	2150
454	2102	2565	2205	2069	604	2408	2846	1555	2193
457	2050	2437	2120	1906	607	2439	3100	1546	2170
460	2010	2357	2209	1895	610	2462	3092	1567	2221
463	1965	2306	2141	1835	613	2445	3142	1600	2218
466	1886	2129	2017	1702	616	2524	3165	1597	2239
469	1836	2182	1967	1699	619	2513	3182	1618	2244
472	1768	2127	1864	1634	622	2515	3240	1628	2263
475	1707	2021	1837	1604	625	2585	3306	1683	2334
478	1673	2006	1829	1582	628	2633	3323	1727	2335
481	1720	1970	1716	1531	631	2625	3367	1736	2349
484	1870	1977	1713	1503	634	2619	3406	1754	2366
487	1819	1888	1651	1489	637	2620	3372	1747	2369
490	1650	1898	1633	1431	640	2646	3313	1798	2357
493	1604	1880	1589	1413	643	2634	3194	1789	2373
496	1566	1868	1585	1389	646	2641	3002	1815	2379
499	1533	1842	1571	1375	649	2616	2919	1788	2396
502	1483	1878	1533	1353	652	2607	2938	1807	2407
505	1461	1840	1532	1312	655	2498	2829	1800	2424
508	1450	1835	1541	1354	658	2187	3188	1793	2438
511	1433	1839	1491	1324	661	2380	3210	1790	2428
514	1423	1833	1496	1309	664	2504	3135	1779	2400
517	1410	1856	1486	1313	667	2443	3121	1756	2350
520	1458	1854	1471	1314	670	2411	3074	1744	2326
523	1473	1880	1477	1326	673	2372	3023	1845	2319
526	1470	1907	1446	1324	676	2399	3002	1826	2308
529	1475	1932	1438	1332	679	2377	2953	1811	2301
532	1482	1941	1451	1364	682	2344	2922	1786	2310
535	1490	1977	1447	1398	685	2328	2850	1798	2250
538	1496	1987	1490	1425	688	2307	2843	1822	2234
541	1790	2094	1440	1481	691	2282	2824	1763	2182
544	1818	2073	1474	1496	694	2252	2791	1796	2184
547	1885	2164	1457	1512	697	2237	2760	1802	2136
					700	2246	2767	1803	2134

Spectra corrected for photomultiplier tube sensitivity (Fig.9.6(a))

Sample No / Curve No.	VHG131 (MA4)	VHG131 (MA5)	Synth. Qtz. (QZ1)	Synth. Qtz. (QZ3)	Sample No / Curve No.	VHG131 (MA4)	VHG131 (MA5)	Synth. Qtz. (QZ1)	Synth. Qtz. (QZ3)
400	10788	11159	6473	6964	550	1830	1693	4474	3763
403	10462	10634	6046	6395	553	1890	1733	4709	3866
406	10041	10165	5551	5994	556	1954	1779	4407	3919
409	9530	9648	5251	5401	559	1997	1841	4514	3977
412	9081	9142	5074	5096	562	2057	1886	5167	4053
415	8654	8728	4750	4629	565	2130	1897	5602	4125
418	8236	8316	4452	4394	568	2155	1979	5755	4170
421	7763	7730	4215	4052	571	2224	2022	5836	4230
424	7110	7213	3931	3729	574	2290	2076	5983	4264
427	6612	6721	3649	3450	577	2342	2118	6216	4269
430	6193	6239	3301	3363	580	2379	2162	6347	4358
433	5741	5830	3036	3035	583	2437	2222	6498	4075
436	5366	5458	2807	2760	586	2473	2286	6217	4063
439	5065	5099	2664	2717	589	2517	2340	5965	4073
442	4745	4793	2567	2589	592	2569	2385	6134	4058
445	4404	4491	2467	2490	595	2595	2415	6949	4057
448	4172	4242	2411	2591	598	2632	2450	7071	4022
451	3919	3981	2339	2460	601	2669	2477	7115	4055
454	3707	3746	2264	2307	604	2697	2532	7091	4067
457	3485	3547	2207	2249	607	2711	2553	7182	4098
460	3304	3359	2314	2221	610	2713	2565	7225	4136
463	3107	3167	2117	2281	613	2740	2573	7255	4180
466	2961	3028	2135	2211	616	2744	2622	7278	4238
469	2830	2852	2143	2147	619	2739	2622	7338	4301
472	2654	2710	2039	2113	622	2766	2650	7362	4366
475	2526	2588	2034	2106	625	2787	2642	7374	4475
478	2411	2455	1991	2096	626	2806	2631	7346	4560
481	2296	2340	1990	2115	631	2800	2653	7374	4606
484	2195	2233	2006	2108	634	2808	2666	7373	4662
487	2097	2113	2010	2126	637	2816	2658	7281	4649
490	2012	2048	2040	2138	640	2806	2636	7216	4634
493	1945	1963	2077	2159	643	2765	2631	7071	4574
496	1869	1883	2121	2176	646	2764	2632	6983	4515
499	1791	1806	2172	2210	649	2758	2603	6804	4389
502	1745	1757	2201	2269	652	2704	2556	6671	4343
505	1713	1699	2286	2339	655	2688	2525	6510	4191
508	1651	1648	2353	2371	658	2631	2484	6318	4310
511	1653	1612	2420	2438	661	2585	2463	6097	4030
514	1623	1580	2517	2510	664	2510	2413	5922	4020
517	1604	1560	2621	2608	667	2457	2394	5727	3935
520	1574	1548	2740	2687	670	2418	2322	5511	3822
523	1577	1515	2853	2722	673	2346	2274	5317	3675
526	1594	1538	3005	2817	676	2294	2227	5087	3530
529	1598	1526	3130	2891	679	2242	2185	4895	3425
532	1608	1518	3318	2960	682	2188	2124	4679	3276
535	1653	1549	3513	3059	685	2156	2115	4489	2771
538	1665	1550	3664	3163	688	2109	2037	4349	2238
541	1686	1560	3788	3434	691	2048	2022	4097	2295
544	1743	1607	4009	3525	694	2007	1985	3889	2178
547	1802	1657	4249	3670	697	1965	1952	3668	2056
					700	1951	1921	3473	1919

Spectra corrected for photomultiplier tube sensitivity (Fig.9.6(b))

Sample No	VHG163(A)	VHG163(A)	Sample No	VHG163(A)	VHG163(A)
Curve No.	(JB3)	(JB6)	Curve No.	(JB3)	(JB6)
400	6754	7810	550	1271	2092
403	6127	7793	553	1273	2052
406	5800	7280	556	1273	2118
409	5446	7299	559	1262	2065
412	5233	6963	562	1256	2059
415	4827	6679	565	1236	2077
418	4591	6385	568	1257	2045
421	4453	5976	571	1226	2039
424	4138	5647	574	1250	2092
427	3753	5305	577	1256	2030
430	3515	5007	580	1239	2004
433	3294	4672	583	1230	2021
436	3109	4488	586	1253	2017
439	3015	4271	589	1238	2022
442	2817	4069	592	1253	2009
445	2668	3897	595	1261	2029
448	2532	3721	598	1254	2049
451	2442	3595	601	1275	2053
454	2344	3472	604	1291	2135
457	2246	3309	607	1292	2034
460	2109	3222	610	1285	2019
463	2068	3146	613	1285	2010
466	2000	3036	616	1318	2102
469	1962	2983	619	1329	2160
472	1855	2857	622	1351	2156
475	1781	2754	625	1375	2207
478	1724	2727	628	1398	2288
481	1700	2645	631	1439	2270
484	1662	2604	634	1474	2354
487	1633	2572	637	1553	2407
490	1605	2476	640	1508	2418
493	1533	2424	643	1499	2432
496	1528	2443	646	1551	2424
499	1471	2344	649	1520	2442
502	1472	2375	652	1546	2405
505	1422	2357	655	1563	2424
508	1415	2302	658	1560	2345
511	1405	2280	661	1617	2360
514	1398	2260	664	1594	2324
517	1364	2174	667	1598	2312
520	1340	2217	670	1589	2281
523	1309	2156	673	1579	2262
526	1295	2132	676	1602	2198
529	1300	2138	679	1548	2220
532	1284	2065	682	1556	2254
535	1280	2096	685	1523	2191
538	1278	2094	688	1500	2190
541	1310	2041	691	1513	2193
544	1258	2078	694	1497	2224
547	1253	2105	697	1524	2224
			700	1516	2206

Spectra corrected for photomultiplier tube sensitivity (Fig.9.8(c))

Sample No	VHG062	VHG062	VHG063(A)	VHG063(A)	Sample No	VHG062	VHG062	VHG063(A)	VHG063(A)
Curve No.	(NC1)	(NC4)	(Q4S1)	(Q4S5)	Curve No.	(NC1)	(NC4)	(Q4S1)	(Q4S5)
400	4799	2595	6621	5288	550	1426	700	3569	3707
403	4279	2463	6348	5082	553	1427	715	3646	3754
406	3973	2274	6059	4990	556	1423	731	3718	3813
409	3707	2080	5618	4742	559	1505	761	3796	3893
412	3648	2013	5300	4689	562	1668	818	3911	3951
415	3848	1881	5068	4494	565	1881	835	4003	3982
418	3684	1808	4752	4395	568	1952	856	4133	3992
421	3278	1658	4443	4172	571	1952	867	4238	3993
424	2701	1556	4033	3935	574	2081	898	4328	4067
427	2479	1435	3627	3711	577	2163	920	4426	4070
430	2227	1347	3362	3561	580	2124	958	4506	4056
433	2159	1285	3171	3452	583	2179	963	4515	4051
436	2213	1205	3030	3351	586	2212	988	4529	4112
439	2294	1154	2906	3289	589	2247	996	4557	4179
442	2231	1107	2799	3172	592	2269	1033	4554	4180
445	2202	1043	2674	3100	595	2315	1060	4569	4205
448	2025	977	2579	3062	598	2363	1072	4605	4248
451	1765	959	2537	3026	601	2367	1078	4658	4345
454	1553	882	2450	2953	604	2393	1118	4738	4350
457	1725	891	2368	2877	607	2365	1127	4812	4314
460	1813	855	2315	2838	610	2392	1140	4898	4322
463	1760	812	2280	2812	613	2432	1035	5009	4337
466	1786	794	2232	2797	616	2424	1144	5112	4407
469	1561	771	2205	2769	619	2430	1168	5203	4509
472	1783	732	2182	2763	622	2514	1190	5257	4565
475	2105	717	2139	2682	625	2496	1205	5292	4691
478	2159	694	2107	2665	628	2499	1251	5363	4841
481	2129	679	2108	2651	631	2517	1226	5412	4922
484	2090	652	2104	2670	634	2550	1237	5404	4968
487	2058	643	2094	2692	637	2536	1245	5402	4975
490	1979	639	2123	2699	640	2561	1221	5388	4979
493	1858	624	2147	2708	643	2565	1200	5333	5002
496	1690	607	2154	2732	646	2523	1110	5324	4915
499	1642	598	2174	2746	649	2538	1007	5285	4779
502	1669	602	2209	2773	652	2503	906	5259	4696
505	1673	582	2274	2844	655	2486	911	5156	4641
508	1611	572	2330	2896	658	2515	861	5052	4470
511	1474	582	2374	2945	661	2456	911	4916	4347
514	1301	574	2441	2963	664	2419	849	4738	4214
517	1179	574	2488	3008	667	2416	1069	4578	4139
520	1154	583	2542	3083	670	2495	862	4383	4039
523	1275	573	2637	3088	673	2437	849	4189	3921
526	1233	594	2725	3154	676	2412	836	4012	3792
529	1153	600	2830	3219	679	2393	790	3861	3643
532	1155	609	2910	3306	682	2211	754	3732	3485
535	1222	615	3024	3364	685	2376	733	3588	3371
538	1299	633	3137	3419	688	2452	737	3494	3243
541	1375	647	3251	3503	691	2450	700	3376	3063
544	1431	661	3379	3529	694	2425	737	3262	2957
547	1423	674	3481	3625	697	2448	711	3154	2854
					700	2448	671		